12-2017

Phase Difference Index: A Frequency-domain Analysis Tool for Structural Mode Identification

Li-Hui Cheng
Purdue University

PHASE DIFFERENCE INDEX: A FREQUENCY-DOMAIN ANALYSIS TOOL FOR STRUCTURAL MODE IDENTIFICATION

A Dissertation

Submitted to the Faculty

of

Purdue University

by

Li-Hui Cheng

In Partial Fulfillment of the

Requirements for the Degree

of

Doctor of Philosophy

December 2017

Purdue University

West Lafayette, Indiana

THE PURDUE UNIVERSITY GRADUATE SCHOOL
STATEMENT OF DISSERTATION APPROVAL

Dr. Ayhan Irfanoglu, Chair

Lyles School of Civil Engineering

Dr. Santiago Pujol

Lyles School of Civil Engineering

Dr. Robert L. Nowack

School of Earth, Atmospheric, and Planetary Sciences

Dr. Mete A. Sozen

Karl H. Kettelhut Distinguished Professor Emeritus of Civil Engineering, Lyles School of Civil Engineering

Approved by:

Dr. Dulcy M. Abrham

Head of the School Graduate Program

To my wife Wan Shan and lovely daughter Carol,
who always stand by my side
sharing all the joy and sorrow with me.

ACKNOWLEDGMENTS

I would like to express my deepest gratitude to my advisor and graduate committee chair, Professor Ayhan Irfanoglu. In the past few years, he has been always willing to offer assistance and suggestion in my school and research life. I would also like to appreciate my graduate committee members, Professor Robert L. Nowack, Professor Santiago Pujol, and Professor Mete A. Sozen who not only gave me useful advice in my research but also taught me practical knowledge about earthquake engineering and seismology.

I would like to thank Ministry of Education, Taiwan(R.O.C) for the financial support. Without the funding from my government, studying abroad would have been an impossible dream to me.

I also would like to say thank you to Lucas Laughery, Aishwarya Puranam, Alana Lund, and Rih-Teng Wu, who were my teammates of the Tainan earthquake investigation. Working with you in the research of damaged buildings in Taiwan was an unforgettable experience in my life. In addition, I am also grateful to Pedram Hesam, who always shared helpful experiences with me.

At the same time, I have to acknowledge the website "Center for Engineering Strong Motion Data" supported by USGS, and the database of Central Weather Bureau of Taiwan, because all analyzed cases in my research are downloaded from these two websites.

At last, I also want to say thank you to Ms. Molly A. Stetler and Ms. Jenny Ricksy for helping me with related administrative procedures.

TABLE OF CONTENTS

Page

Page

Page

Page

Page

LIST OF TABLES

Table Page

Table Page

LIST OF FIGURES

Figure Page

Figure Page

Figure Page

Figure Page

ABSTRACT

Cheng, Li-Hui Ph.D., Purdue University, December 2017. Phase Difference Index: A Frequency-domain Analysis Tool for Structural Mode Identification. Major Professor: Ayhan Irfanoglu.

A new structural mode-identification approach, called the Phase Difference Index plot (PDI plot), is used to identify the natural modes in a building from its acceleration records response to earthquake ground motion. The phase difference index can be calculated by the Hilbert transform of displacement response curves obtained from acceleration records at two different floors in the building. The torsional mode can also be identified if two accelerometers are installed on opposite sides in a floor. To demonstrate the power of the new approach, earthquake acceleration records from ten buildings in Taiwan and the U.S. are used. After applying narrow band-pass filter (frequency bandwidth of 0.05-0.1 Hz) to the acceleration records, and then using Hilbert transform on pairs of displacement records on chosen floors (obtained from the acceleration records), the phase difference between the corresponding pair of designated floors can be calculated. The cosine of the phase difference angle of the two displacement curves is defined as the phase difference index (PDI). The phase difference index versus frequency graph forms a PDI plot. Structural behavior at chosen floors and in various frequency bands can be found by studying the PDI plot. From comparison of PDI plot and typical building mode shapes obtained based on estimated stiffness and mass distribution, the natural modes can be identified. The method has been tested for accuracy and limitations by applying it to data obtained from numerical simulations. Response of one full scale four-story model in Japan, and ten actual buildings in U.S. and Taiwan have been studied using the proposed method. It is shown that using the PDI plot method more modes of a building can

be identified confidently compared to traditional frequency-domain and time-domain based methods.

1. INTRODUCTION

1.1 Background and Previous Research

System identification is the most common approach used to estimate characteristic dynamic parameters of a building from dynamic response data. Using harmonic vibration generators, natural frequency and damping of natural modes of a building can be found experimentally. Results obtained from studying records before and after an earthquake can be compared. Permanent reduction in natural frequency of a building often indicates that the stiffness of the structure has decreased. Some government agencies have begun to install accelerometers in various kinds of buildings to collect earthquake response data and observe the behavior of those buildings. For instance, in Taiwan, more than 30 buildings have been selected for monitoring under seismic excitation [1]. In the U.S., over 100 buildings, bridges and dams have been instrumented with accelerometers [2].

Methods to find the dynamic parameters of buildings can be grouped into two types: time-domain methods and frequency-domain methods. A comparison of these methods is given in Table 1.1.

Most of the time, the first (fundamental) lateral mode is regarded as the most important mode of a building. One practical and intuitive way to identify the fundamental mode is to plot frequency spectrum (obtained through Fourier transform of a record) and searching for the peak with the maximum spectral (Fourier) amplitude. However, the maximum peak is often blurred by noise, mixed with and shifted due to torsional mode interaction, or cannot be identified clearly due to change in stiffness properties within the time window studied. Fig. 1.1 illustrates the difficulty. In this figure, the frequency response function, i.e. the ratio of the Fourier spectra of acceleration recorded at the roof and at the ground floor, of the 7-story hotel building in

Van Nuys, CA is shown. The records are from the June 1, 2014 Westeood Village earthquake. The first translational mode and torsional mode are with the range of $f = 2 \sim 4$Hz. However, the identification cannot be accomplished without using other tools. In addition, sometimes the maximum peak does not correspond to the fundamental mode of the building but to a higher mode or site soil mode, as often observed in high-rise buildings, especially in the ambient noise analysis [3]. Besides, there is no way to tell the ordering of the various modes only by looking at a frequency spectrum. Frequency-domain analysis not only loses the time-dependent information but also has difficulty to provide enough information to tell which frequency peak corresponds to the fundamental mode or other modes. One often needs to use a time-domain analysis, such as subspace method, to identify the natural modes and corresponding frequencies [4] [5] [6].

By means of time-domain analysis, the eigenvalues (modal frequencies) and eigenvectors (mode shapes) may be calculated, and thus the order of modes can be confirmed. However, the computational demand of time-domain methods is very heavy, especially in high-rise buildings where large number of modes are present. Inevitably, influenced by noise, the time-domain analysis sometimes generates dummy eigenvalues or spurious mode shapes. Therefore, a frequency-domain tool called "stability diagram" [5] may need to be drawn and used for checking. The idea behind a stability diagram is simple: for the same system, the first few eigenvalues should be the same regardless the order of the model chosen to represent the system and regardless how many input and output data were used to describe the system. If the same set of signals were tested with different order models, the eigenvalues persisting in different order models are accepted as the real parameters of the system.

From the above discussion, it is seen that frequency-domain analysis only identifies the frequencies with relatively high energy without knowing whether these frequencies correspond to natural modes of the structure, and if so, to which modes, while time-domain analysis can calculate the eigenvalues and the corresponding mode shapes without assurance that no mode is missed.

Another branch of system identification is the analysis method of seismic interferometry. Seismic interferometry reconstructs wavefields propagating between receivers using the waves originally generated by earthquakes [7]. For example, Nakata [7] applied the method based on deconvolution to earthquake data observed in a building at Tokyo Metropolitan University and successfully extracted building response and estimated velocities and frequencies of traveling waves inside the building. Also, Prieto [3] used the method and analyzed the instrumented University of California, Los Angeles, Factory building, while Petrovic [8] identified eight buildings of different construction types by this method.

In addition to time-domain analysis and frequency-domain analysis, an integrated concept, i.e, time-frequency domain analysis is also widely used in signal processing. Timefrequency analysis techniques decompose signal data into forms that separate the time-varying amplitude, frequency, and phase content [9]. Several kinds of tools can be applied to the structural health monitoring, such as short-term Fourier transform, Hilbert-Huang transform, wavelet transform. These approaches may provide good insight into structural dynamic properties.

Although there are many ways to do the signal processing, one question remains. There is no way to tell the order of modes from the identified results only by either time-domain analysis or frequency-domain analysis. Displacements corresponding to the identified modes from all sensors in the building need to be calculated and corresponding mode shapes need to be plotted determine the mode order.

1.2 Outline of the Research

In this proposed research, a new approach called the "Phase difference Index plot (PDI plot)" is developed to help identify the natural modes of a building from its response to ground shaking.

The main idea of the proposed method is based on the fact that there are patterns in the mode shapes of typical buildings. Thus, the phase difference between modal

displacements at different floors should also have patterns. By analyzing the common patterns of mode shapes, the natural frequencies of buildings can be identified.

In this dissertation, Chapter two introduces the concept of the phase difference of the inter-story displacements of SDOF and MDOF buildings. Then, Chapter three discusses the methodology in the research, including defining the"phase difference index (PDI)" and three different ways to calculating the phase difference of two waves. Thereafter, a real building is offered as an example to illustrate the calculation of PDI.

In Chapter four, four different numerical models are analyzed to test the feasibility of PDI with both white noise acceleration input and the Ji-Ji earthquake record(Station-WNT, Jiji-Earthquake, Taiwan, 1999/09/20). Chapter five discusses the issue of torsion. The chapter not only shows how the torsion influences the frequency spectrum and phase, but also uses four types of numerical models to confirm this.

In Chapter six and seven, five real buildings in the U.S. and another five buildings in Taiwan are adopted to test the PDI method to see if the recommended method is feasible. In Chapter eight, the time-frequency application in PDI method is introduced and two cases including one building studied in Chapter seven and a full scale model tested in Japan were studied and compared with the subspace method. At last, Chapter nine and ten are conclusion and recommendation for the PDI method.

Table 1.1.
Comparison of time-domain analysis and frequency-domain analysis

	Time-domain analysis	**Frequency-domain analysis**
Time-dependent information	Yes	No
Mode order identification	possible	No
Torsional mode identification	possible	No
Graphical analysis	No	Yes
Phase information	No	Yes
System stability judgment	cumbersome	easy

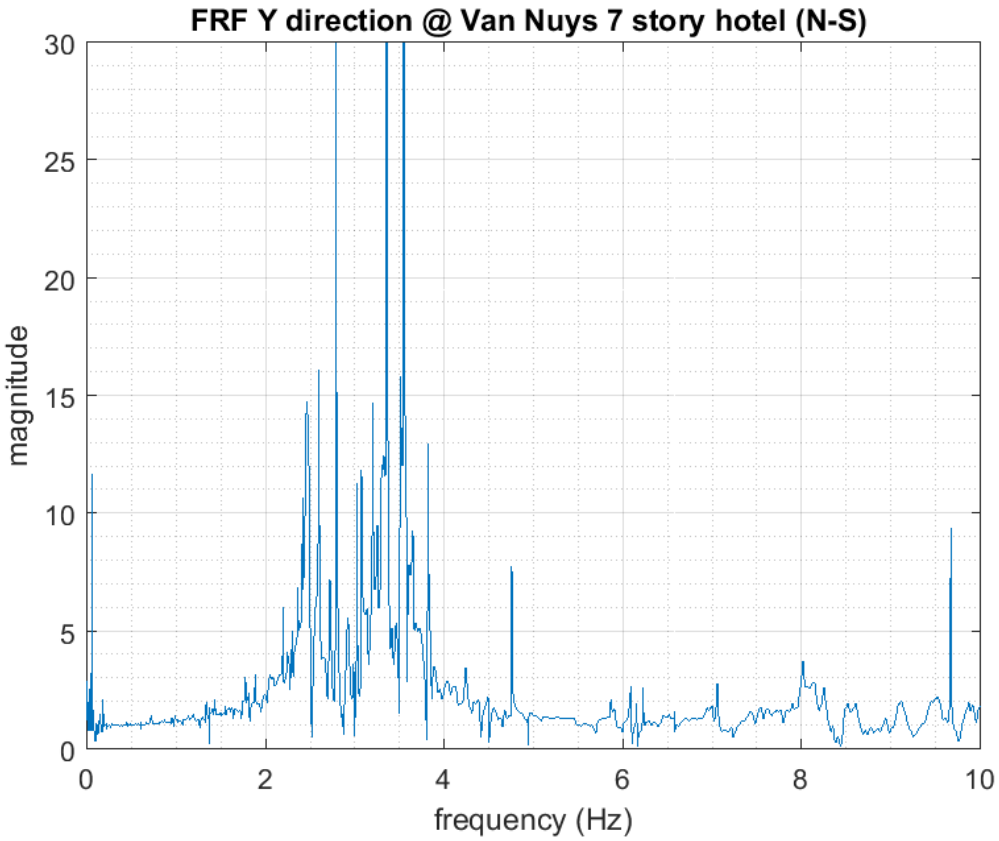

Fig. 1.1. Frequency response function obtained as ratio of Fourier Spectra of the roof acceleration record and the ground acceleration record. The data are from Ch.03 an Ch.14 of the 7-story hotel building in Van Nuys, CA, and recorded during the June, 1, 2014 Westwood Village earthquake.

2. PHASE DIFFERENCE CONCEPT FOR BUILDING RESPONSE MODE IDENTIFICATION

2.1 Phase Angle in SDOF System

A linear single degree of freedom (SDOF) system with linear viscous damping, shown in Figure 2.1, has the following governing equation of motion when subject to harmonic excitation [10]:

$$m\ddot{u} + c\dot{u} + ku = p_0 sin\omega t \tag{2.1}$$

where m, c, and k are mass, damping and stiffness of the system, and the harmonic excitation with forcing frequency ω acts on the mass directly. If the structure is damped subcritically (as in civil structures), the steady-state solution will be:

$$u(t) = (u_{st})_0 R_d sin(\omega t - \phi) \tag{2.2}$$

where $(u_{st})_0$ is the displacement if peak load was applied statically,R_d is the displacement amplification factor, and ϕ is the phase angle.

The displacement dynamic amplification factor of the system is:

$$R_d = \frac{1}{\sqrt{(1-\beta^2) + (2\varepsilon\beta)^2}} \tag{2.3}$$

where:

$\beta = \frac{\omega}{\omega_n}$: (forcing frequency/ natural frequency)

$\varepsilon = \frac{C}{C_c}$: damping ratio of viscous damping

$\omega_n = \sqrt{\frac{k}{m}}$: natural frequency of the system

$C_c = 2\sqrt{m\omega_n}$: critical damping coefficient

The complex frequency response function(FRF) $H(\omega)$ is:

$$H(\omega) = \frac{1}{(1-\beta^2) + 2\varepsilon\beta j} \tag{2.4}$$

The phase angle of the SDOF system is:

$$\phi = tan^{-1}\frac{2\varepsilon\beta}{1-\beta^2} \tag{2.5}$$

Dynamic amplification factor and phase angle plots are shown as Figure 2.2. It is observed that when the excitation frequency is equal to the natural frequency, i.e. ω_n of the SDOF system, the amplification factor reaches its maximum value. When the frequency of excitation is equal to the natural frequency of the SDOF system, the phase angle is 90 degrees, i.e. $\pi/2$ radians. The physical meaning can be illustrated in Figure 2.2. This gives us important insight to develop a phase difference method for multiple degrees of freedom structures (buildings). The phase is related to direction relative of motion no matter how big or small the amplitude of the movement may be. This property is key in making identification of a natural frequency simpler.

2.2 Phase Angle in MDOF System

2.2.1 2DOF System

Similar to SDOF systems, the same notion of phase difference also applies in a linear MDOF structure. A 2-DOF system under seismic force shown in Figure 2.4 is used to illustrate to concept. An illustration of phase difference in response for the 2-DOF system considered is given in Figure 2.5. The middle part of Figure 2.5 shows the mode shape of the first mode, indicating that the roof and ground move in phase if the external excitation is equal to the first mode frequency. Similarly, the right part of Figure 2.5 reveals that the roof and ground move out of phase in case that the external excitation is equal to the second mode frequency.

If it is assumed that the diaphragms of a building move horizontally under seismic excitation, the theoretical mode shapes of a building dictate the relative movement

of each floor. Taking Figure 2.5 as an example, the first floor and second floor move in phase in the first mode, but out of phase in the second mode. Thus, if acceleration records are available, the displacements corresponding to any specific range of frequencies can be obtained. Thus, the phase difference from the displacement curves in first and second floors, i.e, $\Delta\phi$ with the corresponding forcing frequency, i.e., f_{ext} can be calculated. By analyzing the relationship between $\Delta\phi$ and f_{ext}, the frequency band corresponding to a specific mode can be identified.

Time-domain analysis

The equation of motion of a 2DOF system with two identical floor masses, story stiffness can be expressed as follows. The modal damping matrix is assumed to be diagonal:

$$\begin{bmatrix} m & 0 \\ 0 & m \end{bmatrix} \begin{bmatrix} \ddot{u}_1 \\ \ddot{u}_2 \end{bmatrix} + \begin{bmatrix} c_{c1} & -c_{c1} \\ -c_{c1} & c_{c1}+c_{c2} \end{bmatrix} \begin{bmatrix} \dot{u}_1 \\ \dot{u}_2 \end{bmatrix} + \begin{bmatrix} k_1 & -k_1 \\ -k_1 & k_1+k_2 \end{bmatrix} \begin{bmatrix} u_1 \\ u_2 \end{bmatrix} = - \begin{bmatrix} m \\ m \end{bmatrix} \times \ddot{u}_g \tag{2.6}$$

Calculating the natural frequencies for the 2DOF system in Fig. 2.4 is a traditional eigenvalue problem. First, without considering the damping terms, let $x_1(t) = e^{\omega t}$ and $x_2(t) = e^{\omega t}$. The determinant of Eq.2.6 becomes:

$$\begin{vmatrix} k - m\omega^2 & -k \\ -k & 2k - m\omega^2 \end{vmatrix} = k^2 - 3km^2 + m^2\omega^4 \tag{2.7}$$

$$\omega^2 = \frac{1}{2} \times \left(\frac{3k}{m} \pm \sqrt{(\frac{3k}{m})^2 - 4(\frac{k}{m})^2}\right) \tag{2.8}$$

Thus, $\omega = 2.62(\frac{k}{m})$ or $0.38(\frac{k}{m})$. Let m=1 $(kgsec^2/m)$ and k=2500 (kg/m), the natural frequencies $(f = \frac{\omega}{2\pi})$ of the system are 4.92 and 12.88 Hz. By modal superposition method, the steady state solution of displacements can be obtained as:

$$\begin{bmatrix} u_1 \\ u_2 \end{bmatrix} = \begin{bmatrix} 1.17 \\ 0.72 \end{bmatrix} \times \frac{-\ddot{u}_g(t)/\omega_1^2}{\sqrt{(1-\beta_1^2)^2 + (2\varepsilon\beta_1)^2}} + \begin{bmatrix} -0.17 \\ 0.28 \end{bmatrix} \times \frac{-\ddot{u}_g(t)/\omega_2^2}{\sqrt{(1-\beta_2^2)^2 + (2\varepsilon\beta_2)^2}} \tag{2.9}$$

where:

- $\beta_1 = \frac{f}{f_{n1}}$, $\beta_2 = \frac{f}{f_{n2}}$
- $\begin{bmatrix} fn_1 \\ fn_2 \end{bmatrix} = \begin{bmatrix} 4.92 \\ 12.88 \end{bmatrix} (Hz)$
- $[\phi] = \begin{bmatrix} 1 & 1 \\ 0.62 & -1.62 \end{bmatrix}$
  (mode shape vectors are normalized to unit value at top(roof) degree of freedom)

From Eq.2.9, the displacement dynamic amplification factor of this 2DOF system can be computed. It is shown as Figure 2.6. This figure gives us clear information that the response will be amplified when the excitation frequency is around 4.92 or 12.88 Hz. Although Eq.2.9 is very useful to find the amplified response, it is not helpful to derive the relationship between phase angle and excitation frequency. Thus, another approach, namely the frequency-domain analysis is adopted to determine the phase angle of the 2DOF system.

Frequency-domain analysis

Frequency-domain analysis (FDA) is another approach to study structural dynamics. For a undamped MDOF system, the governing equation can be written as:

$$[M]\{\ddot{u}(t)\} + [K]\{u(t)\} = \{f(t)\} \tag{2.10}$$

The general solution by FDA is expressed as [11]:

$$\{U\} = [\alpha(\omega)]\{F\} \tag{2.11}$$

where: $\alpha(\omega)$ is defined as the receptance frequency response function (FRF) matrix of the system [11], i.e.:

$$[\alpha(\omega)] = \begin{bmatrix} \alpha_{11}(\omega) & \alpha_{12}(\omega) & ... & \alpha_{1n}(\omega) \\ \alpha_{21}(\omega) & \alpha_{22}(\omega) & ... & \alpha_{2n}(\omega) \\ ... & ... & ... & ... \\ \alpha_{n1}(\omega) & \alpha_{n2}(\omega) & ... & \alpha_{nn}(\omega) \end{bmatrix} \tag{2.12}$$

And the definition of one single receptance can be given as:

$$[\alpha(\omega)] = [\Phi][\omega_r^2 - \omega^2]^{-1}[\Phi]^T \tag{2.13}$$

For a single receptance FRF $\alpha_{pq}(\omega)$, the equation can be expressed as:

$$\alpha_{pq}(\omega) = \frac{\Phi_{p1}\Phi_{q1}}{\omega_1^2 - \omega^2} + \frac{\Phi_{p2}\Phi_{q2}}{\omega_2^2 - \omega^2} + ... + \frac{\Phi_{pn}\Phi_{qn}}{\omega_n^2 - \omega^2} \tag{2.14}$$

where:

$[\Phi]$ is the mass-normalized mode shape(given in Eq.2.15).

m_r is orthogonal mass for r_{th} mode(given in Eq.2.16).

$$[\Phi]_r = \frac{1}{\sqrt{m_r}} \{\phi\}_r \quad (r = 1, 2, ..., n) \tag{2.15}$$

and

$$m_r = [\phi]_r^T [M][\phi]_r \quad (r = 1, 2, ..., n) \tag{2.16}$$

In a similar way, Eq.2.11 can be applied to damped MDOF system as long as the receptance term $\alpha(\omega)$ is modified by adding the damping ratio term [11]:

$$\alpha_{pq} = \sum_{r=1}^{N} \frac{{}_rA_{pq}}{\omega_r^2 - \omega^2 + \omega_r^2 \eta_r j} \quad (structural\ damping) \tag{2.17}$$

or

$$\alpha_{pq} = \sum_{r=1}^{N} \frac{{}_rA_{pq}}{\omega_r^2 - \omega^2 + 2\omega\omega_r \varepsilon j} \quad (\ viscous\ \ damping) \tag{2.18}$$

where:${}_rA_{pq} = \Phi_{pr}\Phi_{qr}$ (the product of the pth and qth elements in the rth mode shape), and j is the unit imaginary number.

In Eq.2.18 , α_{pq} is a frequency response function or a kind of transfer function of the system. For a 2DOF system, ${}_rA_{pq}$ can be expressed as:

$$\alpha_{pq} = \frac{{}_1A_{pq}}{\omega_1^2 - \omega^2 + 2\omega\omega_1\varepsilon j} + \frac{{}_2A_{pq}}{\omega_2^2 - \omega^2 + 2\omega\omega_2\varepsilon j} \tag{2.19}$$

In Eq. 2.19, ${}_1A_{pq}$ and ${}_2A_{pq}$ represent the contribution factors of 1st mode and 2nd mode. If ${}_2A_{pq}$ is much smaller than ${}_1A_{pq}$, it means the 2nd mode can be ignored, and this 2DOF system can be regarded as a SDOF. In order to observe the phase plot of 2DOF and even higher MDOF systems, all ${}_rA_{pq}$ are assumed to be equal to 1 in the following MDOF system.

α_{pq} is written in complex form. Taking α_{1q} as an example, we can draw the Nyquist plot as Fig. 2.7. If we focus on the relationship between the real part and the imaginary part, the Nyquist plot is shown in Figure 2.8. By means of the Nyquist plot, it is easy to derive the phase angle of α_{1q} in this 2DOF system:

$$\theta_1 = arctan(\frac{imag[\alpha_{1q}(\omega)]}{real[\alpha_{1q}(\omega)]}) \tag{2.20}$$

or, avoiding the infinity occurring in $tan\theta$,

$$\theta_1 = arctan2(\frac{imag[\alpha_{1q}(\omega)]}{real[\alpha_{1q}(\omega)]}) \tag{2.21}$$

For the 2DOF shown in Fig. 2.4, the frequency response function of α_{1q} can be expressed as:

$$\alpha_{1q}(\omega) = \frac{1.17}{(4.92^2 - \omega^2) + 2 * 4.92 * \omega * \varepsilon j} + \frac{-0.17}{(12.88^2 - \omega^2) + 2 * 12.88 * \omega * \varepsilon j} \tag{2.22}$$

The coefficients [1.17 , -0.17] in Eq. 2.22 match the numbers in the first row of Eq.2.9. As mentioned, because -0.17 is small compared to 1.17, if we want to make the phase of 2nd mode more observable, we need to adjust the coefficients. Thus, the frequency response function of α_{1q} can be expressed as:

$$\alpha_{1q}(\omega) = \frac{1}{(4.92^2 - \omega^2) + 2 * 4.92 * \omega * \varepsilon j} + \frac{-1}{(12.88^2 - \omega^2) + 2 * 12.88 * \omega * \varepsilon j} \tag{2.23}$$

Using relationship given in Eq.2.21, the phase angle of α_{1q} can be plotted in Fig. 2.9. The lower part of Fig.2.9 is very similar to the phase angle plot of SDOF in Fig.

2.5. However, the plot is not very practical to identify the natural frequency of the 2DOF system easily. Another index–"$cos\theta$" is adopted to observe the fluctuation of phase angle2.10. One benefit of $cos\theta$ plot is that the zero-crossing point matches the corresponding natural frequency so it is easier to identify the natural modes of the system.

2.2.2 MDOF System

Multiple-degree of system(MDOF) system shares the same equations as 2DOF system. For any degree of freedom system, Eq.2.15 $\sim$ 2.21 are valid to calculate the transfer function and phase angle. In this section, an eight degrees of freedom system shown in Fig. 2.11 is used to develop relevant Nyquist plot and phase angle plot. For a building system, the coefficient of the 1st mode is usually larger than the rest. It is unfavorable to observe the variation of phase plots. Thus, similar to the 2DOF example mentioned in previous sections, the summation of each ${}_rA_{pq}$ for each mode in this case are also adjusted to be 1 so that the phase angle plot is more identifiable. The 3D and 2D Nyquist plots of the 8 DOF system are shown as Fig. 2.13 and 2.14. The phase angle plots are given as Fig. 2.15 and 2.16 respectively. In Fig. 2.16, the calculated natural frequencies of this 8 DOF system match the zero-crossing points in the $cos\theta$ phase plot.

Moreover, the same idea of phase difference as developed for a 2DOF system, though more complicated, also holds true in MODF, and the mode shapes corresponding to different modes also help us to locate the natural frequency of a building. Figure 2.12 presents all mode shapes of the 8 DOF system considered. For a typical simple structure, by observing the relative motion of each floor corresponding to each mode, we can conjecture the sign (positive or negative) of phase difference of each diaphragm under external force with specific frequency. For instance, under ideal circumstance, given the acceleration records of the 9th floor (roof) and 2nd floor,

the sign of the phase difference between the displacement curves of the the 9th floor (roof) and 2nd floor should be positive, negative, positive, negative, i.e. alternating.

In a well monitored building, usually multiple accelerometers are installed in the building. We can acquire different and useful information from all accelerometers in each floor. In the perspective of system identification, the most useful information would be on the roof, the 2nd floor and the ground. First, if we refer to Eq. 2.11, the frequency response function on the roof of a building can be expressed as:

$$H(\omega) = \frac{\ddot{U}(\omega)_{roof}}{\ddot{U}(\omega)_{ground}} \tag{2.24}$$

where:

$\ddot{U}(\omega)_{roof}$: The frequency spectrum of roof acceleration.

$\ddot{U}(\omega)_{ground}$: The frequency spectrum of ground acceleration.

For most buildings, the largest inertial force driven by the earthquake is on the roof. It is because the largest displacement occurs on the roof in the first mode. Therefore, it is easy to identify the first mode only by observing the frequency response function from Eq. 2.24. Second, as for the acceleration record on the 2nd floor, by observing the mode shapes of MDOF system such as Fig. 2.12, we can see that the phase of displacement direction corresponding to each mode frequencies is always opposite between roof and 2nd floor. This characteristic gives us a convenient tool to target the frequency bandwidth for each mode.

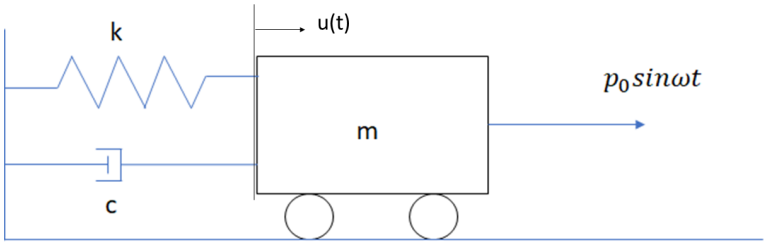

Fig. 2.1. SDOF system. m: mass of the system, c :viscous damping coefficient, k: stiffness, and $p_0 sin\omega t$: external force.

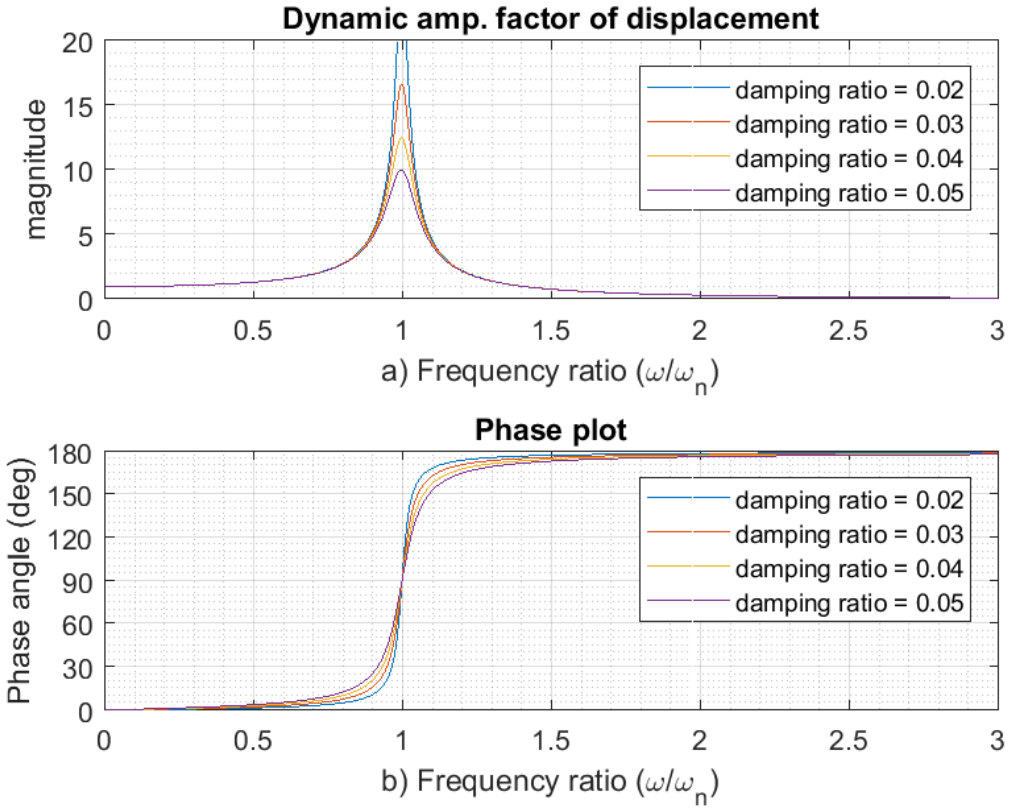

Fig. 2.2. a) Dynamic amplification factor and b) phase angle versus forcing-to-modal frequency ratio (ω/ω_n)

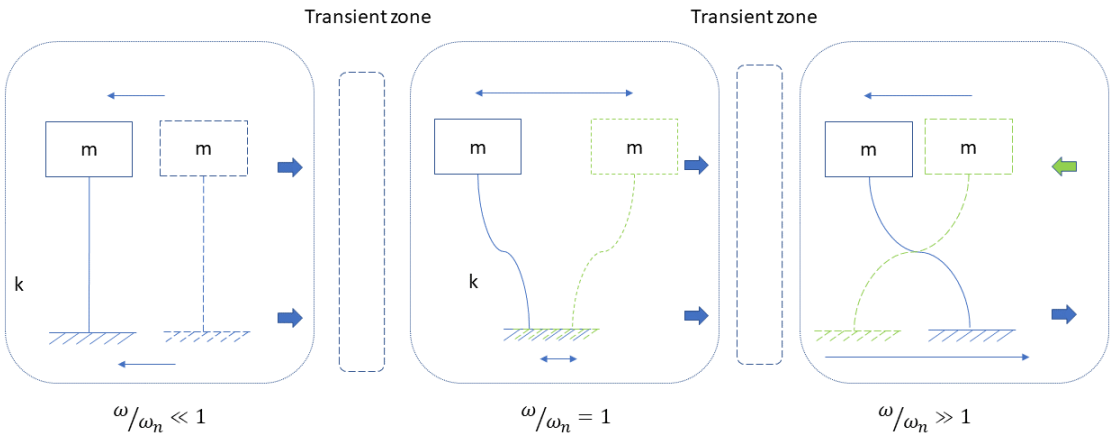

Fig. 2.3. Physical interpretation of phase in SDOF: $\omega/\omega_n << 1$ the mass and the ground move in-phase; $\omega/\omega_n = 1$ the resonance occurs in the system; $\omega/\omega_n > 1$ the mass and the ground move out-of-phase

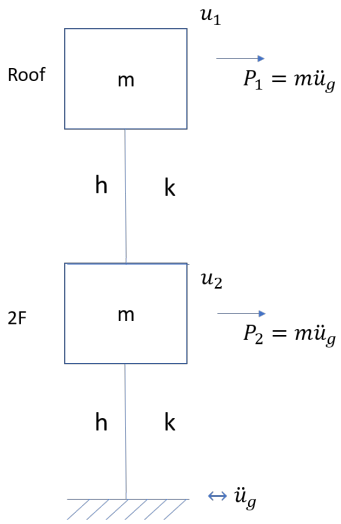

Fig. 2.4. 2DOF system (a simplified shear frame).

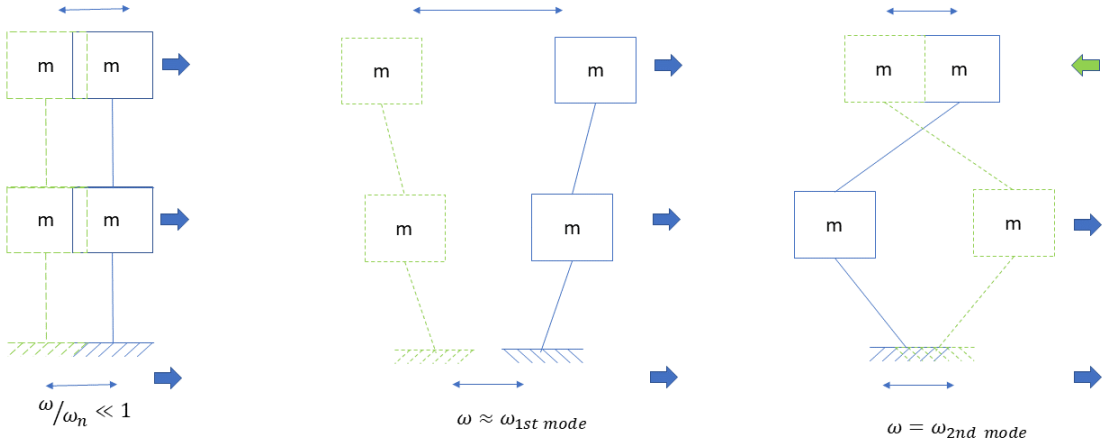

Fig. 2.5. Physical interpretation of phase in 2DOF system (a simplified shear frame). $\omega/\omega_n << 1$ the 2 masses and the ground move in-phase; $\omega/\omega_n 1 = 1$ the resonance occurs in the system and the building shakes in the first mode ; $\omega/\omega_n 2 = 1$ the resonance occurs in the system and the building shakes in the second mode.

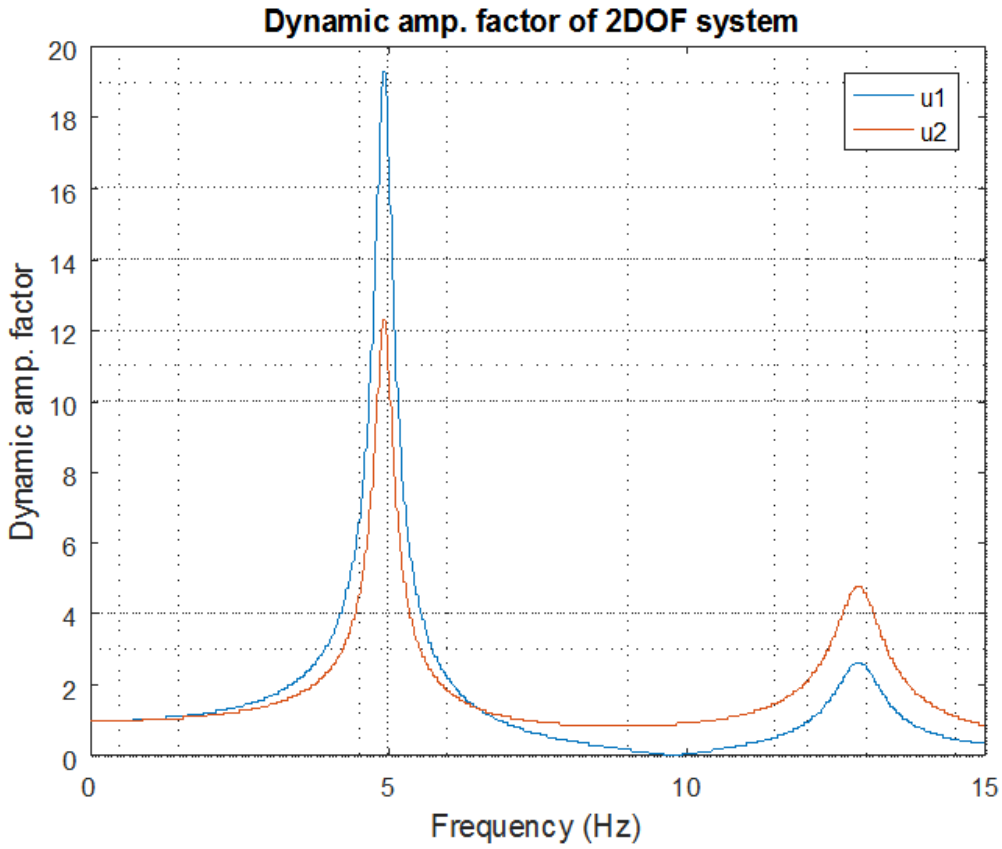

Fig. 2.6. Dynamic amplification factor of 2DOF system (with undamped natural frequencies of 4.92 & 12.88 Hz, 3% viscous damping ratio). Referring to Fig.2.4, u_1 is the displacement of roof, and u_2 is the displacement of the 2nd floor

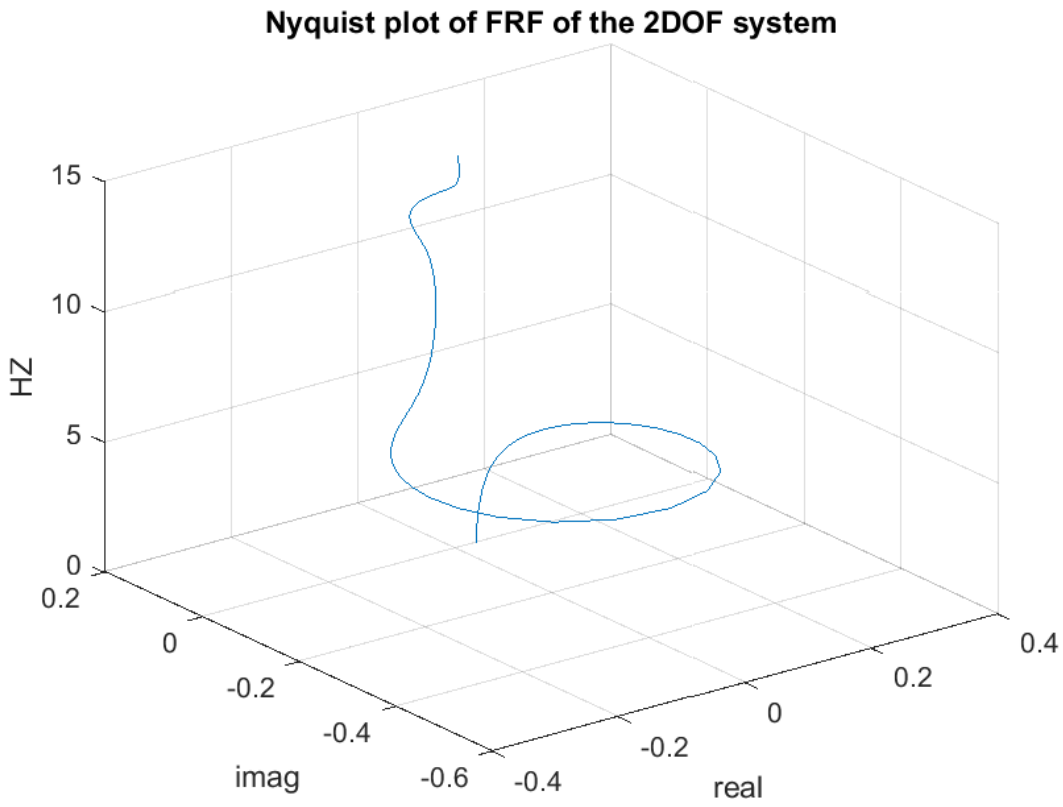

Fig. 2.7. 3D view of Nyquist plot of α_{1q} in the 2DOF system (f_n = 4.92 & 12.88 Hz, ε =0.05)

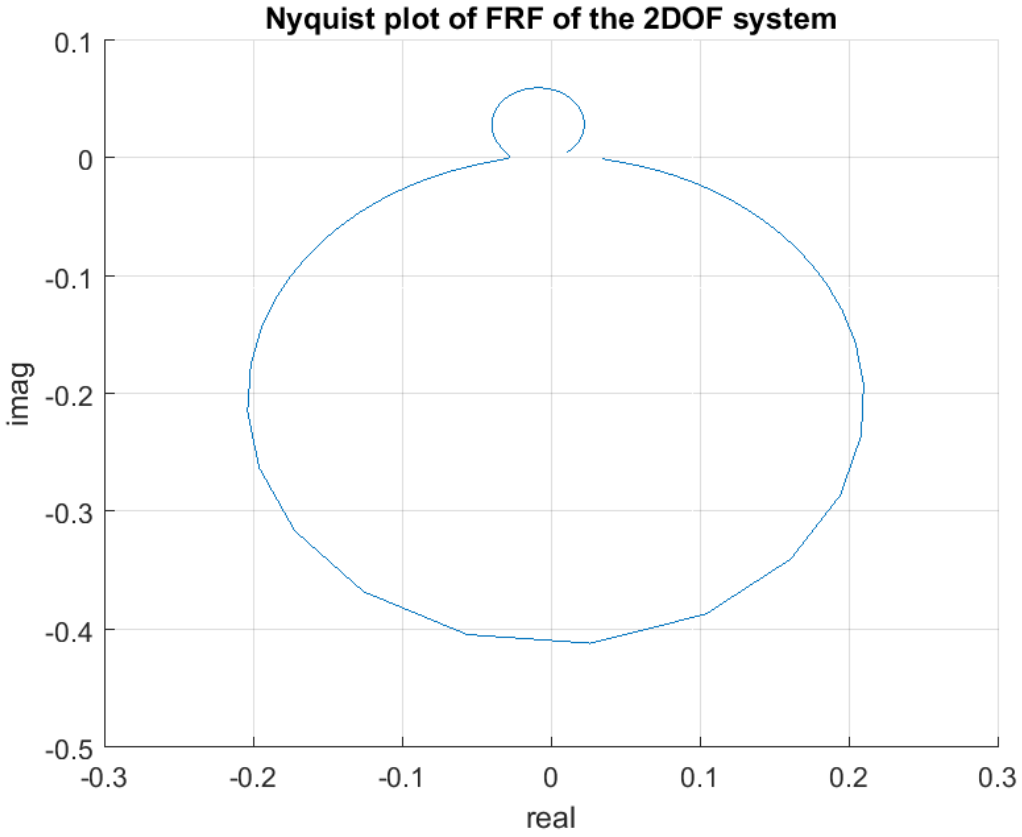

Fig. 2.8. 2D view of Nyquist plot of α_{1q} in 2DOF system (f_n = 4.92 & 12.88 Hz, ε =0.05)

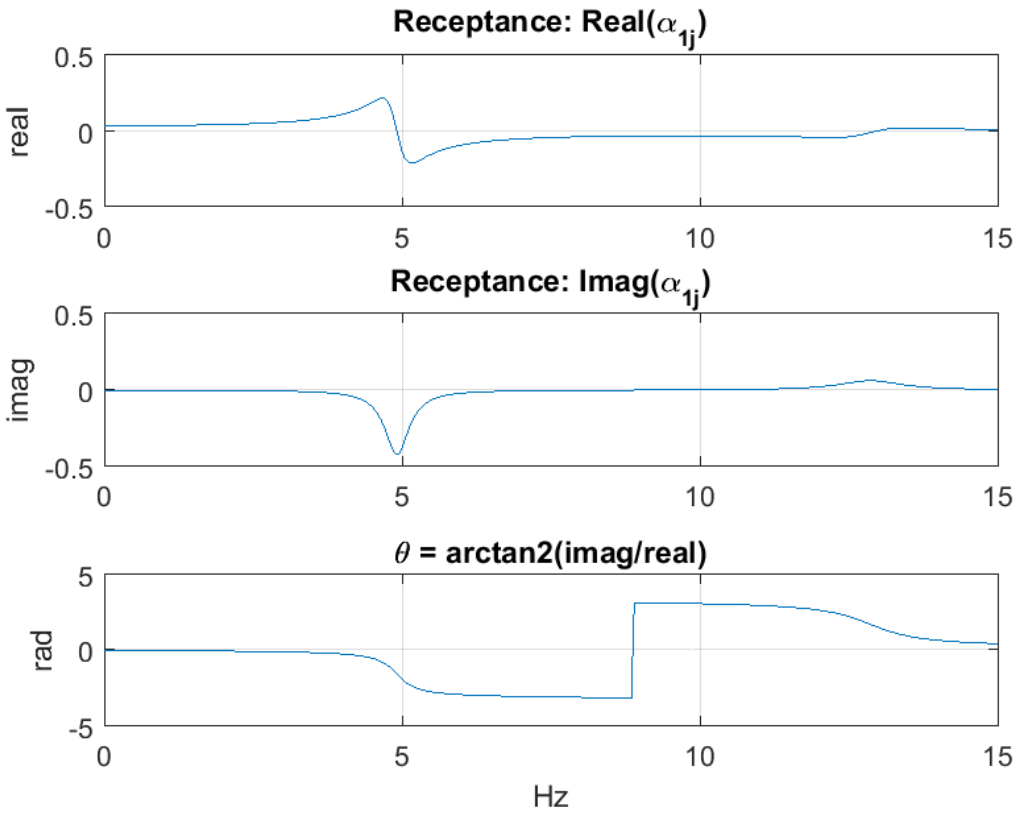

Fig. 2.9. Real part, imaginary part and phase angle of α_{1q} in 2DOF system (f_n = 4.92 & 12.88 Hz, ε =0.05)

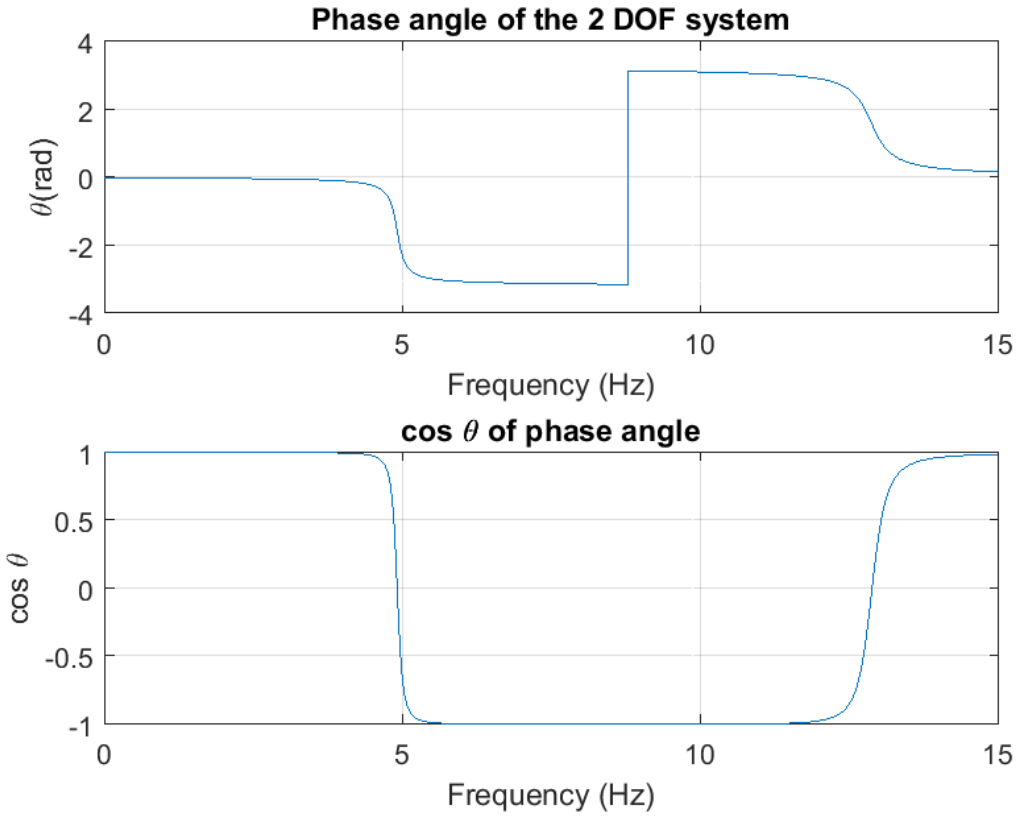

Fig. 2.10. Phase angle of α_{1q} and $\cos\theta_{1q}$ in 2DOF system (f_n = 4.92 & 12.88 Hz, ε =0.05)

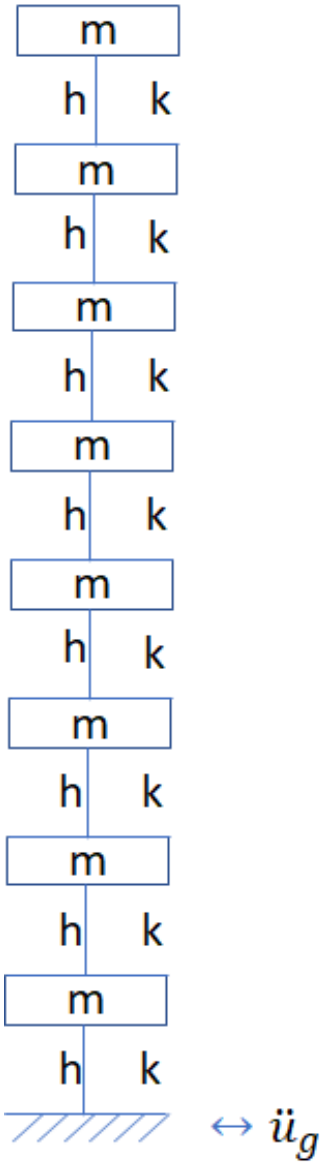

$\leftrightarrow \ddot{u}_g$

$$k=\frac{12EI}{h^3}=1800$$

Fig. 2.11. 8 DOF system(f_n = [1.25, 3.70, 6.02, 8.14, 9.98, 11.48, 12.59, 13.27] Hz)(a simplified shear frame)

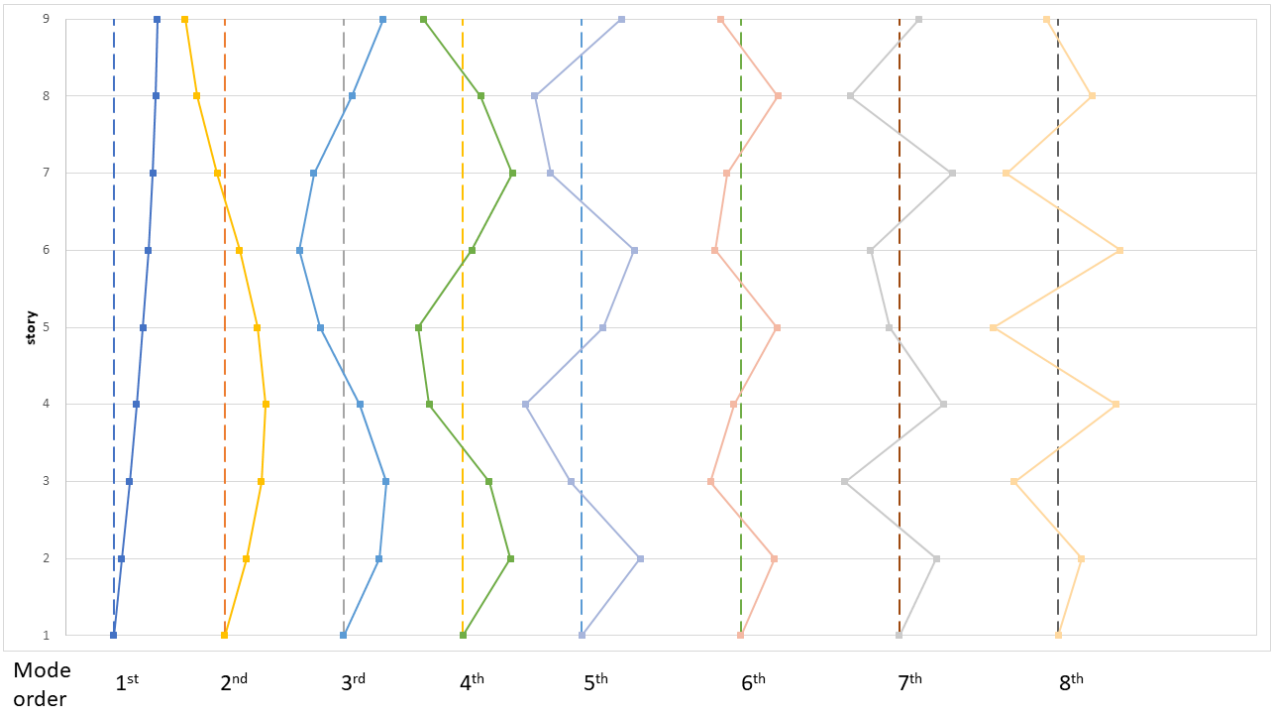

Fig. 2.12. Mode shapes of 8 DOF system(f_n = [1.25, 3.70, 6.02, 8.14, 9.98, 11.48, 12.59, 13.27] Hz)

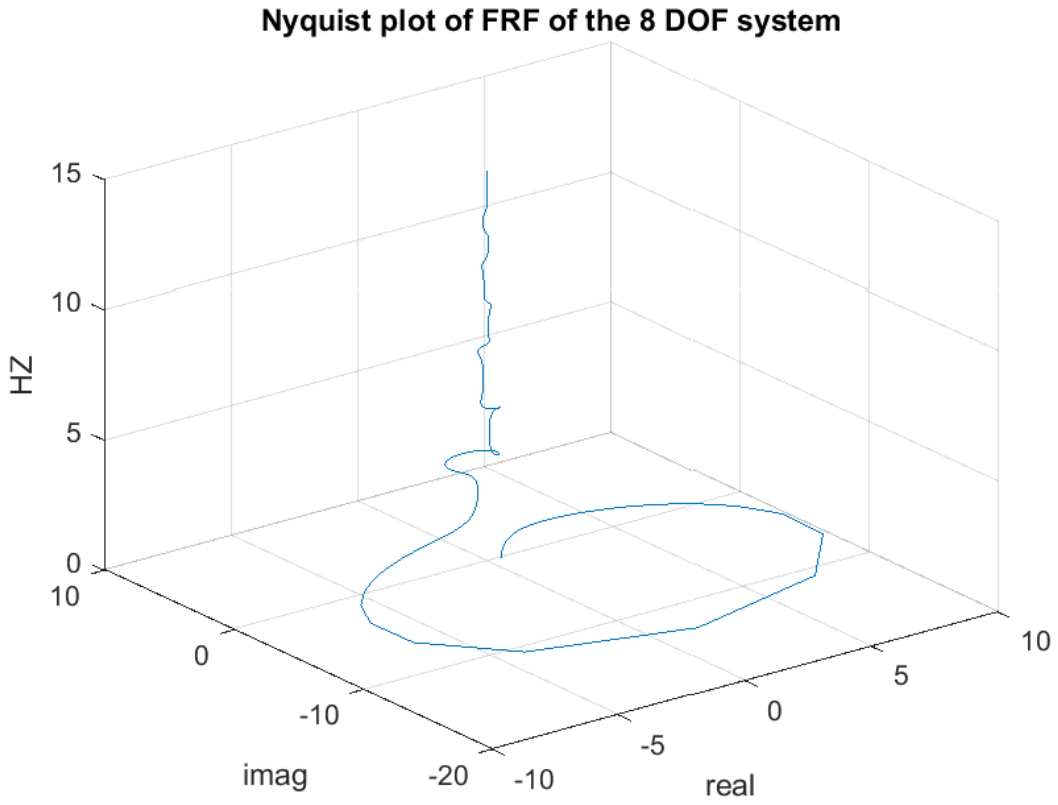

Fig. 2.13. 3D view of Nyquist plot of α_{1q} in the 8 DOF system (f_n = [1.25, 3.70, 6.02, 8.14, 9.98, 11.48, 12.59, 13.27] Hz, ε =0.02)

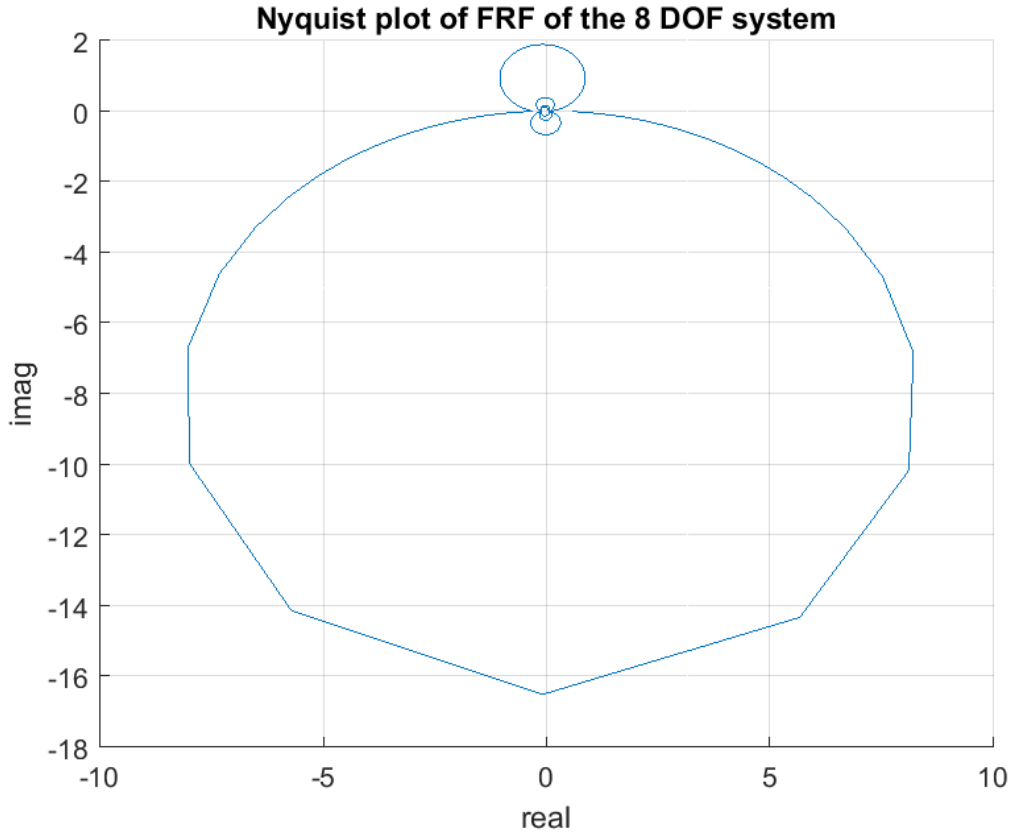

Fig. 2.14. 2D view of Nyquist plot of α_{1q} in 8 DOF system (f_n= [1.25, 3.70, 6.02, 8.14, 9.98, 11.48, 12.59, 13.27] Hz, ε =0.02)

javascript:void(0);

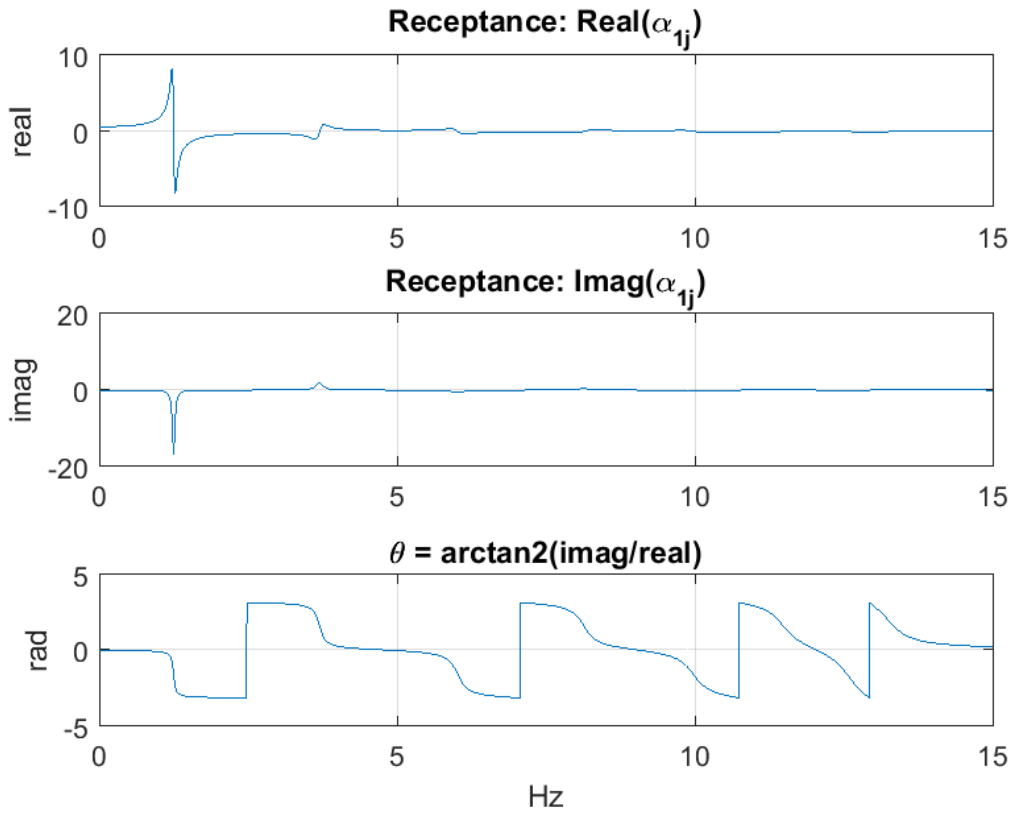

Fig. 2.15. Real part, imaginary part and phase angle of α_{1q} in 8 DOF system (f_n = [1.25, 3.70, 6.02, 8.14, 9.98, 11.48, 12.59, 13.27] Hz, ε =0.02)

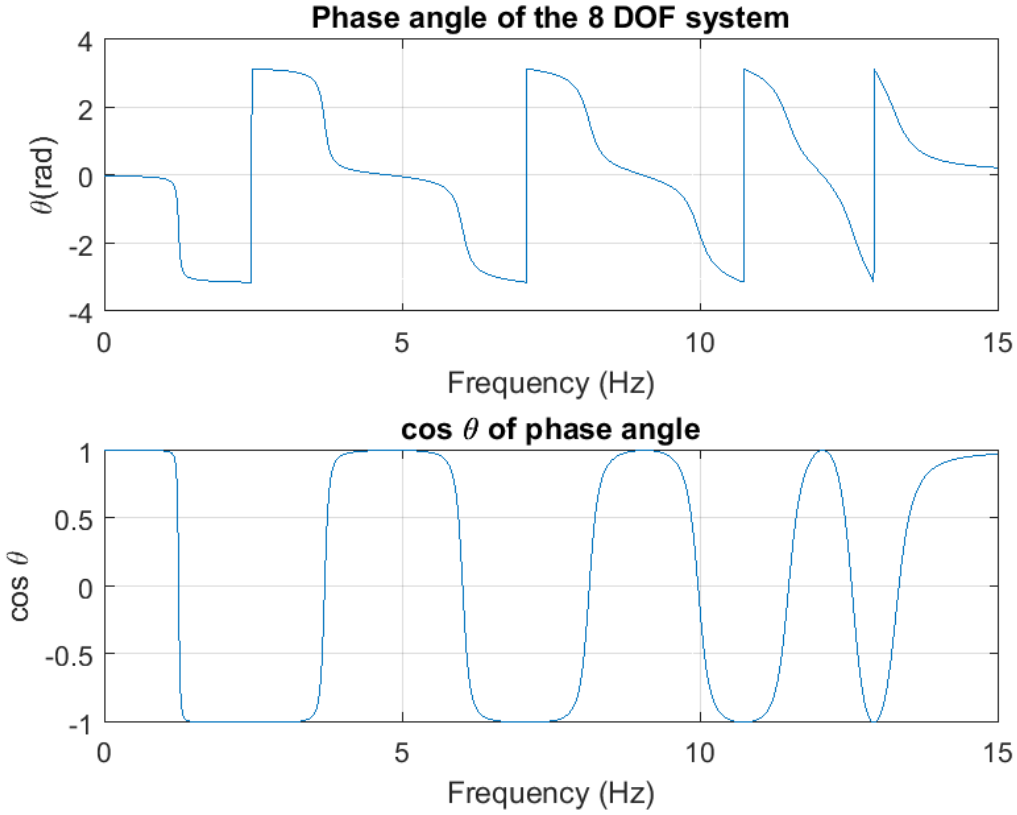

Fig. 2.16. Phase angle of α_{1q} and cosθ in 8 DOF system (f_n = [1.25, 3.70, 6.02, 8.14, 9.98, 11.48, 12.59, 13.27] Hz, ε =0.02)

3. PHASE DIFFERENCE INDEX APPLICATION

3.1 Properties of Linear Time-invariant System

Key properties of linear time-invariant systems, i.e., linear elastic systems, are introduced in order to illustrate various applications of the phase difference index (PDI).

3.1.1 Fundamental Properties of Fourier Transform

In frequency domain analysis, two fundamental properties of Fourier transform hold true [12]. For any two functions $f(t)$ and $g(t)$ in time domain:

- Linearity
  $\mathscr{F}[f(t) + g(t)] = \mathscr{F}[f(t)] + \mathscr{F}[g(t)]$
- For any constant k
  $\mathscr{F}[kf(t)] = k\mathscr{F}[f(t)]$

3.1.2 Definition of A Linear Time-invariant System

In engineering, the simplest and most common assumption is to consider a dynamic system to be a linear time-invariant (LTI) system. In this dissertation, all systems are LTI unless stated otherwise. LTI system is a system which satisfies the following relationships between input $x(n)$ and output $y(n)$ (See Table 3.1) : a single input $x_1[n]$ produces a single output $y_1[n]$; sum of $x_1[n] + x_2[n]$ as input produces $y_1[n] + y_2[n]$, input $ax_1[n] + bx_2[n]$ produces $ay_1[n] + by_2[n]$ [13].

Figure 3.1 illustrates the idea of LTI system in an intuitive way. In the left part of Figure 3.1, the response of an object exerted by a group of forces: $\sum_{i=1}^{n} F_i(\omega) =$

$F_1(\omega_1) + F_2(\omega_2) + F_3(\omega_3)$ shall be equal to the superposition of response caused by each force separately.

3.2 Phase Difference Index Calculation

There are four major steps to calculate the phase difference index from acceleration records of a monitored building:

1. Frequency spectrum decomposition:
   Decompose frequency spectrum of roof and another selected floor acceleration records by band-pass finite impulse response (FIR) filter with a very narrow frequency bandwidth to get acceleration records corresponding to each narrow frequency bandwidth. In this research, the bandwidth is 0.05$\sim$ 0.1 Hz, and the related issues will be discussed in Section 3.2.1. In addition, the "selected floor" in this research means ground floor (GF) or the 2nd floor (2F).

2. Obtain displacement curve from acceleration records:
   To find all displacement curves for roof and ground (or 2nd Floor (2F)) corresponding to each narrow frequency bandwidth.

3. Calculate the phase difference:
   Estimate the phase difference of displacement curves between roof and ground (or 2F), i.e. relative displacement, obtained from step 2.

4. Draw the Phase Difference Index plot.

The details of the four steps are explained in the following sections.

3.2.1 Frequency Spectrum Decomposition

Frequency spectrum decomposition is to use a continuous set of band-pass filters to separate the Fourier spectrum into many narrow bandwidth spectra. The main idea could be inferred from Figure 2.5 and Figure 3.1: 2.5 shows us an interesting

dynamic property of a 2DOF system. For a 2DOF system, if the external excitation frequency is close to ω_{n1}, the resulting displacements will follow the first mode shape(ϕ_1). In other words, when the external excitation frequency is close to ω_{n1}, the contribution of the first mode response to the displacement would be much larger than the contribution of the second mode, if any. In a similar way, when the external excitation frequency is close to ω_{n2}, the response will be dominated by the second mode shape(ϕ_2). Thus, if we use the notion of "frequency sweep" to observe the mode shape corresponding to each different frequency of external excitation, it would be possible to determine the first mode and the second mode period (or natural frequency) for the 2DOF system. The same idea applies in structures with greater degrees of freedoms. Figure 3.1 provides a vague indication of how to achieve "frequency sweep" for a frequency spectrum. If we need to "frequency sweep" a frequency spectrum, referring to figure 3.1, we can use band-pass filters with consecutive cutoff frequencies to filter the original frequency spectrum and get consecutive "filtered" signals. The concept of the band-pass filter is illustrated in figure 3.2. The frequency bandwidth of the original signal ranges from f_1 to f_4. If the original signal is applied with a band-pass filter,the bandwidth of which is $f_1 \sim f_2$, only components within f_1 to f_2 bandwidth would be left in the filtered signal.

For instance, in a given acceleration record, if the preferable analyzed frequency range is from f=0 Hz to f =10 Hz, and the cutoff frequency bandwidth is assumed to be 0.1 Hz, one can use band-pass filters with the cutoff frequencies such as: [0∼0.1] Hz, [0.1∼0.2] Hz, [0.2∼0.3] Hz, [0.3∼0.4] Hz.....[9.8∼9.9] Hz, [9.9∼10] Hz to analyze the given acceleration record and then get the corresponding filtered signals.

Another issue is about the value n which represents the number frequency bands used [14]. In general, the number "n" must obey the uncertainty principle of short-time Fourier transform analysis. In this principle, the following equation dominates the relationship between time interval and frequency bandwidth:

$$\Delta T \times \Delta\omega \geq \frac{1}{4\pi} \tag{3.1}$$

or

$$\Delta t \times \Delta f \geq \frac{1}{2} \tag{3.2}$$

where: Δt: time interval of (sec), ω: frequency (rad), and f: frequency (Hz)

Thus, in the PDI plot analysis, the minimum frequency bandwidth should obey the following equation:

$$\Delta f_{b.pfilter} \geq \frac{1}{2 \times \Delta t_{accel.}} \tag{3.3}$$

: where: $f_{b.pfilter}$: the cutoff frequency of bandpass filter, $\Delta t_{accel.}$: time range of the given acceleration record.

For example, if one considers no less than 60 seconds long earthquake acceleration records, i.e. $\Delta T \geq 60s$ in a strong ground motion, from Eq. 3.3, the minimum window length of frequency bandwidth should be:

$$\Delta f \geq \frac{1}{2 \times 60(sec)} \approx 0.008(Hz)$$

In addition, the window function of an FIR filter is a also a concern in signal processing. Different window has its own pros and cons. In PDI analysis, the behavior in the main lobe of each filtered signal is still the major concern. Therefore, the Hamming widow [15] is adopted in this research.

3.2.2 Obtaining Displacement Curves from Acceleration Records

Most of the dynamic response monitoring instruments installed in buildings are accelerometers. If we need to obtain the displacement history curves of a specific story in a monitored building, we have to integrate over time the acceleration records twice. However, because of back ground noise or unknown conditions, when we integrate directly the acceleration twice, large deviation inevitably occurs in displacement curves. Such outcome often confuses the researchers in earthquake analysis. For example, according to Chiu's research [16], such deviations might be caused by instrument errors and constant Drift, background noise, initial values and manipulation errors.

Proposed Procedures for Strong Motion Data Processing

Chiu [16] proposed three steps to correct the deviation:

1. Least-squares fitting in acceleration:

   The purpose of the step is to reduce the low-order baseline errors. As previously mentioned, any signal inevitably has initial errors. Ideally, displacement is the integral of velocity, and velocity is the integral of acceleration. If all initial conditions are zero, the relationships for displacement, velocity and acceleration are:

   - $A(t)$
   - $V(t) = \int A(t)dt + C_1$
   - $D(t) = \int V(t)dt + C_2$

   However, due to the existence of initial terms, the true acceleration, velocity and displacement would be:

   - $\overline{A}(t) = A_0 + A(t)$
   - $V(t) = V_0 + \int \overline{A}(t)dt + C_3$
   - $D(t) = V_0 t + \frac{1}{2}A_0 t^2 + \iint \overline{A}(t)dt + C_4$

   In order to eliminate the A_0 term, we can use the least-squares fitting for the acceleration record. In general, the least-squares fitting is just shifting the base line of original acceleration curve. In Matlab [17], "detrend" can be used to remove the trend from an acceleration record.

2. High-pass (or band-pass) filtering in acceleration:

   - $\overline{A}(t) = A_{01} + A_{02}(t) + A(t)$
   - $V(t) = V_0 + A_{01}t + \int A_{02}(t)dt + \int A(t)dt + C_5$
   - $D(t) = V_0 t + \frac{1}{2}A_{01}t^2 + \iint A_{02}(t)dt + \iint A(t)dt + C_6$

where:

A_{01}: linear initial acceleration

$A_{02}(t)$: nonlinear initial acceleration

$A(t)$: acceleration response

$C_1 \sim C_6$: constant

In order to eliminate the $A_0(t)$ term, we can use frequency domain analysis to process the record. The first step is to apply the Fourier Transform to the acceleration record and then use the high-pass filter or band-pass filter to remove the low frequency signals. The band range or the cutoff frequency depends on the ratio of noise and earthquake signals. According to Chiu [16], high -pass filter is enough to achieve the goal of removing the unnecessary signals. However, according to reference [18], band-pass filter is recommended to remove the low and high frequency background noise. The recommended frequency pass for the band filter is between 0.5 Hz and 25Hz.

3. Subtracting the initial value in the velocity

   The purpose of the step is to reduce the low-order baseline errors. From step 1 and step 2, we have removed A_{01} and $A_{02}(t)$ terms shown as follows:

   - $\overline{A}(t) = \cancel{A_{01}} + \cancel{A_{02}(t)} + A(t)$
   - $V(t) = V_0 + \cancel{A_{01}t} + \cancel{\int A_{02}(t)dt} + \int A(t)dt$
   - $D(t) = V_0 t + \cancel{\frac{1}{2}A_{01}t^2} + \cancel{\iint A_{02}(t)dt} + \iint A(t)dt$

   In the above equations, all $A(t)$ terms are what's desired to have, and the V_0 terms are what are sought to be removed. Chiu [16] has three alternatives to achieve this goal:

   (a) Use Fourier transform analysis of the acceleration signal: $V_0 = \sum_0^n \frac{b_n}{2\pi f_n}$

   (b) Find the least-squares fit for the new velocity curve.

(c) Find linear trend in new displacement curve.

In this dissertation, (b) alternative is adopted to remove the V_0 term.

Following three steps mentioned above, well-fitting displacement curves would be obtained from acceleration records. However, if the deviation still exists, the problem may be caused by the band width of band-pass filter. One feasible approach is to use trial and error to adjust the lower cutoff frequency to improve the deviation.

3.2.3 Calculating the Phase Difference

Following the steps described in Section 3.2.2 step, two filtered displacement signals corresponding to specific narrow frequency bandwidth are obtained. By analyzing the phase difference of the two signals, the phase difference of displacement between roof and ground (or 2F) are obtained. Thus, one can identify whether a mode shape exists at the specific frequency and determine if the given frequency is a natural frequency. Three different methods may be used to calculate the phase difference of two displacement curves:

1. Phase difference by Fourier spectrum of two signals
2. Cross correlation of two signals
3. Instantaneous phase difference of two signals

The above three methods are explained in section 3.3.

3.2.4 Draw the Phase Difference Index Plot

Three different methods are proposed above to calculate the phase difference index between two signals. For any linear time-invariant system, theoretically, results from the three methods should be equal. However, after testing them on actual earthquake

records from Taiwan and U.S, it is found that there are still some differences among the three methods, and the third method seems more favorable for analysts (see as Appendix A for a discussion). Therefore, in the following chapters, the PDI will mainly be calculated using Eq. 3.12 unless otherwirse noted.

In section 3.2.1, the notion of frequency spectrum decomposition by band-pass filter was introduced. If the frequency bandwidth is divided into n equal parts, the i^{th} unit narrow frequency bandwidth is $f_i \sim f_{i+1}$ and i is from 0 to n. Therefore, the representative frequency of the i^{th} frequency bandwidth is: $\frac{f_i+f_{i+1}}{2}$.

Each narrow bandwidth spectrum represents the summation of a few sinusoid or cosine waves with approximately equal frequencies. Such characteristic causes the beat frequency occurring in the corresponding wave in time domain. To prevent unfavorable influence in the PDI analysis by such phenomenon. Removal of low amplitude is a feasible measure adopted by this research. Related concept is discussed in Appendix B.

For each unit narrow frequency bandwidth of roof and ground(or 2F) response, one can calculate the phase difference index by Eq. 3.12, and then obtain a corresponding PDI_i. Since the frequency bandwidth is divided into n parts, repeating the procedure for n times results in n pairs of $(\frac{f_i+f_{i+1}}{2}, PDI_i)$ coordinate points. Let frequency(Hz) be the x axis, and PDI to be the y axis. These n pairs of $(\frac{f_i+f_{i+1}}{2}, PDI_i)$ points shall compose a phase difference index plot(PDI).

3.3 Three Methods to Calculate Phase Difference of Two Signals

3.3.1 Phase Difference by Fourier Spectrum of Two Signals

For a given periodic signal, the phase angle form of the Fourier series can be expressed as:

$$u(t) = \frac{1}{2}a_0 + \sum_{n=1}^{\infty} c_n \cos(n\omega_0 t + \theta) \tag{3.4}$$

where:

$c_n = \sqrt{a_n^2 + b_n^2}$

$\theta = -arctan(\frac{b_n}{a_n})$

$a_n = \frac{2}{p} \int_{x_0}^{x_0+p} u(t) \cos(n\omega_0 t) dt$

$b_n = \frac{2}{p} \int_{x_0}^{x_0+p} u(t) \sin(n\omega_0 t) dt$

p: period

Therefore, the phase difference of any two signals can be calculated by the following equation:

$$\Delta\theta = \theta_1 - \theta_2 = -\arctan(\frac{b_n}{a_n})_1 + \arctan(\frac{b_n}{a_n})_2 \tag{3.5}$$

In section 2.2.1, $cos(\Delta\theta)$ was introduced. The phase difference index by Fourier Spectrum can be defined as:

$$PDI_{Fourier} = \cos(\Delta\theta)$$

or

$$PDI_{Fourier} = \cos(-\arctan(\frac{b_n}{a_n})_1 + \arctan(\frac{b_n}{a_n})_2) \tag{3.6}$$

3.3.2 Cross-Correlation of Two Signals

In signal processing, cross-correlation is a tool to measure the similarity of two series of data as a function of one relative to the other. For continuous functions f and g, the cross-correlation is defined as:

$$(f * g)(\tau) = \int_{-\infty}^{\infty} f^*(t) g(t + \tau) dt \tag{3.7}$$

where

f^*: the complex conjugate of f.

τ is the lag (or difference).

For discrete signals, the cross correlation is defined as:

$$(f * g)[n] = \sum_{m=-\infty}^{\infty} f^*[t]g[m+n] \tag{3.8}$$

Cross-correlation is also called sliding dot product, the phase difference of two signals occur at the peak (or maximum) of the dot product of two signals.

Thus, with two known signals as input and calculating the cross-correlation, the phase difference finds where maximum absolute cross-correlation occurs. For this method, the Phase difference index can be defined as follows:

$$PDI_{c.c} = cos(lagDiff) \tag{3.9}$$

where:

c.c : abbreviation for cross-correlation

lagDiff: phase difference(or lag) of s_1 and s_2

3.3.3 Instantaneous Frequency Difference by Hilbert Transform

Although Fourier spectrum or cross-correlation can calculate the phase difference of two signals, they are based on the assumption that the system is linear and time-invariant at all times. Such an assumption implies that the frequency response corresponding to specific external excitation would not change when the external force is applied. This can be too strong an assumption for structures. Thus, another approach is used here to calculate the instantaneous frequency and instantaneous phase of two signals. Then, the instantaneous phase difference of two signals at any time step would be obtained.

Analytic Signal and Hilbert Transform

An analytic signal is a complex-valued function that has no negative frequency components [19]. The real and imaginary parts of an analytic signal are real-valued functions related to each other by the Hilbert transform.

The analytic signal can be expressed as the following form [9]:

$$S_a(t) = s(t) + j\hat{s}(t) \tag{3.10}$$

where: $\hat{s}(t)$ is Hilbert transform of $s(t)$; j is the the imaginary unit

Instantaneous Amplitude, Phase, and Frequency

Hilbert transform calculates the envelope of an oscillating signal with a slowly varying amplitude, phase, and frequency. Once an signal is obtained, the following parameters can be found
citeD.Huston2010:

- Instantaneous amplitude: $A(t) = |S_a(t)|$
- Instantaneous phase: $\phi(t) = arg\{S_a(t)\}$
- Instantaneous frequency: $\omega(t) = \frac{d}{dt}\phi(t)$

Another issue is the instantaneous phase of analytic signal. Since the analytic signal operates in complex domain, it is favorable to use $arctan2$ rather than $arctan$ when there is a need to calculate the phase. The definition of $arctan2$ is shown as below:

$$arg(x+jy) = atan2(y,x) = \begin{cases} arctan(\frac{y}{x}), & x > 0 \\ \frac{\pi}{2} - arctan(\frac{y}{x}), & y > 0 \\ -\frac{\pi}{2} - arctan(\frac{y}{x}), & y < 0 \\ \pi + arctan(\frac{y}{x}), & x < 0, y \geq 0 \\ -\pi + arctan(\frac{y}{x}) & x < 0, y < 0 \\ undefined & x = 0, y = 0 \end{cases} \tag{3.11}$$

The purpose to use $arctan2$ rather than $arctan$ is that $arctan2$ uses two inputs, i.e. (y, x) while $arctan$ only needs one input,$(\frac{y}{x})$. Accordingly, one can obtain the sign information and determine the appropriate quadrant of the computed angle. Another benefit is that $arctan2$ can avoid the infinity caused by zero denominator i.e. $x = 0$.

From the discussion in the section, if the difference between phase angles of response of two floors or, simply, of records (duration = T) obtained by two accelerometers at any time step (t=i) is $\Delta\phi_i$, Phase Difference Index (PDI) of instantaneous phase difference is defined as:

$$PDI_{i.p.} = \frac{\sum_{i=1}^{N} cos(\Delta\phi_i)}{N} \tag{3.12}$$

where:

i.p. : instantaneous phase

$\Delta\phi_i$: phase difference of two signals in any time step (t=i)

N= sampling rate$\times$ duration of the acceleration record.

The Phase Difference Index can also be comprehended intuitively. For any lateral movement of a building:

- If two floors move in-phase, $PDI = cos(0 \pm 2\pi) = 1$
- If two floors move fully out-of-phase, $PDI = cos(\pm\pi) = -1$
- If two floors move randomly, $(PDI) = 0$ where average is taken over a time window.

3.4 Example of Phase Difference Index Calculation

A simple case is presented in this section to demonstrate how to use those equations mentioned in this chapter and draw the phase difference index (plot). The related information about the station and earthquake record are listed below:

3.4.1 Station Information

- Station No.: CGS - CSMIP Station 24386
- Station name: Van Nuys - 7-story Hotel, LA
- Location: 34.220N, 118.471W
- Earthquake: Westwood Village Earthquake of 01 Jun 2014
- Start Time: 6/02/14, 02:36:24.0 UTC
- Record Length(sec): 57.00
- Sample Rate(Hz): 200
- Sensor Locations plan : Fig. 3.3
- Selected Sensor: Ch.09 (Roof), & Ch.16 (ground)
- Peak acceleration = -9.502 cm/sec^2 at 25.545 sec.
- Data Source : Center For Engineering Strong Motion Data
  http://www.strongmotioncenter.org/

3.4.2 Example of Frequency Spectrum Decomposition

The steps of spectrum decomposition are as follows:

1. The total frequency bandwidth in Fig.3.4 (b) and Fig.3.4 (d) is 0$\sim$ 15 Hz. Base on Eq. 3.12, N is selected to be 150 i.e. the unit narrow bandwidth $\Delta f = 0.1$ Hz. Therefore, the sequence of narrow bandwidth = [0, 0.1, 0.2....., 14.9, 15] Hz.

2. Apply a band-pass filter (Hamming window) to the roof acceleration and ground acceleration records. The cut off frequencies shall be [0, 0.1],[0.1, 0.2],[0.2, 0.3].....[14.9, 14.9],[14.9, 15.0] by turns. In this section, we use two different narrow bandwidths:[2.2$\sim$ 2.3] Hz and [3.2$\sim$ 3.3] Hz as examples to demo the effect of band-pass filter.

   (a) Case 1: frequency bandwidth=[2.2 $\sim$ 2.3] Hz :
   The comparison of original acceleration signal and filtered acceleration signal is shown as Fig. 3.5. It is obviously observed that the plot $(c)\&(d)$ only have apparent frequency of [2.2$\sim$ 2.3] Hz while other frequency components are filtered.

   (b) Case 2: frequency bandwidth=[3.2 $\sim$ 3.3] Hz :
   The comparison of original acceleration signal and filtered acceleration signal is shown as Fig. 3.6. It is obviously observed that the plot $(c)\&(d)$ only have apparent frequency of [3.2$\sim$ 3.3] Hz while other frequency components are filtered.

3.4.3 Example of Obtaining Displacement from Double Integral of Acceleration

The procedures are as follows:

1. Integrate the acceleration into velocity, and then remove the trend to get the velocity without deviation.

2. Integrate the velocity into displacement, and then remove the trend to get the displacement without deviation.

3. (a) Case 1: frequency bandwidth=[2.2∼2.3] Hz :

   The displacement curves from double integral of filtered acceleration are shown as Fig.3.7. Fig.3.7 (a) and (b) are the same plots. The difference is that (a) represents the response in whole duration while (b) only focuses on the time interval from 30 second to 42 second.

   (b) Case 2: frequency bandwidth=[3.2∼3.3] Hz :

   The displacement curves from double integral of filtered acceleration are shown as Fig.3.8. Fig.3.8 (a) and (b) are the same plots. The difference is that (a) represents the response in whole duration while (b) only focuses on the time interval from 20 second to 32 second.

From the two cases given above, it is clear that Fig. 3.7 is an "in phase" movement of Ch.09 and Ch.16, while the Fig. 3.8 represents an "out of phase" movement.

3.4.4 Example of Calculating the PDI of Two Filtered Displacement Curves

1. Case 1: frequency bandwidth=[2.2∼2.3] Hz :

   The PDI_i corresponding to the external excitation of which bandwidth =(2.2∼2.3)Hz is shown as Fig. 3.9. By Eq. 3.12, PDI (Phase difference index) is the mean of all PDI_i of all time steps. In this case, $PDI = 0.76$. Judging from Fig.3.9, we can observe that in most of the time steps, the PDI_i is close to 1. Thus, it seems that we can conjecture that frequency bandwidth=[2.2∼2.3]Hz is very close to the natural frequency of the system. But unless we finish the whole picture of PDI, we have no idea at which order of mode does this frequency bandwidth belongs to.

2. Case 2: frequency bandwidth=[3.2∼3.3] Hz :

   The PDI_i corresponding to the external excitation of which bandwidth =(3.2∼3.3)Hz is shown as Fig. 3.10. By Eq. 3.12, PDI (Phase difference index) is the mean of all PDI_i of all time steps. In this case, $PDI = 0.8$. Judging from Fig.3.10,

we can observe that in most of the time steps, the PDI_i is close to -1. Thus, it seems that we can conjecture that the roof(Ch.09) and ground(ch.16) always move out of phase under the external excitation. But unless we finish the whole picture of PDI, we have no idea that which order of mode does this frequency bandwidth belongs to.

3.4.5 Example of Drawing the PDI Plot

The final step is to use the notion of "frequency sweep" to calculate the PDI for the whole frequency bandwidth of a system. For a building, the frequency range of $1 \sim 10$ Hz is more important than others. In this example, only $f = 1 \sim 10Hz$ are presented in the final result.

Let frequency(Hz) be the x axis, and PDI to be the y axis. Now we have 100 pairs of $(\frac{f_i+f_{i+1}}{2}, PDI_i)$ points, and these points shall compose a phase difference index plot in x-y coordinate.

Figure 3.11-(a) is the result of PDI plot for the given example. Because the zero-crossing point of a PDI curve should be a natural frequency of the building, it is easy to identify that $f_{n1} = 2.43$. The second mode f_{n2} seems between $7.73 \sim 8.1$ Hz. It seems a little unstable. Without further information, the research just assumes the first zero-crossing point to be the 2nd mode. Figure 3.11-(b) is frequency response function(FRF) of Ch.09 over Ch.16. The FRF can be calculated by Eq. 2.24 i.e. the deconvolution of $\mathscr{F}(\omega)_{Ch.09}$ and $\mathscr{F}(\omega)_{Ch.16}$.

It should be pointed out that the original FRF of Ch.09 over Ch.16. is not smooth. In order to smooth the FRF curve, Welch's method was used [20]. In Figure 3.11-(b), two vertices can be observed in the FRF curve, the left one is more obvious while the right one is more flat. The first peaks match the zero-crossing points in Figure 3.11-(a) very well while the 2nd one approximately matches well. It is easier to identify the natural modes of the system by cross-checking PDI plot and FRF plot.

Table 3.1.
Properties of linear time-invariant(LTI) system

Input	**Output**
$x_1[n]$	$y_1[n]$
$ax_1[n]$	$ay_1[n]$
$x_2[n]$	$y_2[n]$
$x_1[n] + x_2[n]$	$y_1[n] + y_2[n]$
$ax_1[n] + bx_2[n]$	$ay_1[n] + by_2[n]$

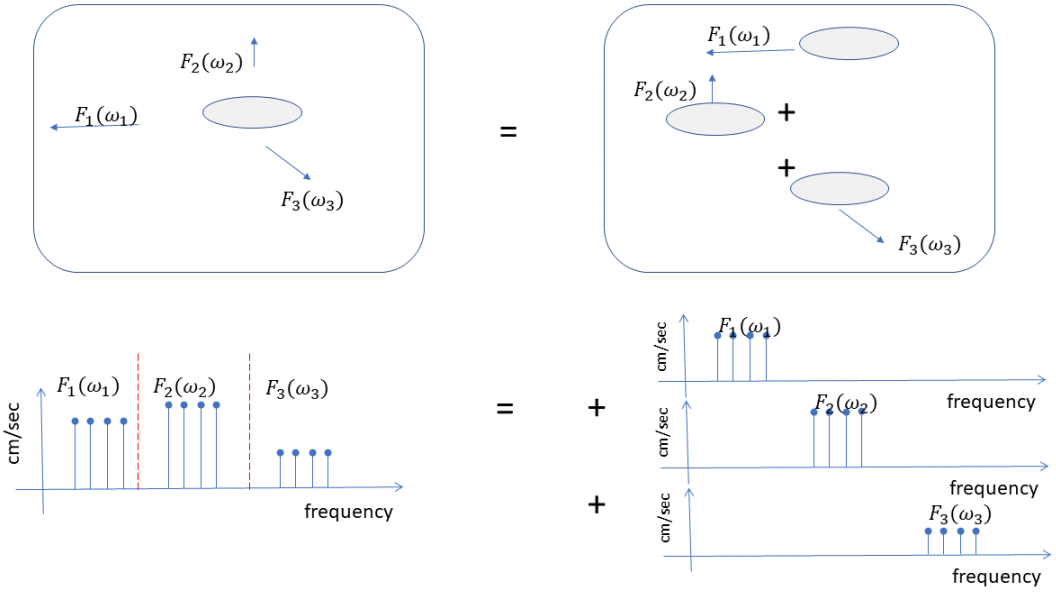

Fig. 3.1. Illustration of frequency spectrum decomposition: the Fourier spectrum could be decomposed into the superposition of three equal parts.

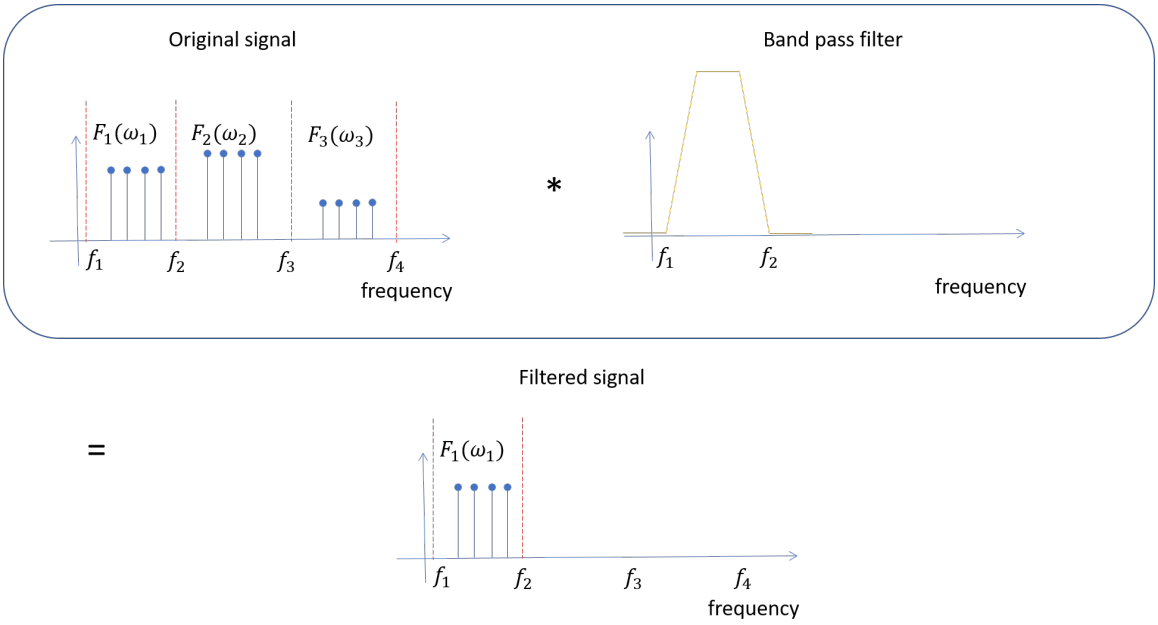

Fig. 3.2. Concept of band-pass filter

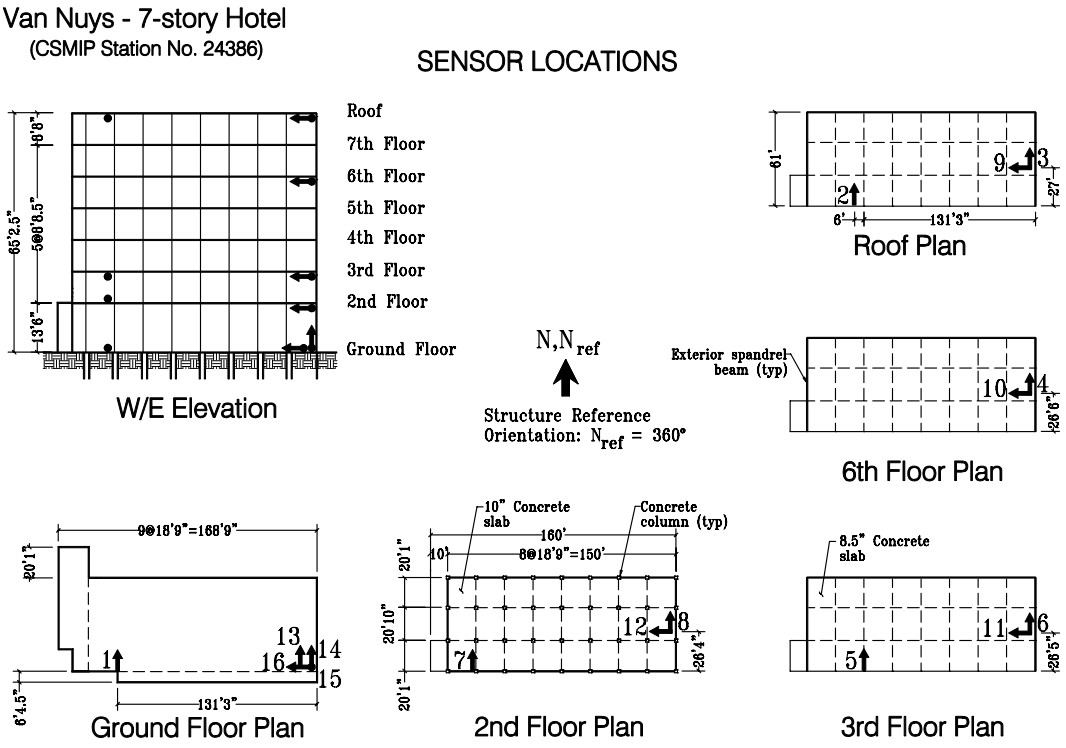

Fig. 3.3. Sensor locations of Van Nuys 7 story building, [21]

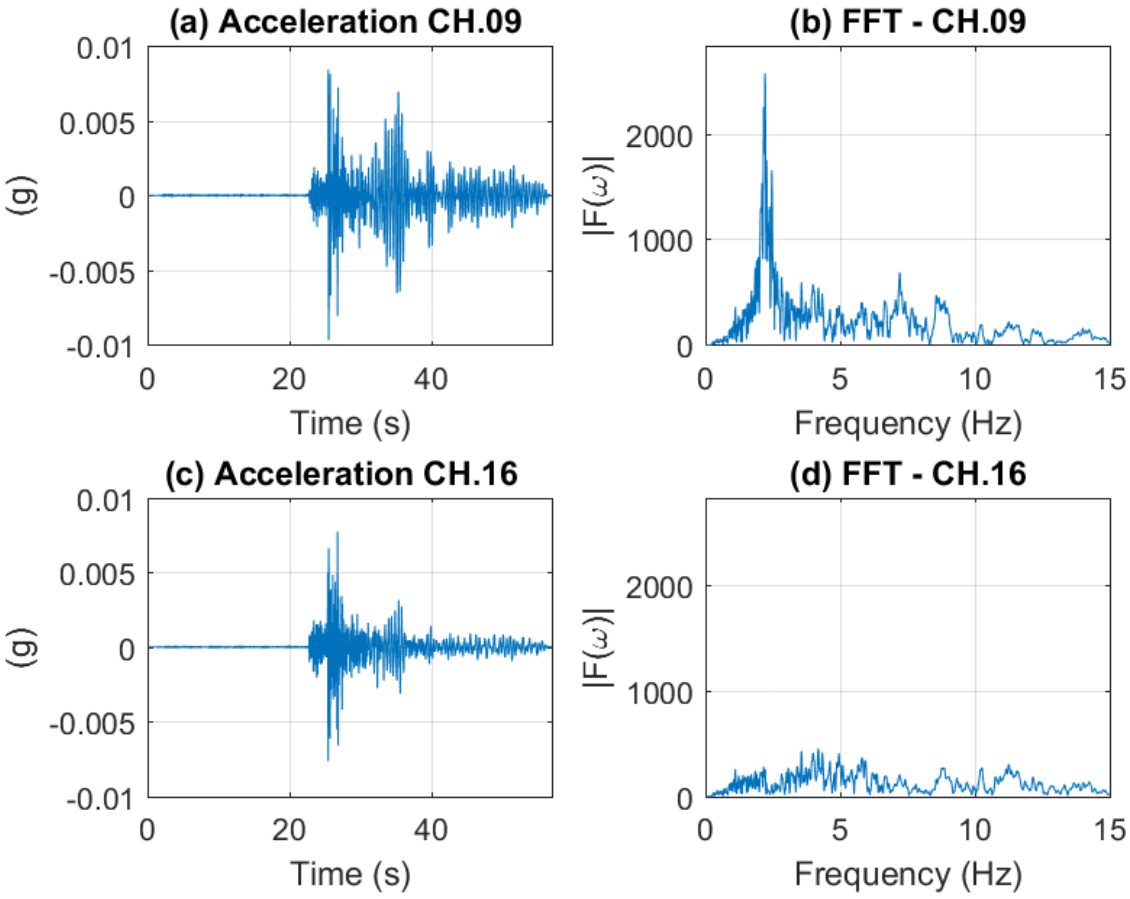

Fig. 3.4. Acceleration records of Ch.09 & Ch.16 of Van Nuys 7-story building Westwood Village Earthquake of 01 Jun 2014: (a) Ch.09 Acceleration time history curve, (b) Ch.09 Fourier Spectrum of Acceleration Ch.09 record, (c) Ch.16 Acceleration time history curve, (d) Fourier Spectrum of Acceleration Ch.16 record

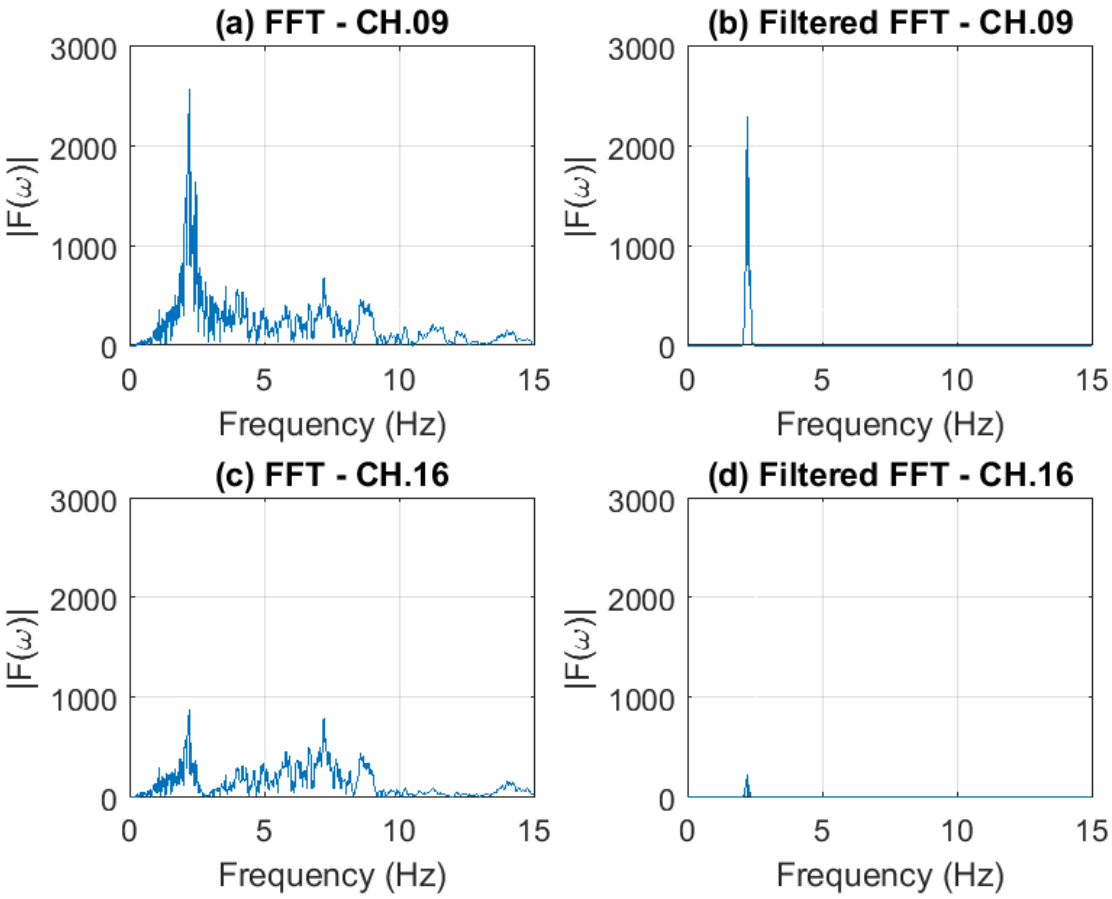

Fig. 3.5. Original & filtered Fourier Spectrum of acceleration records of Ch.09 & Ch.16 with cutoff frequency =[2.2, 2.3] Hz. (a) Ch.09 original acceleration signal, (b) Ch.09 filtered acceleration signal, (c)original Ch.16 acceleration signal, (d) filtered Ch.16 acceleration signal.

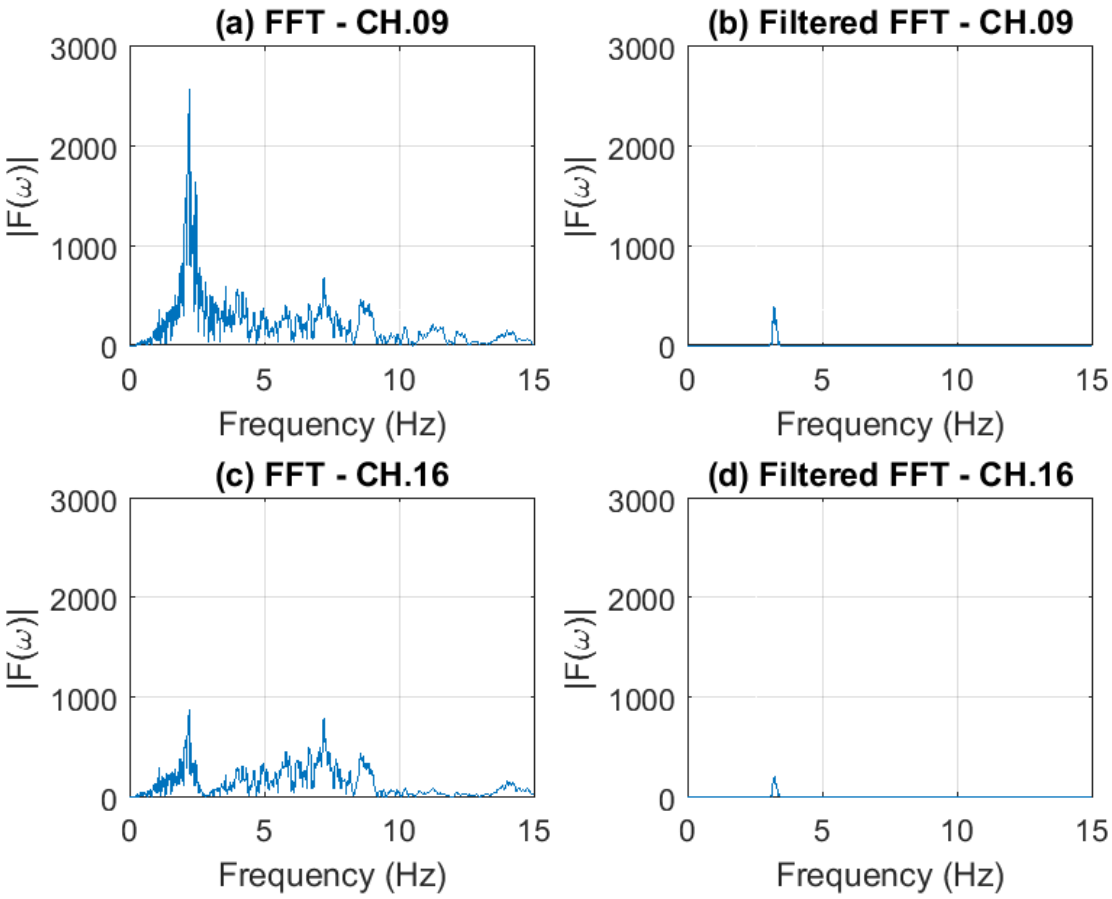

Fig. 3.6. Original & filtered Fourier Spectrum of acceleration records of Ch.09 & Ch.16 with cutoff frequency =[3.2, 3.3] Hz. (a) Ch.09 original acceleration signal, (b) Ch.09 filtered acceleration signal, (c)original Ch.16 acceleration signal, (d) filtered Ch.16 acceleration signal.

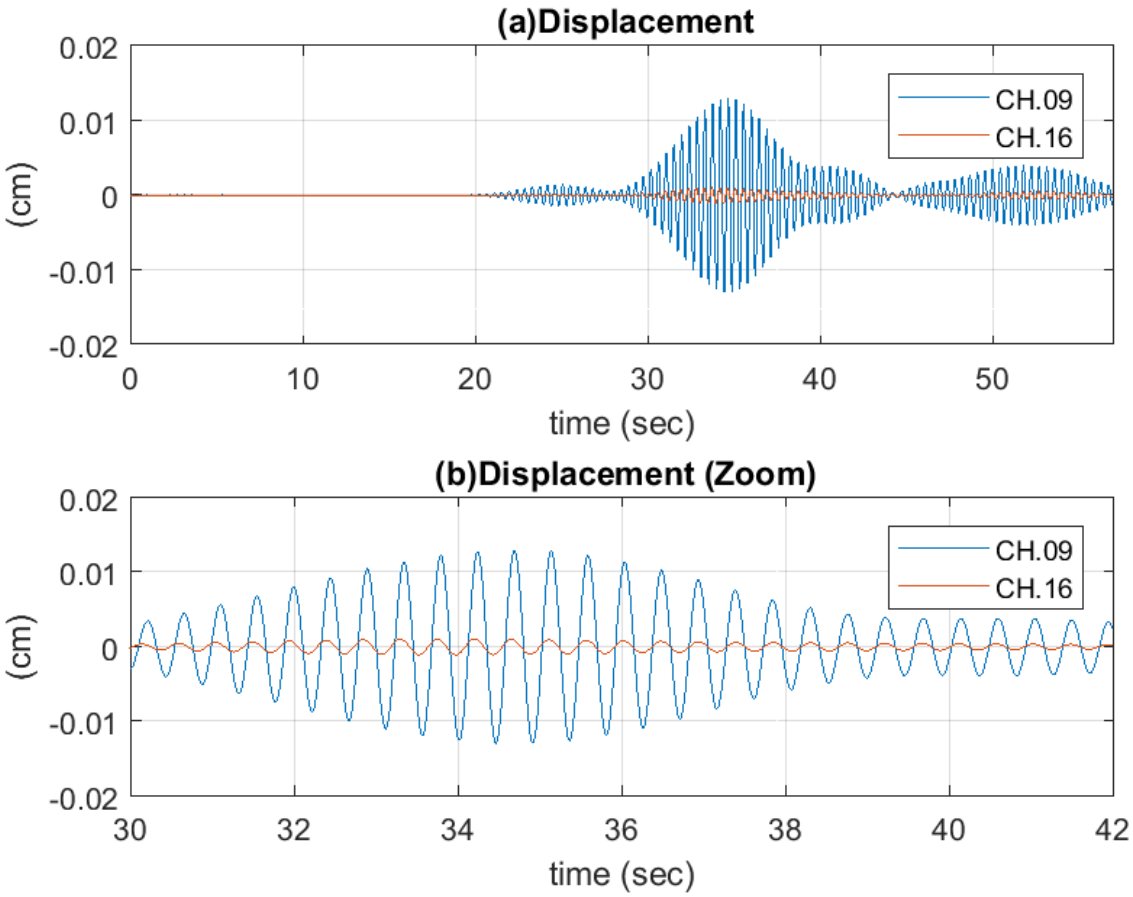

Fig. 3.7. Displacement curve integrated twice from filtered acceleration.(a) Displacement curve of whole duration. (b) Displacement curve zoom in 30∼42 second. ** cutoff frequency of band-pass filter =[2.2∼2.3]Hz

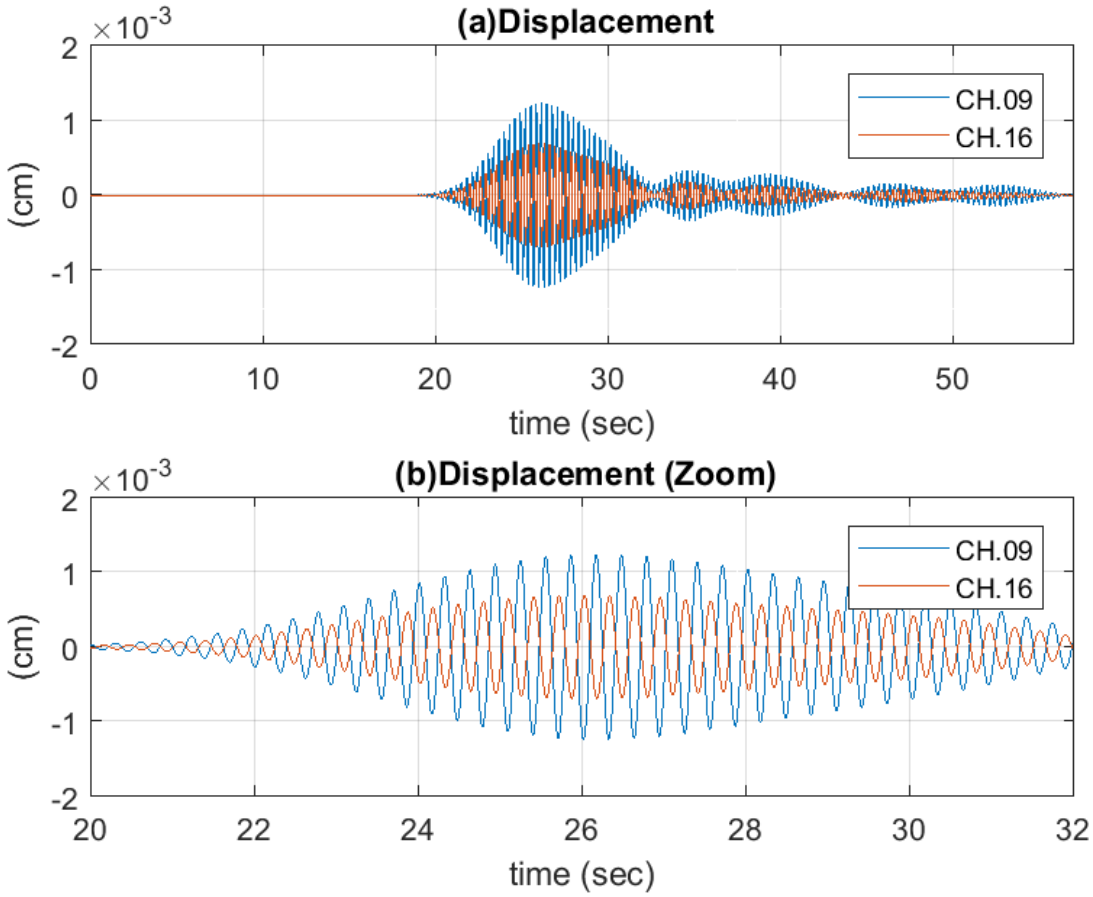

Fig. 3.8. Displacement curve integrated twice from filtered acceleration.(a) Displacement curve of whole duration. (b) Displacement curve zoom in 30∼42 second. The cutoff frequency of band-pass filter =[3.2∼3.3]Hz

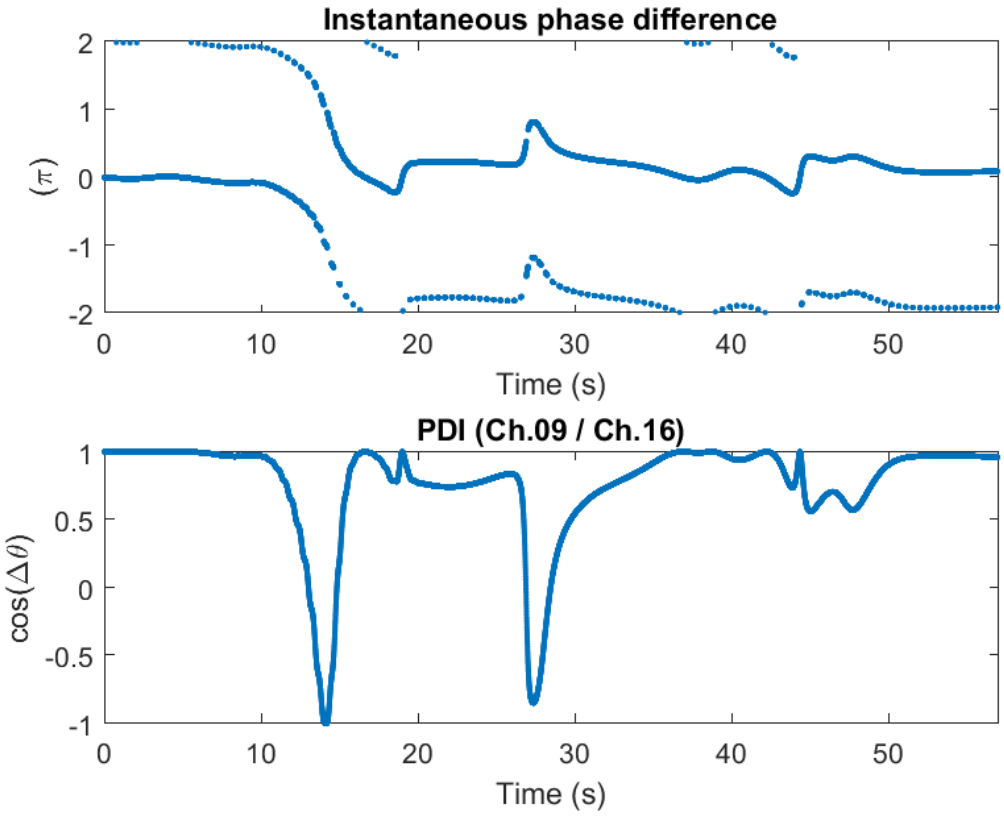

Fig. 3.9. PDI_i (Phase difference index) corresponding to the external excitation of which bandwidth =(2.2∼2.3)Hz. The average PDI_i = 0.76

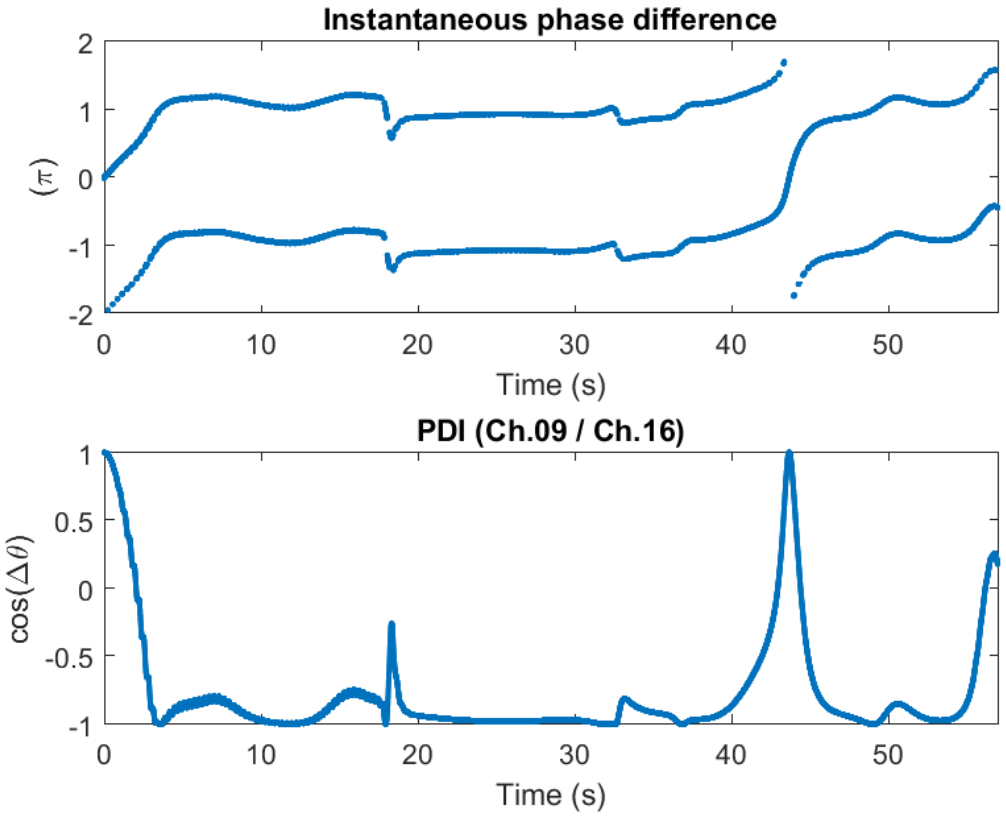

Fig. 3.10. PDI_i (Phase difference index) corresponding to the external excitation of which bandwidth =(3.2∼3.3)Hz. The average $PDI_i = -0.8$

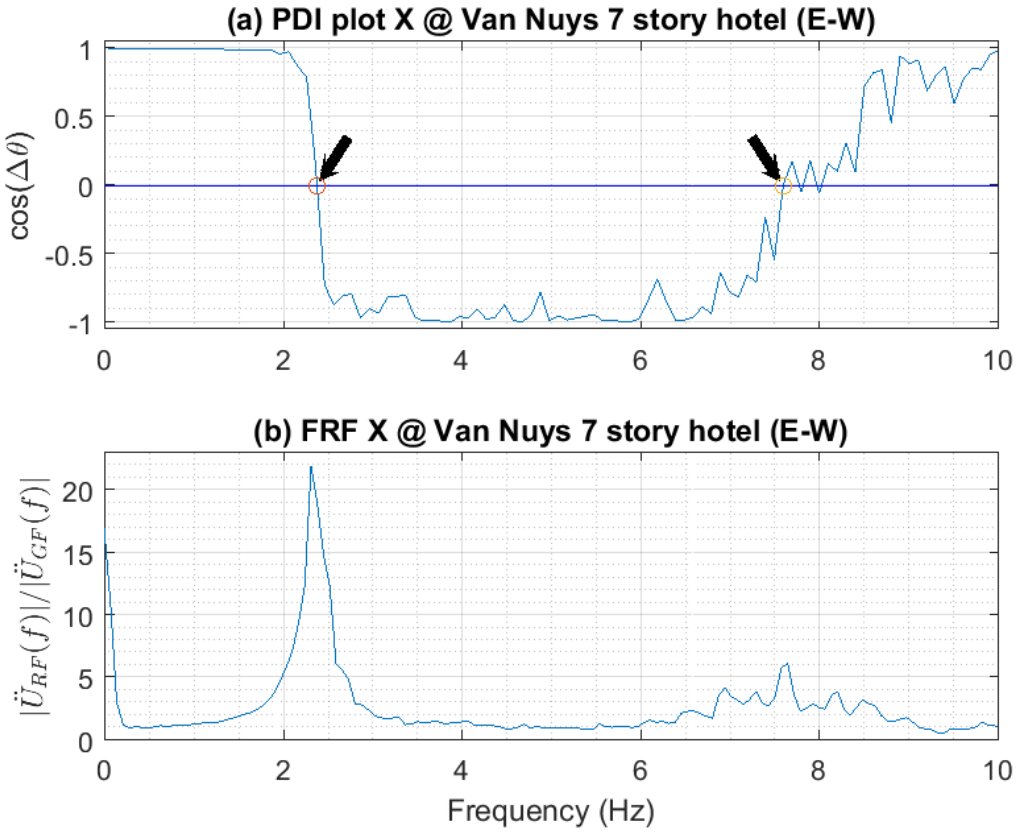

Fig. 3.11. PDI-X plot vs. FRF-X of Van Nuys 7 story Hotel (E-W) This plot use Ch.09 & Ch.16 to analyze PDI and FRF. Earthquake record: Westwood Village Earthquake of 01 Jun 2014. The FRF curve is modified by Welch method, the window size is 25% of signal length.

4. NUMERICAL MODELS FOR PDI ANALYSIS

4.1 Introduction

In this chapter, numerical models are used to test the idea of phase difference index. Four types of frame buildings; namely a 2-story building, a 4-story building, a 7-story building, and a 10-story building are adopted to demonstrate how the PDI plots help identify the natural frequencies of these buildings. Two kinds of ground acceleration are selected to be the input acceleration of numerical models. The first one is white noise (1 cm/sec^2 for 60 seconds) input, and the second one is a record from the 1999 Ji Ji earthquake in Taiwan.

4.2 Numerical Model Description

Four types of numerical models are illustrated as Figure 4.3 and 4.4. Among them, Figure 4.3(a) is 2DOF system, and 4.3(b) is 4-DOF system. In addition, Figure 4.4(a) is 7DOF system, while Fig. 4.4(b) is 10-DOF system. Specific conditions are given to all four models as follows. The number $\frac{12EI}{h^3}$ will be assigned to certain values in order to manipulate the first mode period of each model to be 0.1 H (H:Total height of structure). The conditions of each model are:

- mass of each story = 1 (i.e., unit mass)
- height of each story = h
- $\frac{12EI}{h^3}$ =
  - 2500 (2-DOF system)
  - 2000 (4-DOF system)

  - 1800 (7-DOF system)
  - 1600 (10-DOF system)

- damping ratio (ε) of each mode = 0.05
- All models are linear (Time-invariant elastic system).

4.2.1 Governing Equation of Translational Motion

For moment frame buildings (also known as shear beam models), the governing equation of earthquake response in an N-DOF system can be expressed as:

$$[M]\{\ddot{u}(t)\} + [C]\{\dot{u}(t)\} + [K]\{u(t)\} = -[M]\{\ddot{u}_g\} \tag{4.1}$$

For N degrees of freedom system with the conditions given in Section 4.2, Eq. 4.1 can be expanded as:

$$m[I]_{n\times n}\{\ddot{u}(t)\}_{n\times 1} + [C]_{n\times n}\{\dot{u}(t)\}_{n\times 1} + \frac{12EI}{h^3}\begin{bmatrix} 1 & -1 & 0 & 0 & ..... & 0 \\ -1 & 2 & -1 & 0 & ..... & 0 \\ 0 & & . & & & : \\ : & & & . & & : \\ : & & & & . & -1 \\ 0 & & & ... & -1 & 2 \end{bmatrix}_{n\times n} \{u(t)\}_{n\times 1}$$

$$= -m[I]_{n\times n}\{\ddot{u}_g\}_{n\times 1} \tag{4.2}$$

where: $u_1(t)$ relates to the top mass, and $u_n(t)$ relates to the bottom mass.

4.2.2 Natural Frequencies of Numerical Models

Eq. 4.2 comprises a traditional eigenvalue problem. Natural frequencies of the systems can be acquired by finding the eigenvalues. For the four selected systems(2-

DOF, 4-DOF, 7-DOF, 10-DOF) with given conditions, the natural frequencies are as follows:

- 2-DOF system
  - f_n = [4.92 , 12.88] Hz
- 4-DOF system
  - f_n = [2.47, 7.12, 10.90, 13.38] Hz
- 7-DOF system
  - f_n = [1.41, 4.17, 6.75, 9.04, 10.93, 12.34, 13.21] Hz
- 10-DOF system
  - f_n = [0.98, 2.92, 4.79, 6.56, 8.18, 9.62, 10.84, 11.82, 12.54, 12.98] Hz

4.2.3 Steady State Solution of Displacement on the Roof

The displacement solutions of four models can be found easily by modal superposition method. The PDI plot form (Roof/Ground) reveal the natural frequencies by observing the zero-crossing points. Thus, only steady state solutions on the roof, i.e $u_1(t)$ of four numerical models when the forcing acceleration is $\ddot{u}_g$ are listed as below:

- 2-DOF system:

$$u_1(t) = \begin{bmatrix} \frac{-\ddot{u}_g(t)/\omega_1^2}{\sqrt{(1-\beta_1^2)^2+(2\varepsilon\beta_1)^2}} & \frac{-\ddot{u}_g(t)/\omega_2^2}{\sqrt{(1-\beta_2^2)^2+(2\varepsilon\beta_2)^2}} \end{bmatrix} \times \begin{bmatrix} 1.17 \\ -0.17 \end{bmatrix} \tag{4.3}$$

- 4-DOF system:

$$u_1(t) = \begin{bmatrix} \frac{-\ddot{u}_g(t)/\omega_1^2}{\sqrt{(1-\beta_1^2)^2+(2\varepsilon\beta_1)^2}} & \frac{-\ddot{u}_g(t)/\omega_2^2}{\sqrt{(1-\beta_2^2)^2+(2\varepsilon\beta_2)^2}} & \frac{-\ddot{u}_g(t)/\omega_3^2}{\sqrt{(1-\beta_3^2)^2+(2\varepsilon\beta_3)^2}} & \frac{-\ddot{u}_g(t)/\omega_4^2}{\sqrt{(1-\beta_4^2)^2+(2\varepsilon\beta_4)^2}} \end{bmatrix} \times \begin{bmatrix} 1.24 \\ -0.33 \\ 0.12 \\ -0.03 \end{bmatrix} \tag{4.4}$$

- 7-DOF system:

$$u_1(t) = \left[\frac{-\ddot{u}_g(t)/\omega_1^2}{\sqrt{(1-\beta_1^2)^2+(2\varepsilon\beta_1)^2}} \quad \frac{-\ddot{u}_g(t)/\omega_2^2}{\sqrt{(1-\beta_2^2)^2+(2\varepsilon\beta_2)^2}} \quad \cdots \quad \frac{-\ddot{u}_g(t)/\omega_7^2}{\sqrt{(1-\beta_7^2)^2+(2\varepsilon\beta_7)^2}} \right] \times \begin{bmatrix} 1.26 \\ -0.39 \\ 0.20 \\ -0.11 \\ 0.057 \\ -0.024 \\ 0.006 \end{bmatrix} \tag{4.5}$$

- 10-DOF system

$$u_1(t) = \left[\frac{-\ddot{u}_g(t)/\omega_1^2}{\sqrt{(1-\beta_1^2)^2+(2\varepsilon\beta_1)^2}} \quad \frac{-\ddot{u}_g(t)/\omega_2^2}{\sqrt{(1-\beta_2^2)^2+(2\varepsilon\beta_2)^2}} \quad \cdots \quad \frac{-\ddot{u}_g(t)/\omega_{10}^2}{\sqrt{(1-\beta_{10}^2)^2+(2\varepsilon\beta_{10})^2}} \right] \times \begin{bmatrix} 1.26 \\ -0.41 \\ 0.23 \\ -0.14 \\ 0.093 \\ -0.06 \\ 0.037 \\ -0.02 \\ 0.009 \\ -0.002 \end{bmatrix} \tag{4.6}$$

where:

$\beta_i = \frac{f}{fn_i}$

fn_i: natural frequency of i_{th} mode (Hz)(see section 4.2.2)

$\varepsilon = 0.05$ for each mode

ω_i: natural frequency of i_{th} mode (rad)

4.2.4 Calculating Dynamic Response Numerically

In this dissertation, linear acceleration method is used to solve the dynamic response problem. The procedure is listed as follows [10]:

For any dynamic linear system, in any time step t_{i+1}, the dynamic equilibrium equation can be expressed as:

$$m\ddot{u}_{i+1} + c\dot{u}_{i+1} + ku_{i+1} = p_{i+1} \tag{4.7}$$

For linear acceleration method, $\gamma = 1/2$, and $\beta = 1/6$

1. initial calculations

   (a) $\ddot{u}_0 = \frac{p_0 - c\dot{u}_0 - ku_0}{m}$

   (b) select Δt

   (c) $a_1 = \frac{1}{\beta(\Delta t)^2}m + \frac{\gamma}{\beta\Delta t}c$;
   $a_2 = \frac{1}{\beta\Delta t}m + (\frac{\gamma}{\beta} - 1)c$;
   $a_3 = (\frac{1}{2\beta} - 1)m + \Delta t(\frac{\gamma}{\beta} - 1)c$

   (d) $\widehat{k} = k + a_1$

2. Calculations for each time step, i =0,1,2,...

   (a) $\widehat{p}_{i+1} = p_{i+1} + a_1 u_i + a_2\dot{u}_i + a_3\ddot{u}_i$

   (b) $u_{i+1} = \frac{\widehat{p}_{i+1}}{\widehat{k}}$

   (c) $\dot{u}_{i+1} = \frac{\gamma}{\beta\Delta t}(u_{i+1} - u_i) + (1 - \frac{\gamma}{\beta})\dot{u}_i + \Delta t(1 - \frac{\gamma}{2\beta}\ddot{u}_i)$

   (d) $\ddot{u}_{i+1} = \frac{1}{\beta(\Delta t)^2}(u_{i+1} - u_i) - \frac{1}{\beta\Delta t}\dot{u}_i - (\frac{1}{2\beta} - 1)\ddot{u}_i$

3. Repetition for the next time step. Replace i by i+1 and implement steps 2.(a) to 2.(d) for the next time step.

4.3 Numerical Model Tests with White Noise Input

First, white noise signal is used to test whether the phase difference index analysis works for the selected numerical models effectively when the input ground motion is expected to excite all natural modes of the structure. White noise is a random signal and theoretically has equal intensity at different frequencies. In Matlab, the function-"wgn" can be used to generate white noise. For 1 cm/sec^2 white noise with 60 second duration, the time history and frequency spectrum are plotted as Figure 4.5.

4.3.1 Result from 2DOF Numerical Model with White Noise Input

By using linear acceleration method and white noise input mentioned in section 4.3 and 4.2.4, we can generate the Power Spectrum of the roof of the 2DOF system. Since the natural frequencies of this system are set at 4.92 and 12.88 Hz, it is predictable that the response peaks shall occur at both 4.92 and 12.88 Hz in power spectrum.

Figure 4.6 indicates that the response fully matched the above prediction. Although many rapid variations appear in the spectrum, two peaks occurring at the natural frequencies of the set structure(model) are obvious.

In addition, Figure 4.7-(a) includes the frequency response spectrum of the roof(blue line), 2nd floor(orange line), and ground(yellow line). If we let the blue curve(roof) of the frequency spectrum be divided by the yellow curve(ground), the frequency response function(FRF) of roof (shown as the blue curve in Figure 4.7-(b)) can be obtained. The procedure is also called "deconvolution" of the spectrum. Theoretically, the FRF of roof should be identical as Eq. 4.3. By observing Figure 4.7, the FRF(blue curve at the (b) plot) matches our prediction. Accordingly, it is shown that the 2DOF numerical model with white noise input is working properly.

Phase Difference Index of 2-DOF Numerical Model with white noise input

PDI method is applied to the response data on the roof, 2nd floor as well as the input at ground. The results are illustrated in Fig. 4.8 which comprises three parts:

a. Phase difference index plot (Roof vs. ground)

b. Phase difference index plot (Roof vs. 2F)

c. Frequency response function plot (Roof)

In Figure 4.8-(a) plot, there are two zero-crossing points, which represent the natural frequencies of the model. In this numerical model, the identification results match the default frequencies quite well. The comparison is shown in Table 4.1. In general, the error is equal or less than 1 %.

In Figure 4.8-(b) plot, the coordinate plot is separated by the PDI double curvature curve. Technically, when PDI=1, it means the roof and the second floor move in the same direction at all times, i.e. moving in-phase. On the contrary, if PDI=-1, the roof and the second floor move toward the opposite direction at all times, i.e. moving out of phase. From visual judgment, we can divide the PDI coordinate into 3 parts:

- $f < 5$: RF and 2F move always in-phase
- $5 < f < 11$: RF and 2F not always in-phase or out-of-phase
- $f > 11$: RF and 2F move always out-of-phase

It should be noticed that the above demarcation points are only determined by visual judgment so they are not precise. The real points should be 4.92 and 12.88 rather than 5 and 11. Nevertheless, the plot offers a useful information to assist evaluators to identify the modes of buildings. For example, if we identify some building by peak-picking method or subspace method and need to determine the order of mode, a figure like Figure 4.8-(b) can help exclude some spurious modes.

Figure 4.8-(c) is a traditional FRF plot, and evaluators can judge the natural frequencies by peak-picking method. However, peak-picking method becomes subjective

when the peak is not clear. On the contrary, if we use Figure 4.8-(a) to determine the natural frequency, it is easier and clearer because only one zero-crossing point corresponds to the specific mode in the PDI plot if the data quality is good.

Conclusion of 2DOF Numerical Model with White Noise Input

From previous discussion, Figure 4.8 provides a good format for identifying the modes of buildings. The first crossing point in plot (a) should match the peak in plot(c), and both of them should fall into the area of first mode in plot(b). Similarly, the second crossing point in plot (a) should match the peak in plot(c), and both of them should align with the area of second mode in plot(b). In fact, the peaks in higher modes are usually flatter so that they are harder to recognize. By interactive reference from multiple plots, one can have greater confidence in detection of the modes of buildings.

4.3.2 Result from 4-DOF Numerical Model with White Noise Input

Similar to 2-DOF system, we can also generate the Power Spectrum of the roof of the 4-DOF system. The default natural frequencies of this system are 2.47, 7.12, 10.90, and 13.38 Hz so there should be four peaks. However, Figure 4.9 partially matches the above prediction. Besides many rapid variation appear in the spectrum, only first three peaks clearly can be observed at the default natural frequencies. Referring to Eq. 4.4, the mode contribution factor of the fourth mode is only 0.03. The factor is so small that the fourth mode can be seen barely in the power spectrum.

Phase Difference Index of 4DOF Numerical Model with White Noise Input

PDI method is applied to the response data on the roof, 2nd floor as well as the input at ground. The results are illustrated in Fig. 4.11 which comprises three parts:

a. Phase difference index plot (Roof vs. ground)

b. Phase difference index plot (Roof vs. 2F)

c. Frequency response function plot (Roof)

In Figure 4.11-(a) plot, there are four zero-crossing points, which represent the natural frequencies of the model. In this numerical model, the identification results match the default frequencies well. The comparison is shown in Table 4.2. In general, the error is less than 2 %, and there is no error in the 1st mode.

In Figure 4.11-(b) plot, the coordinate plot is separated by the PDI curve into approximate four parts. From visual judgment, we can define the four parts as:

I. $f < 3$: The first mode frequency bandwidth.

II. $3 < f < 9$: The second mode frequency bandwidth.

III. $9 < f < 13$: The third mode frequency bandwidth.

IV. $f > 13$: The fourth mode frequency bandwidth.

Figure 4.11-(c) is a traditional FRF plot. In this plot (c) , the first peak is not definite. In addition, the third mode and the fourth mode are barely recognized. Thus, some better way has to be proposed. If we use Figure 4.11-(a) to determine the natural frequencies, it is easier and clearer since there is only one zero-crossing point corresponding to each mode in the PDI plot.

Conclusion of 4-DOF Numerical Model with White Noise Input

From previous discussion, Figure 4.11 provides a good format for identifying the modes of buildings. The first crossing point in plot (a) should match the first peak in plot(c), and both of them should align with the area of first mode in plot(b). Similarly, the second, third and fourth crossing points in plot (a) should match the peak in plot(c), and all]of them should fall into the area of the corresponding modes

in plot(b). In fact, the peaks in higher modes in FRF spectrum are usually flatter so that it is harder to recognize those modes. By interactive reference from multiple plots, one can have greater confidence in detection of the modes of buildings.

4.3.3 Result from 7DOF Numerical Model with White Noise input

The Power Spectrum of the roof of the 7DOF system is shown as Figure 4.12. The default natural frequencies of this system are [1.41, 4.17, 6.75, 9.04, 10.93, 12.34, 13.21] Hz so there should be seven peaks in the spectrum. However, there are only three obvious peaks in Figure 4.12. Referring to Eq. 4.5, the mode contribution factors from the fourth mode to the seventh mode are [-0.11, 0.057, -0.024, 0.006]. These factors are so small that they can barely be seen in the power spectrum.

Phase Difference Index of 7-DOF Numerical Model with White Noise Input

PDI method is applied to the response data on the roof, 2nd floor as well as the input at ground. The results are illustrated in Fig. 4.14 which comprises three parts:

a. Phase difference index plot (Roof vs. ground)

b. Phase difference index plot (Roof vs. 2F)

c. Frequency response function plot (Roof)

In Figure 4.14-(a) plot, there should be seven zero-crossing points, which represent the natural frequencies of the model. However, only six zero-crossing points are recognized. In this numerical model, the identification results of the first six points exactly match the default frequencies.The comparison is shown in Table 4.3. In general, the error is less than 1.2 %, and no error occurs in the 1st mode.

In Figure 4.14-(b) plot, the coordinate plot is separated by the PDI curve into approximate six parts. From visual judgment, we can define the six parts as:

I. $f < 2$: The first mode frequency bandwidth.

II. $2 < f < 5$: The second mode frequency bandwidth.

III. $5 < f < 8$: The third mode frequency bandwidth.

IV. $8 < f < 10$: The fourth mode frequency bandwidth.

V. $10 < f < 12$: The fifth mode frequency bandwidth.

VI. $12 < f$: The sixth mode frequency bandwidth.

** The seventh mode frequency bandwidth can not be determined.

Figure 4.14-(c) is a traditional FRF plot for 7-DOF system, and evaluators can judge the natural frequencies by peak-picking method. Taking this plot (c) as an example, the third mode and after modes are barely recognized. If we use Figure 4.14-(a) to determine the natural frequencies, it is easier and clearer to identify the higher modes.

Conclusion of 7-DOF Numerical Model with White Noise Input

From previous discussion, Figure 4.14 provides a good format for identifying the modes of buildings. The first crossing point in plot(a) should match the first peak in plot(c), and both of them should fall into the area of first mode in plot(b). Similarly, the second, third and fourth crossing point in plot (a) should match the peak in plot(c), and all of them should align with the area of the corresponding modes in plot(b). In fact, the peaks in higher modes in FRF spectrum are usually flatter so that it is harder to recognize those modes. By interactive reference from multiple plots, one can have greater confidence in detection of the modes of buildings.

4.3.4 Result from 10DOF Numerical Model with White Noise Input

The Power Spectrum of the roof of the 10DOF system is shown as Figure 4.15. The default natural frequencies of this system are [0.98, 2.92, 4.79, 6.56, 8.18, 9.62, 10.84, 11.82, 12.54, 12.98] Hz so there should be 10 peaks in the spectrum. However, there are only four obvious peaks in Figure 4.15. Referring to Eq. 4.6, the mode contribution factors from the fifth mode to the tenth mode are [0.093, -0.06, 0.037, -0.02, 0.009,-0.002]. These factors are so small that they can barely be seen in the power spectrum.

Phase Difference Index of 10DOF Numerical Model with White Noise Input

PDI method is applied to the response data on the roof, 2nd floor as well as the input at ground. The results are illustrated in Fig. 4.17 which comprises three parts:

a. Phase difference index plot (Roof vs. ground)

b. Phase difference index plot (Roof vs. 2F)

c. Frequency response function plot (Roof)

In Figure 4.17-(a) plot, there should be seven zero-crossing points, which represent the natural frequencies of the model. However, only nine zero-crossing points are recognized. In this numerical model, the identification results of the first nine points exactly match the default frequencies. The comparison is shown in Table 4.4. In general, the error is less than 1.2 %, and no error occurs in the 1st mode.

In Figure 4.17-(b), the coordinate plot is separated by the PDI curve into approximate eight parts. From visual judgment, we can define the eight parts as:

I. $f < 1$: The first mode frequency bandwidth.

II. $1 < f < 3$: The second mode frequency bandwidth.

III. $3 < f < 5.5$: The third mode frequency bandwidth.

IV. $5.5 < f < 7.5$: The fourth mode frequency bandwidth.

V. $7.5 < f < 9$: The fifth mode frequency bandwidth.

VI. $9 < f < 10.5$: The sixth mode frequency bandwidth.

VII. $10.5 < f < 11.5$: The seventh mode frequency bandwidth.

VIII. $11.5 < f < 12.5$: The eighth mode frequency bandwidth.

X. $12.5 < f$: The ninth mode frequency bandwidth.

** The tenth mode frequency bandwidth can not be determined.

Figure 4.17-(c) is a traditional FRF plot for 10-DOF system, and evaluators can judge the natural frequencies by peak-picking method. In this plot (c), the fifth mode and after modes are barely recognized. If we use Figure 4.17-(a) to determine the natural frequencies, it is easier and clearer since there is only one zero-crossing point corresponding to each mode in the PDI plot.

Conclusion of 10-DOF Numerical Model with White Noise Input

From previous discussion, Figure 4.17 provides a good format for identifying the modes of buildings. The first crossing point in plot (a) should match the first peak in plot(c), and both of them should correspond to the area of first mode in plot(b). Similarly, the second and after crossing points in plot (a) should match the peak in plot(c), and all of them should align with the area of the corresponding modes in plot(b). In fact, the peaks in higher modes in FRF spectrum are usually flatter so that it is harder to recognize those modes. By interactive reference from multiple plots, one can have greater confidence in detection of the modes of buildings.

4.4 Numerical Model Tests with Earthquake Record Input

In this section, an actual earthquake record from a free field station in Taiwan is adopted to test the same numerical structural models. The related information of the ground acceleration are as follows:

- Station Code: WNT
- Station Name: Xin-Jie elementary school, Nantou County, Taiwan
- Location: 122.1 E, 23.27 N
- Start Time: 1999/09/20 -17:47:12.000
- Record Length(sec): 60.00
- Sample Rate(Hz): 200
- Direction: E-W ground acceleration
- Amplitude MAX. E-W: 808.691, -921.143 cm/s^2
- Acceleration time history : given in Fig. 4.18 (a)
- Acceleration frequency spectrum: given in Fig. 4.18 (b)
- Data Source : Central Weather Bureau, Taiwan.
  ftp://gdms.cwb.gov.tw/19990921/FreeField/

4.4.1 Result from 2DOF Numerical Model with Earthquake Record Input

The same as section 4.3, in this model test, three kinds of plots are generated to make comparison with the outcome of white noise test:

a. Power Spectrum of 2DOF system : Fig. 4.19

b. Frequency spectrum & Frequency response function of 2DOF system : Fig. 4.20

c. Phase difference index plot of roof of 2DOF system : Fig. 4.21

d. Comparison of identification results with actual frequencies: Table 4.5

4.4.2 Result from Higher Degree of Freedom Numerical Model with Earthquake Record Input

The 4-DOF, 7-DOF, 10-DOF models also have the same category of plots:

a. Power Spectrum:

- 4-DOF system: Fig. 4.22
- 7-DOF system: Fig. 4.25
- 10-DOF system: Fig. 4.28

b. Frequency spectrum & Frequency response function:

- 4-DOF system: Fig. 4.23
- 7-DOF system: Fig. 4.26
- 10-DOF system: Fig. 4.29

c. Phase difference index plot of roof:

- 4-DOF system: Fig. 4.24
- 7-DOF system: Fig. 4.27
- 10-DOF system: Fig. 4.30

d. Comparison of identification results with actual frequencies:

- 4-DOF system: Table 4.6
- 7-DOF system: Table 4.7

– 10-DOF system: Table 4.8

Comparing the results of white noise test with earthquake record test for higher degree of freedom models, the plots are almost the same. The only difference is that the FRF and PDI curves of the models with earthquake records input are smoother than the plots of white noise test.

In addition, from Table 4.6, Table 4.7 and Table 4.8, the error of identification results all are within 5 % , and most of them are smaller than 1 %. Thus, it is convincing that the PDI plot can identify the natural frequencies by checking the zero-crossing points.

4.5 Limit of Modal Order Identification in Different Stories

In this chapter, the numerical model analysis are presented with three Figures:

a. Phase difference index plot (Roof vs. ground)

b. Phase difference index plot (Roof vs. 2F)

c. Frequency response function plot (Roof)

Figures (a) and (c) undoubtedly play vital roles in system identification because we can obtain the natural frequencies from PDI for roof vs. ground as well as FRF for roof. Figure (b) can help us locate the possible frequency bandwidth of natural frequencies. However, sometimes the accelerometers are not installed on the second floor in buildings. For example, as will be seen, some buildings in U.S and Taiwan, from which these are acceleration records, no data from 2F are available. Therefore, a good question to consider is whether records from another could be used as an alternative for second floor acceleration data. Before answering the question, a 4DOF typical building is used to explain the feasibility.

The typical 4DOF building was shown in Figure 4.3-(b). By Modal superposition method, we can obtain the steady solution of displacement of each floor:

$$\begin{pmatrix} u_1 \\ u_2 \\ u_3 \\ u_4 \end{pmatrix} = \begin{pmatrix} 1.24 & -0.33 & 0.12 & -0.028 \\ 1.09 & -0 & -0.16 & 0.07 \\ 0.81 & 0.33 & -0.06 & -0.08 \\ 0.43 & 0.33 & 0.18 & 0.05 \end{pmatrix} \begin{pmatrix} U_1 \\ U_2 \\ U_3 \\ U_4 \end{pmatrix}$$

where:

u_i : The displacement of i_{th} mass

U_i : The displacement of i_{th} modal mass

Available Records Only on Roof and 2F

In case that the record from roof, i.e. u_1 and the record from 2F, i.e. u_4 are available, the sign of phase difference index between u_1&u_4 would be as shown in table 4.9. The result is a sequence of +, -, +, - which results in a PDI illustrated in Figure 4.1. Therefore, the f_{n1} must be located in the first zone, the f_{n2} must be located in the second zone, and so on.

Available Records Only from Roof and 3F

In case that the record from roof, i.e. u_1 and the record of 3F, i.e. u_3 are available, the sign of phase difference index between u_1&u_3 would be shown as table 4.10. The result is not preferable, because the sign in sequence is +, -, -, + which results in a PDI illustrated in Figure 4.2. The f_{n1} is located in the first zone. But f_{n2} and f_{n3} would be located in the same zone. Therefore, one could not distinguish the possible bandwidth of f_{n3}. Since aliasing occurs, the identification limit can only reach to the second mode. Thus,we define a simple index for for the identification limit.

Limit of Modal Order Identification

$LMOI(N)_{ij}$: (Limit of Modal Order Identification)

The definition of the index is:“ The maximum modal order which can be detected by PDI between i_{th} and j_{th} degrees of mass in an N-DOF system”. Taking the 4DOF system as an example, in the case that only data from roof(the fourth story, i=1) and the third floor (the second story, j=3) are available, the Limit of Modal Order Identification of this case can be expressed as:

$$LMOI(4)_{13} = 2$$

Also, $LMOI(4)_{14} = 4$. Generally, the larger the index is, the more modal zones can be detected in the corresponding PDI curve. However, each building has different structural system(stiffness & mass distribution). It is impractical to calculate all LMOI for all buildings. However, one can do is to calculate the index for standard models and make a general judgment. Several general cases are listed in Table 4.11. Some of them will be used in ensuing cases analysis.

Table 4.1.
Comparison of identification results of 2-DOF system (white noise input)

Mode Order	**No.**	**Actual frequency (Hz)**	**PDI method (Hz)**	**Error %**
1	f_{1x}	4.92	4.97	1.02
2	f_{2x}	12.88	12.91	0.23

Related PDI plot is shown in Fig.4.8

Table 4.2.
Comparison of identification results of 4-DOF system (white noise input)

Mode Order	**No.**	**Actual frequency (Hz)**	**PDI method (Hz)**	**Error %**
1	f_{1x}	2.47	2.47	0
2	f_{2x}	7.12	7.16	0.56
3	f_{3x}	10.9	11.04	1.3
4	f_{4x}	13.38	13.67	2.17

Related PDI plot is shown in Fig.4.11

Table 4.3.
Comparison of identification results of 7-DOF system (white noise input)

Mode Order	**No.**	**Actual frequency (Hz)**	**PDI method (Hz)**	**Error** %
1	f_{1x}	1.41	1.41	0
2	f_{2x}	4.17	4.22	1.2
3	f_{3x}	6.75	6.80	0.74
4	f_{4x}	9.04	9.07	0.33
5	f_{5x}	10.93	10.96	0.27
6	f_{6x}	12.34	12.48	1.13
7	f_{7x}	13.21	-	-

Related PDI plot is shown in Fig.4.14

Table 4.4.
Comparison of identification results of 10-DOF system (white noise input)

Mode Order	**No.**	**Actual frequency (Hz)**	**PDI method (Hz)**	**Error %**
1	f_{1x}	0.98	1.01	3.06
2	f_{2x}	2.92	2.95	1.03
3	f_{3x}	4.79	4.84	1.68
4	f_{4x}	6.56	6.58	0.3
5	f_{5x}	8.18	8.26	0.98
6	f_{6x}	9.62	9.69	0.73
7	f_{7x}	10.84	10.9	0.55
8	f_{8x}	11.82	11.94	1.02
9	f_{9x}	12.54	12.82	2.23
10	f_{10x}	12.98	-	-

Related PDI plot is shown in Fig.4.17

Table 4.5.
Comparison of identification results of 2-DOF system (earthquake input)

Mode Order	**No.**	**Actual frequency (Hz)**	**PDI method (Hz)**	**Error %**
1	f_{1x}	4.92	4.97	1.02
2	f_{2x}	12.88	12.84	0.23

Related PDI plot is shown in Fig.4.21

Table 4.6.
Comparison of identification results of 4-DOF system (earthquake input)

Mode Order	**No.**	**Actual frequency (Hz)**	**PDI method (Hz)**	**Error %**
1	f_{1x}	2.47	2.51	0.02
2	f_{2x}	7.12	7.12	0
3	f_{3x}	10.9	10.94	0.37
4	f_{4x}	13.38	13.60	1.64

Related PDI plot is shown in Fig.4.24

Table 4.7.
Comparison of identification results of 7-DOF system (earthquake input)

Mode Order	**No.**	**Actual frequency (Hz)**	**PDI method (Hz)**	**Error** %
1	f_{1x}	1.41	1.44	0.02
2	f_{2x}	4.17	4.21	0.96
3	f_{3x}	6.75	6.77	0.3
4	f_{4x}	9.04	9.02	0.22
5	f_{5x}	10.93	10.97	0.37
6	f_{6x}	12.34	12.44	0.81
7	f_{7x}	13.21	-	-

Related PDI plot is shown in Fig.4.27

Table 4.8.
Comparison of identification results of 10-DOF system (earthquake input)

Mode Order	**No.**	**Actual frequency (Hz)**	**PDI method (Hz)**	**Error %**
1	f_{1x}	0.98	1.02	4.08
2	f_{2x}	2.92	2.92	0
3	f_{3x}	4.79	4.79	0
4	f_{4x}	6.56	6.58	0.3
5	f_{5x}	8.18	8.24	0.73
6	f_{6x}	9.62	9.65	0.31
7	f_{7x}	10.84	10.92	0.74
8	f_{8x}	11.82	11.86	0.34
9	f_{9x}	12.54	12.84	2.39
10	f_{10x}	12.98	-	-

Related PDI plot is shown in Fig.4.30

Table 4.9.
Sign of PDI corresponding to each natural frequency of typical 4DOF structure

Mode	f_{n1}	f_{n2}	f_{n3}	f_{n4}
	$sign(1.24 \times 0.43)$	$sign(-0.33 \times 0.33)$	$sign(0.12 \times 0.18)$	$sign(-0.028 \times 0.05)$
Sign	+	-	+	-

Table 4.10.
Sign of PDI corresponding to each natural frequency of typical 4-DOF structure

N	f_{n1}	f_{n2}	f_{n3}	f_{n4}
	$sign(1.24 \times 0.81)$	$sign(-0.33 \times 0.33)$	$sign(0.12 \times -0.06)$	$sign(-0.028 \times -0.08)$
Sign	+	-	-	+

Table 4.11.
$LMOI(N)_{1j}$ of standard N-DOF structure

j \ N	4	6	7	8	11	20	26	54
1	0	0	0	0	0	0	0	0
2	0	0	0	0	0	0	0	0
3	2	1	0	0	0	0	0	0
4	4	1	1	1	0	0	0	0
5		2	1	1	1	0	0	0
6		6	4	2	1	0	0	0
7			7	4	1	0	0	0
8				8	3	1	0	0
9					4	1	0	0
10					6	1	1	0
11					11	1	1	0
12						1	1	0
13						2	1	0
14						2	1	0
15						2	1	0
16						3	1	0
17						4	2	0
18						5	2	0
19						9	2	1
20						20	3	1
21							3	1
22							4	1
23							5	1
24							7	1
25							12	1
26							26	1
27								1
28								1
29								1
30								1
31								1
32								1
33								1
34								2
35								2
36								2
37								2
38								2
39								2
40								3
41								3
42								3
43								4
44								4
45								4
46								5
47								6
48								7
49								8
50								10
51								13
52								17
53								26
54								54

1. In yellow highlight, j = N/2
2. Story No. = j -54+1
3. N= degree of freedom

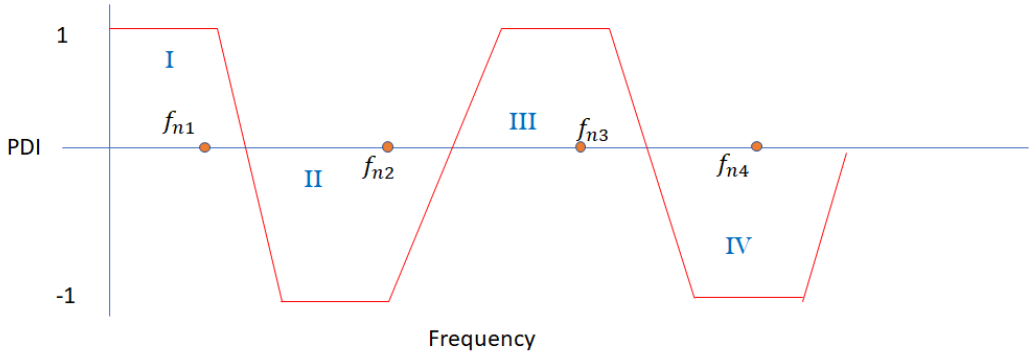

Fig. 4.1. Phase difference plot of (Roof/2F) of a typical 4-DOF building.

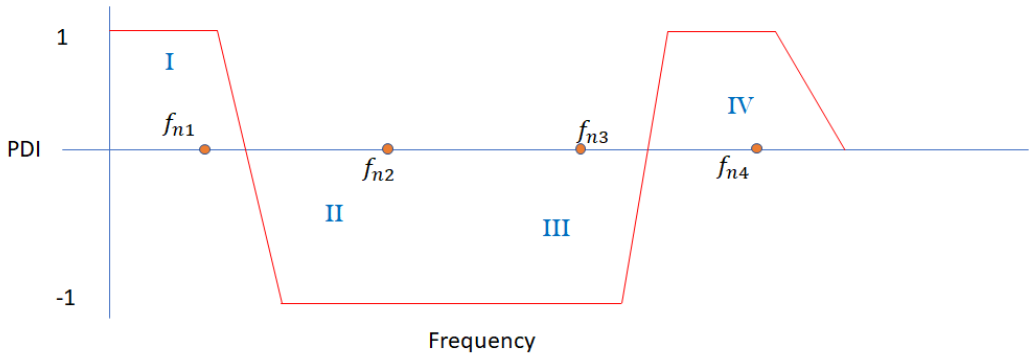

Fig. 4.2. Phase difference plot of (Roof/3F) of a typical 4-DOF building.

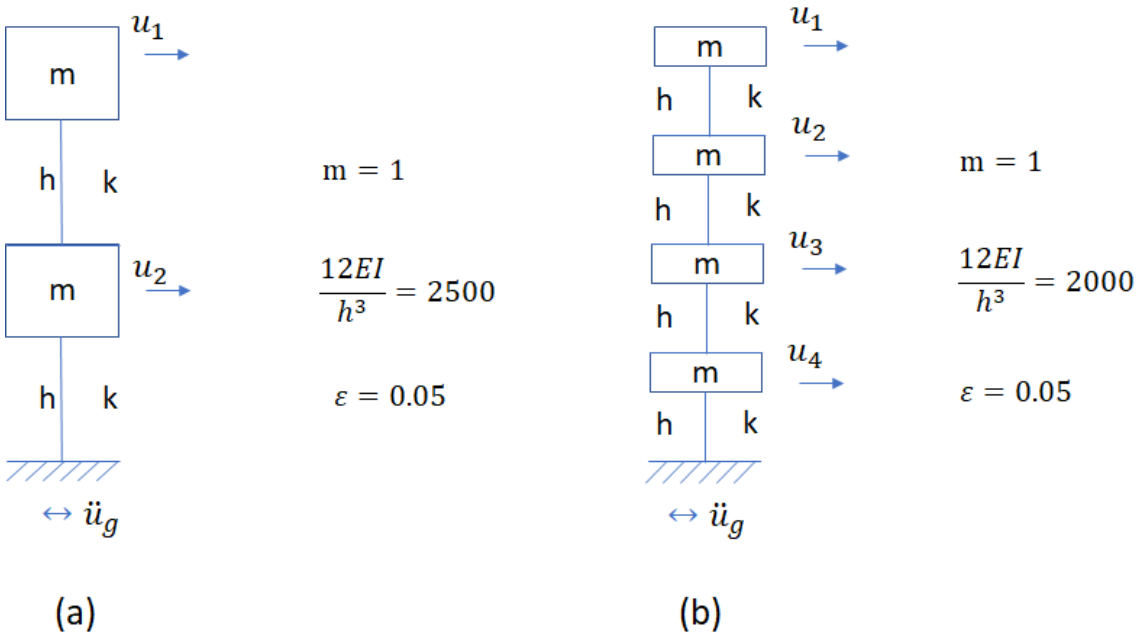

Fig. 4.3. Numerical model of 2-DOF and 4-DOF systems.(Simplified Shear frames)

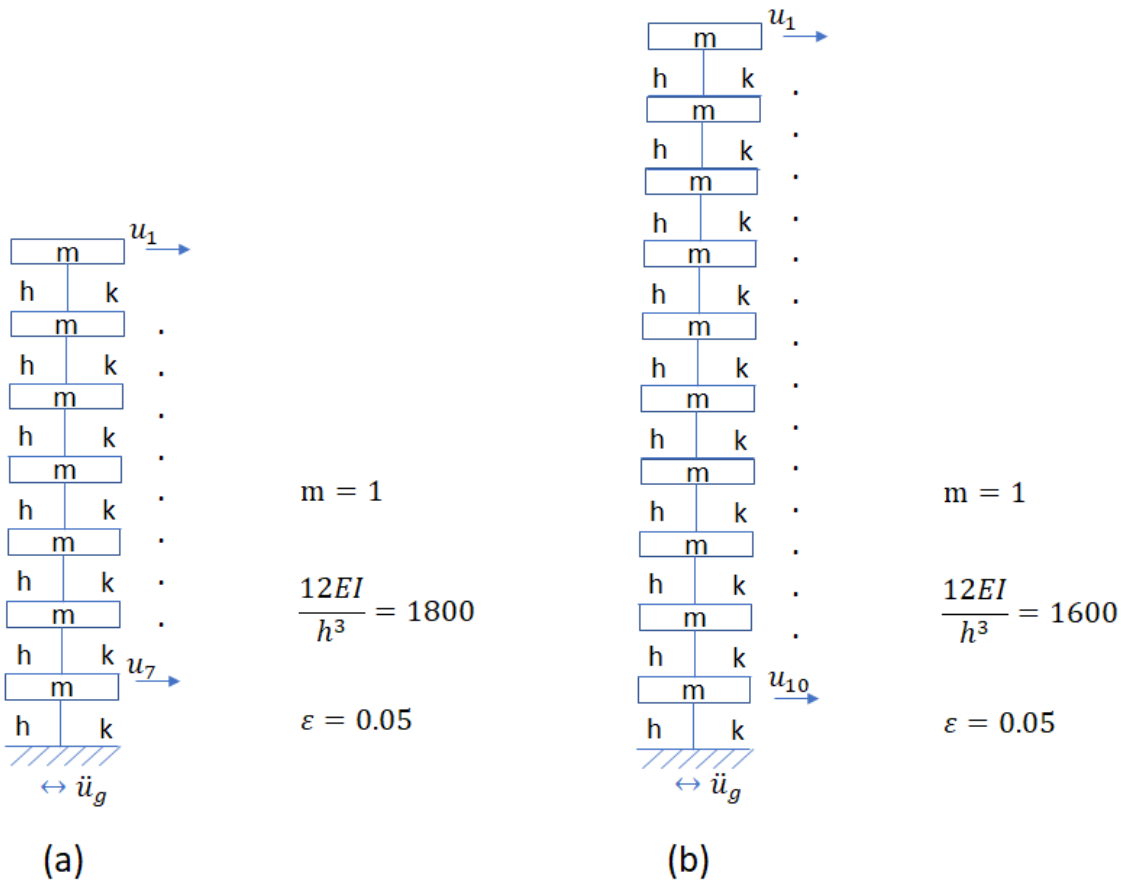

Fig. 4.4. Numerical model of 7-DOF and 10-DOF systems.(Simplified Shear frames)

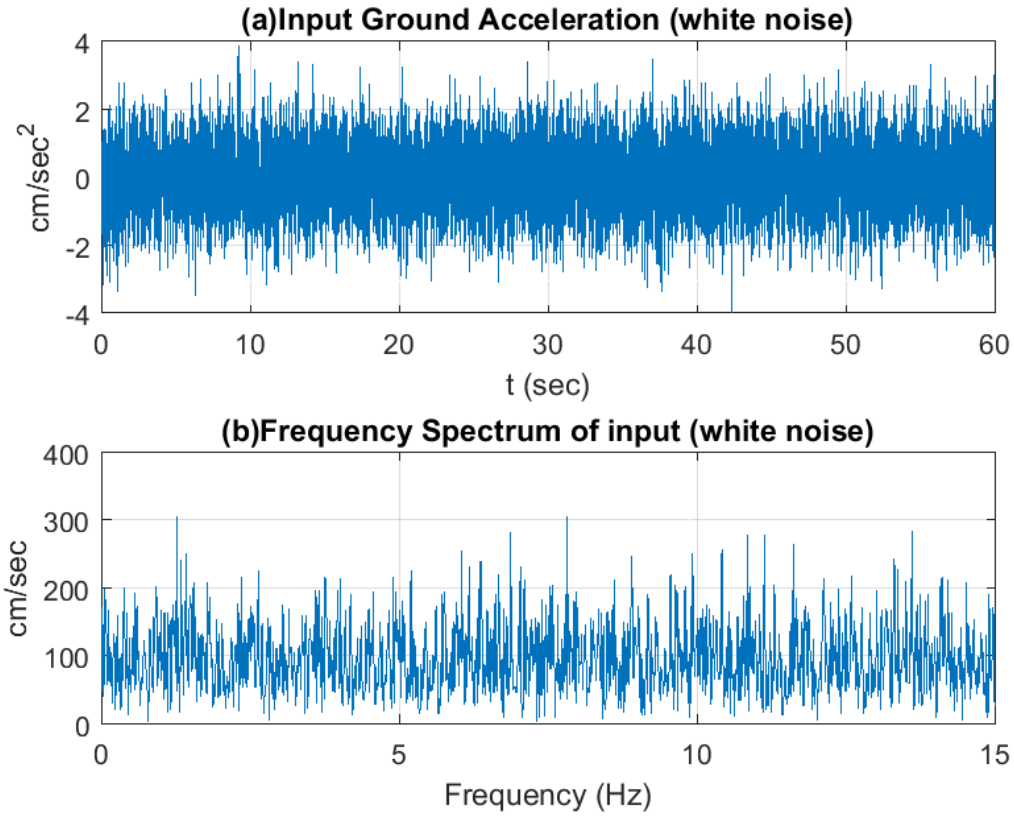

Fig. 4.5. White noise input:(a) input record, (b) frequency spectrum

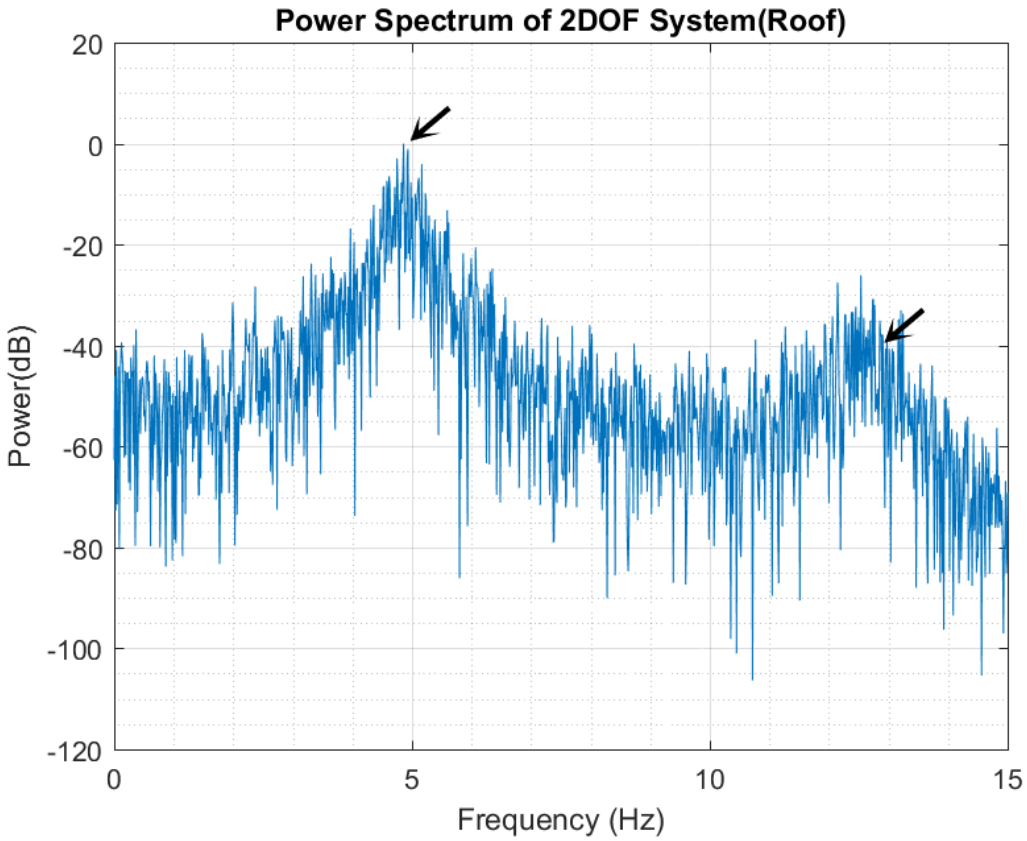

Fig. 4.6. Roof Power Spectrum of 2-DOF system with white noise input. (f_n = 4.92 & 12.88 Hz, ε =0.05). The black arrow marks point at the actual frequencies. In this power spectrum, the two peaks of the curve are approximately identified.

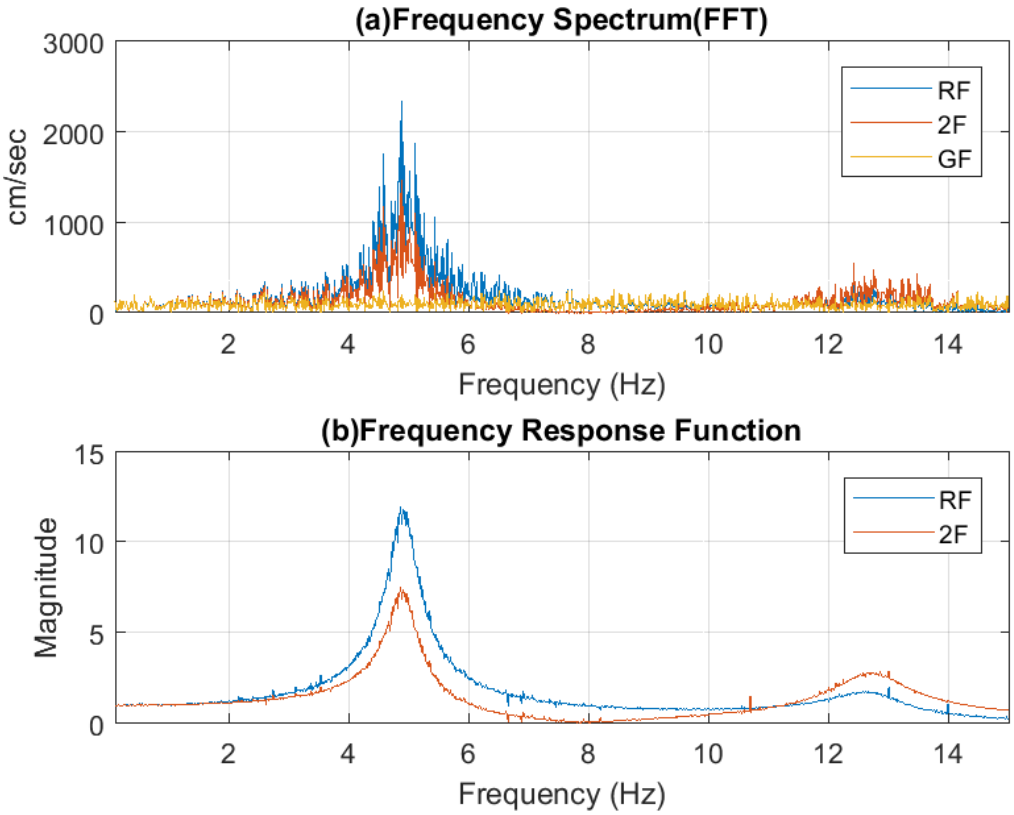

Fig. 4.7. Frequency spectrum & Frequency response function of 2DOF system (White noise input) a. Frequency spectrum of Roof, 2F and Ground floor. b. Frequency response function of Roof and 2F (f_n = 4.92 & 12.88 Hz, ε =0.05).

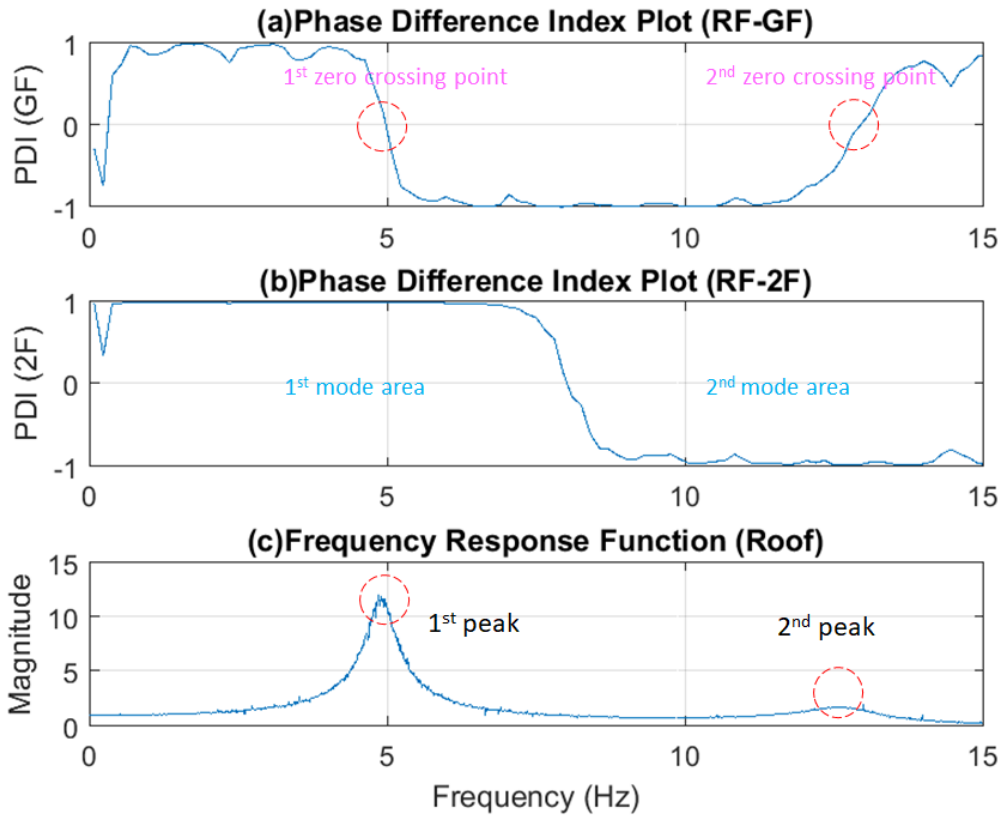

Fig. 4.8. Phase difference plot of 2DOF system (White noise input). a. PDI plot (Roof vs. Ground). The zero-crossing points indicate the natural frequencies of the 2DOF system. b. PDI plot (Roof vs. 2F). The PDI curve points out the theoretical zone of natural frequencies. c. Frequency response function of Roof(f_n = 4.92 & 12.88 Hz, ε =0.05). In figure (a), the two zero-crossing points match the actual frequencies. In figure(c), the two peaks of FRF are also identified although the second seems a little flat.

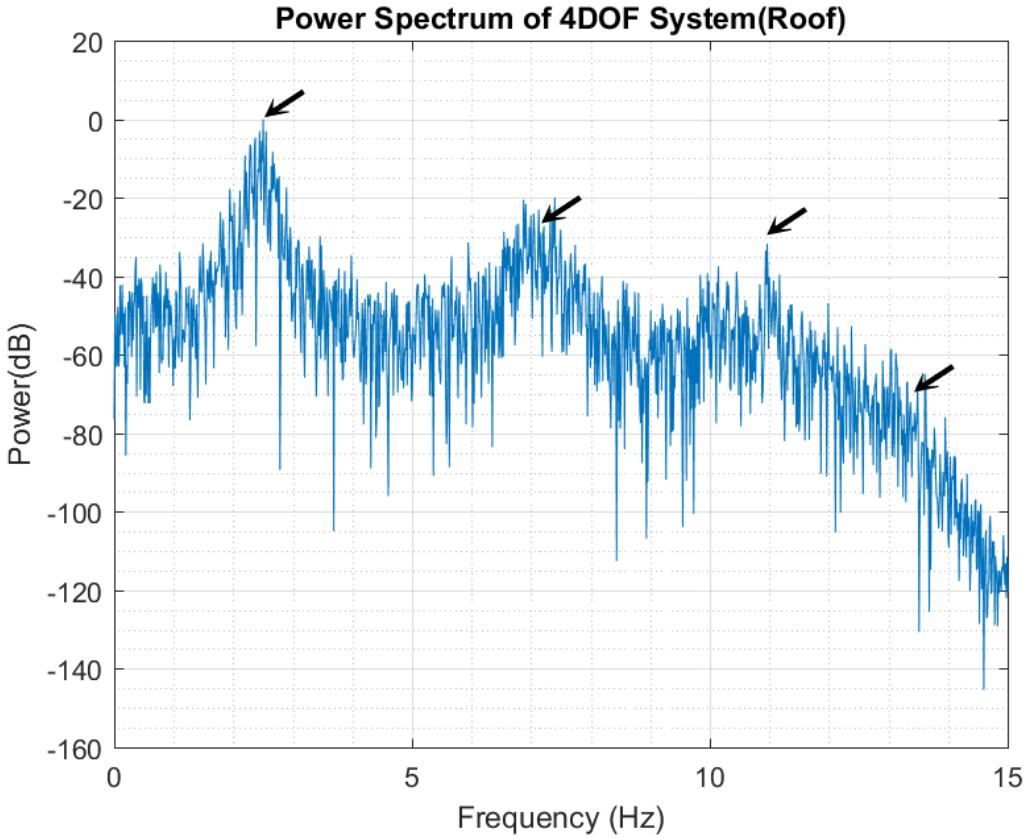

Fig. 4.9. Power Spectrum of 4DOF system (White noise input) (f_n = [2.47, 7.12, 10.90, 13.38] Hz, ε =0.05). The black arrow marks point at the actual frequencies. In this power spectrum, the first two peaks of the curve are approximately identified while others are missing.

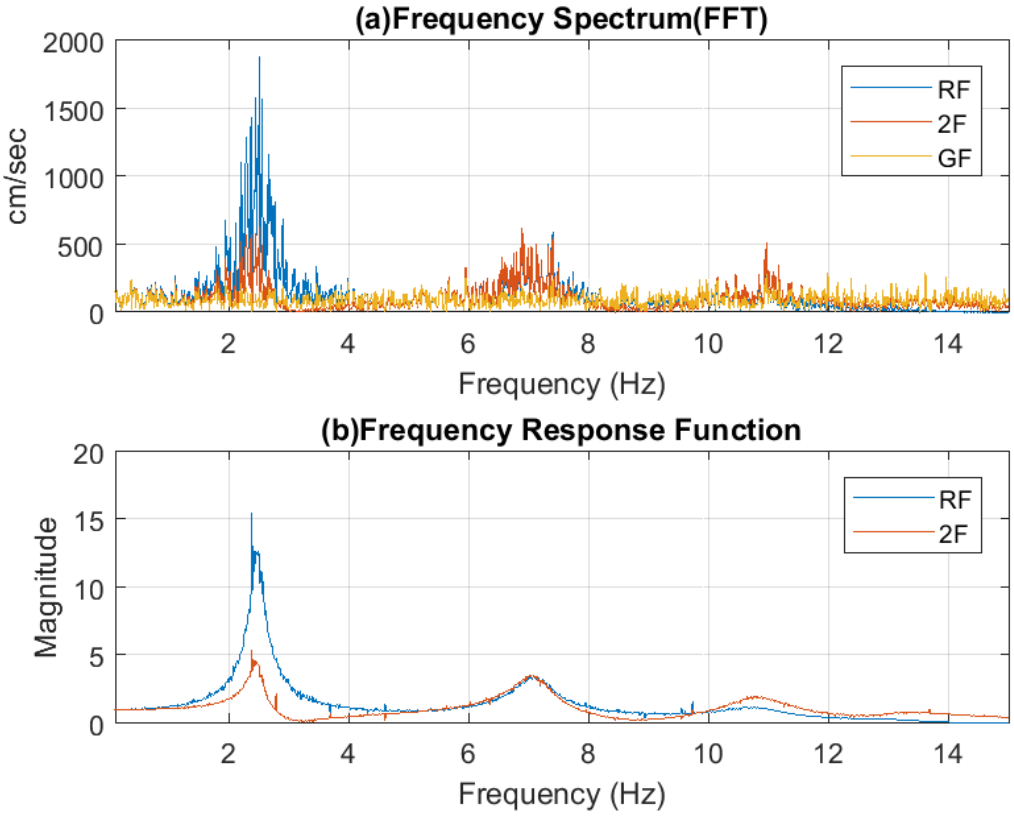

Fig. 4.10. Frequency spectrum & Frequency response function of 4-DOF system (White noise input) a. Frequency spectrum of Roof, 2F and Ground floor. b. Frequency response function of Roof and 2F (f_n = [2.47, 7.12, 10.90, 13.38] Hz, ε =0.05)

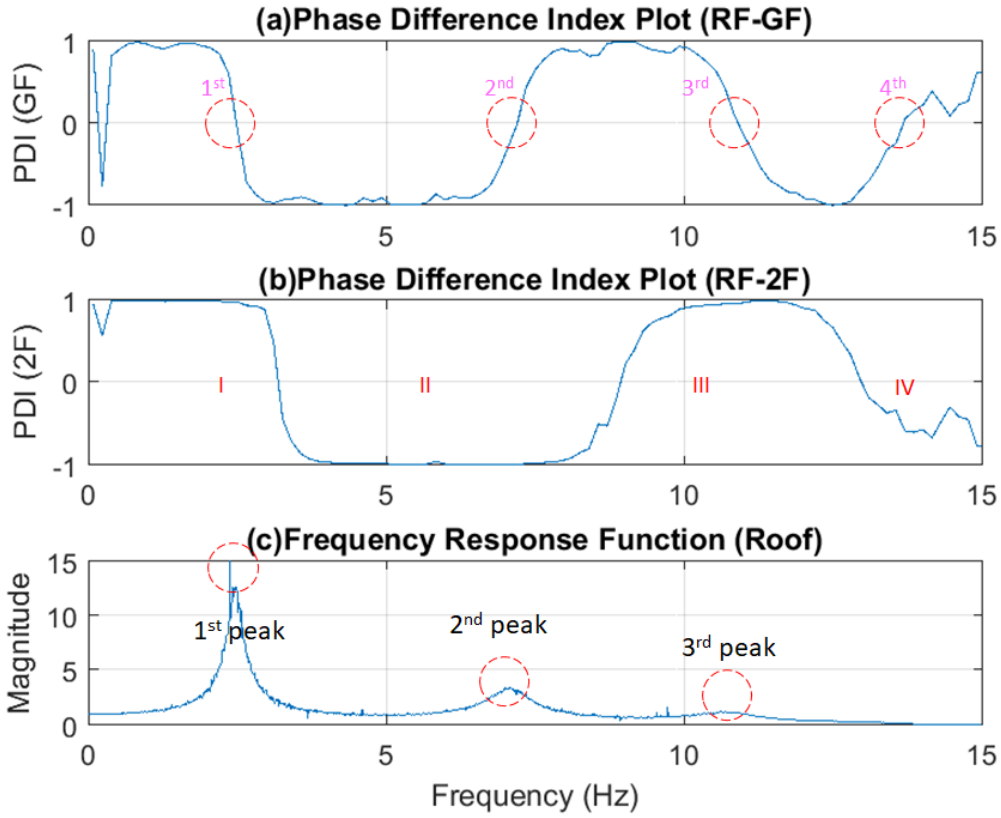

Fig. 4.11. Phase difference plot of 4-DOF system (White noise input). a. PDI plot (Roof vs. Ground). The zero-crossing points indicate the natural frequencies of the 4-DOF system. b. PDI plot (Roof vs. 2F). The PDI curve points out the theoretical zone of natural frequencies. c. Frequency response function of Roof(f_n = [2.47, 7.12, 10.90, 13.38] Hz, ε =0.05). In figure (a), the first three zero-crossing points match the actual frequencies, while the last one has a little deviation with tolerable error. In figure(c), only the first two peaks of FRF are clearly identified, and the third seems a little flat.

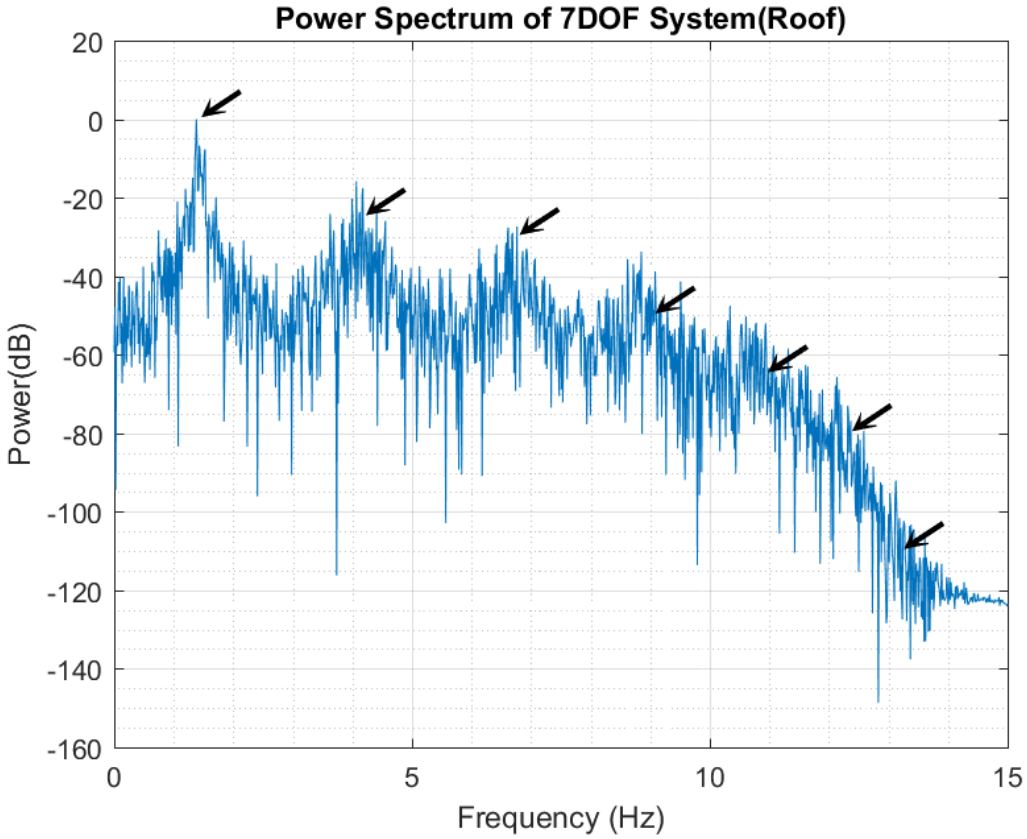

Fig. 4.12. Power Spectrum of 7-DOF system (White noise input) (f_n = [1.41, 4.17, 6.75, 9.04, 10.93, 12.34, 13.21] Hz, ε =0.05). The black arrow marks point at the actual frequencies. In this power spectrum, the first three peaks of the curve are approximately identified while others are missing.

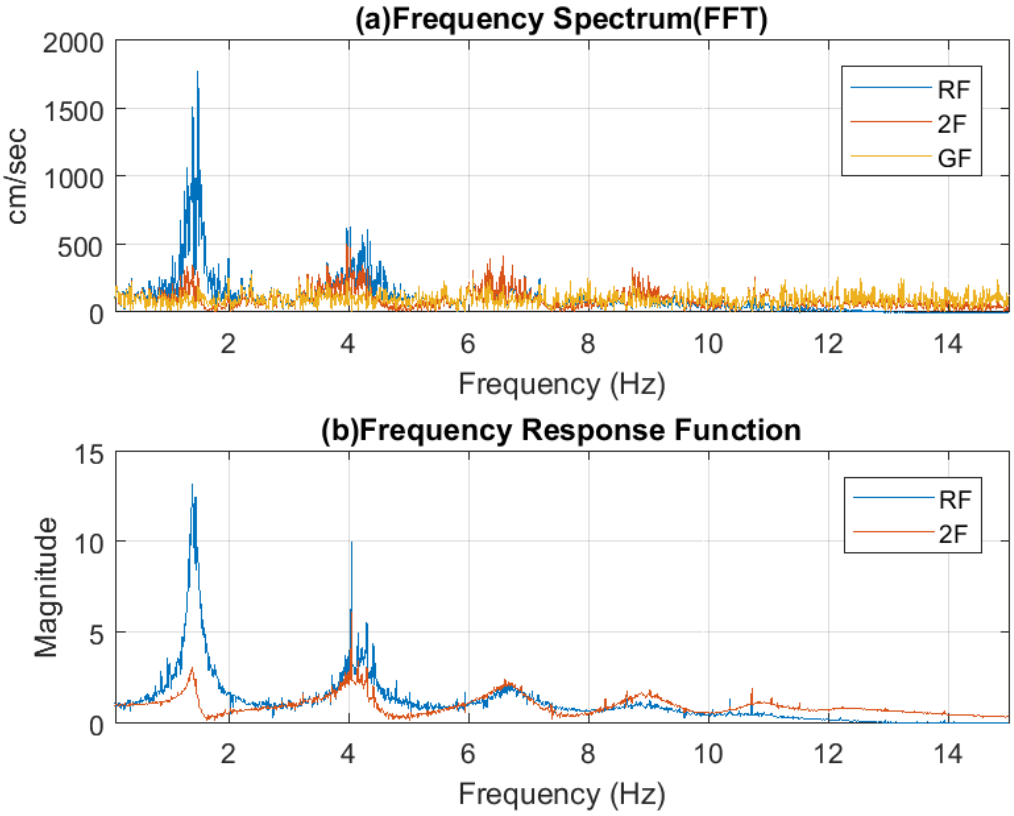

Fig. 4.13. Frequency spectrum & Frequency response function of 7-DOF system (White noise input) a. Frequency spectrum of Roof, 2F and Ground floor. b. Frequency response function of Roof and 2F (f_n = [1.41, 4.17, 6.75, 9.04, 10.93, 12.34, 13.21] Hz, ε =0.05)

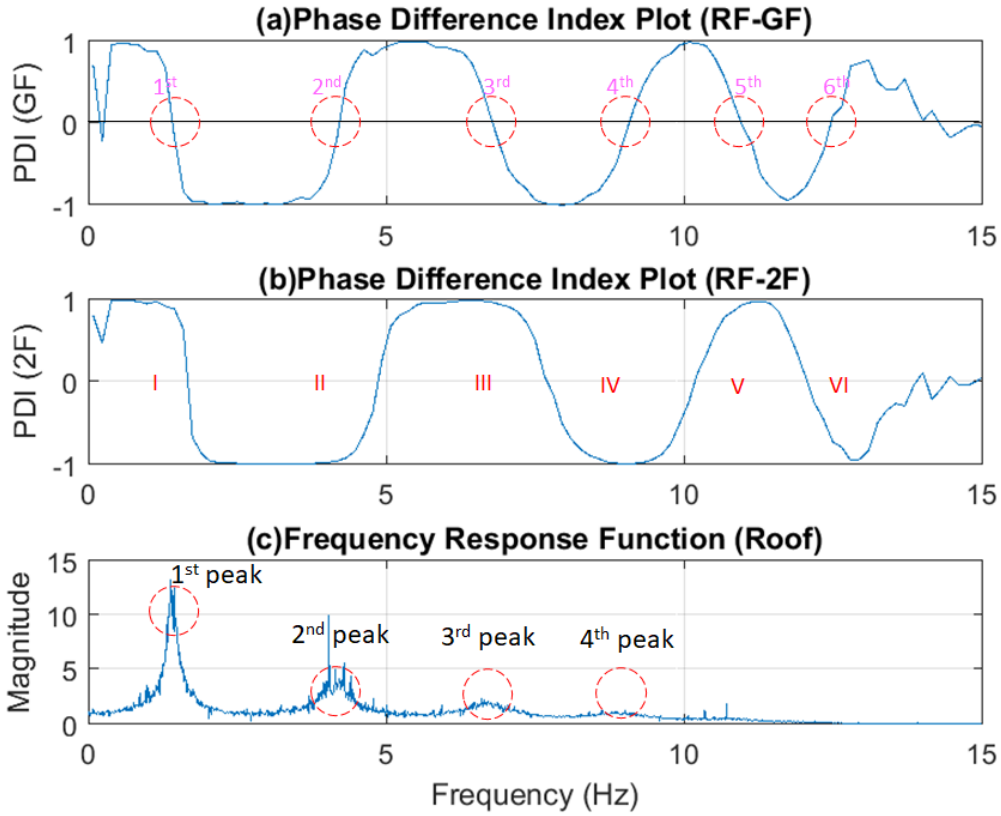

Fig. 4.14. Phase difference plot of 7-DOF system (White noise input). a. PDI plot (Roof vs. Ground). The zero-crossing points indicate the natural frequencies of the 7-DOF system. b. PDI plot (Roof vs. 2F). The PDI curve points out the theoretical zone of natural frequencies. c. Frequency response function of Roof(f_n = [1.41, 4.17, 6.75, 9.04, 10.93, 12.34, 13.21] Hz, ε =0.05). In figure (a), the first six zero-crossing points match the actual frequencies, while the last one seem missing. In figure(c), only the first three peaks of FRF are clearly identified. The forth peak is flatter.

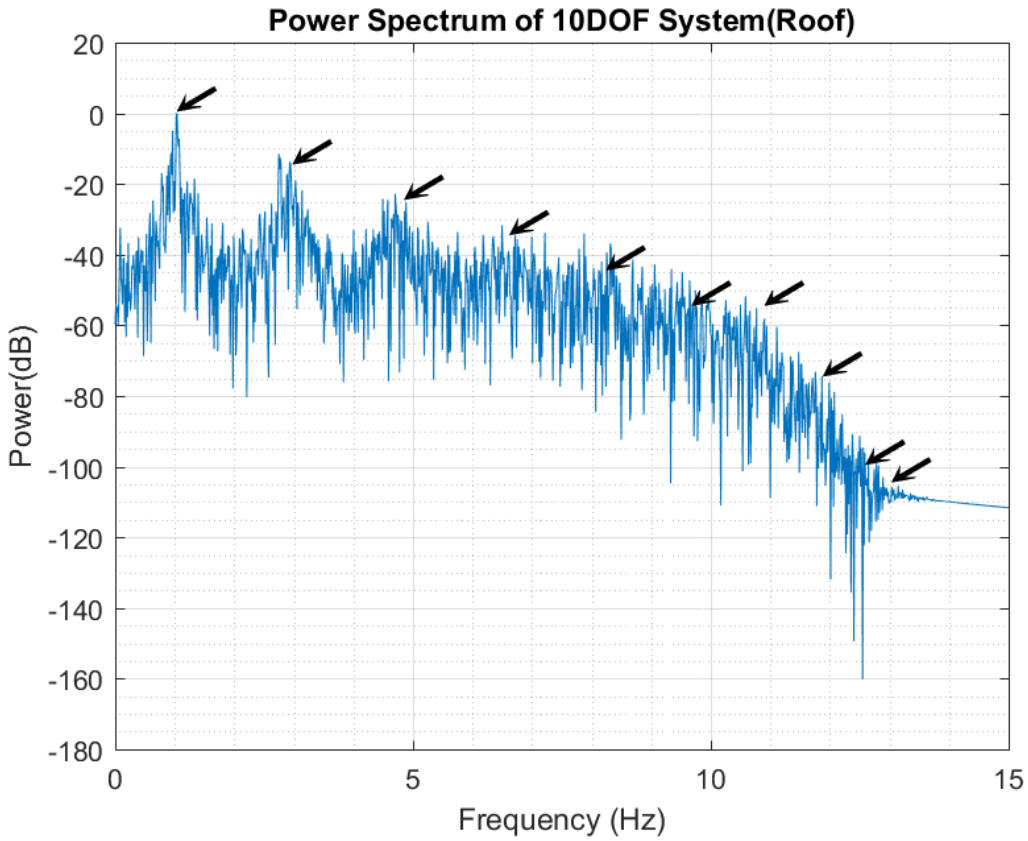

Fig. 4.15. Power Spectrum of 10-DOF system (White noise input)(f_n = [0.98, 2.92, 4.79, 6.56, 8.18, 9.62, 10.84, 11.82, 12.54, 12.98] Hz, ε =0.05). The black arrow marks point at the actual frequencies. In this power spectrum, the first three peaks of the curve are approximately identified while others are missing.

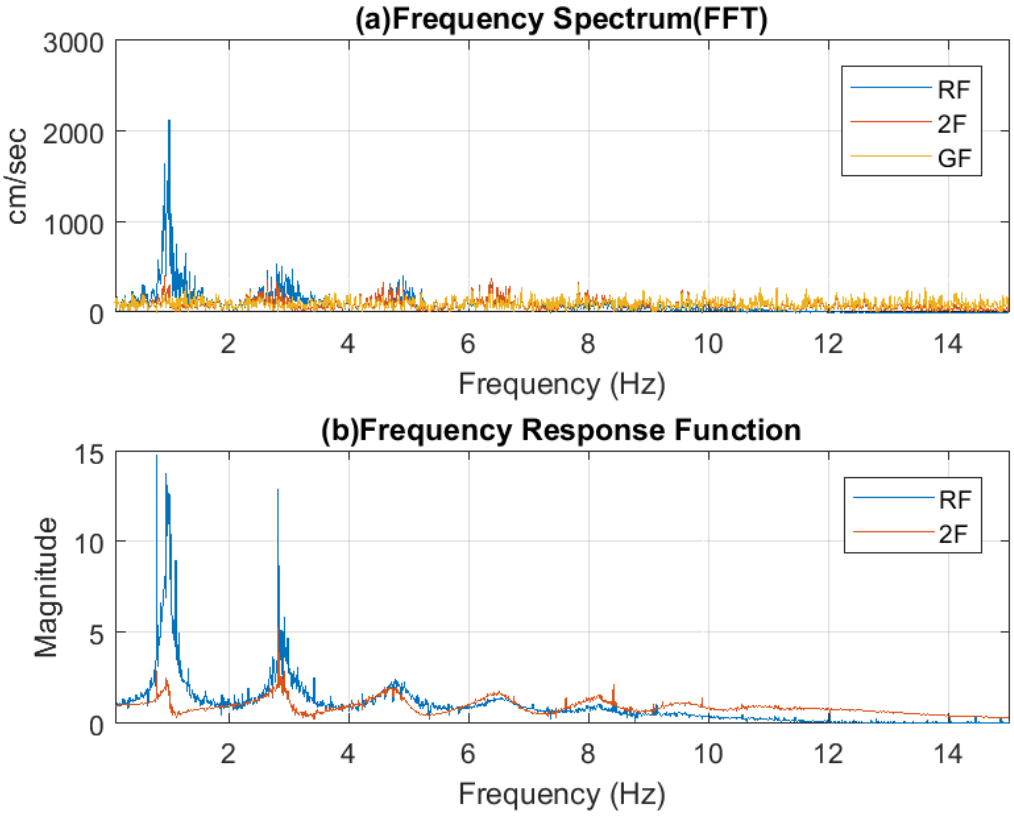

Fig. 4.16. Frequency spectrum & Frequency response function of 10-DOF system (White noise input): a. Frequency spectrum of Roof, 2F and Ground floor. b. Frequency response function of Roof and 2F (f_n = [0.98, 2.92, 4.79, 6.56, 8.18, 9.62, 10.84, 11.82, 12.54, 12.98] Hz, ε =0.05)

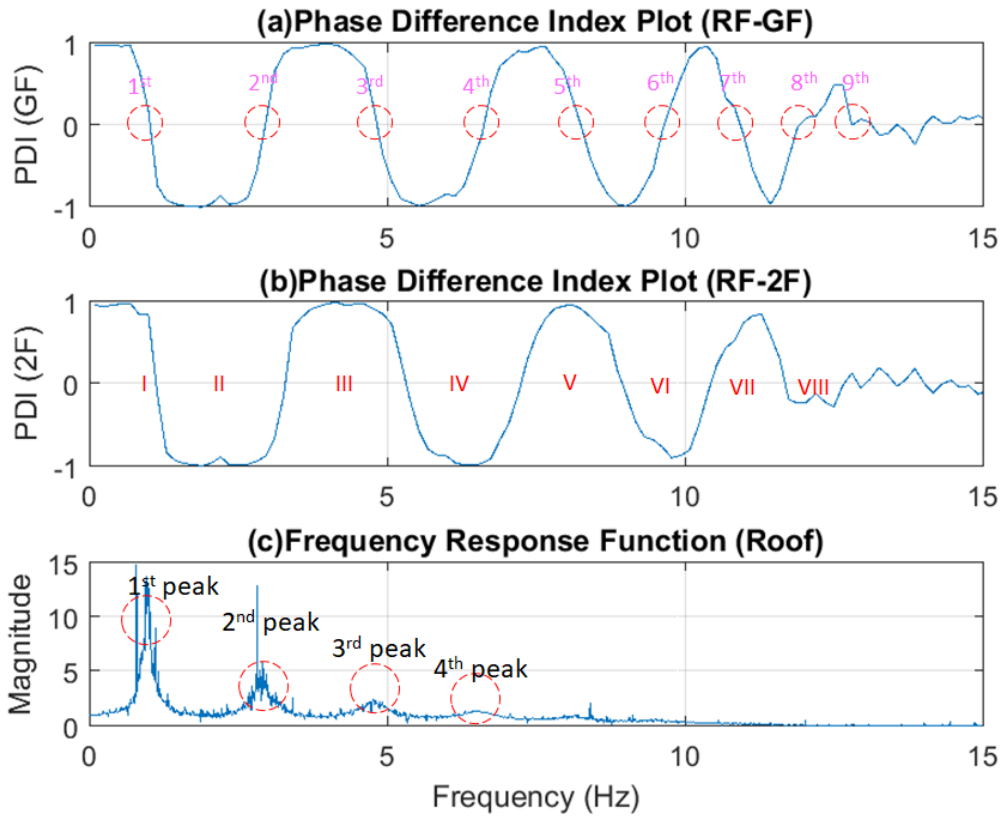

Fig. 4.17. Phase difference plot of 10-DOF system (White noise input). a.PDI plot (Roof vs. Ground). The zero-crossing points indicate the natural frequencies of the 10-DOF system. b. PDI plot (Roof vs. 2F). The PDI curve points out the theoretical zone of natural frequencies. c. Frequency response function of Roof(f_n = [0.98, 2.92, 4.79, 6.56, 8.18, 9.62, 10.84, 11.82, 12.54, 12.98] Hz, ε =0.05). In figure (a), the first eight zero-crossing points match the actual frequencies, while the last two seem mixed by each other. In figure(c), only the first three peaks of FRF are clearly identified. The forth peak is much flat.

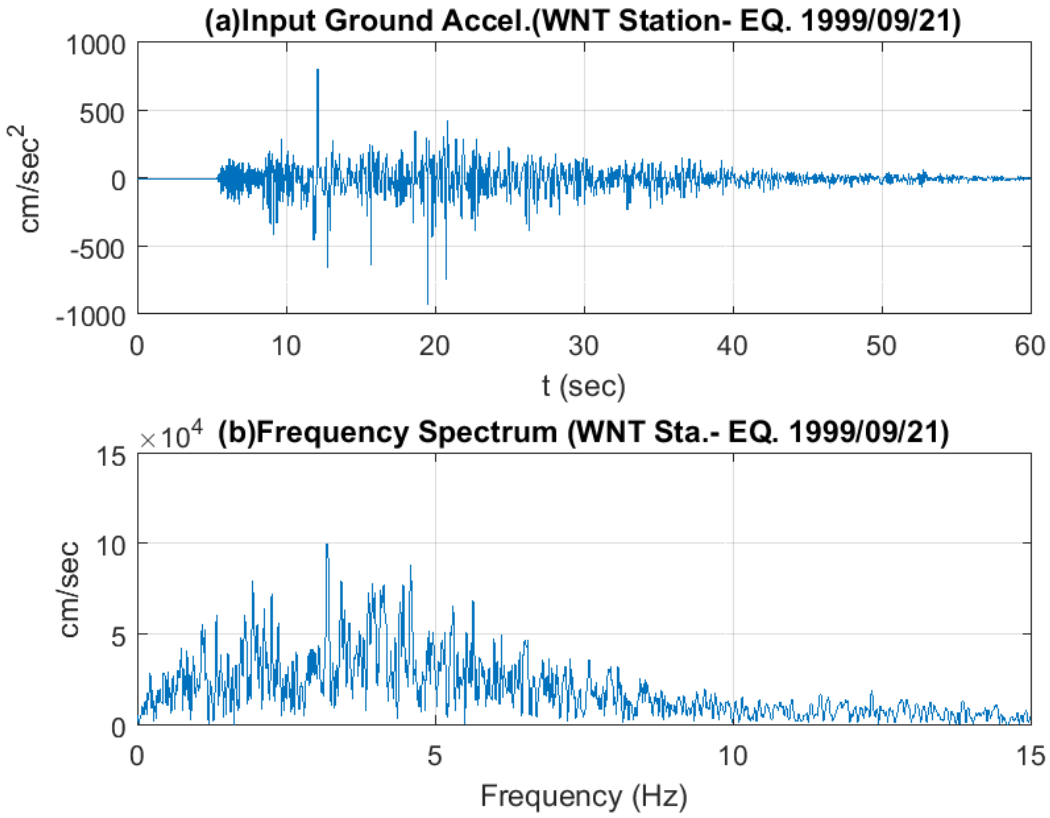

Fig. 4.18. Input Ground Acceleration: Station-WNT, Jiji-Earthquake, Taiwan, 1999/09/20

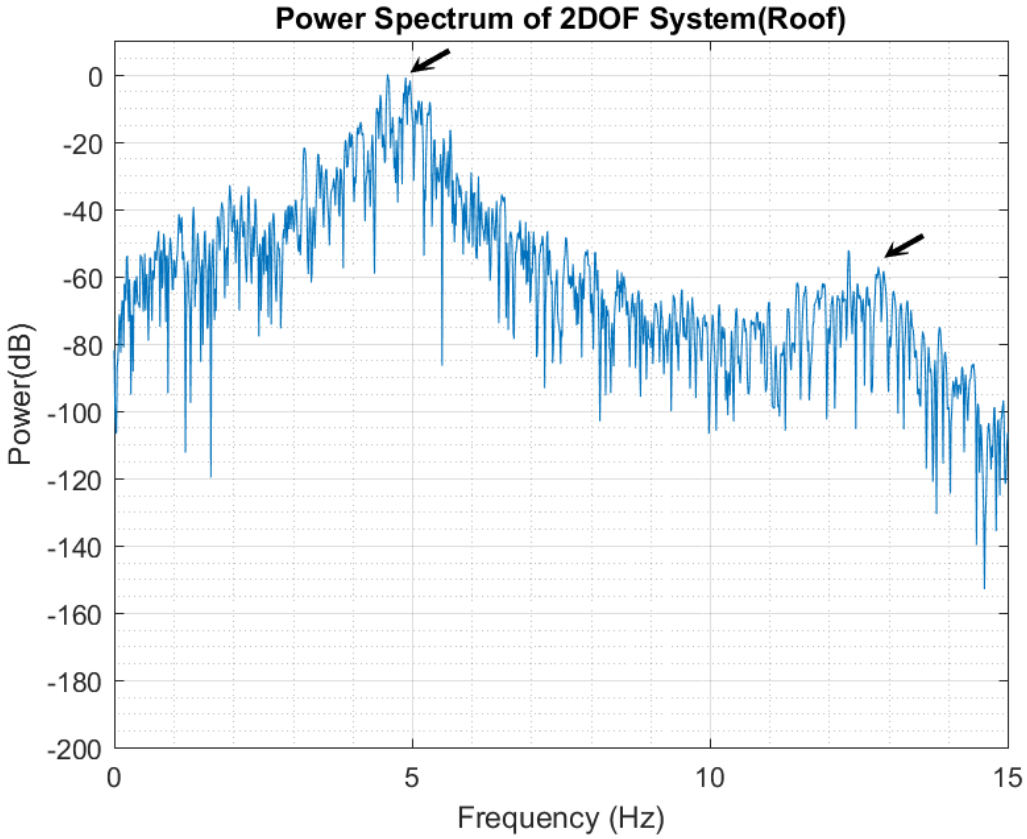

Fig. 4.19. Power Spectrum of Roof of 2-DOF system (Input: Station-WNT, Jiji-Earthquake, Taiwan, 1999/09/20) (f_n = 4.92 & 12.88 Hz, ε =0.05). The black arrow marks point at the actual frequencies. In this power spectrum, the two peaks of the curve are approximately identified.

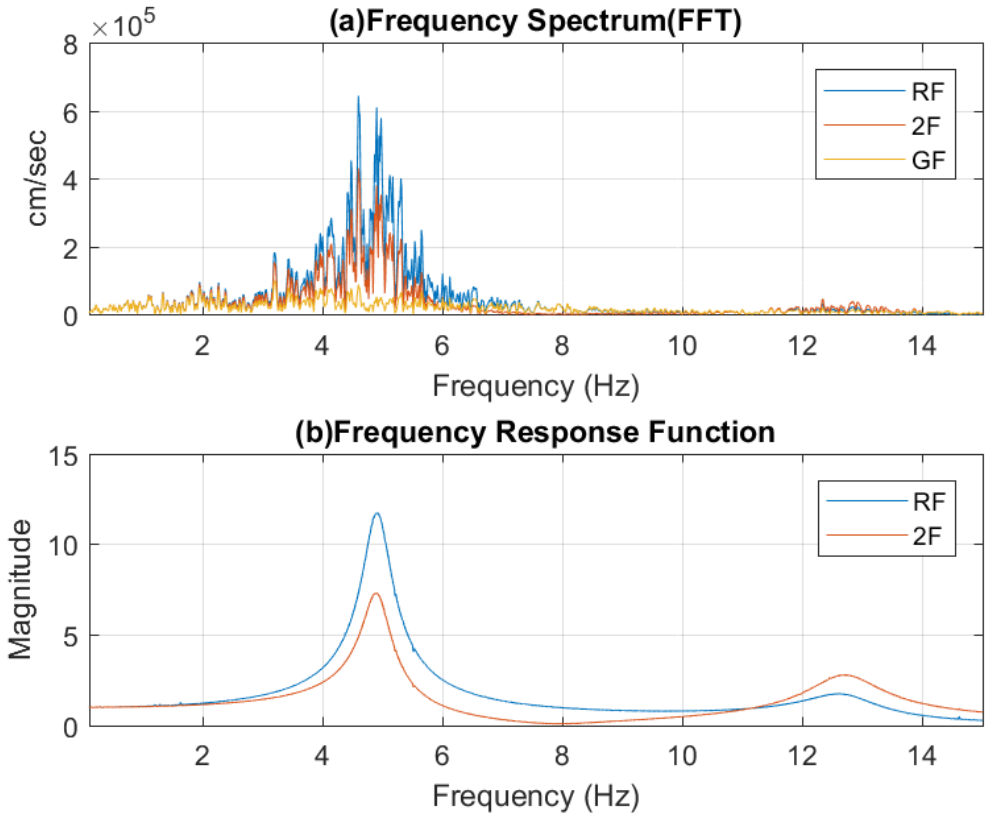

Fig. 4.20. Frequency spectrum & Frequency response function of 2-DOF system (Input: Station-WNT, Jiji-Earthquake, Taiwan, 1999/09/20) a. Frequency spectrum of Roof, 2F and Ground floor. b. Frequency response function of Roof and 2F (f_n = 4.92 & 12.88 Hz, ε =0.05)

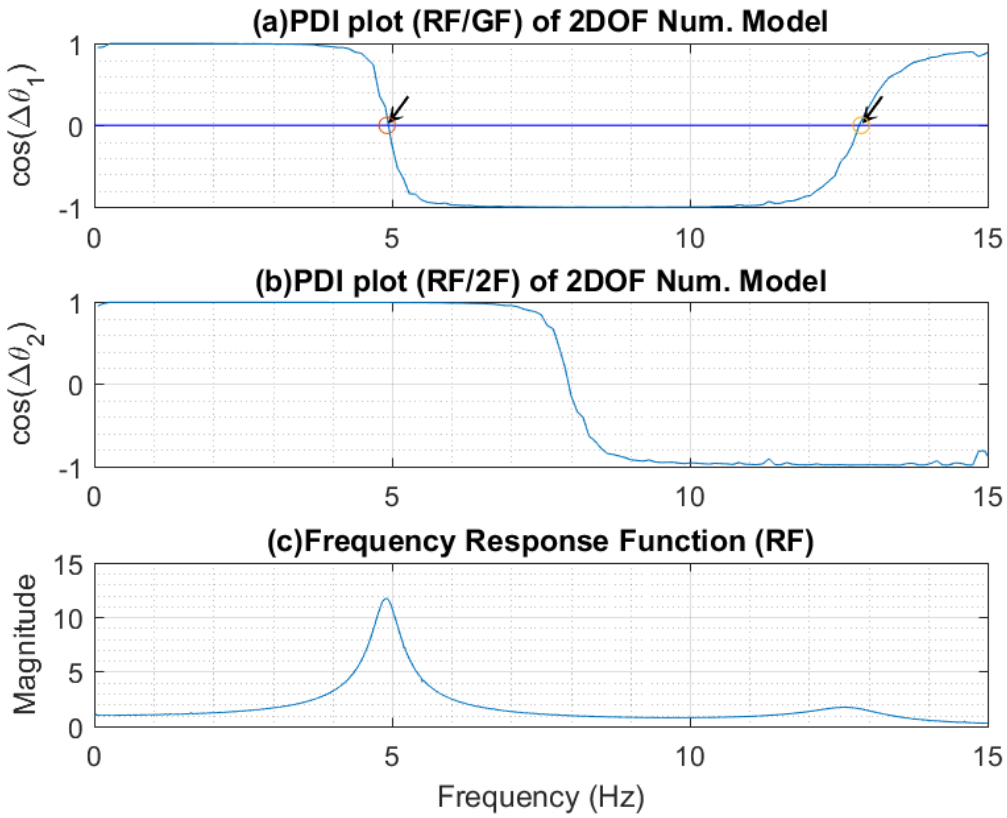

Fig. 4.21. Phase difference plot of 2-DOF system (Input: Station-WNT, Jiji-Earthquake, Taiwan, 1999/09/20). a. PDI plot (Roof vs. Ground). The zero-crossing points theoretically indicate the natural frequencies of the 2DOF system. b. PDI plot (Roof vs. 2F). The PDI curve points out the theoretical zone of natural frequencies. c. Frequency response function of Roof(f_n = 4.92 & 12.88 Hz, ε =0.05). In figure (a), the two zero-crossing points match the actual frequencies. In figure(c), the two peaks of FRF are also identified although the second seems a little flat.

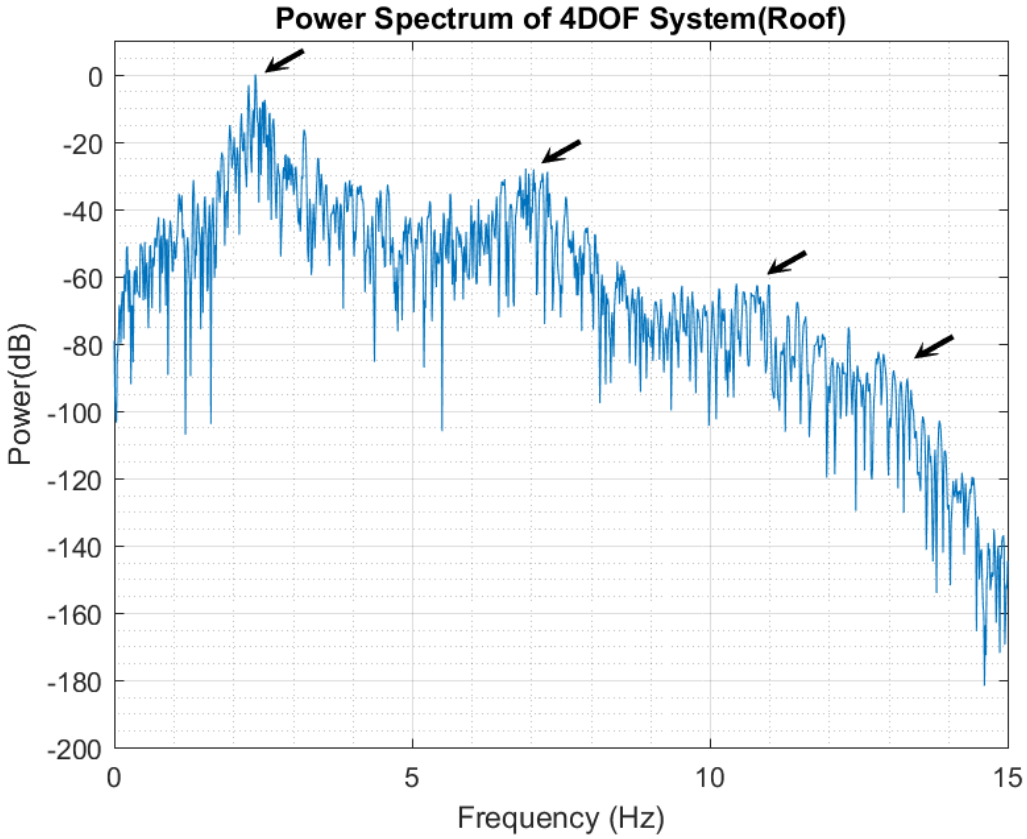

Fig. 4.22. Power Spectrum of 4-DOF system (Input: Station-WNT, Jiji-Earthquake, Taiwan, 1999/09/20) (f_n = [2.47, 7.12, 10.90, 13.38] Hz, ε =0.05). The black arrow marks point at the actual frequencies. In this power spectrum, the first two peaks of the curve are approximately identified while others are missing.

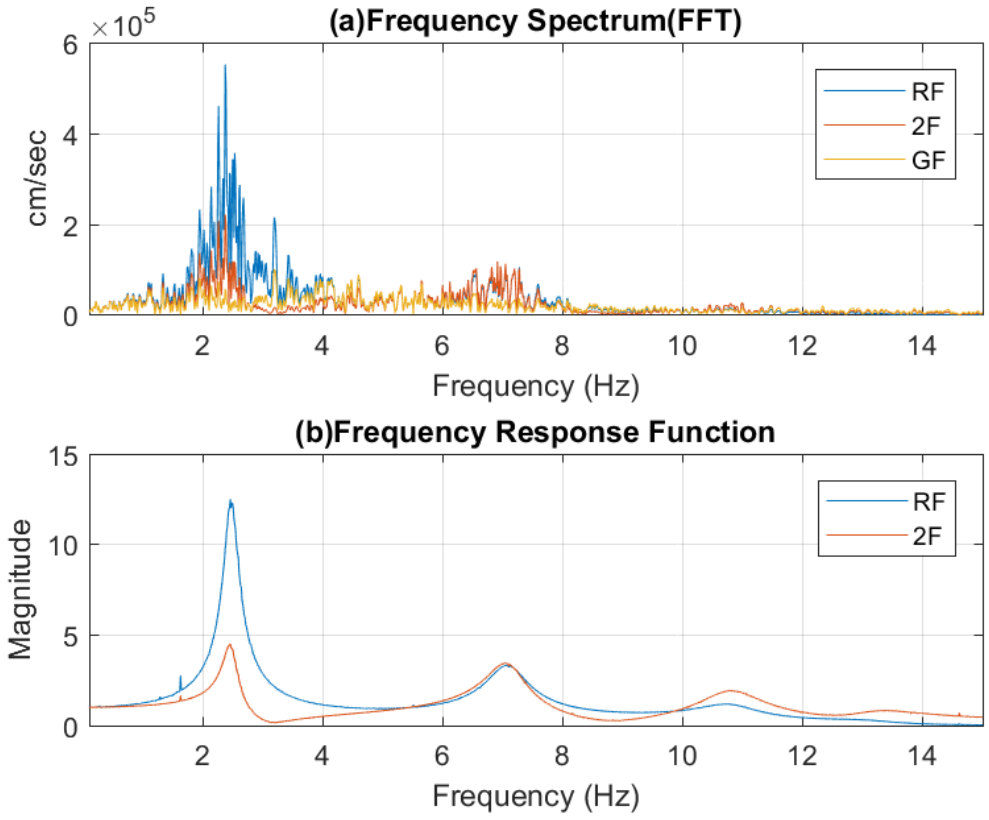

Fig. 4.23. Frequency spectrum & Frequency response function of 4-DOF system (Input: Station-WNT, Jiji-Earthquake, Taiwan, 1999/09/20) a. Frequency spectrum of Roof, 2F and Ground floor. b. Frequency response function of Roof and 2F (f_n = [2.47, 7.12, 10.90, 13.38] Hz, ε =0.05)

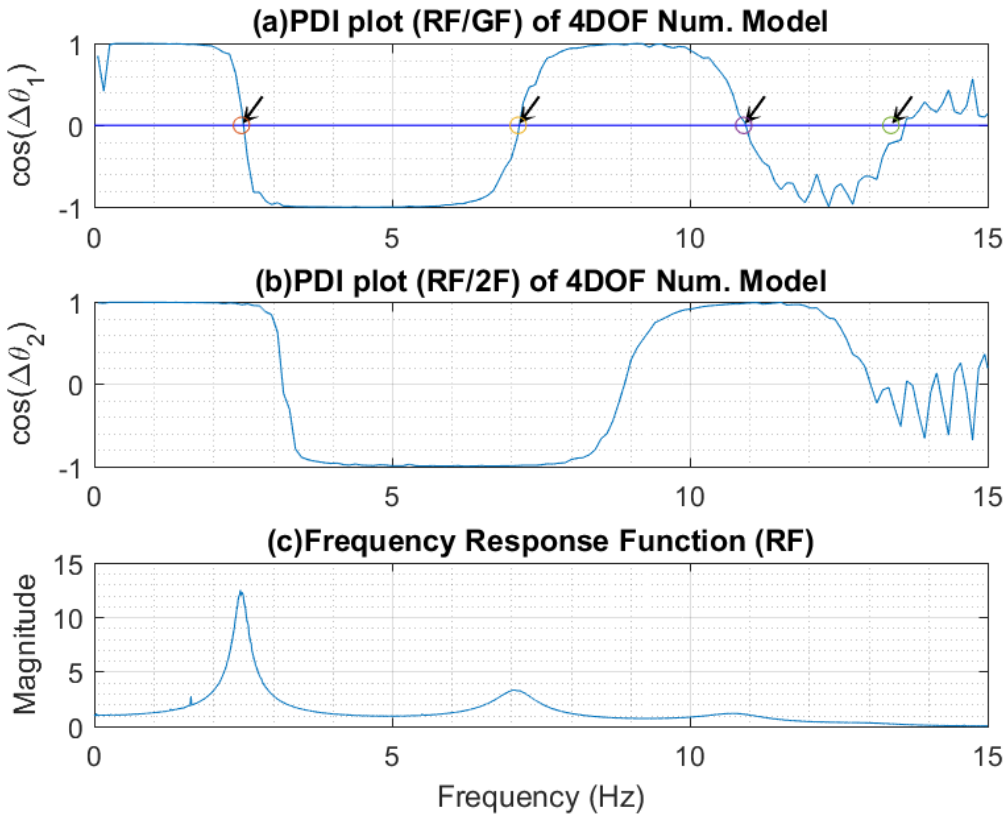

Fig. 4.24. Phase difference plot of 4-DOF system (Input: Station-WNT, Jiji-Earthquake, Taiwan, 1999/09/20). a. PDI plot (Roof vs. Ground). The zero-crossing points theoretically indicate the natural frequencies of the 4-DOF system. b. PDI plot (Roof vs. 2F). The PDI curve points out the theoretical zone of natural frequencies. c. Frequency response function of Roof(f_n = [2.47, 7.12, 10.90, 13.38] Hz, ε =0.05). In figure (a), the first three zero-crossing points match the actual frequencies, while the last one has a little deviation with tolerable error. In figure(c), only the first two peaks of FRF are clearly identified.

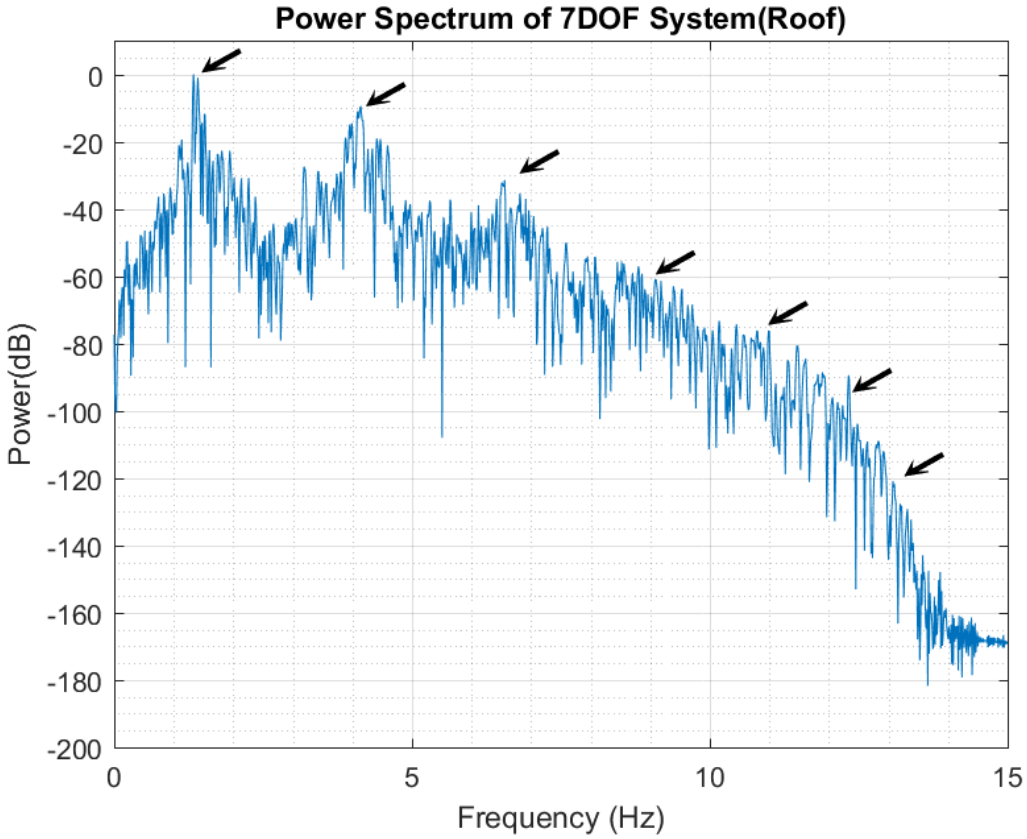

Fig. 4.25. Power Spectrum of 7-DOF system (Input: Station-WNT, Jiji-Earthquake, Taiwan, 1999/09/20) (f_n = [1.41, 4.17, 6.75, 9.04, 10.93, 12.34, 13.21] Hz, ε =0.05). The black arrow marks point at the actual frequencies. In this power spectrum, the first four peaks of the curve are approximately identified while others are missing.

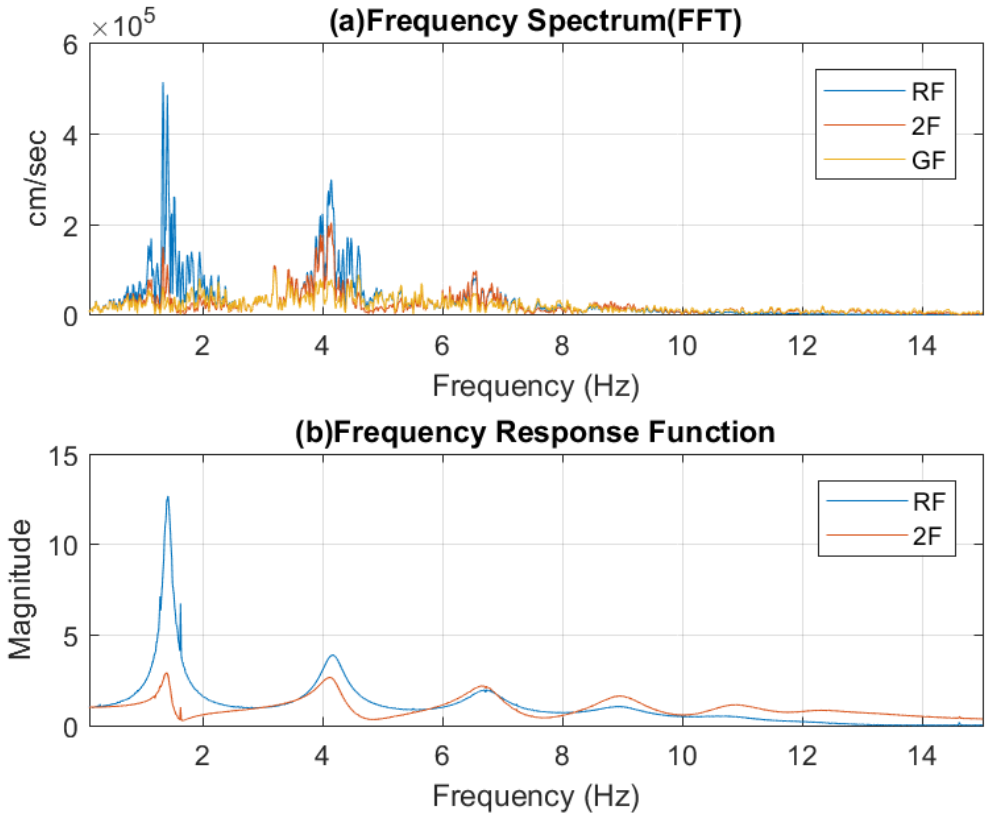

Fig. 4.26. Frequency spectrum & Frequency response function of 7-DOF system (Input: Station-WNT, Jiji-Earthquake, Taiwan, 1999/09/20) a. Frequency spectrum of Roof, 2F and Ground floor. b. Frequency response function of Roof and 2F (f_n = [1.41, 4.17, 6.75, 9.04, 10.93, 12.34, 13.21] Hz, ε =0.05)

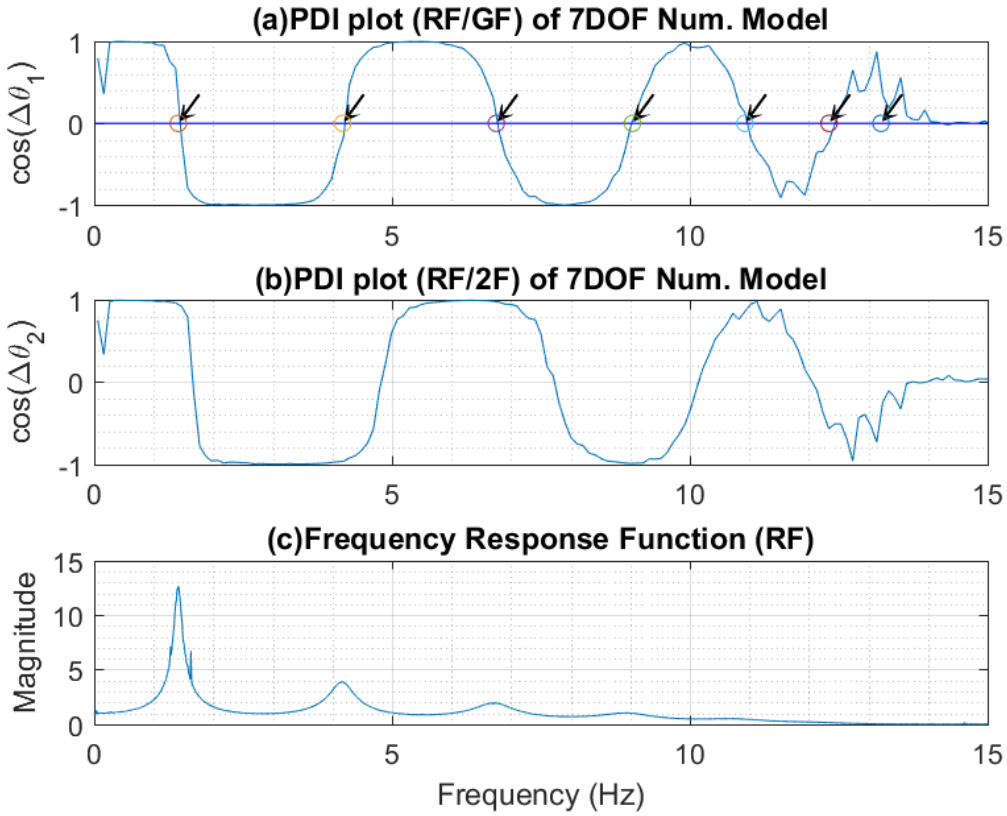

Fig. 4.27. Phase difference plot of 7-DOF system (Input: Station-WNT, Jiji-Earthquake, Taiwan, 1999/09/20). a. PDI plot (Roof vs. Ground). The zero-crossing points theoretically indicate the natural frequencies of the 7-DOF system. b. PDI plot (Roof vs. 2F). The PDI curve points out the theoretical zone of natural frequencies. c. Frequency response function of Roof(f_n = [1.41, 4.17, 6.75, 9.04, 10.93, 12.34, 13.21] Hz, ε =0.05). In figure (a), the first six zero-crossing points match the actual frequencies, while the last one seem missing. In figure(c), only the first three peaks of FRF are clearly identified.

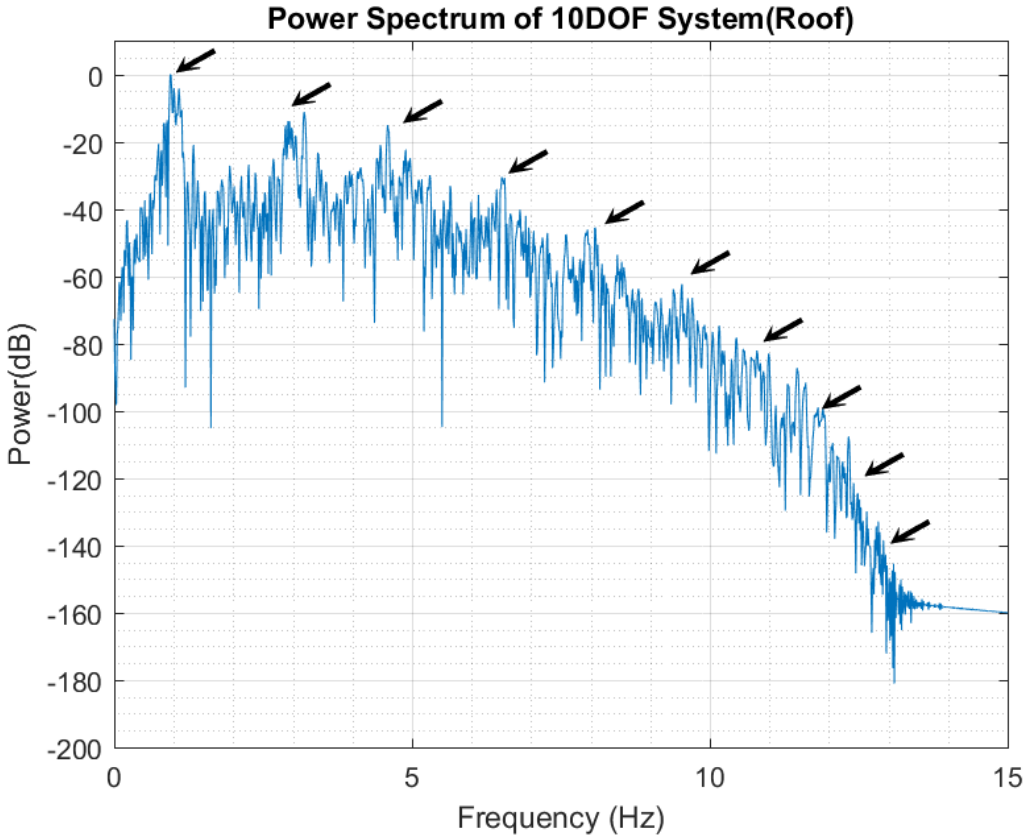

Fig. 4.28. Power Spectrum of 10-DOF system (Input: Station-WNT, Jiji-Earthquake, Taiwan, 1999/09/20)(f_n = [0.98, 2.92, 4.79, 6.56, 8.18, 9.62, 10.84, 11.82, 12.54, 12.98] Hz, ε =0.05). The black arrow marks point at the actual frequencies. In this power spectrum, the first three peaks of the curve are approximately identified while others are missing.

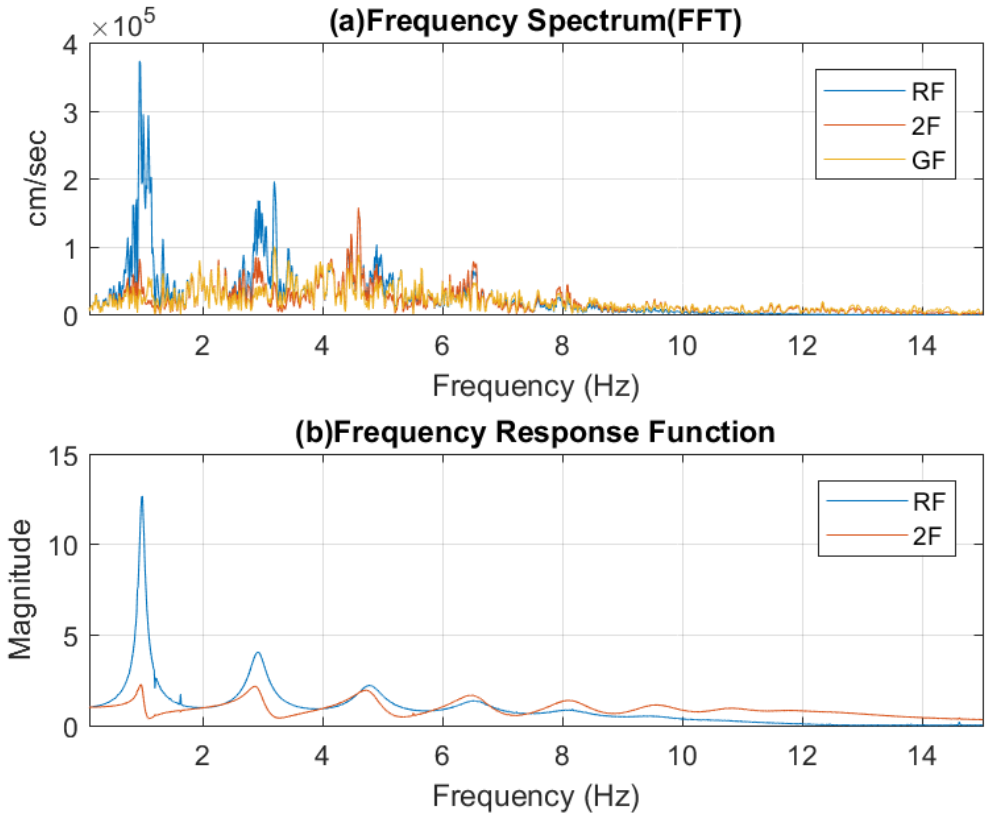

Fig. 4.29. Frequency spectrum & Frequency response function of 10-DOF system (Input: Station-WNT, Jiji-Earthquake, Taiwan, 1999/09/20): a. Frequency spectrum of Roof, 2F and Ground floor. b. Frequency response function of Roof and 2F (f_n = [0.98, 2.92, 4.79, 6.56, 8.18, 9.62, 10.84, 11.82, 12.54, 12.98] Hz, ε =0.05)

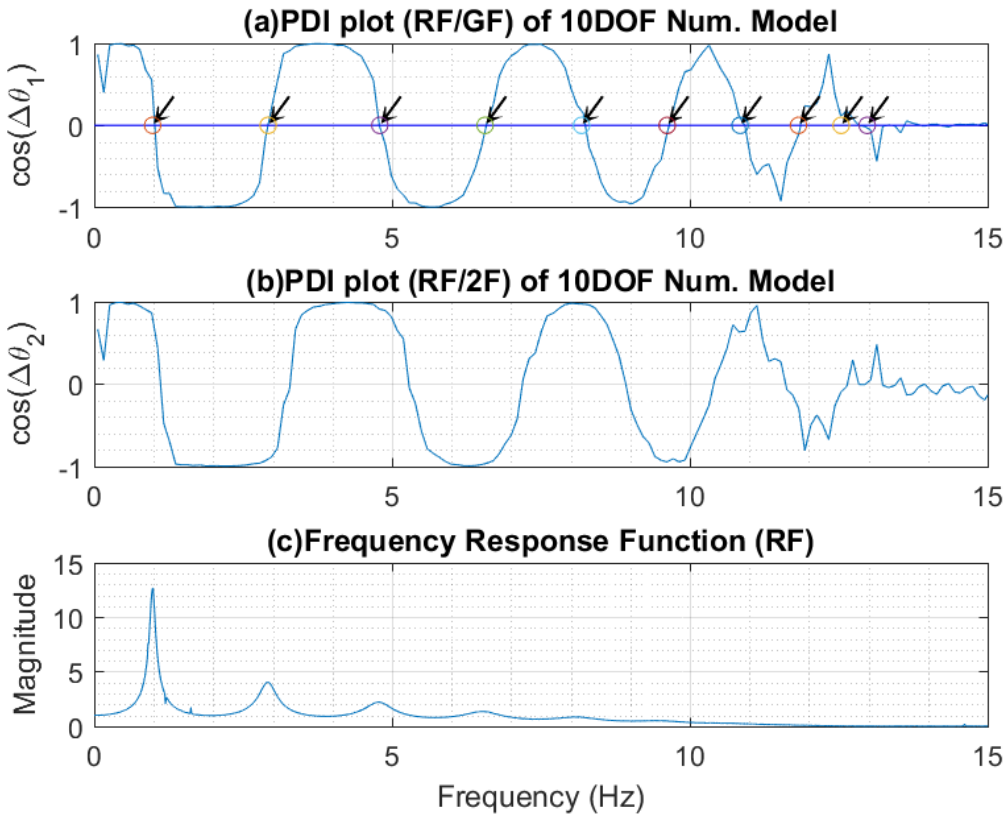

Fig. 4.30. Phase difference plot of 10-DOF system (Input: Station-WNT, Jiji-Earthquake, Taiwan, 1999/09/20). a.PDI plot (Roof vs. Ground). The zero-crossing points theoretically indicate the natural frequencies of the 10-DOF system. b. PDI plot (Roof vs. 2F). The PDI curve points out the theoretical zone of natural frequencies. c. Frequency response function of Roof(f_n = [0.98, 2.92, 4.79, 6.56, 8.18, 9.62, 10.84, 11.82, 12.54, 12.98] Hz, ε =0.05). In figure (a), the first eight zero-crossing points match the actual frequencies, while the last two seem mixed by each other. In figure(c), only the first three peaks of FRF are clearly identified.

5. PHASE DIFFERENCE IN TORSION

5.1 Introduction

Since most buildings have eccentricities in plane, torsion inevitably occurs when the earthquake ground motion excites the building. The torsional response happens because eccentric response generates additional inertial force which twists the building. In ASCE code, a minimum of 5% accidental torsion is required to be taken into consideration in the building design [22]. Therefore, when it comes to system identification for a building, it is impractical to exclude the torsional mode. In fact, several factors may generate torsion, such as asymmetric stiffness distribution in plane or elevation, asymmetric mass distribution in plane or elevation, external torsional force, asymmetric geological condition at foundation, and so on. Each factor has different influence on the building. As finding the analytic solutions for all kinds of torsional problems is not within the scope of the dissertation, only pure torsion problems and plate-mass problems will be discussed to illustrate how torsion affects the frequency spectrum in order to find a way to identify the torsional frequency of a building.

5.2 Pure Torsion

For a simple system structure (shown in Figure 5.1), there is a theoretical solution for rotational mode [10]. The solution is based on the assumption that displacements of the structure are very small, and the whole system remains linear elastic under rotational excitation. In earthquake engineering, since the first translational mode of low-rise building always dominates the dynamic response, similar notion might also hold true in the rotational frequency for a multiple degrees of freedom system.

In an undamped simple system shown as Figure 5.1, the dynamic equation for pure rotational(torsional) response can be expressed as Eq.5.1:

$$I_0\ddot{u}_\theta + k_\theta u_\theta = -I_0\ddot{u}_{g\theta} \tag{5.1}$$

where:

- I_0: moment of inertia of the plate.
- $k_\theta = (k_x d^2 + k_y b^2)$: rotational stiffness of the simple system.
- $\ddot{u}_\theta$: angular acceleration of the simple system.
- $\ddot{u}_{g\theta}$:ground angular acceleration.

Eq.5.1 can be rewritten:

$$\ddot{u}_\theta + \omega_\theta^2 u_\theta = -\ddot{u}_{g\theta} \tag{5.2}$$

If a viscous damping term of the system is considered, the Eq.5.2 becomes:

$$\ddot{u}_\theta + 2\varepsilon_\theta\beta_\theta\dot{u}_\theta + \omega_\theta^2 u_\theta = -\ddot{u}_{g\theta} \tag{5.3}$$

where:

- ε_θ: rotational damping ratio of the system
- $\beta_\theta = \frac{\omega}{\omega_{n\theta}}$: frequency ratio

It is obvious that the governing equation has completely the same form as the translational motion equation. Therefore, it is not surprising that the frequency response function and phase angle of this rotational system have the same forms as the translational motion equation.

The frequency response function(FRF) is:

$$H_\theta(\omega) = \frac{1}{(1-\beta_\theta^2) + 2\varepsilon_\theta\beta_\theta i} \tag{5.4}$$

The phase angle of the rotational system is:

$$\phi_\theta = tan^{-1}\frac{2\varepsilon_\theta\beta_\theta}{1-\beta_\theta^2} \tag{5.5}$$

Similarly, the governing equation of SDOF can also be applied to MDOF rotational system:

$$[I]\{\ddot{u}_\theta(t)\} + [C_\theta]\{\dot{u}_\theta(t)\} + [K_\theta]\{u_\theta(t)\} = -[I]\{\ddot{u}_{g_\theta}\} \tag{5.6}$$

If the modal damping matrix is diagonal, by modal superposition method, n sets of independent dynamic equations for n-DOF system would be obtained:

$$\ddot{U}_{\theta i}(t) + 2\varepsilon_{\theta i}\beta_{\theta i}\dot{U}_{\theta i}(t) + \omega_\theta^2 U_{\theta i}(t) = -\ddot{U}_{g\theta i} \tag{5.7}$$

Thus, by modal superposition method, we can find the steady solution of u_θ to be the linear combination of U_θ corresponding to each fundamental mode.

Therefore, from Eq.5.3 and Eq.5.7, we know that all equations and plots related to translational motion are also applicable to rotational motion.

5.3 Torsion with Lateral Force

The equation of motion of a single story building is [10]:

$$\begin{bmatrix} m & & \\ & m & \\ & & I_0 \end{bmatrix}\begin{Bmatrix} \ddot{u}_x \\ \ddot{u}_y \\ \ddot{\theta} \end{Bmatrix} + \begin{bmatrix} k_{xx} & k_{xy} & k_{x\theta} \\ k_{yx} & k_{yy} & k_{y\theta} \\ k_{\theta x} & k_{\theta y} & k_{\theta\theta} \end{bmatrix}\begin{Bmatrix} u_x \\ u_y \\ \theta \end{Bmatrix} = -\begin{bmatrix} m & & \\ & m & \\ & & I_0 \end{bmatrix}\left(\begin{Bmatrix} 1 \\ 0 \\ 0 \end{Bmatrix}\ddot{u}_{gx} + \begin{Bmatrix} 0 \\ 1 \\ 0 \end{Bmatrix}\ddot{u}_{gy} + \begin{Bmatrix} 0 \\ 0 \\ 1 \end{Bmatrix}\ddot{u}_{g\theta}\right) \tag{5.8}$$

From Eq.5.8, the equation of motion governing torsional response can be expressed:

$$I_0\ddot{\theta} + k_{\theta\theta}\theta = -I_0\ddot{\theta}_{g\theta} - k_{\theta x}u_x - k_{\theta y}u_y \tag{5.9}$$

In periodic motion, $\ddot{u}_x \approx \omega_x^2 u_x, \ddot{u}_y \approx \omega_y^2 u_x$.

Then, rearranging the equation:

$$\ddot{\theta} + \omega_\theta^2 \theta = -\ddot{\theta}_{g\theta} - k_{\theta x}\frac{\ddot{u}_x}{I_0\omega_x^2} - k_{\theta y}\frac{\ddot{u}_y}{I_0\omega_y^2} \tag{5.10}$$

Considering that the torsion is driven by the inertia force of eccentric mass, and the eccentricity in both directions are e_x and e_y. Assuming that both eccentricities are small so that the moment inertia remain constant. Then the input torsional acceleration can be expressed:

$$\ddot{\theta}_{g\theta} = \frac{m}{I_0}(e_x\ddot{u}_{gy} + e_y\ddot{u}_{gx}) \tag{5.11}$$

Solving Eq. 5.10 by Fourier Transform, the solution for the angle of rotation is:

$$\theta(t) = -H_\theta(\omega)\mathcal{F}\left\{\ddot{\theta}_{g\theta} + k_{\theta x}\frac{\ddot{u}_x}{I_0\omega_x^2} + k_{\theta y}\frac{\ddot{u}_y}{I_0\omega_y^2}\right\} \tag{5.12}$$

where:

- $H_\theta(\omega)$: frequency response function of this rotation system
- $\mathcal{F}\left\{\ddot{\theta}_{g\theta}\right\} = \ddot{\Theta}_{g\theta}(\omega)$: Fourier Transform of ground angular acceleration.
- $\mathcal{F}\left\{k_{\theta x}\ddot{u}_x/(I_0\omega_x^2)\right\} = \frac{k_{\theta x}}{I_0\omega_x^2}H_x(\omega)\ddot{U}_{gx}(\omega)$:
  - $H_x(\omega)$: frequency response function in X direction
  - $\ddot{U}_{gx}(\omega)$: Fourier Transform of ground acceleration in X direction.
- $\mathcal{F}\left\{k_{\theta y}\ddot{u}_y/(I_0\omega_y^2)\right. \ = \frac{k_{\theta y}}{I_0\omega_y^2}H_y(\omega)\ddot{U}_{gy}(\omega)$
  - $H_y(\omega)$: frequency response function in Y direction
  - $\ddot{U}_{gy}(\omega)$: Fourier Transform of ground acceleration in Y direction.

5.4 Concept of Torsional Mode Spectrum

Figure 5.2 is the top view of figure 5.1. A_1 and A_2 are two accelerometers installed on the two sides of the diaphragm. Referring to Figure 5.2-(b), acceleration a_1 measured by A_1 is:

$$a_1(t) \approx \ddot{u}_x(t) + r_1\ddot{\theta}(t) \tag{5.13}$$

Acceleration a_2 measured by A_2 is:

$$a_2(t) \approx \ddot{u}_x(t) - r_2\ddot{\theta}(t) \tag{5.14}$$

Subtracting a_2 from a_1, the difference can be written as:

$$\Delta a(t) = (r_2 + r_1)\ddot{\theta}(t) = R \times \ddot{\theta}(t) \tag{5.15}$$

where: $R = (r_2 + r_1)$

If we analyze Eq. 5.15 in frequency domain, this equation becomes:

$$\Delta A(\omega) = R \times \Theta(\omega) \tag{5.16}$$

By Eq.5.12, we can rewrite Eq.5.16 as:

$$\Delta A(\omega) = -R \times H_\theta(\omega) \left\{ \ddot{\Theta}_{g\theta}(\omega) + \frac{k_{\theta x}}{I_0\omega_x^2} H_x(\omega)\ddot{U}_{gx}(\omega) + \frac{k_{\theta y}}{I_0\omega_y^2} H_y(\omega)\ddot{U}_{gy}(\omega) \right\} \tag{5.17}$$

Now, we define the absolute value of $\Delta A(\omega)$ to be the "Torsional Mode Spectrum"- $\mathcal{F}_T(\omega)$, then:

$$\mathcal{F}_T(\omega) = R \times |H_\theta(\omega)| \left\{ \ddot{\Theta}_{g\theta}(\omega) + \frac{k_{\theta x}}{I_0\omega_x^2} |H_x(\omega)| \ddot{U}_{gx}(\omega) + \frac{k_{\theta y}}{I_0\omega_y^2} |H_y(\omega)| \ddot{U}_{gy}(\omega) \right\} \tag{5.18}$$

where:

- $|H_\theta(\omega)| = A_\theta / \sqrt{(1 - beta_\theta^2)^2}$: ABS. value of FRF in θ direction
- $|H_x(\omega)| = A_x / \sqrt{(1 - \beta_x^2)^2}$: ABS. value of FRF in X direction
- $|H_y(\omega)| = A_y / \sqrt{(1 - \beta_y^2)^2}$: ABS. value of FRF in Y direction
- A_x, A_y, A_θ: modal contribution factors of MODF system in X, Y and θ direction(see Chapter 2.2.1).
- $\beta_x, \beta_y, \beta_\theta = \omega/\omega_{nx}, \omega/\omega_{ny}$,and $\omega/\omega_{n\theta}$ respectively

Although Eq.5.18 looks a little complicated, there is no need to use it to do any calculation. The reason $\mathcal{F}_T(\omega)$ is called torsional mode spectrum is because in Eq.5.18,

when $\beta_x = 1$, $\beta_y = 1$, or $\beta_\theta = 1$, the torsion spectrum would be close to infinity. Thus, if there are data from two accelerometers on the same floor,and away from each other are available, in low-rise buildings, the Fourier Spectrum of their difference should reveal three peaks which represent ω_x, ω_y, and ω_θ. In high-rise buildings, even more peaks could be observed in torsion spectrum. Normally, one can tell the translational frequencies ω_x and ω_y by peak-picking method from the Fourier Spectra in X and Y direction. Therefore, it is possible to exclude ω_x and ω_y in torsion spectrum and the remaining frequency peak would be ω_θ.

Despite the use of torsion spectrum seems encouraging, there are still some restrictions to its use:

1. The torsional and translational response must be coupled. If the θ and u_x or u_y are orthogonal, it means that in Eq.5.8, $k_{\theta x}$ and $k_{\theta y} = 0$. Thus, the ω_x and ω_y could disappear in torsion spectrum.

2. Two accelerometers should be available on the same floor and their location may not be too close. If their locations are close, the frequency spectrum of their difference would be near zero. In addition, the accelerometers may not be installed close to the stiffness center of the building, or else the torsional response will be too weak to be detected.

3. High-rise buildings often have long periods, so the first modes of ω_x, ω_y and ω_θ are usually very close. Therefore, in high-rise buildings or skyscrapers, sometimes there may be difficulties to distinguish ω_x, ω_y and ω_θ

4. The chosen pair of accelerometers must be on the roof or an upper story because torsional response is weaker at lower stories.

The practical use of torsional mode spectrum shall be introduced in Chapters 6 and 7, and illustrated by actual building examples.

5.5 Phase Difference and Rotation

The idea of phase difference can also be used in the identification of torsional modes. The concept can be illustrated by using Figure 5.3. Figure 5.3 illustrates rigid diaphragm with two accelerometers set on opposite sides in plan on a given floor. In torsional mode, points A and B move out-of-phase; in non-torsional mode, points A and B move in phase. Thus, the concept of PDI also works in torsional mode identification. However, there are still some conditions in using this method to identify torsional modes.

- A pair of accelerometers on the same story must be available.
- Both of the accelerometers must be far away from the center of stiffness. The relative motion (or phase difference of displacement) of two accelerometers would be hard to observe if one of them is too close to the rotation center.
- The chosen accelerometers must be on an upper story.
- In strong ground motions, the first torsional mode would often be mixed with the first translational modes, especially in high-rise buildings.
- For high rise buildings, the ω_x, ω_y and ω_θ are usually very close. If we need to separate ω_x, ω_y and ω_θ by band-pass filter, we need a very narrow bandwidth of frequency and a band-pass filter with high order to achieve the goal.

5.6 Numerical Model for Torsion and PDI Analysis

In this section, we would like to use a simple model to simulate the effects of added torsion in translational motion. Referring to Eq.5.8, and assuming that in K matrix, only k_{xx}, k_{yy} and $k_{\theta\theta} \neq 0$, i.e. a symmetric K system, equation of motion can be written as:

$$\begin{bmatrix} m & & \\ & m & \\ & & I_0 \end{bmatrix} \begin{Bmatrix} \ddot{u}_x \\ \ddot{u}_y \\ \ddot{\theta} \end{Bmatrix} + \begin{bmatrix} k_{xx} & & \\ & k_{yy} & \\ & & k_{\theta\theta} \end{bmatrix} \begin{Bmatrix} u_x \\ u_y \\ \theta \end{Bmatrix} = - \begin{bmatrix} m & & \\ & m & \\ & & I_0 \end{bmatrix} \left(\begin{Bmatrix} 1 \\ 0 \\ 0 \end{Bmatrix} \ddot{u}_{gx} + \begin{Bmatrix} 0 \\ 1 \\ 0 \end{Bmatrix} \ddot{u}_{gy} + \begin{Bmatrix} 0 \\ 0 \\ 1 \end{Bmatrix} \ddot{u}_{g\theta} \right) \tag{5.19}$$

or:

$$\begin{cases} \ddot{u}_x + \omega_x^2 u_x = -\ddot{u}_{gx} \\ \ddot{u}_y + \omega_y^2 u_y = -\ddot{u}_{gy} \\ \ddot{\theta} + \omega_\theta^2 \theta = -\ddot{u}_{g\theta} \end{cases} \tag{5.20}$$

The measured rotational acceleration relates to the sensor location in the numerical model. Taking Figure 5.4 to explain the notion, in the following analysis of numerical models, plots with translational acceleration only and translational plus torsional acceleration will be both presented. In Figure 5.4, the acceleration recored in A1 sensor is translation only, while A2 records translation plus torsional acceleration.

Referring to Figure 5.4 and assuming that the torsional acceleration is driven by eccentric mass inertial force, and the eccentricities in X and Y directions are both 5%$\times$ length (or width). The $\ddot{u}_{g\theta}$ can be expressed as:

$$\begin{cases} \ddot{u}_{gy\theta} = m \times (0.05 \times b) \times \ddot{u}_{gx}/I_0 \\ \ddot{u}_{gx\theta} = m \times (0.05 \times d) \times \ddot{u}_{gy}/I_0 \end{cases} \tag{5.21}$$

where: $I_0 \approx m(b^2 + d^2)/12$ for small e_x and e_y

Normally, 5% accidental torsion is demanded in ASCE code for building design. However, after initial testing the numerical model, the 5% torsion only has little effect in frequency spectra and PDI plots. This is unfavorable to observe the impact of torsion in PDI analysis. Thus, in this section, four times larger than the basic demanded torsion is going to be added in the numerical models analysis.

In addition, the parameters of Figure 5.4 and all numerical models are assumed to be:

- $b = d = 1000(cm)$
- $h = 350(cm)$ per story
- fundamental period (sec):
  - $T_{1x} = T_{1y} \approx 0.2\times$ N (No. of stories) for 1,5 & 10-story building
  - $T_{1x} = T_{1y} \approx 0.1\times$ N for 26-story building
- fundamental torsional period (sec):
  - $T_{1t} \approx T_{1x}/1.4$ for 1, 5 & 10-story building;
  - $T_{1t} \approx T_{1x}/1.2$ for 26-story building;
- viscous damping ratio of each mode: 5%
- ground acceleration: The same as considered in Chapter 4.4
  - E-W acceleration: X direction
  - N-S acceleration: Y direction

In the following examples, since the models are symmetric in X-Y plane, the analysis results in X and Y direction should be the same. Therefore, only results in X direction will be shown.

5.6.1 One Story Structure (Torsional Analysis)

Basic Information

1. Model figure: Figure 5.5
2. Spectrum of input acceleration: Figure 5.6-(a)
3. Spectrum of roof response: Figure 5.6-(b)
4. Frequency response function of X direction
   - FRF measured at center(A1 in Fig.5.2) : Figure 5.7-(a)(pure translation)
   - FRF measured at corner(A2 in Fig.5.2) : Figure 5.7-(b)(translation plus torsion)
5. PDI plot of X direction
   - PDI-X measured at center(A1 in Fig.5.2) : Figure 5.8-(a)(pure translation)
   - PDI-X measured at corner(A2 in Fig.5.2) : Figure 5.8-(b)(translation plus torsion)
6. Triple plots(PDI-X+PDI-T+ FRF-X): Figure 5.9
7. Comparison of identification and actual frequencies: Table 5.1
8. Stiffness per story: $12EI/h^3 = 900$
9. Default f_{nx}: 4.77 Hz
10. Default f_{nt}: 6.94 Hz

Identification Result

1. FRF-X plot

(a) FRF-X(pure trans.): 4.76 Hz

The FRF plot is shown as Fig.5.7)-(a). The peak in FRF is a good approximation as default frequency ($f = 4.77$ Hz), and there is one peak only.

(b) FRF-X(torsion): 4.8 Hz

The FRF plot is shown as Fig.5.7)-(b). The peak in FRF is a good approximation as default frequency ($f = 4.77$ Hz), and there is another peak at $f \approx 7$Hz. Since we let $f_{1t} = 6.94$Hz in this numerical model, we know that the second peak indicates the torsional response. Thus, normally, in a LTI building with approximate symmetric plan, the second peak beside the fundamental mode in frequency spectrum can be inferred as the fundamental torsional mode.

2. PDI plot

(a) PDI-X (pure trans.): 4.79 Hz

The PDI plot of pure translation is shown as Figure 5.8-(a). The first zero-crossing point is at 4.79 Hz. The identification results is a good approximation as default numerical model.

(b) PDI-X (trans.+ torsion): 4.80 Hz

The PDI plot of pure translation is shown as Figure 5.8-(b). The first zero-crossing point is at 4.80 Hz. The identification results is a good approximation as default numerical model. Another minor peak occurs at the frequency bandwidth [6$\sim$7]Hz. Since $f_{1t} = 6.94$Hz in this numerical model, it is clear that the fluctuation is caused by added torsion.

(c) PDI-T (torsion): 6.9 Hz

The PDI plot of torsion is shown as Figure 5.9-(b). The default torsional fundamental frequency is 6.94 Hz. Thus, the identification result is pretty good. However, what has to be pointed out is that the sometimes the PDI-T plot only can show a bandwidth range rather than a certain point. In

that case, we have to use other information such as FRF plot or torsional spectrum to help identify the torsional mode.

3. Triple plots (PDI-X + PDI-T +FRF): The triple plots shown as Figure 5.9 can identify the fundamental modes if one follows the procedure described below:

   (a) The first crossing point of (a) and the corresponding peak in (c) indicates the natural frequency of first mode.

   (b) Three indicators: (1) the vertex of the curve near f =7 Hz in (b), (2) the corresponding peak in (c) and (3) the corresponding minor peak in (a) indicate the torsional fundamental frequency.

5.6.2 Five Story Structure (Torsional Analysis)

Basic Information

1. Model figure: Figure 5.10
2. Spectrum of input acceleration: Figure 5.11-(a)
3. Spectrum of roof response: Figure 5.11-(b)
4. Frequency response function of X direction
   - FRF measured at center(A1 in Fig.5.2) : Figure 5.12-(a)(pure translation)
   - FRF measured at corner(A2 in Fig.5.2) : Figure 5.12-(b)(translation plus torsion)
5. PDI plot of X direction
   - PDI-X measured at center(A1 in Fig.5.2) : Figure 5.13-(a)(pure translation)
   - PDI-X measured at corner(A2 in Fig.5.2) : Figure 5.13-(b)(translation plus torsion)

6. Triple plots(PDI-X+PDI-T+ FRF-X): Figure 5.14
7. Comparison of identification and actual frequencies: Table 5.2
8. Stiffness per story: $12EI/h^3 = 400$
9. Default f_{nx}: [0.91, 2.65, 4.17, 5.36, 6.11] Hz
10. Default f_{nt}: [1.36, 3.97, 6.25, 8.03, 9.16] Hz

Identification Result

1. FRF-X plot

   (a) FRF-X(pure trans.): 0.9 Hz

   The FRF plot is shown as Fig.5.12)-(a). The first peak in FRF is a good identification in comparison with the default frequency($f = 0.91$ Hz), and in the FRF, there are three obvious peaks:[0.9, 2.6, 4.2] Hz, while the actual frequencies=[0.91, 2.65, 4.17]

   (b) FRF-X(with torsion): 0.9 Hz

   The FRF plot is shown as Fig.5.12)-(b). The peak in FRF is a good approximation as default frequency ($f = 0.91$ Hz), and there is another blurry peak at $f \approx 1.4$Hz. Since we let $f_{1t} = 1.36$Hz in this numerical model, we know that the second peak indicates the torsional response. However, in this case, the peak can not be clearly identified, so do other torsional modes.

   In $f \approx 4$Hz, there seems a bifurcation occurring in the response peak. Knowing the acted frequencies, we know that it is clear that a mode aliasing between the third translational(4.17 Hz) mode and the second rotational(3.97 Hz) mode is happening.

2. PDI plot

(a) PDI-X (pure trans.): 0.92 Hz

The PDI plot of pure translation is shown as Figure 5.13-(a). The first zero-crossing point is 0.92 Hz. The identification results is a good approximation as default numerical model. There are three obvious zero-crossing points:[0.92, 2.62, 4.23, 5.35], while the actual frequencies=[0.91, 2.65, 4.17, 5.36].

(b) PDI-X (trans.+ torsion): 0.92 Hz

The PDI plot of pure translation is shown as Figure 5.13-(b). The first zero-crossing point is 0.92 Hz. There are three obvious zero-crossing points:[0.92, 2.65, 4.38, 5.32], while the actual frequencies=[0.91, 2.65, 4.17, 5.36].

There is a minor deviation occurring in the third translational mode and we have known the reason from the discussion of FRF in last paragraph. The third translational mode and the second rotational mode make a mode aliasing so that the phase curve is affected.

Another minor peak occurs at the frequency bandwidth [1.2$\sim$1.4]Hz. Since we let $f_{1t} = 1.359$Hz in this numerical model, we know that the fluctuation is caused by added torsion. Nevertheless, the second and after torsional modes can not be observed in this way.

(c) PDI-T (torsion): 1.4 Hz

The PDI plot of torsion is shown as Figure 5.14-(b). The default torsional fundamental frequency is 1.36 Hz. Thus, the identification result is not bad. However, The concave in the torsional PDI curve is rather smoother so it is a rather a little subjective to determine the torsional mode. Similarly, the second torsional mode can be guessed around 4 Hz, but can not be determined definitely.

In $f \approx 6.3$Hz, third concave point is observed which corresponds to the third default natural torsional frequency($f_{t3} = 6.25$Hz)

3. Triple plots (PDI-X + PDI-T + FRF): The triple plots shown as Figure 5.14 can identify the fundamental modes by following the steps described below:

   (a) The first crossing point of (a) and the corresponding peak in (c) indicates the natural frequency of first mode, and the second mode also can be identified successfully. The third mode in (a) is 10% larger than the default frequency, while the (c) plot can not determine the third mode because there is a bifurcation in the peak around $f = 4$Hz.

   (b) Three indicators-(1) the vertex of the curve near f =1.3 Hz in (b), (2) the corresponding peak in (c) and (3) the corresponding minor peak in (a), indicate the torsional fundamental frequency. However, in this case, on the contrary, (a) is a better indicator to tell us where f_t is.

5.6.3 Ten Story Structure (Torsional Analysis)

Basic Information

1. Model figure: Figure 5.15
2. Spectrum of input acceleration: Figure 5.16-(a)
3. Spectrum of roof response: Figure 5.16-(b)
4. Frequency response function of X direction
   - FRF measured at center(A1 in Fig.5.2) : Figure 5.17-(a)(pure translation)
   - FRF measured at corner(A2 in Fig.5.2) : Figure 5.17-(b)(translation plus torsion)
5. PDI plot of X direction
   - PDI-X measured at center(A1 in Fig.5.2) : Figure 5.18-(a)(pure translation)

- PDI-X measured at corner(A2 in Fig.5.2) : Figure 5.18-(b)(translation plus torsion)

6. Triple plots(PDI-X+PDI-T+ FRF-X): Figure 5.19
7. Comparison of identification and actual frequencies: Table 5.3
8. Stiffness per story: $12EI/h^3 = 400$
9. Default f_{nx}: [0.48, 1.42, 2.33, 3.18, 3.97, 4.67, 5.26] Hz (only the first 7 modes listed)
10. Default f_{nt}: [0.67, 2.00, 3.29, 4.50, 5.61] Hz (only the first 5 modes listed)

Identification Result

1. FRF-X plot

   (a) FRF-X(pure trans.): 0.47 Hz

   The FRF plot is shown as Fig.5.17)-(a). The first peak in FRF is a good identification in comparison with the default frequency ($f = 0.48$ Hz), and in the FRF, there are five obvious peaks:[0.47, 1.42, 2.35, 3.17, 3.92] Hz, while the actual frequencies=[0.48, 1.42, 2.33, 3.18, 3.97]

   (b) FRF-X(with torsion): 0.47 Hz

   The FRF plot is shown as Fig.5.17)-(b). The first peak in FRF is a good identification in comparison with the default frequency ($f = 0.48$ Hz), and in the FRF, there are three obvious peaks:[0.47, 1.42, 2.20] Hz, while the actual frequencies=[0.48, 1.42, 2.33]. From previous cases, we know that the dual peaks in frequency spectrum usually means a torsional response occurring. Since we let $f_{1t} = 0.67$Hz in this numerical model, we know that the second peak indicates the torsional response. In this case, the second peak is exactly 0.67 Hz.

2. PDI plot

   (a) PDI-X (pure trans.): 0.5 Hz

   The PDI plot of pure translation is shown as Figure 5.18-(a). The first zero-crossing point is 0.5 Hz. The identification results is close to default numerical model. There are more than five obvious zero-crossing points:[0.5, 1.43, 2.31, 3.2, 3.98, 4.70, 5.21], while the actual frequencies=[0.48, 1.42, 2.33, 3.18, 3.97, 4.67, 5.26].

   (b) PDI-X (trans.+ torsion): 0.5 Hz

   The PDI plot of pure translation is shown as Figure 5.18-(b). The first zero-crossing point is 0.5 Hz. There are five obvious zero-crossing points:[0.5, 1.43, 2.32, 3.15, 4.00, 4.64], while the actual frequencies=[0.48, 1.42, 2.33, 3.18, 3.97, 4.67].

   (c) PDI-T (torsion): 0.67 Hz

   The PDI plot of torsion is shown as Figure 5.19-(b). The default torsional fundamental frequency is 0.67 Hz. Thus, the identification result is very accurate. In addition, the (b) plot also identify $f = [1.98, 3.49]$, which are close to the default second and third modes:f =[2.00, 3.29].

   In this case, another interesting phenomenon can be observed. The Figure 5.19-(a) and (b) are approximately complementary relationship. The downward concaves in (b) plot, such as f =[0.67m 1.98,3.49] have corresponding concaves in plot (a). This similarity can help us to guess the torsional modes, if the PDI-T is not available in other buildings.

3. Triple plots (PDI-X + PDI-T +FRF): The triple plots shown as Figure 5.19 can identify the fundamental modes following the steps described below:

   (a) The first crossing point of (a) and the corresponding peak in (c) indicates the natural frequency of first mode.

(b) Three indicators: (1) the vertex of the curve near f =0.6 Hz in (b), (2) the corresponding peak in (c) and (3) the corresponding minor peak in (a) indicate the torsional fundamental frequency.

(c) The same procedure can also be applied to other higher modes.

5.6.4 Twenty-Six Story Structure (Torsional Analysis)

Basic Information

1. Model figure: Figure 5.20
2. Spectrum of input acceleration: Figure 5.21-(a)
3. Spectrum of roof response: Figure 5.21-(b)
4. Frequency response function of X direction
   - FRF measured at center(A1 in Fig.5.2) : Figure 5.22-(a)(pure translation)
   - FRF measured at corner(A2 in Fig.5.2) : Figure 5.22-(b)(translation plus torsion)
5. PDI plot of X direction
   - PDI-X measured at center(A1 in Fig.5.2) : Figure 5.23-(a)(pure translation)
   - PDI-X measured at corner(A2 in Fig.5.2) : Figure 5.23-(b)(translation plus torsion)
6. Triple plots(PDI-X+PDI-T+ FRF-X): Figure 5.24
7. Comparison of identification and actual frequencies: Table 5.4
8. Stiffness per story: $12EI/h^3 = 1600$

9. Default f_{nx}: [0.38, 1.13, 1.88, 2.62, 3.36, 4.08, 4.79] Hz (only the first 7 modes listed)

10. Default f_{nt}: [0.45, 1.36, 2.25, 3.14, 4.02, 4.89, 5.74] Hz (only the first 7 modes listed)

Identification Result

1. FRF-X plot

   (a) FRF-X(pure trans.): 0.38 Hz

   The FRF plot is shown as Fig.5.22)-(a). The first peak in FRF is a good identification in comparison with the default frequency ($f = 0.38$ Hz), and in the FRF, there are five obvious peaks:[0.38, 1.13, 1.88, 2.61, 3.34] Hz, while the actual frequencies=[0.38, 1.13, 1.88, 2.62, 3.36]

   (b) FRF-X(with torsion): 0.37 Hz

   The FRF plot is shown as Fig.5.22)-(b). The first peak in FRF is a good identification in comparison with the default frequency ($f = 0.38$ Hz), and in the FRF, there are three obvious peaks:[0.37, 1.14, 1.89] Hz, while the actual frequencies=[0.38, 1.13, 1.88]. From previous cases, we know that the dual peaks in frequency spectrum usually means a torsional response occurring. Since we set $f_{1t} = 0.45$Hz in this numerical model, we know that the second peak indicates the torsional response. In this case, the second peak is 0.46 Hz, very close to the default torsional fundamental mode.

2. PDI plot

   (a) PDI-X (pure trans.): 0.38 Hz

   The PDI plot of pure translation is shown as Figure 5.23-(a). The first

zero-crossing point is 0.38 Hz. The identification results is equal to default numerical model. There are seven obvious zero-crossing points:[0.38, 1.14, 1.89, 2.62, 3.39, 4.04, 4.82], while the actual frequencies=[0.38, 1.13, 1.88, 2.62, 3.36, 4.08, 4.79].

(b) PDI-X (trans.+ torsion): 0.47 Hz

The PDI plot of pure translation is shown as Figure 5.23-(b). The first zero-crossing point is 0.47 Hz. There are seven obvious zero-crossing points:[0.47, 1.15, 1.89, 2.63, 3.45, 4.08, 4.81], while the actual frequencies=[0.38, 1.13, 1.88, 2.62, 3.36, 4.08, 4.79].

Here, we can find that with the effect of torsion, there is a larger deviation occurring in the first zero-crossing point. The first apparent zero-crossing point actually not the real first mode, but the aliasing mode misled by first torsional mode. Because f_{1x} and f_{1t} are too close, the PDI curve can not separate them apart. Such phenomenon will also occurs in other high rise buildings. Thus, to solve the problem, we can use FRF plot to be an auxiliary information for identification. In high rise buildings, the first mode should be determined by the FRF peak rather than the zero-crossing point in PDI plot.

(c) PDI-T (torsion): 0.47 Hz

The PDI plot of torsion is shown as Figure 5.24-(b). The default torsional fundamental frequency is 0.45 Hz. Thus, the identification result is very close. In addition, the (b) plot also identify $f = [1.38, 2.28, 3.15]$, which are also close to the default second and third modes:f =[1.36, 2.25, 3.14].

3. Triple plots (PDI-X + PDI-T +FRF): The triple plots shown as Figure 5.24 can identify the fundamental modes by following thinking procedures:

(a) The first crossing point of (a) and the corresponding peak in (c) indicates the natural frequency of first mode. If the two plot are not consistent in the first mode, in high rise building, the FRF plot would be more accurate.

(b) Three indicators: (1) the vertex of the curve near f =0.4 Hz in (b), (2) the corresponding peak in (c) and (3) the corresponding minor peak in (a) indicate the torsional fundamental frequency.The concave in (b), the corresponding peak in (c) and the corresponding minor peak in (a) indicates the torsional fundamental frequency.

(c) The same procedure can also be applied to other higher modes.‘’

5.7 Conclusion

1. In the studied numerical models, the following are observed about the FRF curves:

   (a) In pure translational analysis, the FRF curves are smooth, and the first few peaks of FRF would be exactly identical to the default natural frequencies.

   (b) If the input is the combination of translation and 5% eccentric torsion, the ideal FRF would be blurred, and rapid variations appear everywhere in the FRF curves.

2. In a typical, symmetric-plan building of LTI system, if there is a dual-peak in the first mode response in the FRF curve, the first peak is usually the translational mode while the second one is the torsional mode. However, this judgment should be double checked by PDI plots.

3. If the FRF curves is blurred by a small amount of torsion, it is difficult to identify the third and following higher modes by peak-picking method. It can be inferred that if a very clear FRF from some building is obtained, the torsion might be small enough to be neglected.

4. In the numerical model studies, the following are found about PDI curves:

   (a) In pure translational analysis, the PDI curves are smooth, and the zero-crossing points of FRF would be exactly identical to the default natural

frequencies. In addition, the PDI curve can detect more modes than the FRF curve.

(b) If the PDI curves are for responses influenced by a small amount of torsion, compared to pick-peaking method it is still possible to identify the third and following higher modes, but in some specific mode where the torsion mode and translational mode are very close, the error would be larger than 10%.

5. In the PDI curve of translation plus torsion, small downward or upward changes would appear and correspond to the torsional modes in PDI-T curve.

6. In the PDI-T(torsion) plot, the apparent local vertex in the PDI curve can be inferred as a torsional mode, and this can be double checked by PDI-X curve(corresponding small concaves) or FRF curves(corresponding bigger frequency response).

7. In high-rise buildings, if the corresponding frequency of the first zero-crossing point of PDI curve is larger than the peak in FRF:

   (a) The first-zero-crossing point in PDI is inferred as the first torsional mode.

   (b) The first peak in FRF is inferred as the first translational mode.

Table 5.1.
Torsion analysis of 1-story system (earthquake input)

Mode Order	**No.**	**Actual freq. (Hz)**	**PDI (Trans.+Torsion) (Hz)**	**Error %**
1	f_{1x}	4.77	4.8	0.63
2	f_{1t}	6.94	6.9	0.58

Related PDI plots are shown in Fig.5.8∼ Fig.5.9

Table 5.2.
Torsion analysis of 4-story system (earthquake input)

Mode Order	**No.**	**Actual freq. (Hz)**	**PDI (Trans.+Torsion) (Hz)**	**Error %**
1	f_{1x}	0.91	0.92	1.1
	f_{1t}	1.36	1.4	2.94
2	f_{2x}	2.65	2.65	0
	f_{2t}	3.97	4	0.76
3	f_{3x}	4.17	4.38	5.04
	f_{3t}	6.25	6.3	0.8
4	f_{4x}	5.36	6.25	0.75
	f_{4t}	8.03	-	-
5	f_{5x}	6.11	-	-
	f_{5t}	9.16	-	-

Related PDI plots are shown in Fig.5.13∼ Fig.5.14

Table 5.3.
Torsion analysis of 10-story system (earthquake input)

Mode Order	**No.**	**Actual freq. (Hz)**	**PDI (Trans.+Torsion) (Hz)**	**Error** %
1	f_{1x}	0.48	0.5	4.17
	f_{1t}	0.67	0.67	0
2	f_{2x}	1.42	1.43	0.7
	f_{2t}	2.00	1.98	1
3	f_{3x}	2.33	2.32	0.43
	f_{3t}	3.29	3.49	6.08
4	f_{4x}	3.18	3.15	0.94
	f_{4t}	4.50	-	-
5	f_{5x}	3.97	4.00	0.76
	f_{5t}	5.61	-	-
6	f_{6x}	4.67	4.64	0.64
	f_{6t}	-	-	-

Related PDI plots are shown in Fig.5.18∼ Fig.5.19

Table 5.4.
Comparison of identification results of 10-DOF system (earthquake input)

Mode Order	**No.**	**Actual freq. (Hz)**	**PDI (Trans.+Torsion) (Hz)**	**Error %**
1	f_{1x}	0.38	0.47	23.68
	f_{1t}	0.45	0.47	4.44
2	f_{2x}	1.13	1.15	1.77
	f_{2t}	1.36	1.38	1.47
3	f_{3x}	1.88	1.89	0.53
	f_{3t}	2.25	2.28	1.33
4	f_{4x}	2.62	2.63	0.38
	f_{4t}	3.14	3.15	0.32
5	f_{5x}	3.36	3.45	2.68
	f_{5t}	4.02	-	-
6	f_{6x}	4.08	4.08	0
	f_{6t}	4.89	-	-
7	f_{7x}	4.79	4.81	0.42
	f_{7t}	5.74	-	-

Related PDI plots are shown in Fig.5.23$\sim$ Fig.5.24

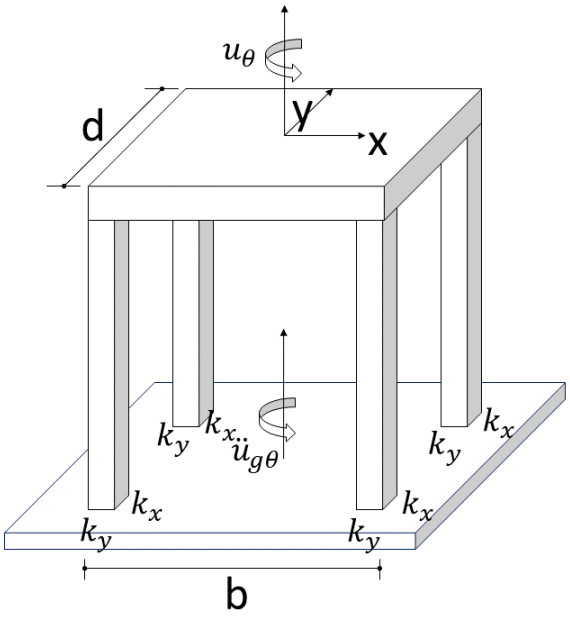

Fig. 5.1. Pure torsion acts on a simple typical structure. [10]

acts

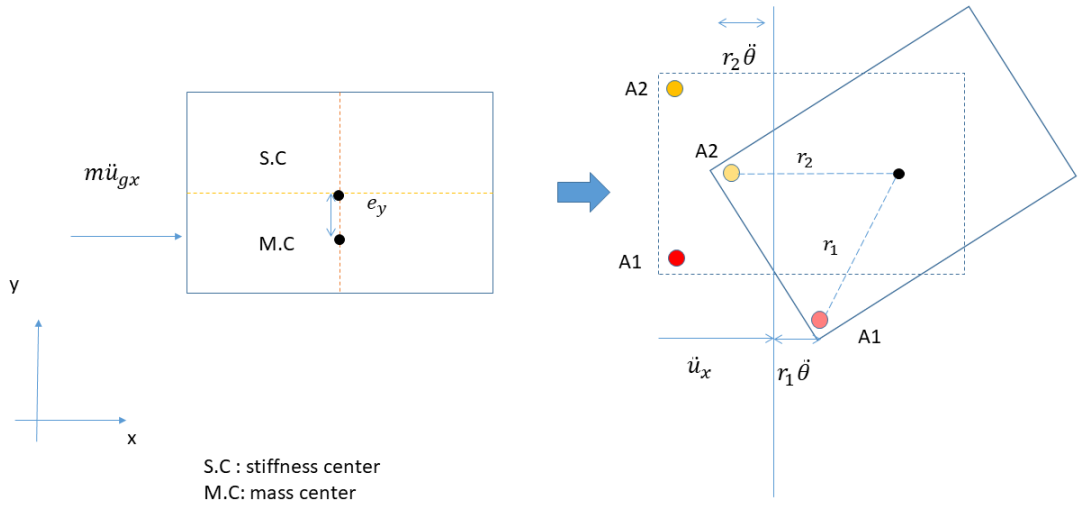

Fig. 5.2. Top view of a simple structure under earthquake and eccentric torsion

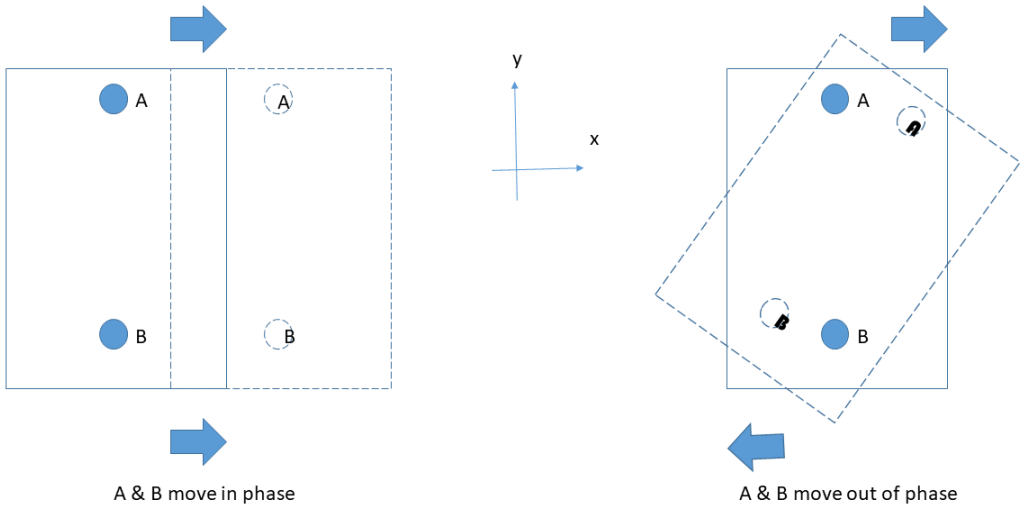

Fig. 5.3. Phase concept in the torsion identification

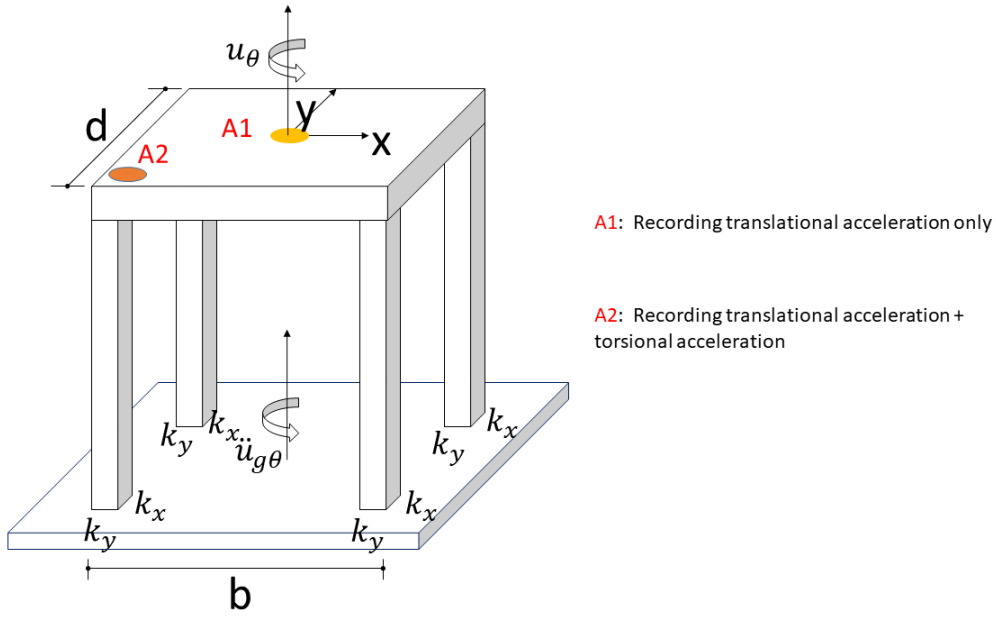

Fig. 5.4. Sensor locations of a 1-story numerical model(torsion analysis).

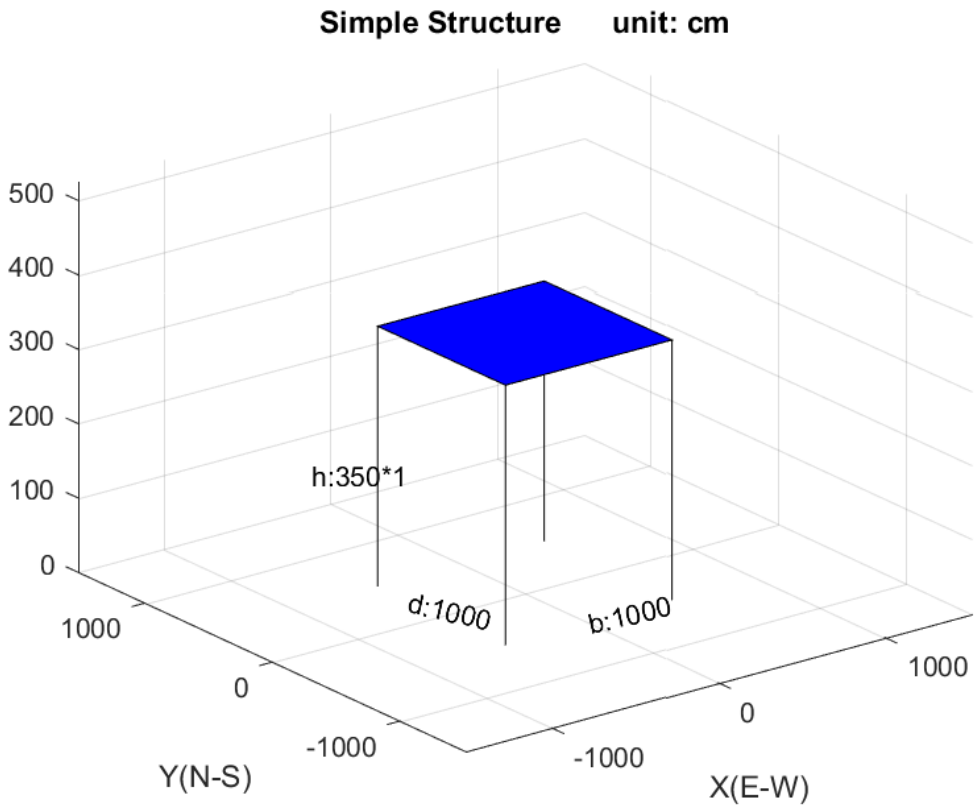

Fig. 5.5. One story structure model (Torsion analysis)

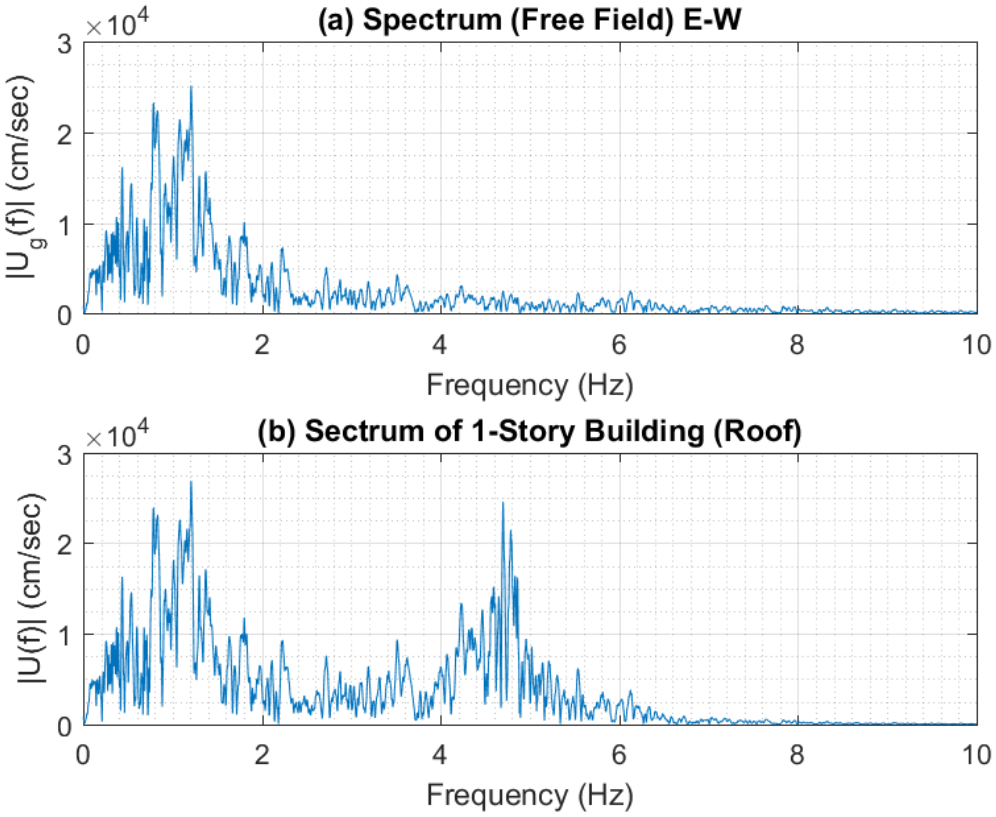

Fig. 5.6. One story structure (torsion analysis)-(a) Spectrum of input ground acceleration. (b) Spectrum of roof response

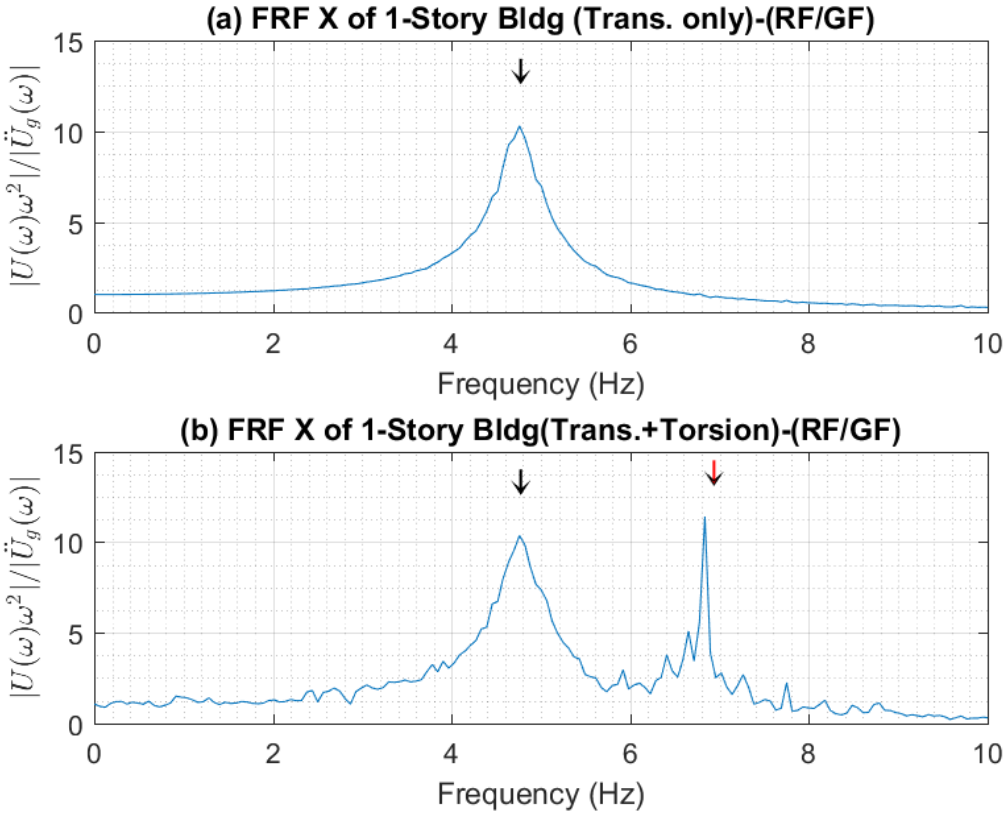

Fig. 5.7. FRF of one story structure (Torsion analysis) (a) Translation. (b)Translation + Rotation. In the two plots, arrow marks are added to help target the actual modes of the system. The black arrows point at the translational modes, and the red arrow points at the torsional mode. In Fig.-(a), the peak of the curve represents the fundamental translational mode of the system. In Fig.-(b), in addition to the first peak, a 2nd peak appears, representing the torsional fundamental mode. However, a slightly deviation between the actual mode and the 2nd peak.

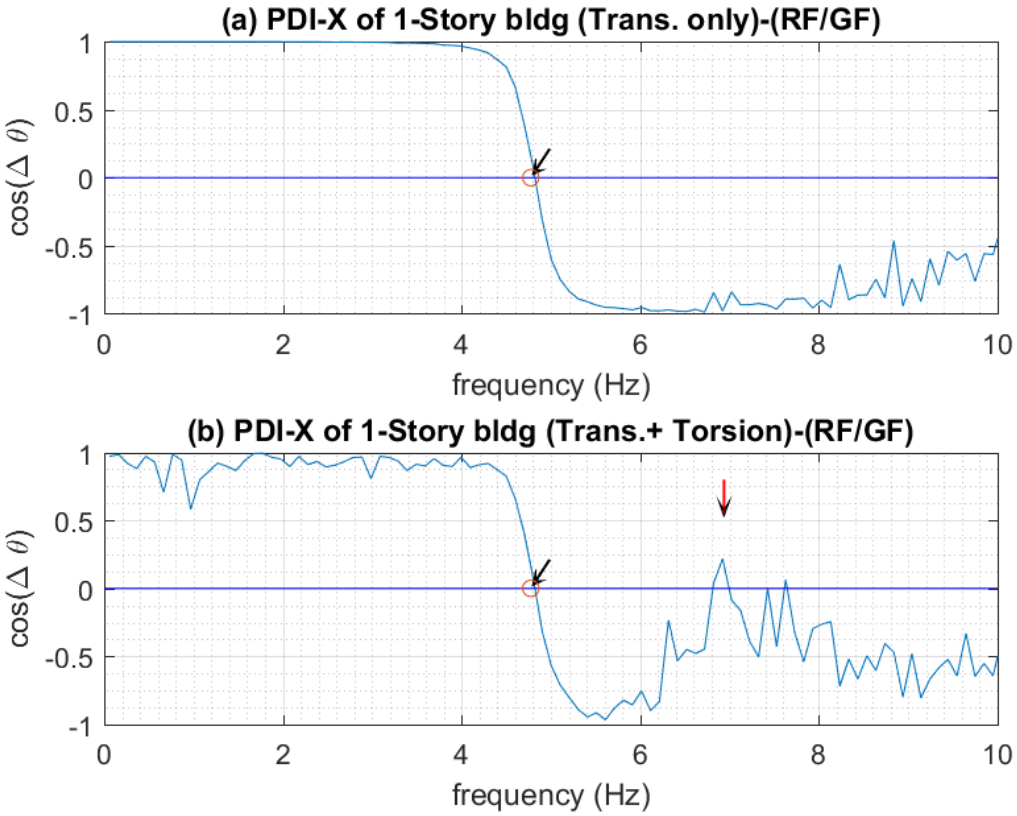

Fig. 5.8. PDI of one story structure (Torsion analysis) (a) Translation. (b)Translation + Rotation. In the two plots, arrow marks are added to help target the actual modes of the system. The black arrows point at the translational modes, and the red arrow points at the torsional mode. In Fig.-(a), the zero-crossing point represents the fundamental translational mode of the system. In Fig.-(b), the sudden peak in the range of $f = 6 \sim 8$ Hz is caused by torsion. This characteristic can be used to detect the torsional mode.

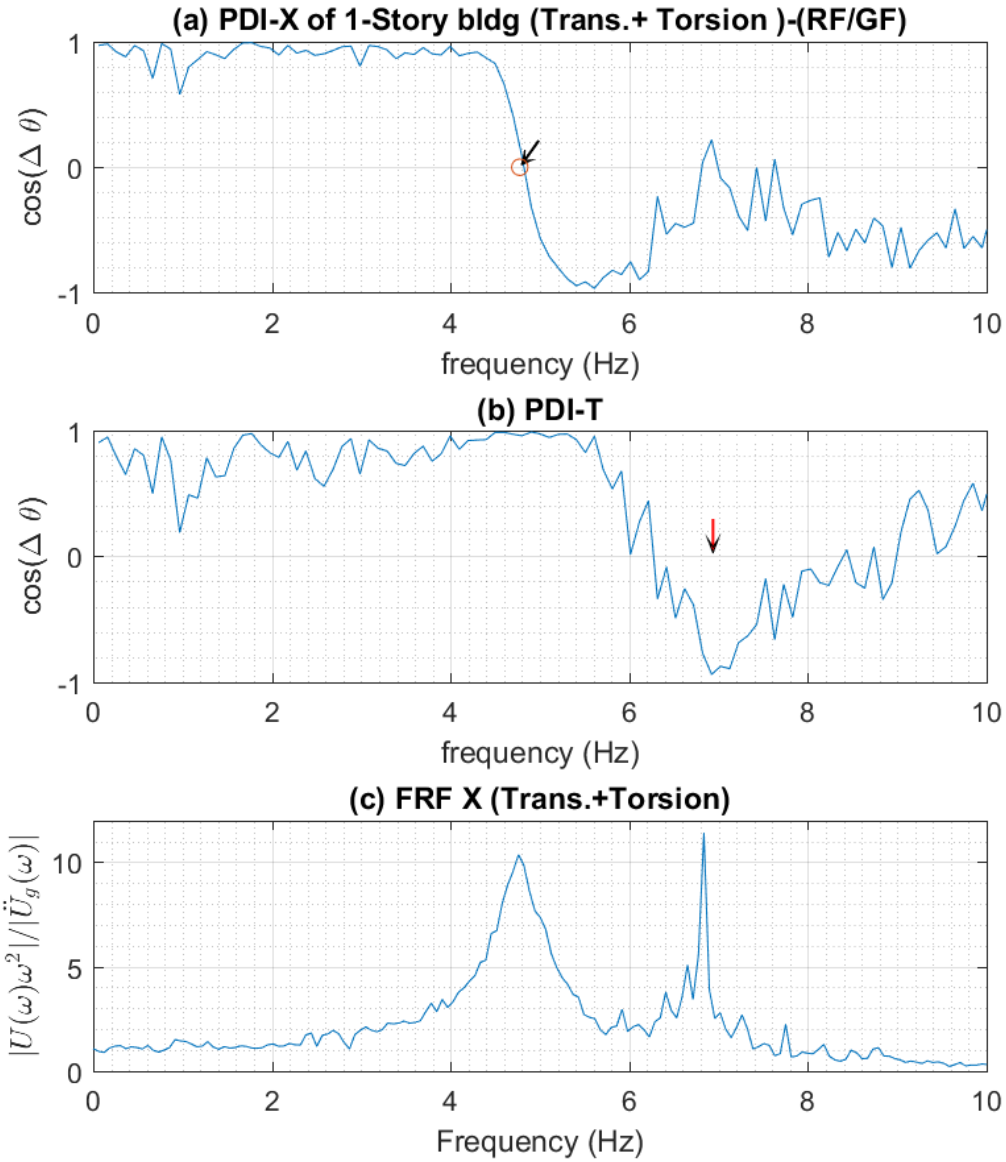

Fig. 5.9. PDI-X + PDI-T +FRF plots of one story structure (Torsion analysis) (a) PDI-X, (b) PDI-T, (c) FRF-X. In (a) and (b) plots, arrow marks are added to help target the actual modes of the system. The black arrow points at the translational modes, and the red arrow points at the torsional mode.

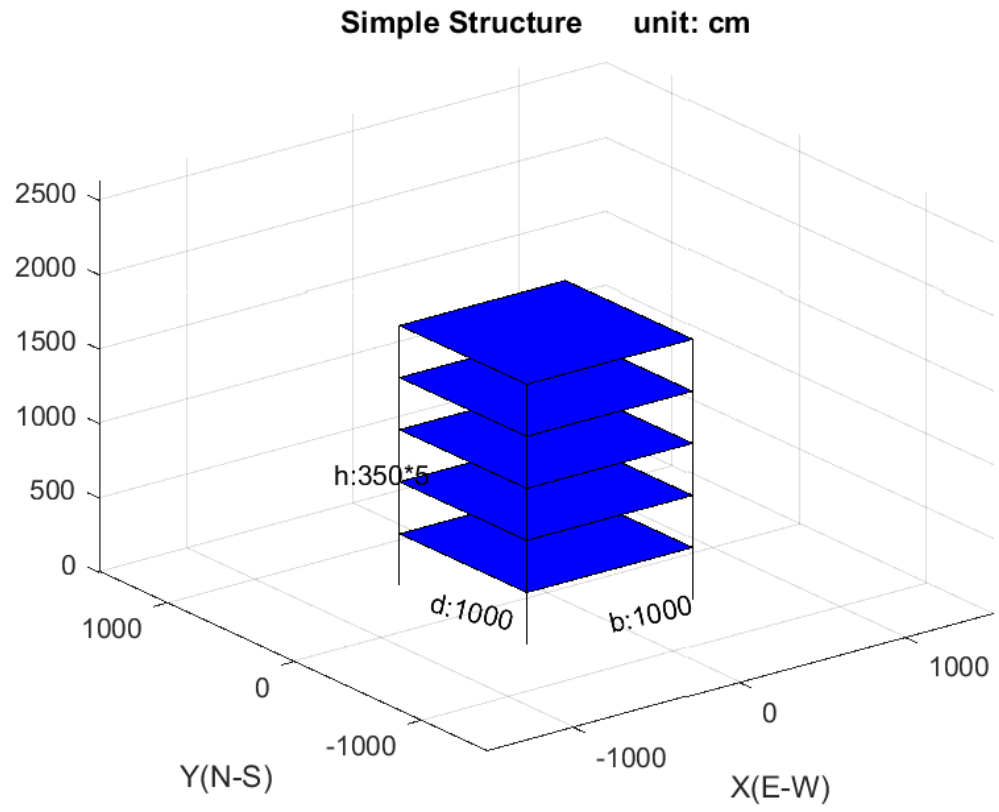

Fig. 5.10. 5 story structure model (Torsion analysis)

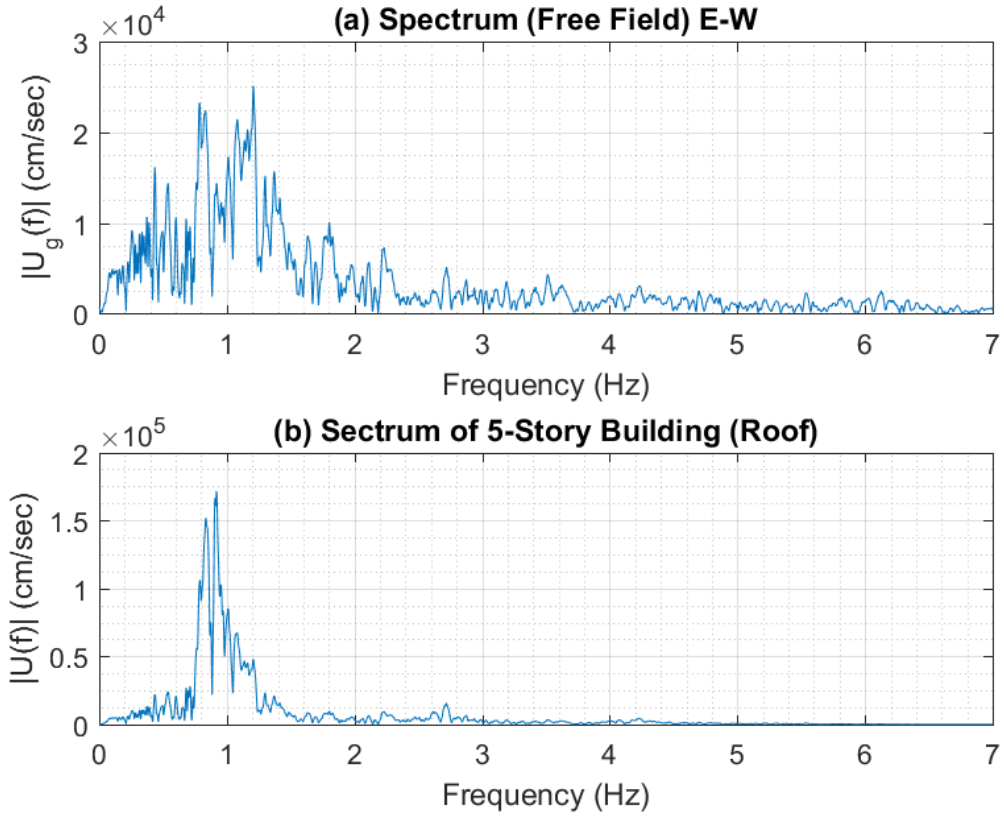

Fig. 5.11. 5-story structure (torsion analysis)-(a) Spectrum of input ground acceleration. (b) Spectrum of roof response

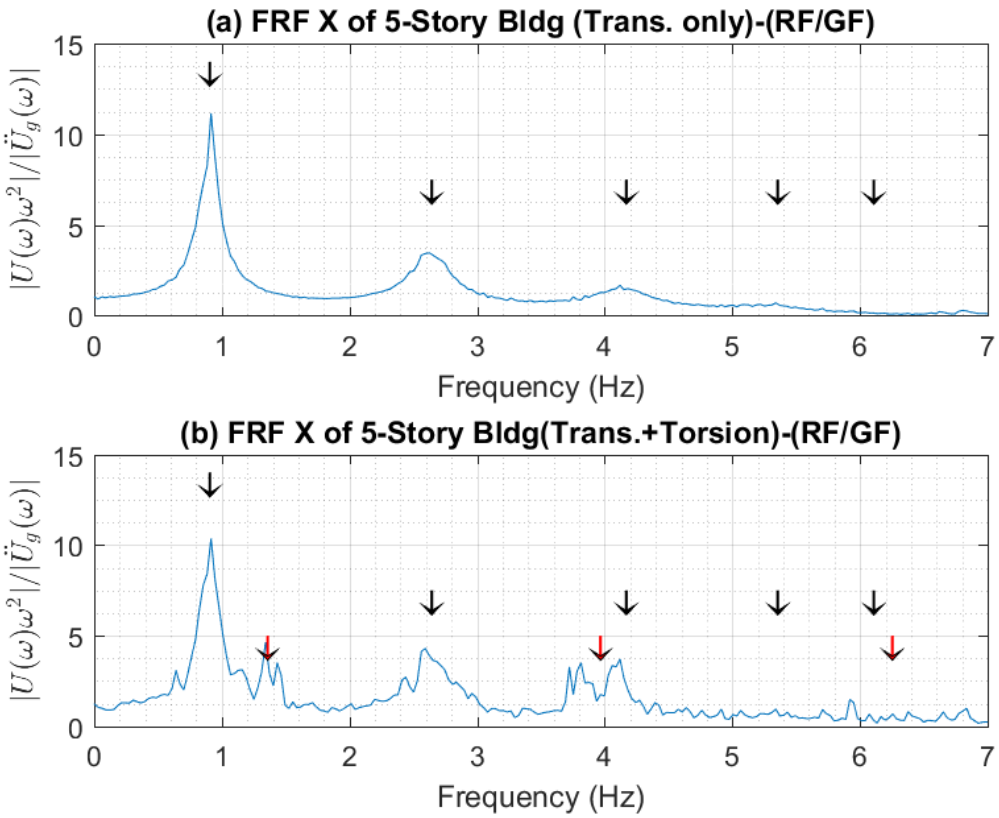

Fig. 5.12. FRF of 5-story structure (Torsion analysis) (a) Translation. (b)Translation + Rotation. In the two plots, arrow marks are added to help target the actual modes of the system. The black arrows point at the translational modes, and the red arrows point at the torsional modes. In Fig.-(a), the peak of the curve represents the fundamental translational modes of the system. In Fig.-(b), small torsion blurs the FRF curve, making it more difficult to identify the translational and torsional modes.However, the small peak in the range of $f = 1.2 \sim 1.4$ Hz can be regarded as the first torsional mode. Thus, it is possible to detect the 1st torsional mode by FRF curve.

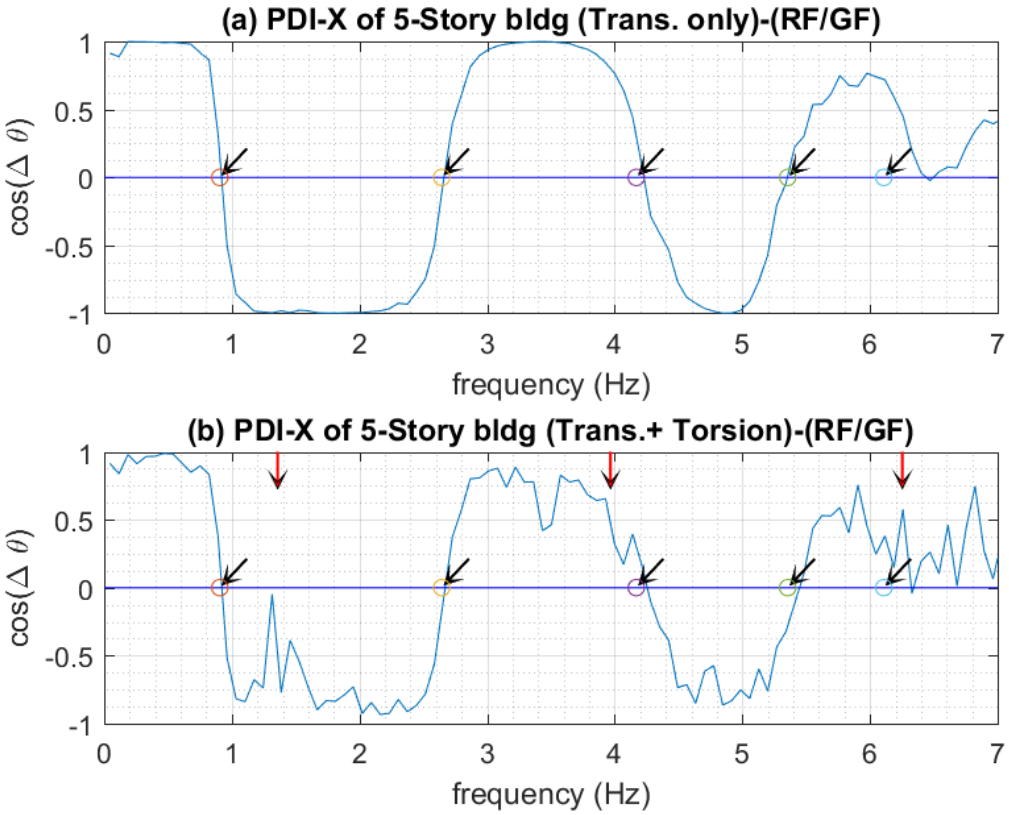

Fig. 5.13. PDI of 5-story structure (Torsion analysis) (a) Translation. (b)Translation+Rotation. In the two plots, arrow marks are added to help target the actual modes of the system. The black arrows point at the translational modes, and the red arrows point at the torsional mode. In Fig.-(a), the zero-crossing points represent the fundamental translational modes of the system. The first four modes are accurate, while the last one is not correct. In Fig.-(b), the sudden peak in the range of $f = 1.2 \sim 1.4$ Hz is caused by torsion. This characteristic can be used to detect the first torsional mode. However, the higher torsional modes are mixed with translational modes and hard to detect.

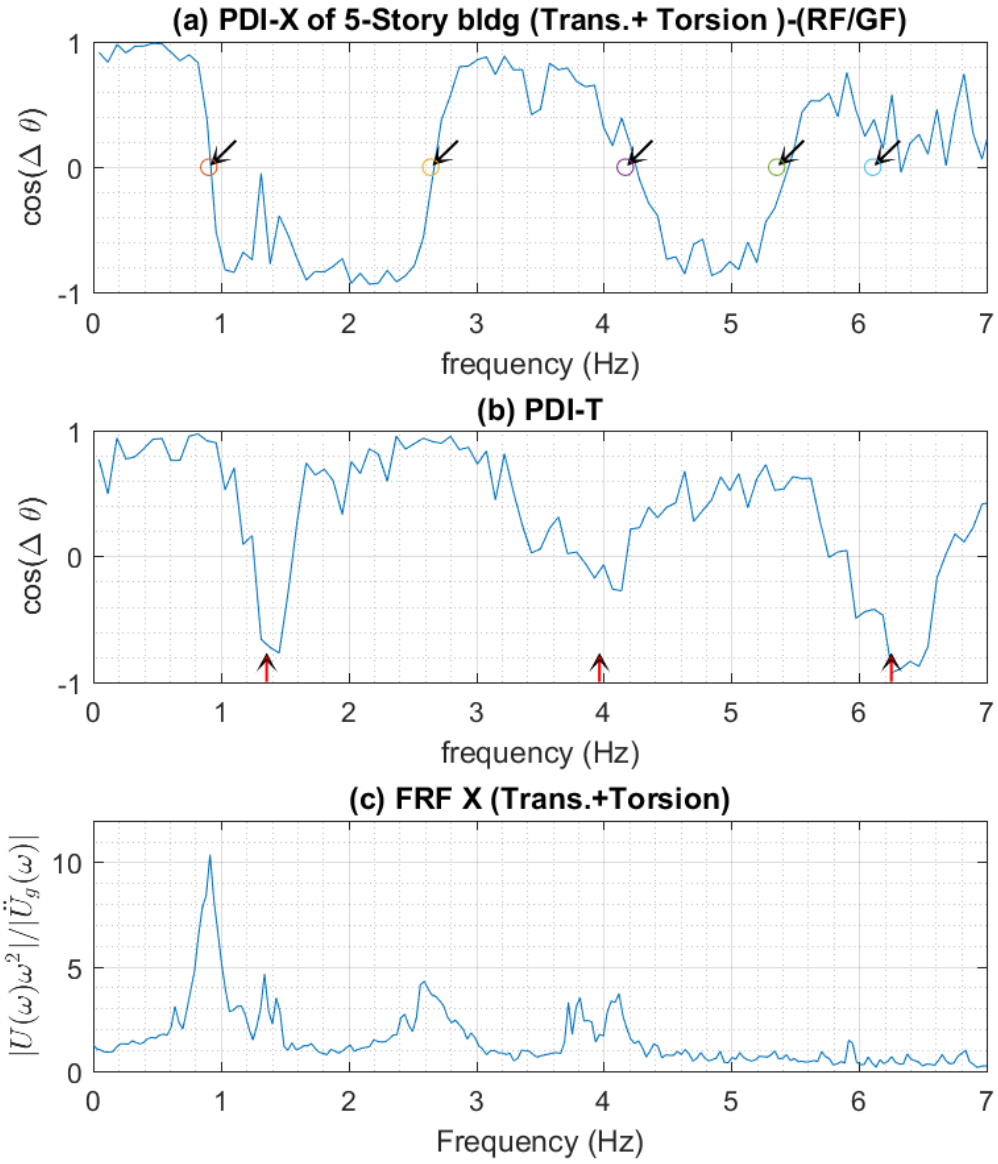

Fig. 5.14. PDI-X + PDI-T + FRF plots of 5-story structure (Torsion analysis) (a) PDI-X, (b) PDI-T, (c) FRF-X. In (a) and (b) plots, the black arrows point at the translational modes, and the red arrows point at the torsional mode. In this case, converging results can not be detected in PDI-T plot for torsional modes, but credible frequency ranges still can be obtained.

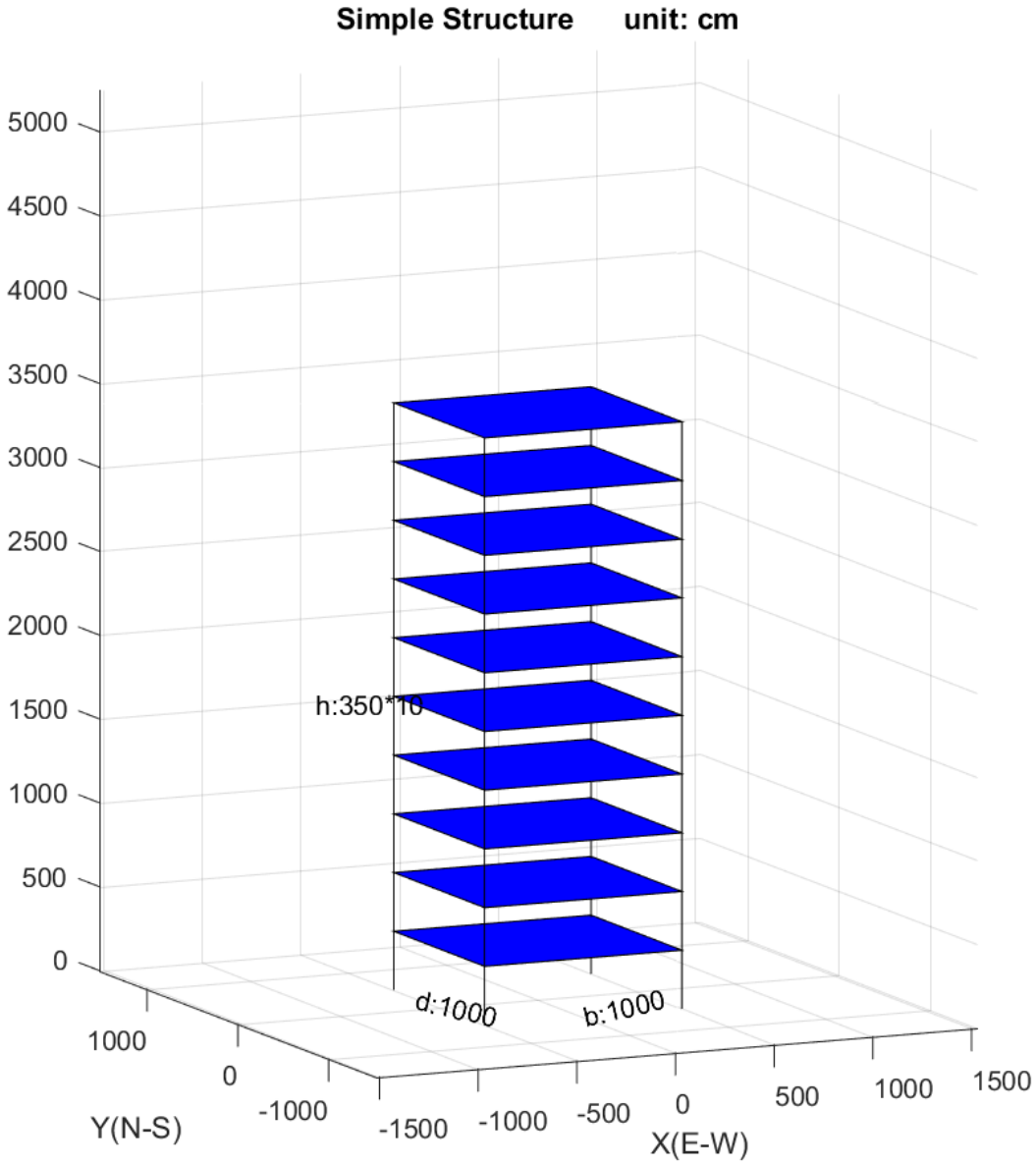

Fig. 5.15. 10-story structure model(Torsion analysis)

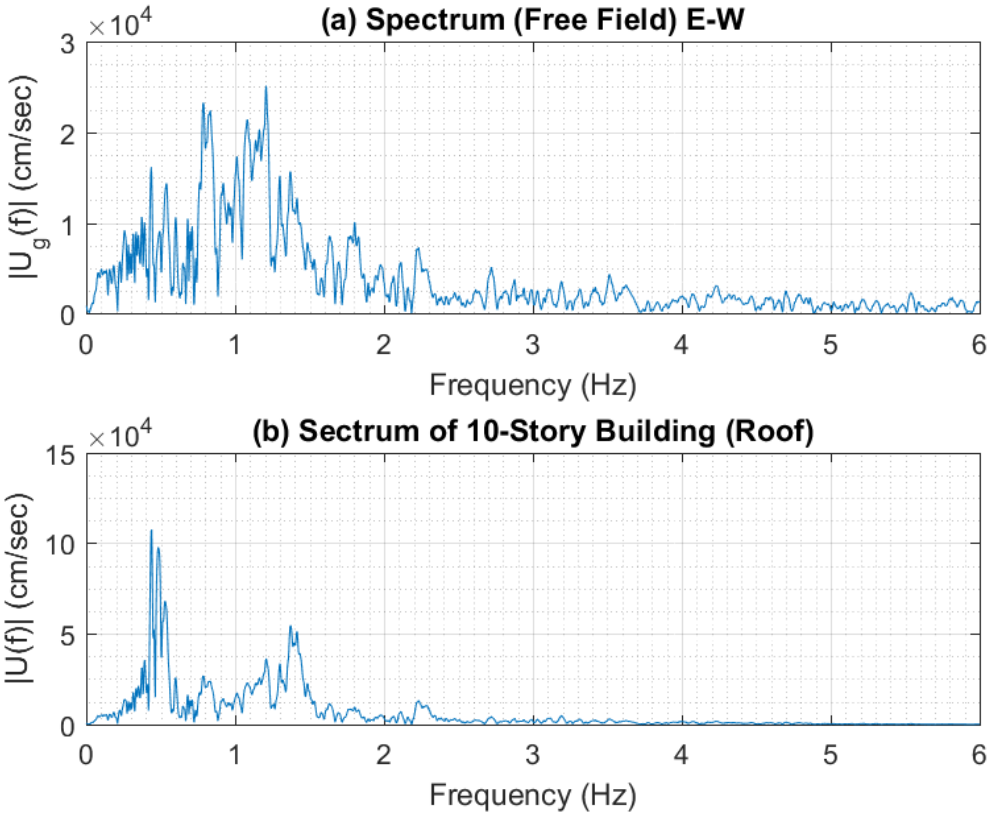

Fig. 5.16. 10-story structure (torsion analysis)-(a) Spectrum of input ground acceleration. (b) Spectrum of roof response

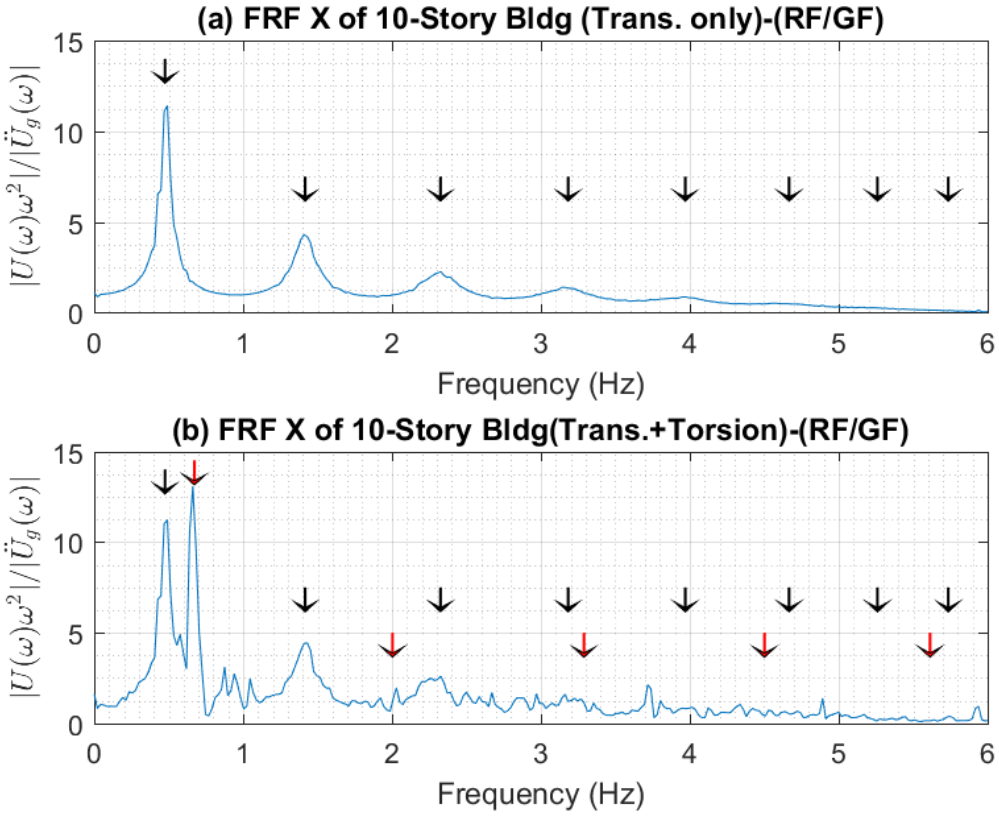

Fig. 5.17. FRF of 10-story structure (Torsion analysis) (a) Translation. (b)Translation + Rotation. In the two plots, arrow marks are added to help target the actual modes of the system. The black arrows point at the translational modes, and the red arrows point at the torsional modes. In Fig.-(a), the peak of the curve represents the fundamental translational modes of the system. In Fig.-(b), small torsion blurs the FRF curve, making it more difficult to identify the translational and torsional modes. However, the peak in the range of $f = 0.6 \sim 0.7$ Hz can be regarded as the first torsional mode.

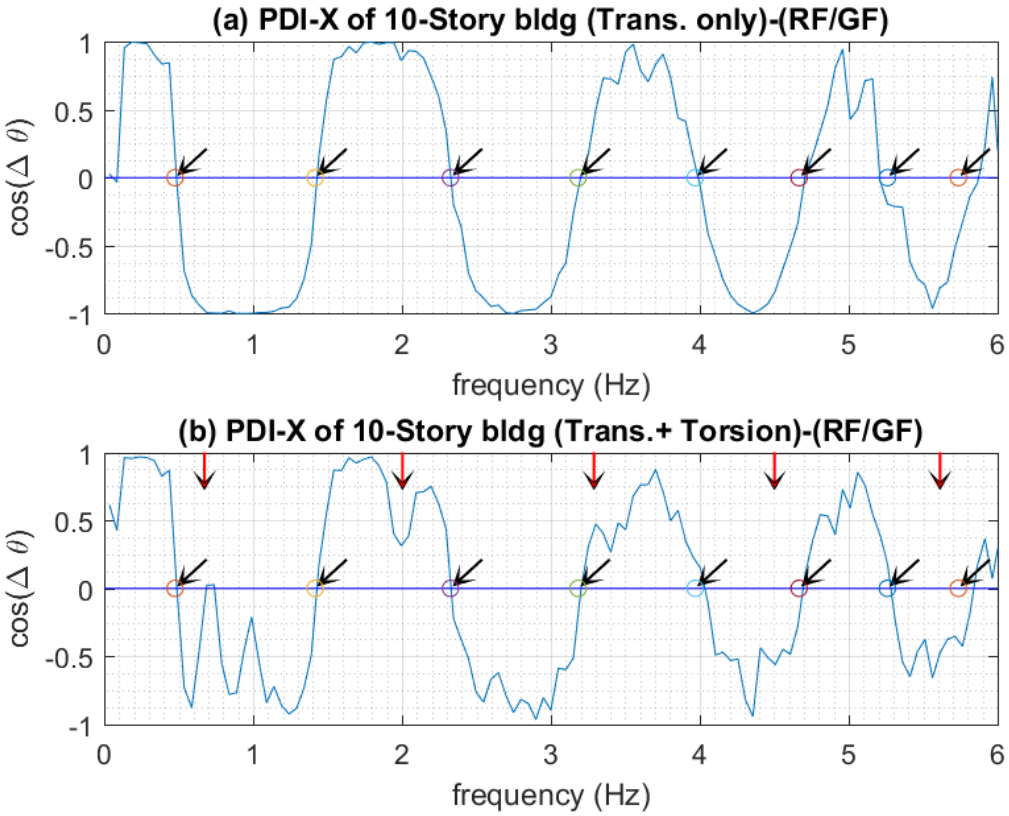

Fig. 5.18. PDI of 10-story structure (Torsion analysis) (a) Translation. (b)Translation + Rotation. In the two plots, arrow marks are added to help target the actual modes of the system. The black arrows point at the translational modes, and the red arrows point at the torsional modes. In Fig.-(a), the zero-crossing points represent the fundamental translational modes of the system. The first six modes are accurate, while the next two are a little deviated. In Fig.-(b), the sudden peak in the range of $f = 0.7$ Hz is caused by torsion. The 2nd mode may be identified because a variation occurs. However, the higher torsional modes are mixed with translational modes and hard to detect.

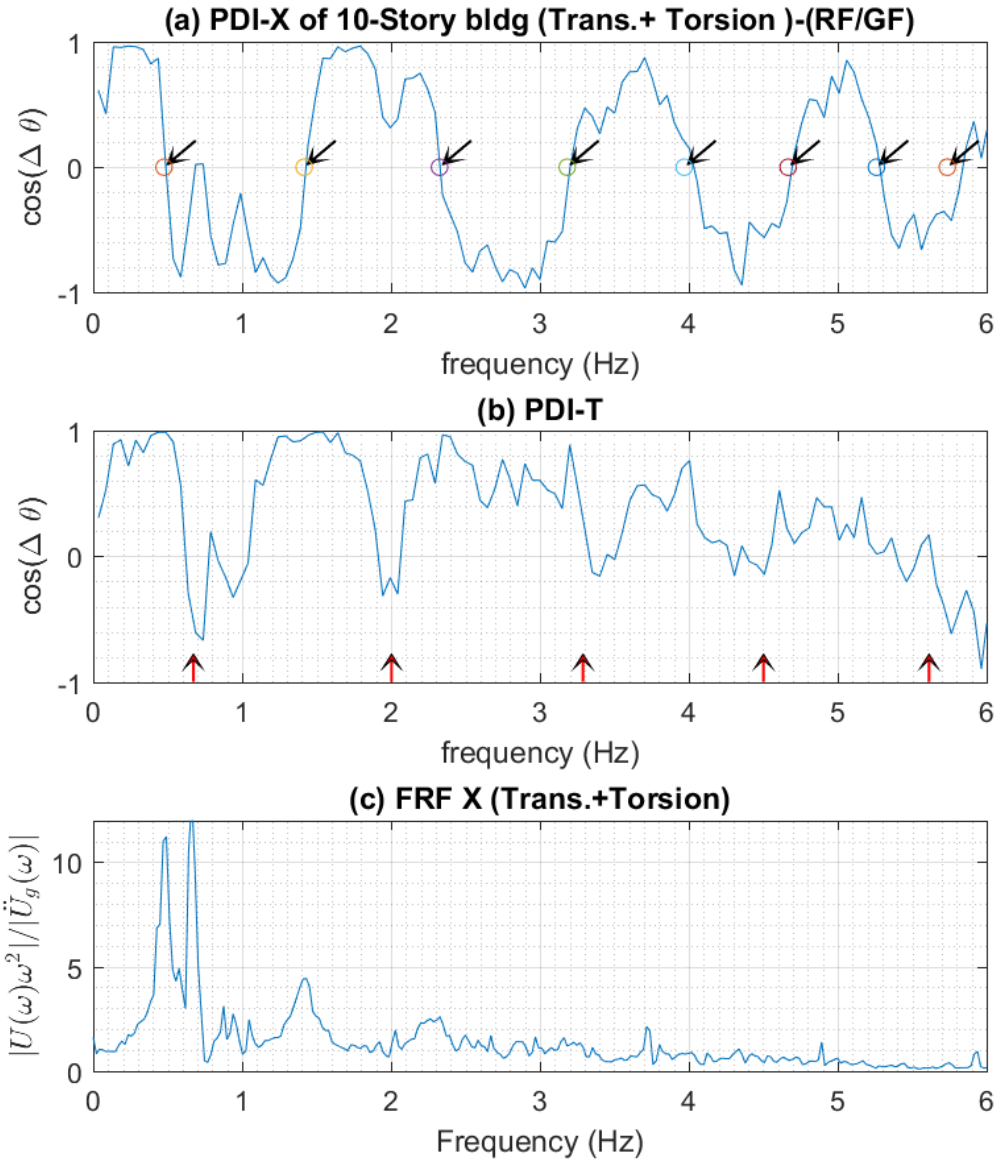

Fig. 5.19. PDI-X + PDI-T + FRF plots of 10-story structure (Torsion analysis) (a) PDI-X, (b) PDI-T, (c) FRF-X. In (a) and (b) plots, the black arrows point at the translational modes, and the red arrows point at the torsional mode. In this case, converging results can not be detected in PDI-T plot for torsional modes. but credible frequency ranges still can be obtained.

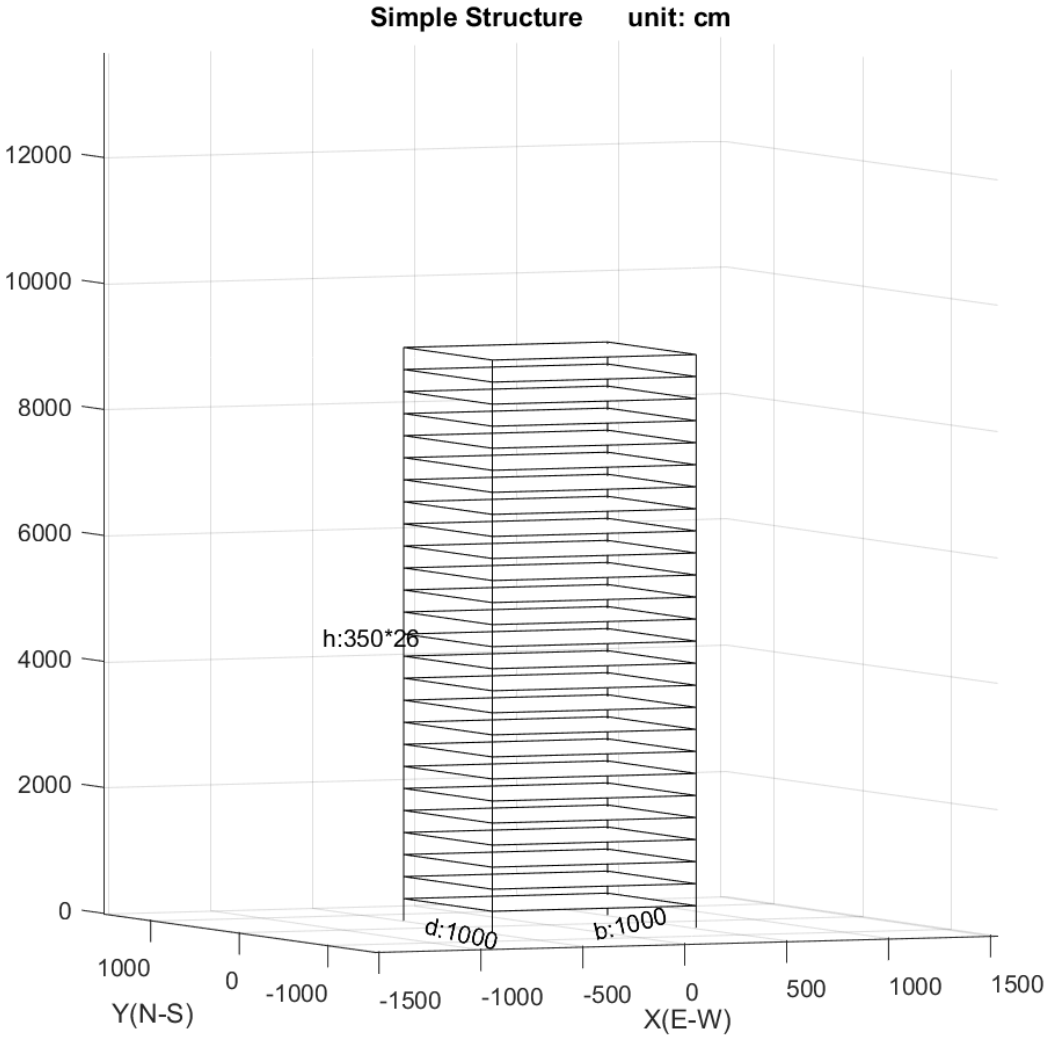

Fig. 5.20. 26-story structure model (Torsion analysis)

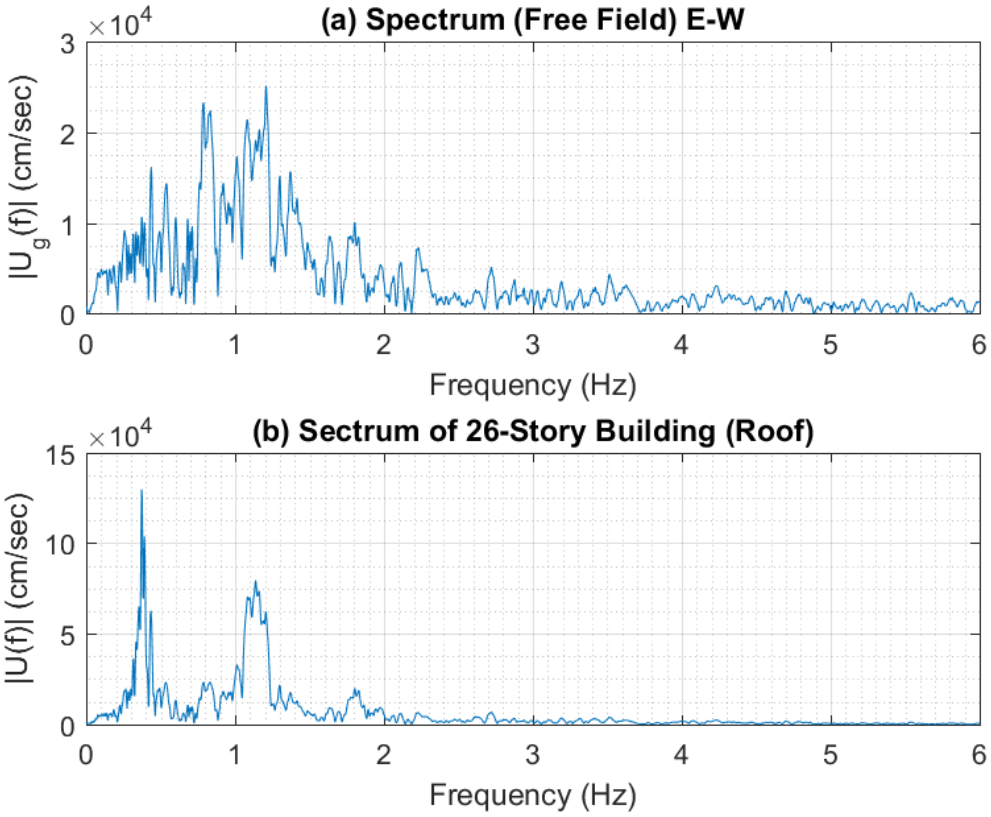

Fig. 5.21. 26-story structure (torsion analysis)-(a) Spectrum of input ground acceleration. (b) Spectrum of roof response

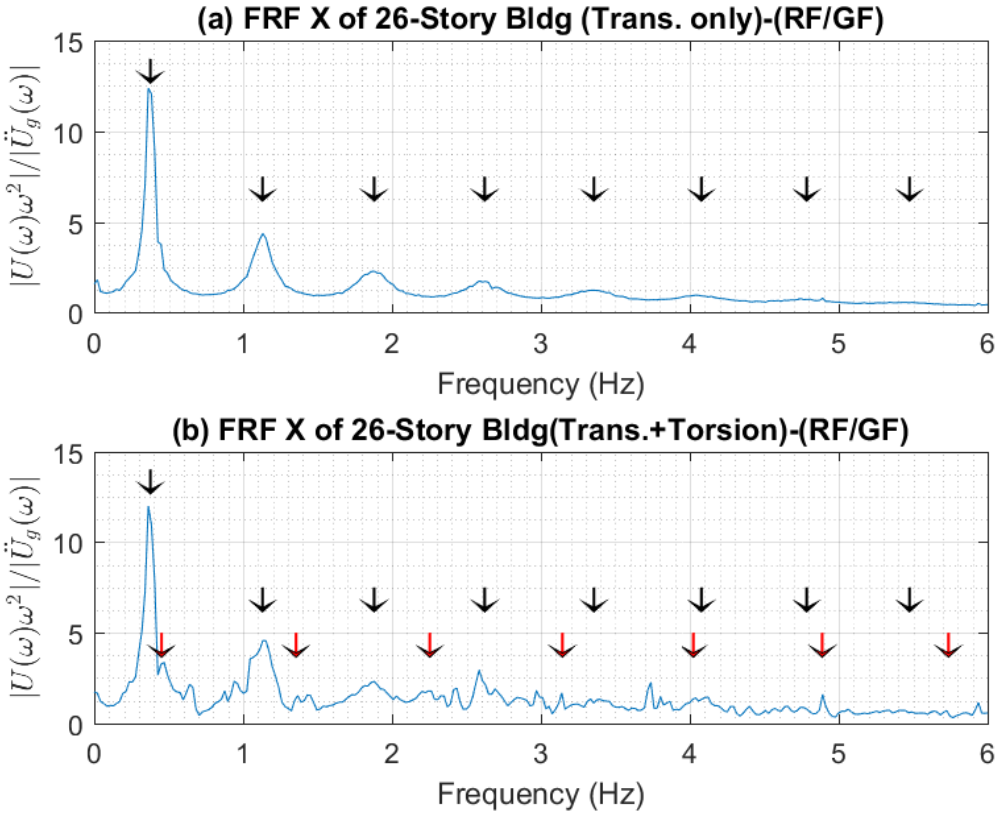

Fig. 5.22. FRF of 26-story structure (Torsion analysis) (a) Translation. (b)Translation + Rotation. In the two plots, arrow marks are added to help target the actual modes of the system. The black arrows point at the translational modes, and the red arrows point at the torsional modes. In Fig.-(a), the peak of the curve represents the fundamental translational modes of the system. In Fig.-(b), small torsion blurs the FRF curve, making it more difficult to identify the translational and torsional modes. Because the the first torsional mode and translational mode are too close, it is even harder to detect this using FRF plot.

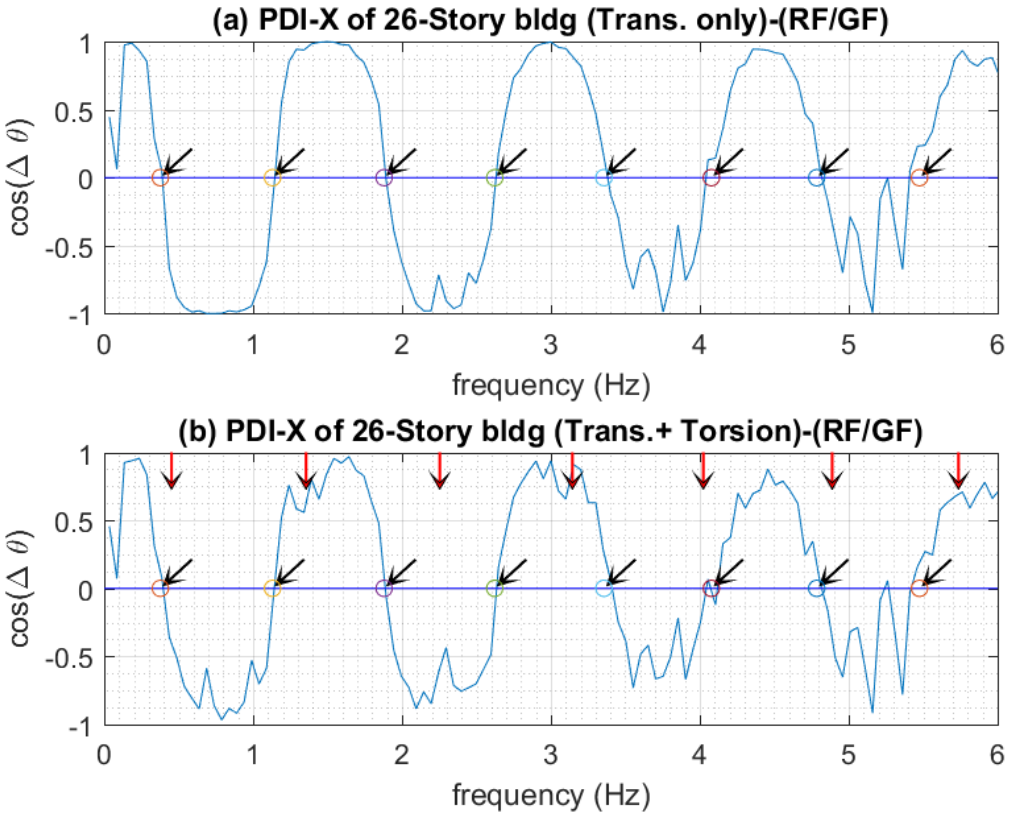

Fig. 5.23. PDI of 26-story structure (Torsion analysis) (a) Translation. (b)Translation + Rotation. In the two plots, arrow marks are added to help target the actual modes of the system. The black arrows point at the translational modes, and the red arrows point at the torsional modes. In Fig.-(a), the zero-crossing points represent the fundamental translational modes of the system. The first seven modes are accurate, while the next one are a little deviated. In Fig.-(b), although the red arrows point at the torsional modes, the PDI curve is blurred and no torsional mode can be detected.

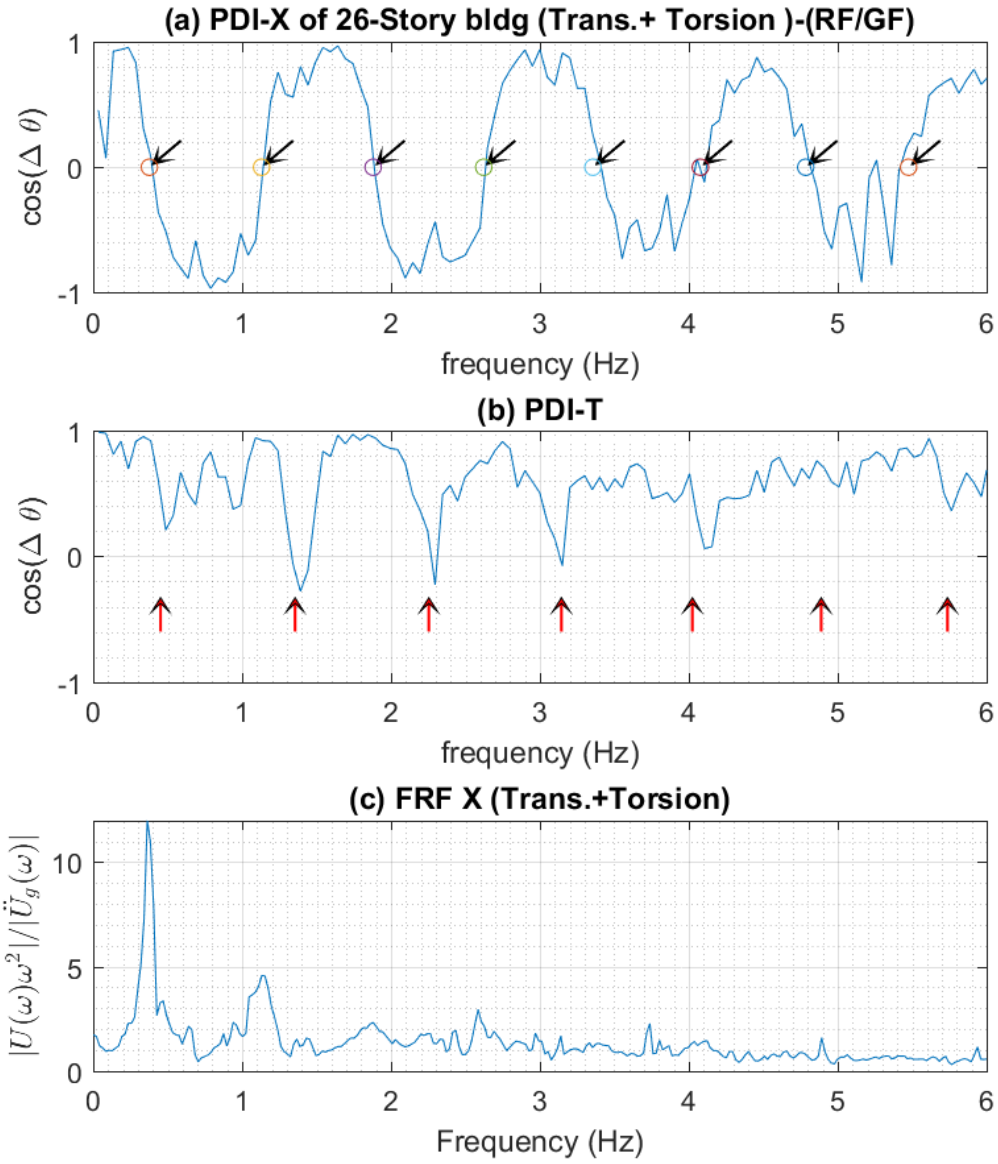

Fig. 5.24. PDI-X + PDI-T + FRF plots of 26-story structure (Torsion analysis) (a) PDI-X, (b) PDI-T, (c) FRF-X. In (a) and (b) plots, the black arrows point at the translational modes, and the red arrows point at the torsional mode. In this case, converging results for torsional modes can be obtained. Although there are slight deviations, it seems tolerable for practical application.

6. CASE STUDY I - PDI ANALYSIS OF SAMPLE BUILDINGS IN U.S.

6.1 Introduction

In this chapter, five actual buildings in U.S.with strong ground motion records are studied to test the PDI analysis. All of the information on the buildings and acceleration records were obtained from the "Center for Engineering Strong Motion Data" website [21]. These five buildings are chosen based on the following criteria:

1. The acceleration records at both horizontal directions on the roof, on any lower floor(2F is preferable), and at ground are available.
2. At least one pair of accelerometers, pointing to the same direction at the roof(or any upper floor) is available.
3. The selected buildings fall in a wide range of height.
4. System identification results from other sources are available.

6.2 Analysis Procedure

The selected five buildings, ranging from 6 to 54 stories are listed in Table 6.1. The basic information of each building are listed in from Table 6.2 to Table 6.6. All of them experienced the 1994 Mw 6.7 Northridge earthquake [23]. Northridge earthquake records from each building were used to test the PDI analysis. All cases include the following information:

1. Identify the frequency in one of the principal plan direction of the building(X-direction, or E-W direction) by three figures:

(a) Draw the PDI plot(Roof/Ground) in X direction:

The obvious zero-crossing points of PDI curve are considered to be the natural frequencies in X direction.

(b) Draw the PDI plot(Roof/2F(or other story)) in X direction:

Although the PDI curve of (Roof/2F) cannot point out the natural frequencies directly, it can divide the frequency domain into several zones which point out the possible bandwidth of each mode. Thus, this kind of PDI curve is also a useful tool for reference.

(c) Draw the FRF in X direction:

The FRF curve can help us to identify the natural frequency. Most of the time, peak picking is the most convenient method to pinpoint the first mode(fundamental mode).

2. Identify the frequency in the other principal plan direction of the building(Y direction) by three figures:

   The procedures is identical to the one used for the X direction.

3. Identify the torsional frequency by two figures:

   The requirement to draw the PDI curve for torsion is that at least a pair of accelerometers installed on the roof (or upper story) are available. Furthermore, these accelerometers must be on the opposite side with respect to the stiffness center on that floor. If one of the accelerometers is close to the stiffness center of the building, it would be difficult to observe the relative motion and phase difference in frequency domain.

   (a) Draw the PDI plot of torsion:

   In each case, two sets of accelerometers are selected to draw the PDI plots. Basically, one pair is in X direction while another pair should be in Y direction. If only one direction is available on the roof, another pair in a different story, if available, is also an option.

(b) Draw the torsional mode spectrum:

In section 5.4, the torsional spectrum is defined as the difference between the frequency spectra of two accelerometers on the same floor. Normally, there should be three obvious peaks in the torsional spectrum which represent the natural modes in X, Y and Rotation. Therefore, when compared the two plots from response in two principal plan direction together, it is possible to identify the torsional mode of the building.

4. Compare PDI-based results with those from other existing system identification work:

Multiple methods are able to identify the natural modes of a building. In order to verify the utility of PDI, results compared provided by PDI plots with results presented in other work. All five buildings were investigated after the 1994 Northridge earthquake. Structural identification results for them are given in a report by Naeim et al. [24] in 2005. In particular, the identified periods presented are relevant. The report mainly focuses on the first mode period of each building. Thus, the comparison are also focused on the first mode while other identified higher modes by PDI plots are still listed.

6.3 Analysis Results

6.3.1 PDI method vs. Other Methods

The five buildings were analyzed by two methods: PDI method and Peak-Picking method. In addition, research works by Naeim et al. [24] in 2005 and Rahmani [25] were cited for comparison. The results are shown in Table 6.7, Table 6.8, Table 6.9, Table 6.10, and Table 6.11. The results were also illustrated by Fig. 6.1. The average difference between PDI method and other method or research works is only 3%. The detailed discussions and PDI figures are collected in Appendix C.

6.3.2 Higher modes to First Mode Frequency Ratios

The natural frequencies ratio of a rigid diaphragm moment resisting frame building is close to a shear beam model, and the ratio is close to 1:3:5.....$2i-1$(i=1.....n) [25]. Therefore, the ratio of frequencies higher modes to that of the first mode can be used to check the identification results. The results of f_{ix}/f_{1x}, f_{iy}/f_{1y} and f_{it}/f_{1t} are also listed in Table 6.7, Table 6.8, Table 6.9, Table 6.10, and Table 6.11, and the results are illustrated by Fig. 6.2. The results approximately match the shear beam model. However, the larger deviations occur in the X direction of Station 24643. It is because in Station 24643, X-braced steel frames are installed in the transverse direction. The behavior of the structure in X direction may be close to a bending beam.

Table 6.1.
Selected buildings and earthquake event in U.S. structure array

NO.	STATION NO.	STATION NAME	NUMBER OF STORIES	EVENT
1	24468	L.A - CSULA Admin. Bldg.	8	Northridge-17Jan1994
2	13589	Newport Beach - Hospital	11	”
3	24629	L.A - Office Bldg.	54	”
4	24655	L.A - Parking Structure	6	”
5	24643	L.A - Office Bldg.	19	”

Table 6.2.
Basic Information of CSMIP-STATION-24468

No.	**Topic**	**Description**
1	Station No.	CSMIP-STATION-24468
2	Location	34.0664 N , 118.1691 W
3	Number of Stories (above/below) Ground	8/1
4	Typical Floor Dimensions	63'-2" x 154'
5	Vertical Load Carrying System	Reinforced concrete slab, beams and columns.
6	Lateral Force Resisting System	Concrete shear walls except between levels 1 and 2 where concrete and steel columns resist lateral forces.
7	Accel. Record for Identification	Northridge-17Jan1994-CE24468P
8	Accel. Peak	Ground: 0.17 g Building: 0.25 g
9	Max. Roof Drift(cm)	10.24
10	Max. Roof Drift Ratio(%)	0.3
11	Sensor Location	Fig. C.1

Table 6.3.
Basic Information of CSMIP-STATION-13589

No.	**Topic**	**Description**
1	Station No.	CSMIP-STATION-13589
2	Location	33.6243 N , 117.9304 W
3	Number of Stories (above/below) Ground	11/0
4	Typical Floor Dimensions	88' x 147'
5	Vertical Load Carrying System	Base to 3rd floor: reinforced concrete columns and walls supporting beams and concrete slab floors. 4th floor to roof: concrete columns and walls supporting concrete flat slab floors with drop panels at supports.
6	Lateral Force Resisting System	Perimeter concrete shear walls (10" to 14" thick) with openings. The north, east and west walls are stepped at the 3rd floor, but the south wall is continuous throughout the height of the building.
7	Accel. Record for Identification	Northridge-17Jan1994-CE13589P
8	Accel. Peak	Ground: 0.08 g Building: 0.26 g
9	Max. Roof Drift(cm)	2.69
10	Max. Roof Drift Ratio(%)	0.06
11	Sensor Location	Fig. C.6

Table 6.4.
Basic Information of CSMIP-STATION-24629

No.	**Topic**	**Description**
1	Station No.	CSMIP-STATION-24629
2	Location	34.0483 N , 118.2617 W
3	Number of Stories (above/below) Ground	54/4
4	Typical Floor Dimensions	196'x121' to 156'x121'
5	Vertical Load Carrying System	Concrete slab (2.5" thick) over 3" steel deck with welded metal studs, supported by steel frames. The spans between columns vary from about 10' to 47".
6	Lateral Force Resisting System	Moment resisting perimeter steel frame (framed tube) with 10' column spacing. There are Virendeel trusses and 48 inch deep transfer girders at the 36th and 46th floors where vertical setbacks occur.
7	Accel. Record for Identification	Northridge-17Jan1994-CE24629P
8	Accel. Peak	Ground: 0.14 g Building: 0.19 g
9	Max. Roof Drift(cm)	16.76
10	Max. Roof Drift Ratio(%)	0.09
11	Sensor Location	Fig. C.11

Table 6.5.
Basic Information of CSMIP-STATION-24655

No.	**Topic**	**Description**
1	Station No.	CSMIP-STATION-24655
2	Location	34.0211 N , 118.2903 W
3	Number of Stories (above/below) Ground	6/0
4	Typical Floor Dimensions	259 x 306 ft (73.2 x 33.5 m)
5	Vertical Load Carrying System	Concrete slabs supported on precast concrete beams and columns.
6	Lateral Force Resisting System	Six cast-in-place concrete shear walls in the N/S direction and two cast-in-place concrete shear walls in E/W direction.
7	Accel. Record for Identification	Northridge-17Jan1994-CE13589P
8	Accel. Peak	Ground: 0.29 g Building: 1.21 g
9	Max. Roof Drift(cm)	6.99
10	Max. Roof Drift Ratio(%)	0.34
11	Sensor Location	Fig. C.16

Table 6.6.
Basic Information of CSMIP-STATION-24643

No.	**Topic**	**Description**
1	Station No.	CSMIP-STATION-24643
2	Location	34.0595 N , 118.4177 W
3	Number of Stories (above/below) Ground	19/4
4	Typical Floor Dimensions	240 x 110 ft (73.2 x 33.5 m)
5	Vertical Load Carrying System	4.5”(11.4 cm) concrete slabs supported on steel frames.
6	Lateral Force Resisting System	Moment resisting steel frames in the longitudinal and X-braced steel frames in the transverse direction.
7	Accel. Record for Identification	Northridge-17Jan1994-CE13589P
8	Accel. Peak	Ground: 0.32 g Building: 0.65 g
9	Max. Roof Drift(cm)	30.92
10	Max. Roof Drift Ratio(%)	0.93
11	Sensor Location	Fig. C.21

Table 6.7.
Comparison of identification results of CSMIP-STATION-24468

Mode Order	**No.**	**PDI plot (Hz)**	f_i/f_1	**Peak-Picking (Hz)**	**Ref. [24] (Hz)**
1st	f_{1x}	0.64	1.0	0.64	0.65
	f_{1y}	0.64	1.0	0.59$\sim$ 0.62	0.62
	f_{1t}	0.80	1.0	-	-
2nd	f_{2x}	1.84	2.9	-	-
	f_{2y}	2.00	3.1	-	-
	f_{2t}	2.30	2.9	-	-
3^{rd}	f_{3x}	4.04	6.3	-	-
	f_{3y}	4.2	6.6	-	-
	f_{3t}	-	-	-	-

Related PDI plots are shown in Fig.C.2$\sim$ Fig.C.5

Table 6.8.
Comparison of identification results of CSMIP-STATION-13589

Mode Order	**No.**	**PDI plot (Hz)**	f_i/f_1	**Peak-Picking (Hz)**	**Ref. [24] (Hz)**
1st	f_{1x}	1.24	1	1.15	1.18
	f_{1y}	1.41	1	1.34	1.35
	f_{1t}	2.00	1	-	-
2nd	f_{2x}	3.85	3.1	3.80	-
	f_{2y}	4.55	3.2	4.70	-
	f_{2t}	5.80	2.9	-	-
3^{rd}	f_{3x}	5.91	4.8	-	-
	f_{3y}	7.95	5.6	-	-
	f_{3t}	-		-	-

Related PDI plots are shown in Fig.C.7$\sim$ Fig.C.10

Table 6.9.
Comparison of identification results of CSMIP-STATION-24629

Mode Order	**No.**	**PDI plot (Hz)**	f_i/f_1	**Peak-Picking (Hz)**	**Ref. [24] (Hz)**	**Rahmani 2014 (Hz) [25]**
1st	f_{1x}	0.18	1	0.18	0.17	0.192
	f_{1y}	0.16	1	0.15	0.16	0.162
	f_{1t}	0.37	1	-	-	0.360
2nd	f_{2x}	0.53	2.9	0.52	-	0.527
	f_{2y}	0.52	3.3	0.49	-	0.500
	f_{2t}	0.98	2.6	-	-	0.936
3^{rd}	f_{3x}	0.85	4.7	0.85	-	0.842
	f_{3y}	0.86	5.4	0.82	-	0.822
	f_{3t}	1.48	4.0	-	-	1.483
4^{th}	f_{4x}	1.21	6.7	1.22	-	1.196
	f_{4y}	1.21	7.6	1.16	-	1.168
	f_{4t}	2.10	5.7	-	-	2.042
5^{th}	f_{5x}	1.57	8.7	1.52	-	1.530
	f_{5y}	1.55	9.7	1.46	-	1.510
	f_{5t}	2.55	6.9	-	-	2.508
6^{th}	f_{6x}	2.00	11.1	-	-	1.960
	f_{6y}	1.89	11.8	-	-	1.828
	f_{6t}	3.25	8.8	-	-	3.200
7^{th}	f_{7x}	2.50	13.9	-	-	-
	f_{7y}	2.35	14.7	-	-	-
	f_{7t}	-	-	-	-	-
8^{th}	f_{8x}	2.80	15.6	-	-	-
	f_{8y}	2.74	17.1	-	-	-
	f_{8t}	-	-	-	-	-
9^{th}	f_{9x}	3.18	17.7	-	-	-
	f_{9y}	3.02	18.9	-	-	-
	f_{9t}	-	-	-	-	-

Related PDI plots are shown in Fig.C.12∼ Fig.C.15

Table 6.10.
Comparison of identification results of CSMIP-STATION-24655

Mode Order	**No.**	**PDI plot (Hz)**	f_i/f_1	**Peak-Picking (Hz)**	**Ref. [24] (Hz)**
1st	f_{1x}	1.95	1	$1.9 \sim 2$	1.89
	f_{1y}	2.60	1	2.4	2.50
	f_{1t}	2.50	1	-	-
2nd	f_{2x}	5.70	2.9	-	-
	f_{2y}	-	-	-	-
	f_{2t}	6.55	2.6	-	-

Related PDI plots are shown in Fig.C.17$\sim$ Fig.C.20

Table 6.11.
Comparison of identification results of CSMIP-STATION-24643

Mode Order	**No.**	**PDI plot (Hz)**	f_i/f_1	**Peak-Picking (Hz)**	**Ref. [24] (Hz)**
1st	f_{1x}	0.30	1	0.29	0.347
	f_{1y}	0.23	1	0.24	0.254
	f_{1t}	0.23	1	-	-
2nd	f_{2x}	1.23	4.1	1.21	-
	f_{2y}	0.72	3.1	0.70	-
	f_{2t}	0.97	4.2	-	-
3^{rd}	f_{3x}	2.58	8.6	2.61	-
	f_{3y}	1.28	5.6	1.19	-
	f_{3t}	2.00	8.7	-	-
4^{th}	f_{4x}	3.83	12.8	-	-
	f_{4y}	1.77	7.7	-	-
	f_{4t}	3.08	13.4	-	-
5^{th}	f_{5x}	4.78	15.9	-	-
	f_{5y}	2.33	10.1	-	-
	f_{5t}	-		-	-
6^{th}	f_{6x}	-	-	-	-
	f_{6y}	2.87	12.5	-	-
	f_{6t}	-		-	-
7^{th}	f_{7x}	-		-	-
	f_{7y}	3.47	15.1	-	-
	f_{7t}	-		-	-
8^{th}	f_{8x}	-		-	-
	f_{8y}	4.19	18.2	-	-
	f_{8t}	-		-	-
9^{th}	f_{9x}	-		-	-
	f_{9y}	4.71	20.5	-	-
	f_{9t}	-		-	-

Related PDI plots are shown in Fig.C.22$\sim$ Fig.C.25

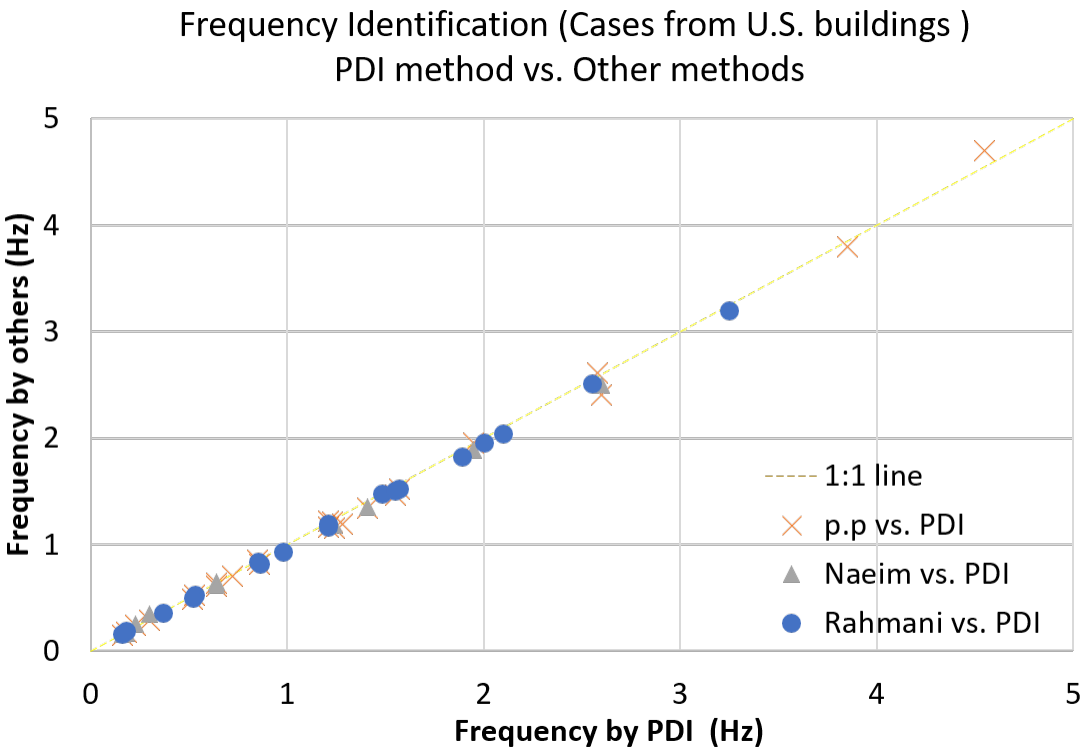

Fig. 6.1. Frequency Identification -PDI method vs. Other methods. The data are from Table 6.7∼ Table 6.11.(** p.p: peak-picking method)

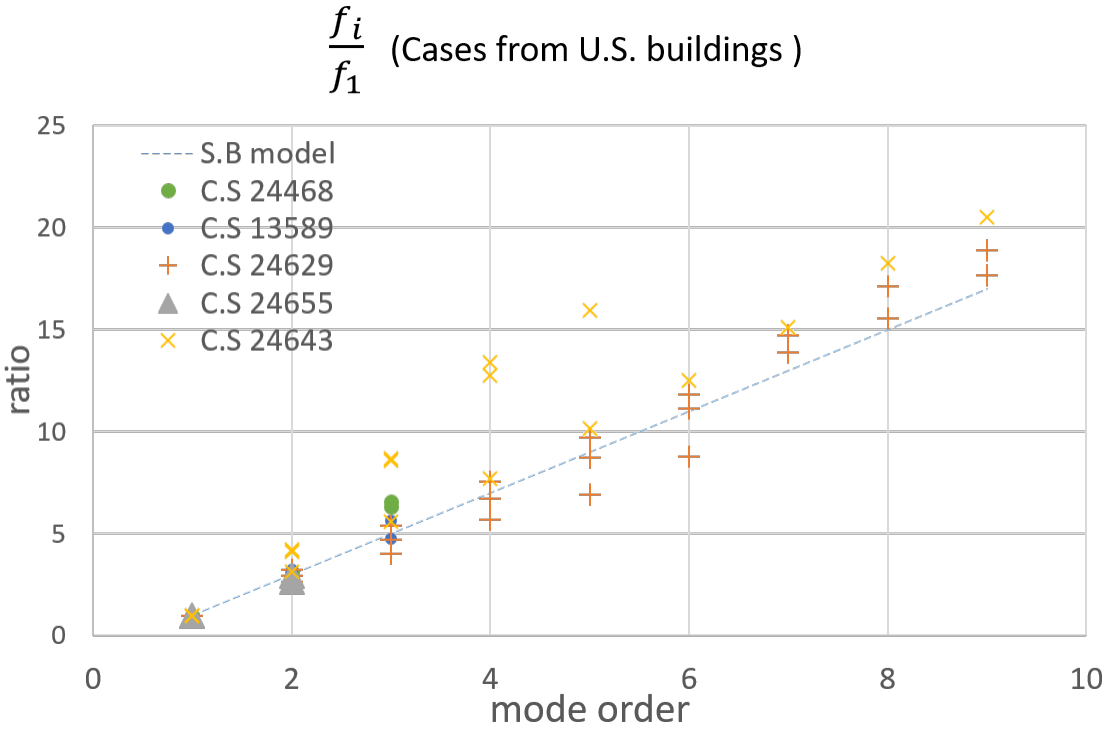

Fig. 6.2. Ratio of higher mode to the first mode (X,Y,T) (Cases in U.S.). The data are from Table 6.7∼ Table 6.11.(** S.B model: shear beam model)

7. CASE STUDY II - PDI ANALYSIS OF SAMPLE BUILDINGS IN TAIWAN

7.1 Introduction

In this chapter, five buildings in Taiwan are studied to test the PDI-based natural mode identification method analysis. All the information about the buildings and acceleration records are acquired from the Central Weather Bureau of Taiwan [26]. The criteria used in choosing these five buildings in Taiwan are identical to those used in choosing the studied sample buildings in U.S.(Chap. 6).

7.1.1 Analysis Procedure

The selected five buildings, ranging from 7 to 26 stories high are listed in Table 7.1. The basic information of each building are listed in from Table 7.2 to Table 7.6. Records from four different earthquakes are used to test the PDI analysis. Similar to investigation of sample buildings in U.S., All cases include the following information::

1. Identify the frequency in X direction by three figures:
   (a) Draw the PDI plot(Roof/Ground) in X direction
   (b) Draw the PDI plot(Roof/2F(or other available story)) in X direction
   (c) Draw the FRF in X direction
2. Identify the frequency in Y direction by three figures:
   (a) Draw the PDI plot (Roof/Ground) in Y direction
   (b) Draw the PDI plot (Roof/2F(or other available story)) in Y direction
   (c) Draw the FRF in Y direction

3. Identify the Torsional frequency by two figures:

   (a) Draw the PDI plot of torsion

   (b) Draw the torsional spectrum

4. Compared the results with other existing work information about in which natural modes of the buildings are presented:

   Multiple methods are available to identify the natural modes of a building. In order to verify the utility of PDI, results compared provided by PDI plots with results presented in other work. All five buildings were investigated from historic earthquake database in Taiwan and compared with the reports "Application of CWB structural earthquake monitoring data to evaluate the horizontal / vertical building seismic design code of Taiwan" in 2014 [27] and 2015 [28] published by the Central Weather Bureau, Taiwan.

7.2 Analysis Results

7.2.1 PDI method vs. Other Methods

In the research, the five buildings were analyzed by two methods: PDI method and Peak-Picking method. In addition, research works about the subspace method by Loh [27], [28] were cited for comparison. Thus, the analysis results by the subspace method are also provided. The identification results are shown in Table 7.7, Table 7.8, Table 7.9, Table 7.10, and Table 7.11. The data points of all (f_{PDI}/f_{others}) were also illustrated by Fig. 7.1. The average difference between PDI method and other method or research works is about 4.5%. The detailed discussions and PDI figures are collected in Appendix D, and the introduction of the subspace method is available in Appendix E.

7.2.2 Ratio of Higher Modes to the First mode

The results of f_{ix}/f_{1x}, f_{iy}/f_{1y} and f_{it}/f_{1t} are listed in Table 7.7, Table 7.8, Table 7.9, Table 7.10, and Table 7.11. The results were also illustrated by Fig. 7.2.

Table 7.1.
Selected buildings and earthquake events in Taiwan

NO.	STATION NO.	STATION NAME	NO. OF STORIES	EVENT
1	TCUBA3	Building of CE, NCHU	7	UT 1999/07/07
2	TAPBA5	Building of CCE,TTU	8	UT 2004/05/16
3	TCUBA6	Dormitory of Faculty & Staff, NCTU	14	UT 1994/10/05
4	TAPBA4	Office building, Taipower Company	26	UT 1999/09/20
5	TCUBAA	Library building, NCTU	8	UT 1999/09/20

Table 7.2.
Basic Information of Station-TCUBA3

No.	**Topic**	**Description**
1	Station No.	TCUBA3
2	Station Name	Building of CE, NCHU
3	Location	E 120.678 ,N 24.120
4	Number of Stories (above/below) Ground	7/1
5	Typical Floor Dimensions	3750 x 6020 cm^2
6	Structure System	RC rigid frame
7	Earthquake record	UT1999/ 7/ 7-13:53:13.37
8	Magnitude (M_L)	5.1
9	Epicenter	E120.735, N23.319, Z 13.78
10	Distance between Epicenter and Station (km)	89.35
11	Accel. Peak	Ground: 0.004 g Building: 0.018 g
12	Max. Roof Drift(cm)	0.57
13	Max. Roof Drift Ratio(%)	0.02
14	Drawing	Elevation: Fig.D.1 Plan: Fig.D.2

Table 7.3.
Basic Information of Station-TAPBA5

No.	Topic	Description
1	Station No.	TAPBA5
2	Station Name	Building of CCE,TTU
3	Location	E 121.541 ,N 25.013 ,
4	Number of Stories (above/below) Ground	8/1
5	Typical Floor Dimensions	8000 x 650 cm^2
6	Structure System	The structure is a ductile moment-resisting frame. The height is about 35.3m. The east side of the building at the first and second floor retreat 7.8m. The third and above floors become a cantilever stretching out.
7	Earthquake record	UT2004/ 5/16- 6: 4: 8.70
8	Magnitude (M_L)	5.72
9	Epicenter	E:121.979, N:23.051, Z:12.85
10	Distance between Epicenter and Station (km)	222.9
11	Accel. Peak	Ground: 0.0013 g Building: 0.007 g
12	Max. Roof Drift(cm)	0.078
13	Max. Roof Drift Ratio(%)	0.016
14	Drawing	Elevation: Fig.D.10 Plan: Fig.D.11

Table 7.4.
Basic Information of Station-TCUBA6

No.	Topic	Description
1	Station No.	TCUBA6
2	Station Name	Dormitory of Faculty & Staff, NCTU
3	Location	E 120.678 , N 24.120 ,
4	Number of Stories (above/below) Ground	14/2
5	Typical Floor Dimensions	2802 x 4650 cm^2
6	Structure System	The structure is a RC rigid frame.
7	Earthquake record	UT2002/ 2/12- 3:27:25.00,
8	Magnitude (M_L)	6.2
9	Epicenter	E:121.723, N:23.741, Z:29.98,
10	Distance between Epicenter and Station (km)	114.4
11	Accel. Peak	Ground: 0.02 g Building: 0.068 g
12	Max. Roof Drift(cm)	0.56
13	Max. Roof Drift Ratio(%)	0.014
14	Drawing	Elevation: Fig.D.19 Plan: Fig.D.20

Table 7.5.
Basic Information of Station-TAPBA4

No.	Topic	Description
1	Station No.	TAPBA4
2	Station Name	Office building, Taipower Company
3	Location	E 121.523 ,N 25.019
4	Number of Stories (above/below) Ground	26/3
5	Typical Floor Dimensions	5,216 x 3,960 cm^2
6	Structure System	A ductile steel rigid frame with bracing in $1 \sim 17$ F along E-W side and $1 \sim 8$ F along N-S side.
7	Earthquake record	UT1999/ 9/20-17:47:15.850
8	Magnitude (M_L)	7.3
9	Epicenter	E:120.8150, N:23.853, Z:8.00,
10	Distance between Epicenter and Station (km)	148.31
11	Accel. Peak	Ground: 0.047 g Building: 0.19 g
12	Max. Roof Drift(cm)	10.44
13	Max. Roof Drift Ratio(%)	0.11
14	Drawing	Elevation: Fig.D.28 Plan: Fig.D.29

Table 7.6.
Basic Information of Station-TCUBAA

No.	Topic	Description
1	Station No.	TCUBAA
2	Station Name	Library building, NCTU
3	Location	E 120.998 ,N 24.787
4	Number of Stories (above/below) Ground	8/1
5	Typical Floor Dimensions	6,400 x 9,600 cm^2
6	Structure System	A ductile RC rigid frame with mat foundation. 8 spans in E-W direction and 12 spans in N-S direction.
7	Earthquake record	UT1999/ 9/20-17:47:15.85
8	Magnitude (M_L)	7.3
9	Epicenter	E:120.8150, N:23.853, Z:8.00,
10	Distance between Epicenter and Station (km)	105.62
11	Accel. Peak	Ground: 0.079 g Building: 0.27 g
12	Max. Roof Drift(cm)	7.77
13	Max. Roof Drift Ratio(%)	0.15
14	Drawing	Elevation: Fig.D.36 Plan: Fig.D.37

Table 7.7.
Comparison of mode identification results of TCUBA3

Mode Order	f_n	**PDI plot (Hz)**	f_i/f_1	**Peak-Picking (Hz)**	**Loh, 2014 [27] (Hz)**
1st	f_{1x}	3.1	1	3.31	3.02
	f_{1y}	3.22	1	3.12	3.05
	f_{1t}	3.8	1	3.54∼ 3.9	3.9
2nd	f_{2x}	9.3	3.0	-	-
	f_{2y}	8.78	2.7	-	-
	f_{2t}	7.8	2.1		-

Related PDI plots are shown in Fig.D.3∼ Fig.D.9

Table 7.8.
Comparison of mode identification results of TAPBA5

Mode Order	f_n	**PDI plot (Hz)**	f_i/f_1	**Peak Picking (Hz)**	**Loh, 2014 [27] (Hz)**
1st	f_{1x}	1.48	1	1.44	1.432
	f_{1y}	2.45	1	2.29	2.238
	f_{1t}	1.75	1	-	1.812
2nd	f_{2x}	5.24	3.5	5.45	-
	f_{2y}	7.70	3.2	-	-
	f_{2t}	5.2	3.0	-	-
3^{rd}	f_{3x}	9.27	6.3	-	-
	f_{3y}	-	-	-	-
	f_{3t}	9.2 ∼ 9.4	5.3	-	-

Related PDI plots are shown in Fig.D.12∼ Fig.D.18

Table 7.9.
Comparison of mode identification results of TCUBA6

Mode Order	f_n	**PDI plot (Hz)**	f_i/f_1	**Peak Picking (Hz)**	**Loh, 2015 [28] (Hz)**
1st	f_{1x}	1.71	1	1.68	1.624
	f_{1y}	2.18	1	2.17	2.015
	f_{1t}	2.4	1	-	-
2nd	f_{2x}	5.85	3.4	-	-
	f_{2y}	8.43	3.9	-	-
	f_{2t}	5.6	2.3	-	-
3^{rd}	f_{3x}	-	-	-	-
	f_{3y}	-	-	-	-
	f_{3t}	8.4∼9.4		-	-

Related PDI plots are shown in Fig.D.21∼ Fig.D.27

Table 7.10.
Comparison of mode identification results of TAPBA4

Mode Order	f_n	**PDI plot (Hz)**	f_i/f_1	**Peak Picking (Hz)**	**Loh, 2015 [28] (Hz)**
1st	f_{1x}	0.37	1	0.35	0.358
	f_{1y}	0.4	1	0.35	0.368
	f_{1t}	0.45	1	-	-
2nd	f_{2x}	1.03	2.8	1.0	1.012
	f_{2y}	1.09	2.7	1.2	1.078
	f_{2t}	1.21	2.7	-	-
3^{rd}	f_{3x}	1.83	4.9	1.82	1.919
	f_{3y}	2.0	5.0	2.0	1.919
	f_{3t}	2.2	4.9	-	-
4^{th}	f_{4x}	-	-	2.4	-
	f_{4y}	2.82	7.1	2.9	-
	f_{4t}	-	-	-	-

Related PDI plots are shown in Fig.D.30∼ Fig.D.35

Table 7.11.
Comparison of mode identification results of TCUBAA

Mode Order	f_n	**PDI plot (Hz)**	f_i/f_1	**Peak Picking (Hz)**	**Loh, 2015 [28] (Hz)**
1st	f_{1x}	1.48	1	1.5	1.45
	f_{1y}	1.10	1	1.15	1.16
	f_{1t}	0.96	1	-	1.02
2nd	f_{2x}	4.8	3.2	4.9	-
	f_{2y}	3.9	3.5	4.4	-
	f_{2t}	-	-	-	-

Related PDI plots are shown in Fig.D.38∼ Fig.D.44

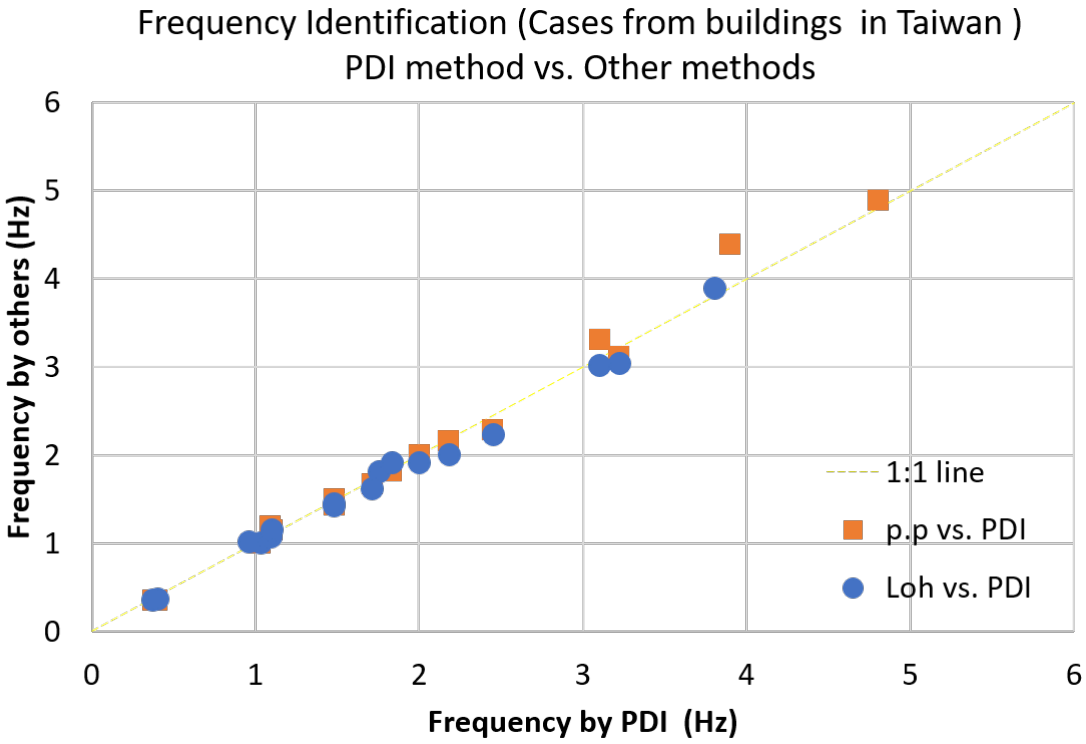

Fig. 7.1. Frequency Identification- PDI method vs. Other methods. The data are from Table 7.7 ∼ Table 7.11.(** p.p: peak-picking method)

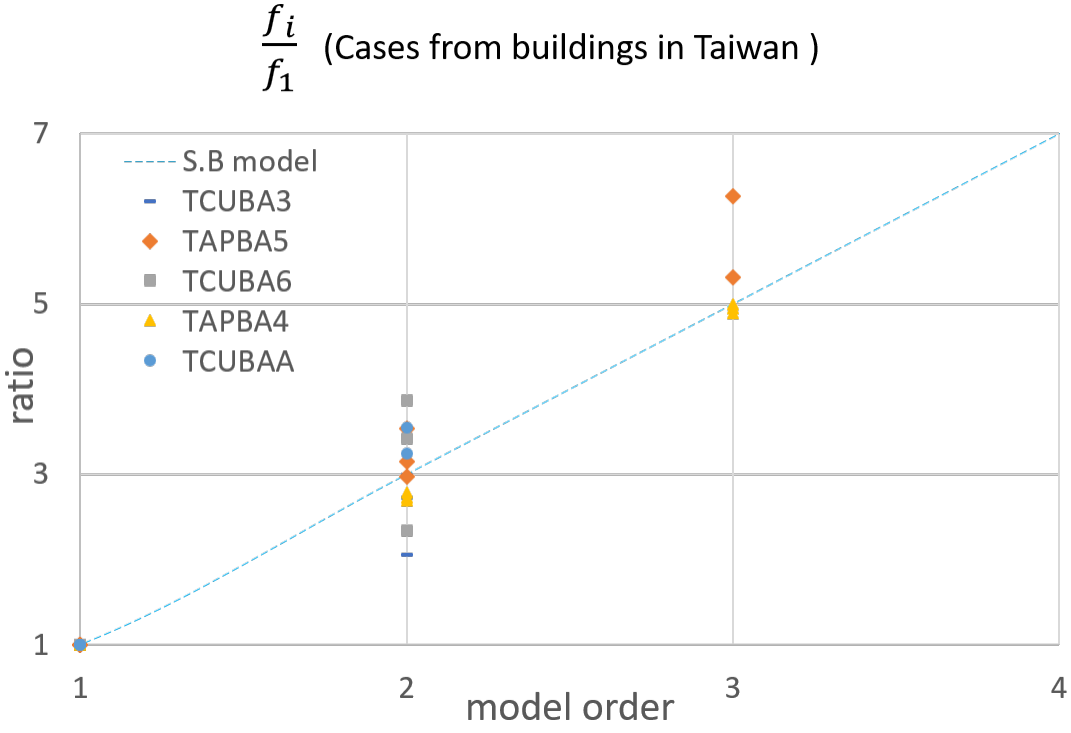

Fig. 7.2. Ratio of higher mode to the first mode (X,Y,T) (Cases in Taiwan). The data are from Table 7.7 ∼ Table 7.11.(** S.B model: shear beam model)

8. TIME-FREQUENCY ANALYSIS

8.1 Introduction of Time-PDI analysis

Time-frequency analysis decomposes signal data into forms that separate the time-varying amplitude, frequency, and phase content [9]. There are several tools available for the structural health monitoring, such as short-term Fourier transform, Hilbert-Huang transform, and wavelet transform. Since most of the buildings are assumed to remain linear elastic under small seismic forces, these techniques were not often used in structural health monitoring. Nevertheless, time-frequency analysis is a time-sensitive technique. By using this method, more detailed information of dynamic properties can be obtained. Therefore, this research would try to broaden the application of PDI method into time-frequency domain analysis.

The concept of the time-frequency analysis in PDI, i.e, Time-PDI analysis is not complicated. The basic idea is to truncate the displacement time history curve into two or more segments such as shown in Fig. 8.1. This figure is the acceleration record on the roof and ground from the case 5 analyzed in Chapter 7, i.e., National Chiao Tung University Library (TCUBAA). In traditional PDI analysis, the instantaneous phase difference between both displacement curves in whole duration, i.e, from 0$\sim$ 120 sec are included to calculate the phase difference index. In the concept of time-frequency analysis, the displacement curves are divided into two segments- T_{d1} and T_{d2}. The two segments are not necessary equal in length. Then, one can calculate the PDI for both sets of displacement curves (T_{d1} and T_{d2}) individually. If this system is an LTI system, the PDI curves in T_{d1} and T_{d2} should be the same. On the contrary, if the PDI curves are not the same, a possible explanation is that the natural frequency changed during the earthquake event.

Time-frequency analysis also works in subspace method, and the concept is shown in Fig.8.2. Instead of using displacements as analysis data, in this building identification case, the subspace method uses the acceleration records as input and output. In Fig.8.2, the acceleration records are truncated into five segments, and each piece represents the dimension of a Hankel matrix. In a LTI system, the obtained eigenvalues should be the same in any T_{di} section. By finding repeated eigenvalues, the natural frequencies may be identified and confirmed. Theoretically, the natural frequencies of a non-linear system also may be traced by this method, but the question is how the eigenvalues on the stable plots can be confirmed as the true frequencies if the eigenvalues keep changing all the time. The answer is: to use the PDI plots to identify the natural frequencies of the buildings.

In the following, two examples are studied to demonstrate how the PDI method work in non-linear-time-invariant system, and help the subspace method to target the possible natural frequencies.

8.2 Case 1: National Chiao Tung University Library (TCUBAA)

8.2.1 introduction

The fifth case in Chapter 7, i.e., National Chiao Tung University Library (TCUBAA) with the same earthquake record is studied again by the perspective of time-frequency analysis. The detailed information is shown in Table 7.6. The first step is to determine the time intervals in Fig. 8.1. By observation, the t_1, t_2, $t_3$and t_4 are set to be 20, 40, 70, and 100 seconds, and the corresponding PDI plots in X and Y direction are shown in Fig. 8.4 and Fig. 8.5. From these Time-PDI plots, it can be inferred that the natural frequencies of the building were not constant during Ji-Ji earthquake. In addition, the analysis results by the subspace method are shown in Fig. 8.7 and Fig. 8.8.

8.2.2 Analysis Result

The identified results by PDI method and subspace method are shown in Table 8.1 and Table 8.2. The variation of frequencies in X and Y direction with time are shown in Fig. 8.6. This figure provides the information of how the frequencies changed with time.

From the above results, it is found that the structure was not an LTI system during the JiJi earthquake event. The first three natural modes of X and Y directions were changing during the response. However, there is no knowing that whether this phenomenon was either due to the original property of the building or because of damage during the earthquake. If the prior and the following events of the building can be analyzed thoroughly, the answer probably might be clearer.

In addition, in this case, from Fig. 8.7 and Fig. 8.8, the subspace method demonstrates extraordinary ability to trace the variation of frequencies of the building with time, especially the fundamental modes. However, it is easier to identify the order of modes by PDI method because spurious modes often occur in the analysis of subspace method.

8.3 Case 2: A Full-Scale, Four-Story RC Building on the NIED E-Defense Shake Table

8.3.1 introduction

The second case is a full-scale, four-story RC building tested on the NIED E-Defense shake table. The full-scale building was tested on December, 2010. The basic information of this building is given in Table 8.3. JMA-Kobe motions (1995) was selected to be the input acceleration. The intensity of input ground motions was gradually increased to observe the damage progress. The adopted factors for JMA-Kobe were 10 %, 25 %, 50 %, and 100 %. In the tests of the first two input records, no obvious damage was observed in the building. The beam-column joints,

beam ends, column and wall bases showed minor cracking after the JMA-Kobe-50% test [29]. It can be inferred that the building became inelastic in this event. Thus, in this research, the 50 % JMA-Kobe input and corresponding output are selected for the time-PDI analysis. The acceleration records on the ground and roof are shown in Fig. 8.9 and Fig. 8.10.

8.3.2 Analysis Result

Fig. 8.14 provides the frequency response function plots in X and Y directions. The first obvious peaks can be regarded as the first modes in X and Y direction, i.e., $f_{1x} = 1.1$Hz, and $f_{1y} = 1.66$Hz. Compared with the initial natural frequencies shown in Table 8.3, the building could be damaged in this event based on the fact that the natural frequencies decreased. However, there is no knowing the variation of frequencies during the 50 % JMA-Kobe motion only by relying on the FRF plots.

By observing Fig. 8.9 and Fig. 8.10, the acceleration records are separated into three sections, and the time intervals are: $[0 \sim 10]$ sec, $[10 \sim 30]$ sec, and $[30 \sim 50]$ sec. The PDI curves are calculated based on the corresponding time intervals separately. The results are shown in Fig. 8.15 and Fig. 8.16.

The identified results by the PDI method and the subspace method are shown in Table 8.5 and Table 8.6. The variation of frequencies in X and Y direction with time are shown in Fig. 8.17. This figure provides the information of how the frequencies changed with time.

In addition, the subspace method is also used to identify the building for comparison. The identified results with the stable plots are shown in Fig. 8.18 and Fig. 8.19. Similar to the first case (TCUBAA), the subspace method also demonstrates extraordinary advantage to trace the variation of frequencies of the building with time. However, it is easier to detect the higher modes by PDI method while spurious modes often appear in high frequency range in stable plot.

8.4 Conclusion

This research truncated the acceleration records into three intervals, i.e.,"before the main shock", "during the main shock", "after the main shock", and the corresponding PDI plots were obtained. From the two studied cases, here are the findings about the time-frequency analysis by the PDI method and the subspace method:

1. The PDI method successfully identified the three-stage natural frequencies of a building during a single event, including the natural frequencies "before the main shock", "during the main shock", "after the main shock".

2. In the two cases, the PDI method identified more modes than the subspace method. In addition, the PDI method does not need the sketches of mode shapes to confirm the mode order.

3. For the fundamental modes, the subspace can be used to trace the change in frequency. However, in the two cases studied, spurious modes occurred in higher frequencies, and the PDI plots can be helpful to exclude them.

Table 8.1.
Identified Frequencies in X Direction of TCUBAA Station

Method	**Time (sec)**	f_{1x} **(Hz)**	f_{2x} (Hz)	f_{3x} (Hz)	Figure
PDI method	$20 \sim 40$ sec	1.98	6.40	8.64	Fig. 8.4
	$40 \sim 70$ sec	1.48	4.86	7.02	
	$70 \sim 100$ sec	1.42	4.69	6.59	
Subspace method	$20 \sim 40$ sec	1.92	6.16	$-^{**}$	Fig. 8.7
	$40 \sim 70$ sec	1.47	5.27	-	
	$70 \sim 100$ sec	1.37	4.65	-	

**The third modes cannot be identified independently by the subspace method.

Table 8.2.
Identified Frequencies in Y Direction of TCUBAA Station

Method	**Time (sec)**	f_{1y} **(Hz)**	f_{2y} (Hz)	f_{3y} (Hz)	Figure
PDI method	$20 \sim 40$ sec	1.59	5.25	9.88	Fig. 8.5
	$40 \sim 70$ sec	1.15	4.08	7.65	
	$70 \sim 100$ sec	1.08	3.90	7.54	
Subspace method	$20 \sim 40$ sec	1.63	5.31	$-^{**}$	Fig. 8.8
	$40 \sim 70$ sec	1.13	4.06	-	
	$70 \sim 100$ sec	1.00	3.69	-	

**The third modes cannot be identified independently by the subspace method.

Table 8.3.
Basic Information of Four-Story RC Building

No.	Topic	Description
1	Elevation of RC specimen	Fig.8.11
2	Plan of RC specimen	Fig.8.12
3	Sensor Location	Fig.8.13
4	Number of Stories (above/below) Ground	4/0
5	Typical Floor Dimensions	14.4 m × 7.2 m
6	Story height	3 m
7	Building weight	5877 KN
8	Structural System	The moment frame system was adopted in the longer (X) direction of two spans of 7.2 m, and a pair of multi-story walls were incorporated in the exterior frames in the shorter (Y) direction of one span of 7.2 m. The foundations were fixed on the shaking table by a number of prestressing post-tensioned bars.
9	Initial natural frequency	X dir.: 2.33 Hz; Y dir.:3.33 Hz
10	Input Accel. Record	JMA-Kobe motions (1995) scaled by 50%
11	Accel. Peak	Ground: 0.33 g Building: 1.1 g
12	Maximum inter-story drift (rad)	0.015 (X dir.)

Data source: [29] [30]

Table 8.4.
Selected Sensors in Four-Story RC Building

Direction	**Floor**	**Channel NO.**
X	Roof	2-RRA1-X
	1F	2-R1A1-X
Y	Roof	2-RRA1-Y
	1F	2-R1A1-Y

Table 8.5.
Identified Frequencies in X Direction of Four-Story RC Building

Method	**Time (sec)**	f_{1x} **(Hz)**	f_{2x} (Hz)	f_{3x} (Hz)	Figure
PDI method	$0 \sim 10$ sec	2.61	8.12	14.75	Fig. 8.15
	$10 \sim 30$ sec	1.35	4.94	9.32	
	$30 \sim 50$ sec	1.49	5.88	10.94	
Subspace method	$0 \sim 10$ sec	2.42	7.88	$-^*$	Fig. 8.18
	$10 \sim 30$ sec	1.39	5.14	-	
	$30 \sim 50$ sec	1.54	6.18	-	

*The third modes cannot be identified independently by the subspace method.

Table 8.6.
Identified Frequencies in Y Direction of Four-Story RC Building

Method	**Time (sec)**	f_{1y} **(Hz)**	f_{2y} (Hz)	f_{3y} (Hz)	Figure
PDI method	$0 \sim 10$ sec	2.73	14.17	-	Fig. 8.16
	$10 \sim 30$ sec	1.62	7.60	-	
	$30 \sim 50$ sec	1.84	7.83	-	
Subspace method	$0 \sim 10$ sec	3.22	5.63**	-	Fig. 8.19
	$10 \sim 30$ sec	1.68	6.81	-	
	$30 \sim 50$ sec	1.91	7.99	-	

** From Fig. 8.16-(a), f_{2y} =5.63 Hz is not a correct identification.

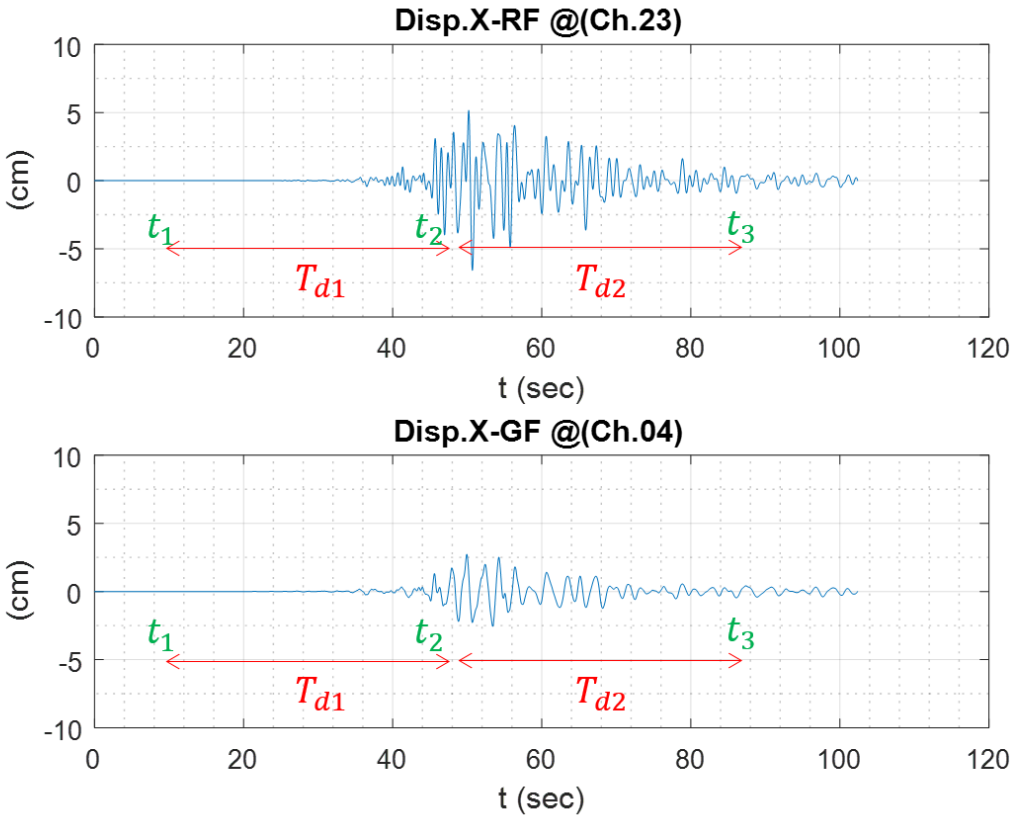

Fig. 8.1. The time-PDI method concept. The displacement signals are truncated into two segments. The first piece is from $t_1$to t_2, and the second piece is from $t_2$to t_3. The phase difference indices are calculated individually so that one can observe the difference between T_{d1} and T_{d2}.

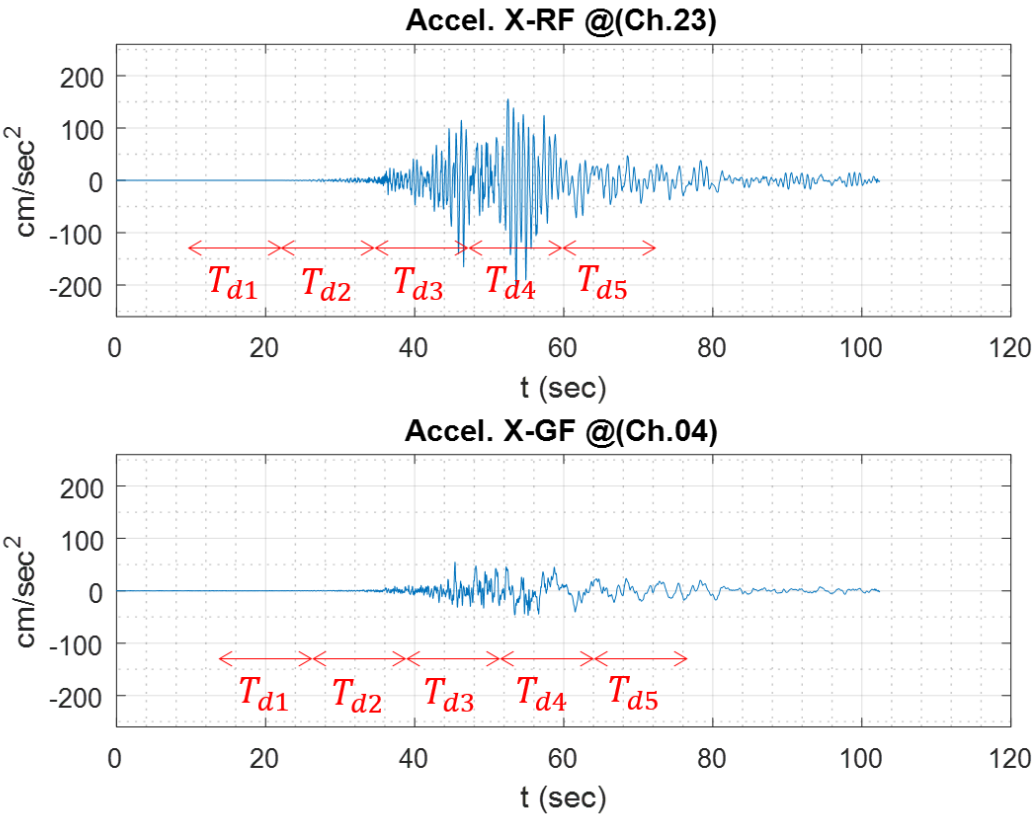

Fig. 8.2. Example of acceleration signal truncation for the subspace method. In this Fig., each T_{di} represents the size of single Hankel matrix. For each pair of input and output matrices, corresponding eigenvalues can be calculated, and the repeated eigenvalues are supposed to be the real frequencies of the structure.

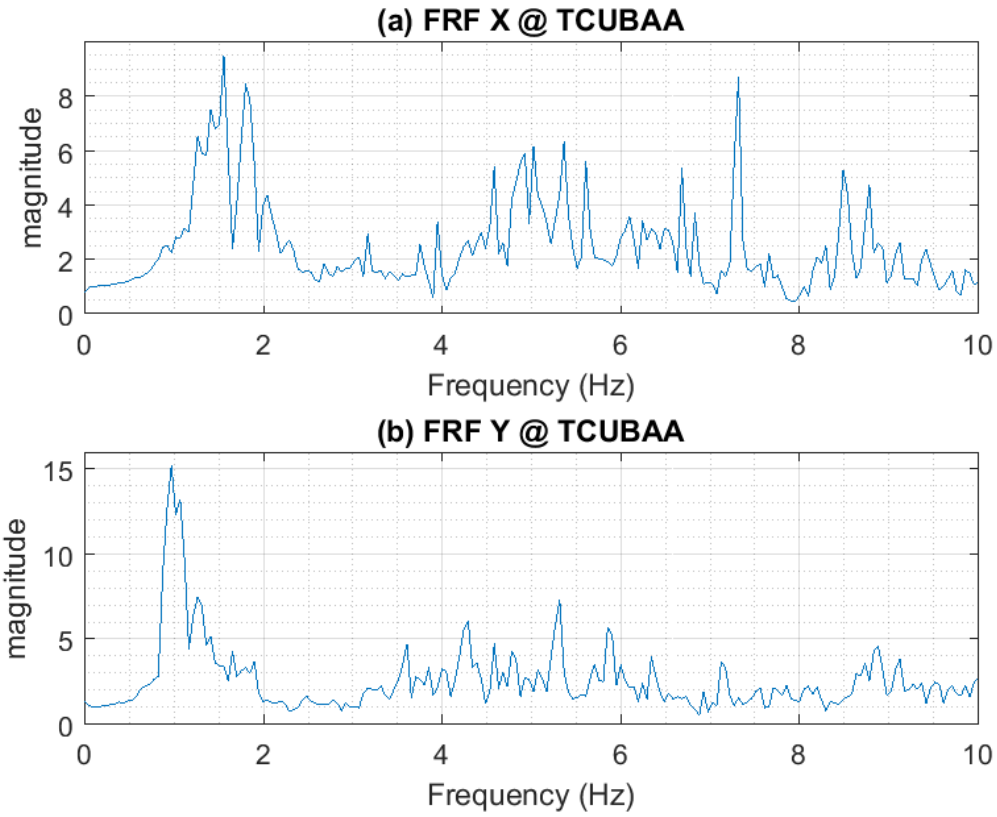

Fig. 8.3. The frequency response function of TCUBAA station. The plot was smoothed by Welch's method with Hamming window of 25% signal length.

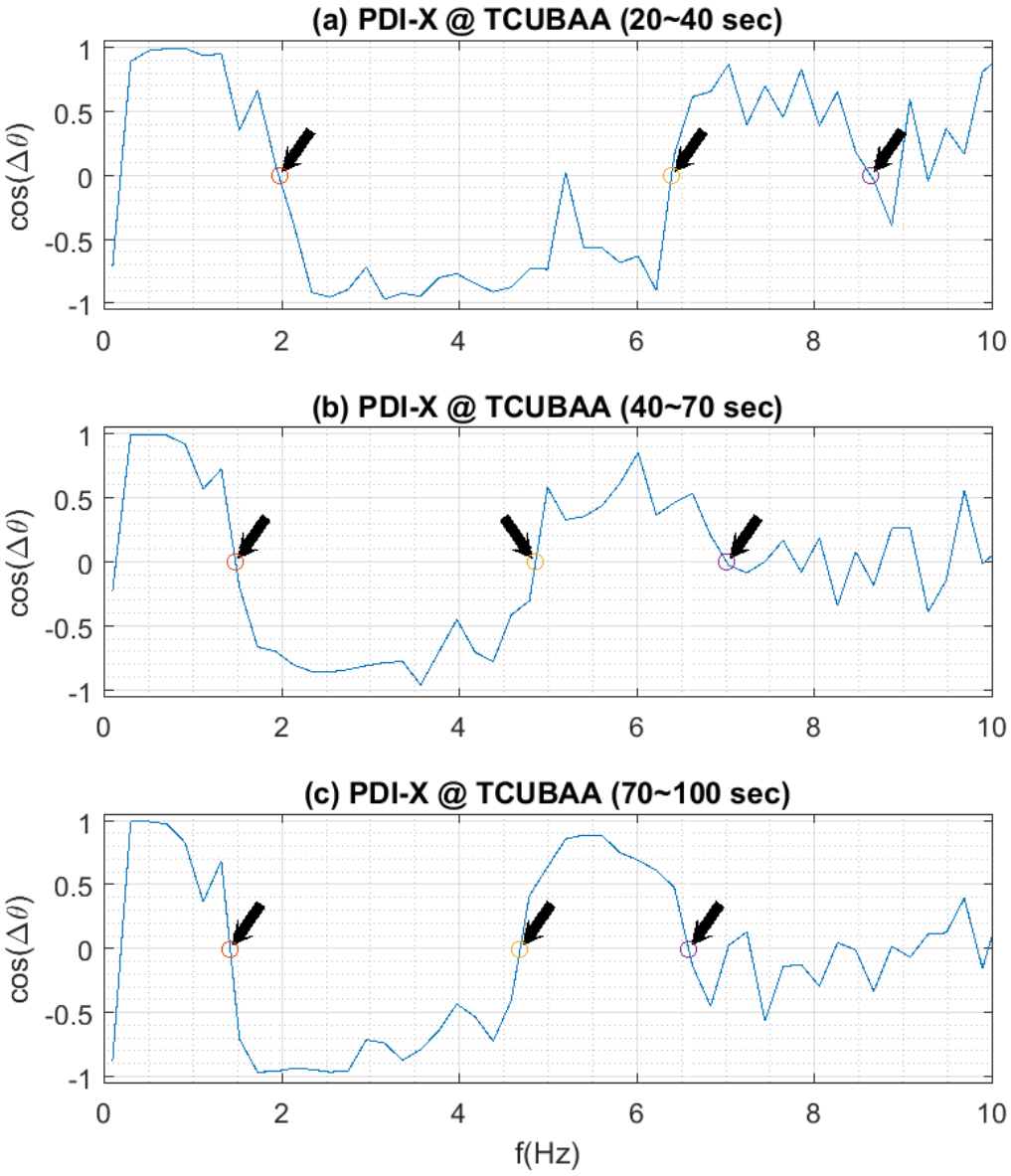

Fig. 8.4. The Time-PDI plots in X direction of the four-story RC building. f_{nx}= (a):[1.98, 6.40, 8.64]Hz, (b):[1.48, 4.86, 7.02]Hz, (c):[1.42, 4.69, 6.59]Hz.

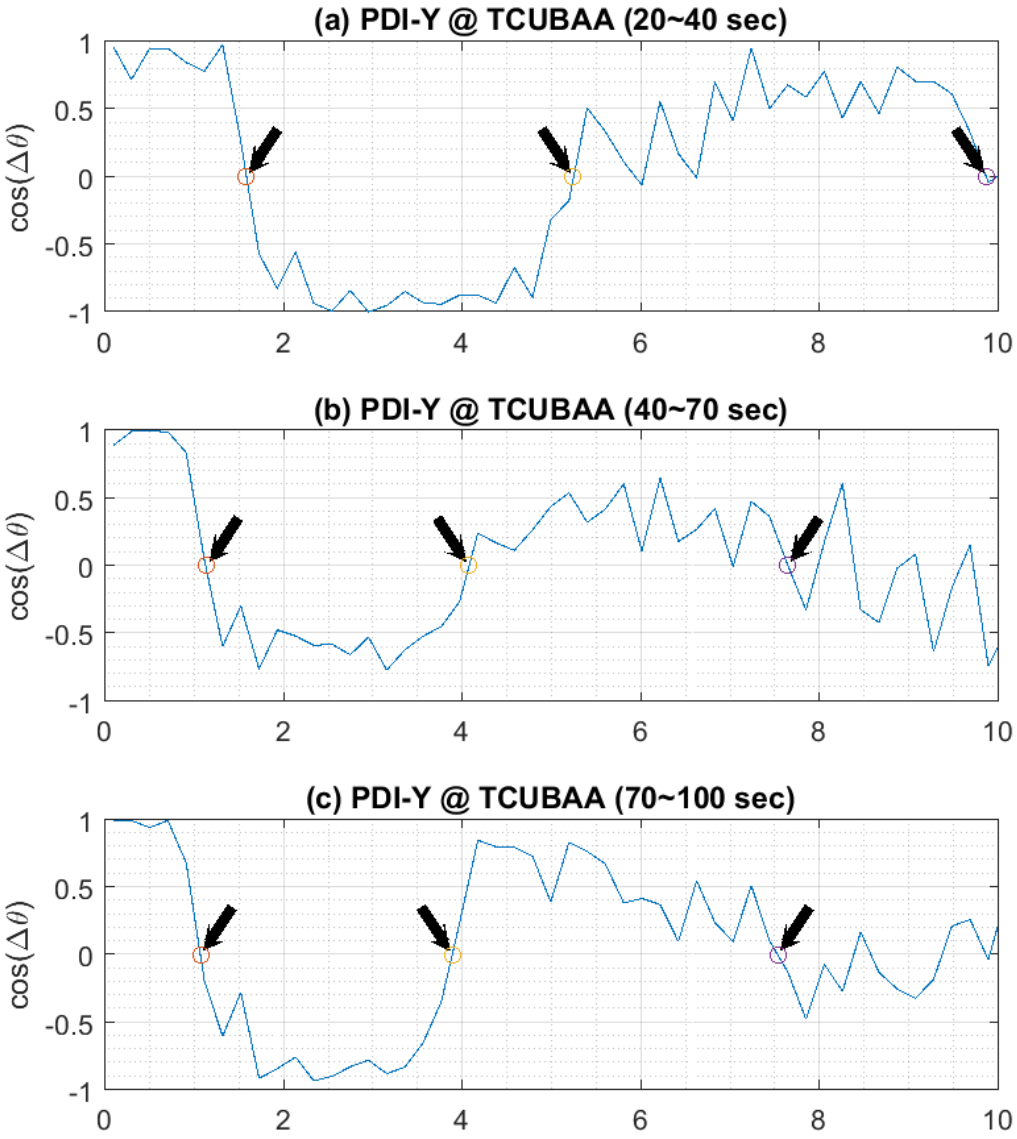

Fig. 8.5. The Time-PDI plots in Y direction of the four-story RC building. f_{ny}= (a):[1.59, 5.25, 9.88]Hz, (b):[1.15, 4.08, 7.65]Hz, (c):[1.08, 3.90, 7.54]Hz.

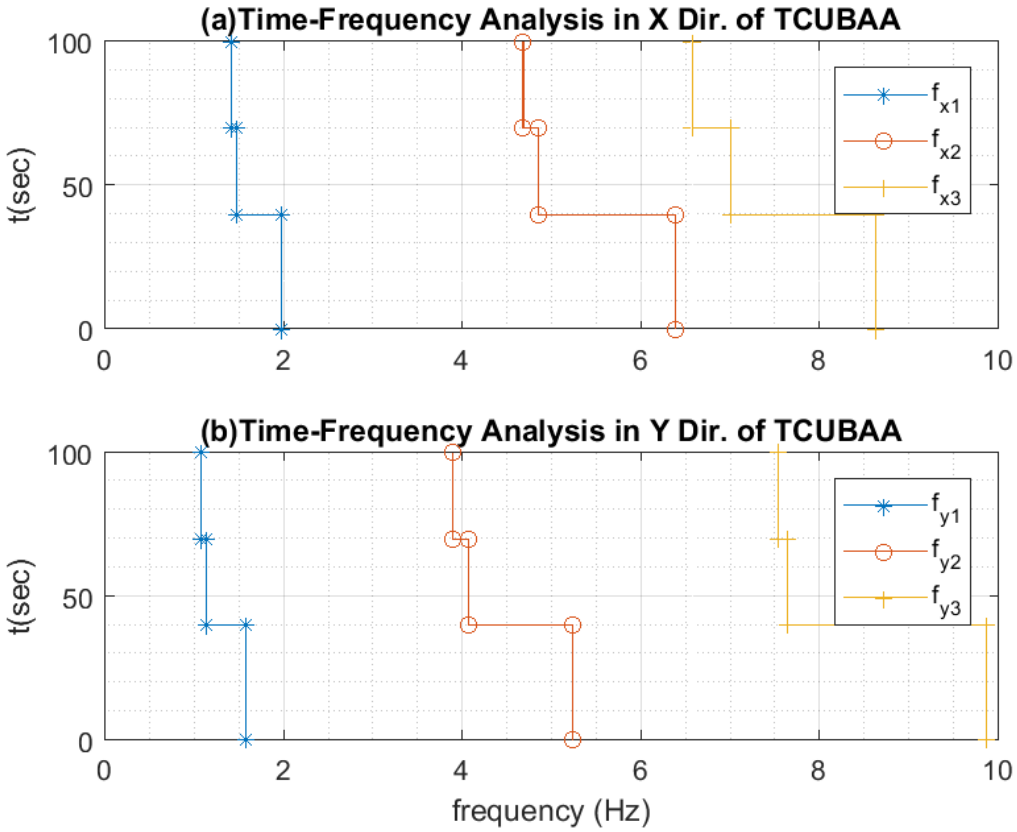

Fig. 8.6. The time-frequency analysis of TCUBAA station, Taiwan. (Ji-Ji earthquake, UT1999/ 9/20-17:47:15.85)

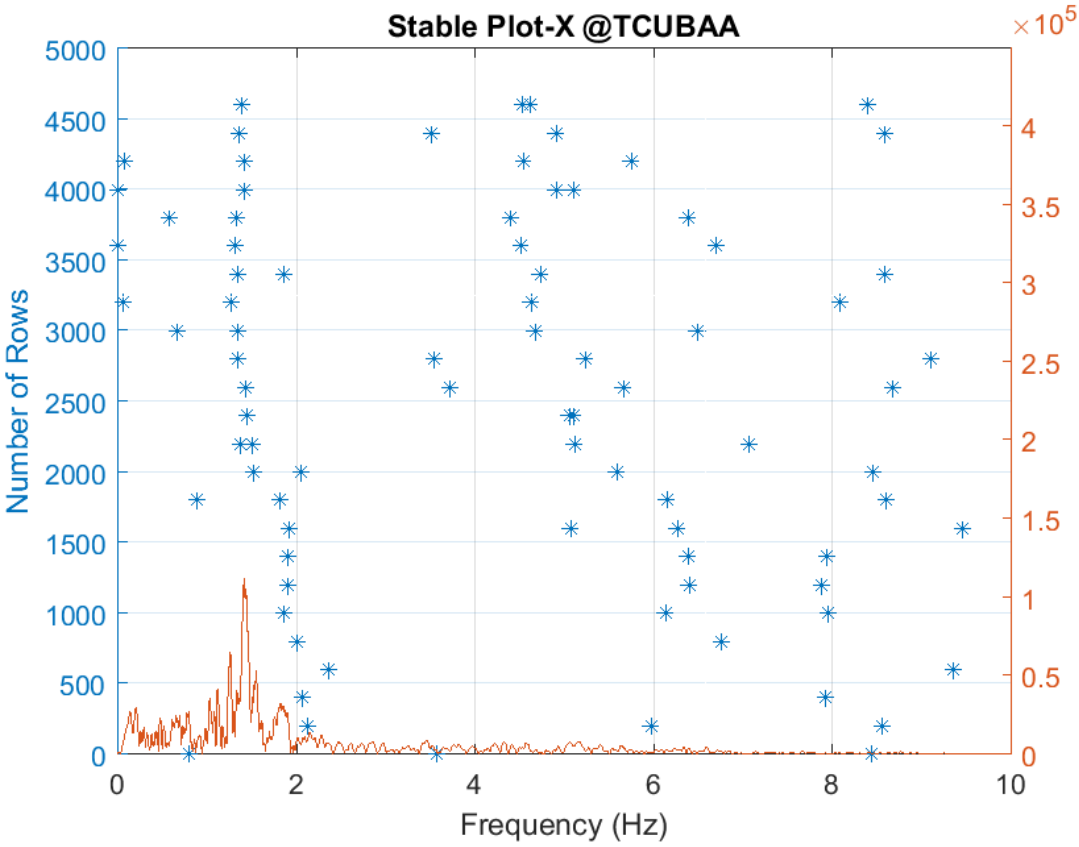

Fig. 8.7. The stable plot by the subspace method in X direction of TCUBAA station. In this case, the conversion of time and rows is: 102.4 seconds ≈4,800 rows. For example, T= 0∼12.8 sec represents Row= 0 ∼600.

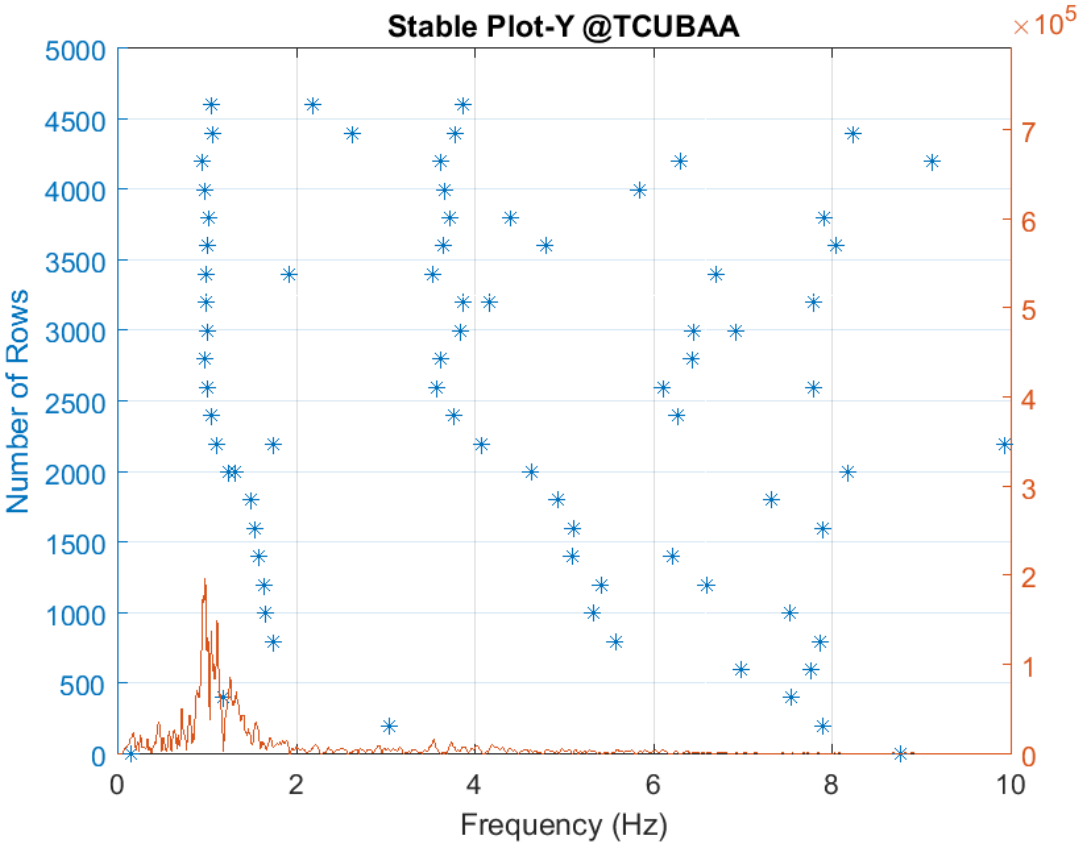

Fig. 8.8. The stable plot by the subspace method in Y direction of TCUBAA station. In this case, the conversion of time and rows is: 102.4 seconds ≈4,800 rows. For example, T= 0∼12.8 sec represents Row= 0 ∼600.

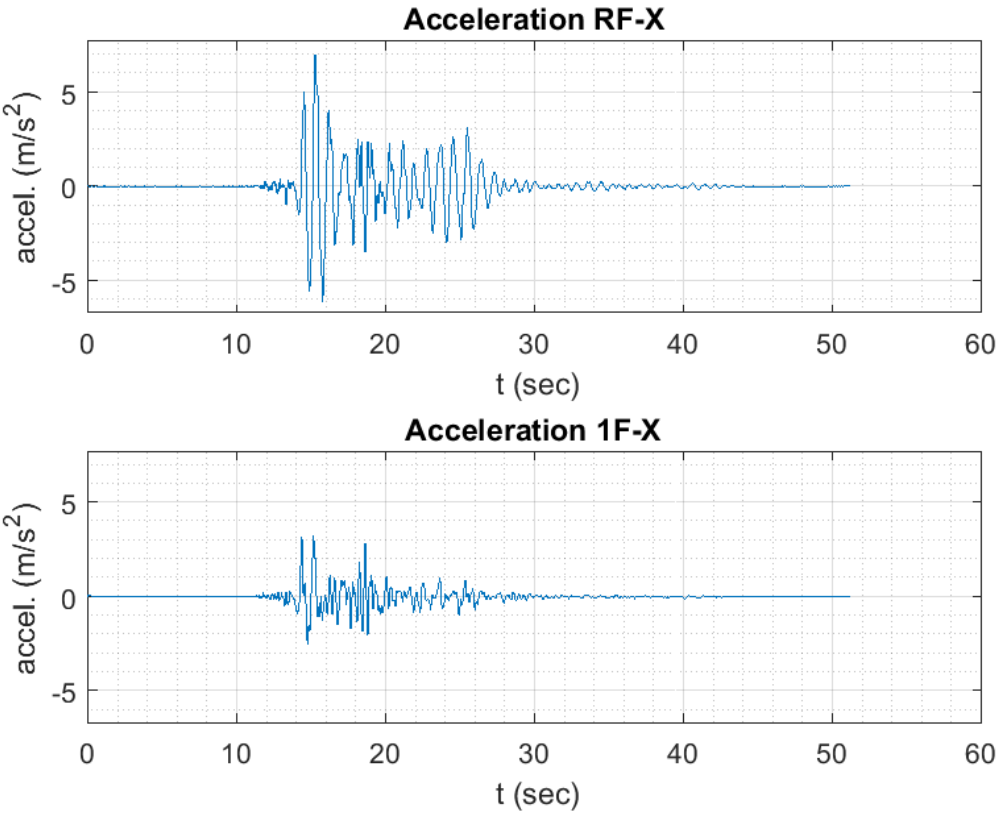

Fig. 8.9. Input acceleration in X direction of four-story RC Building on the NIED E-Defense shake table. The record is JMA-Kobe motions (1995) scaled by 50 % [30].

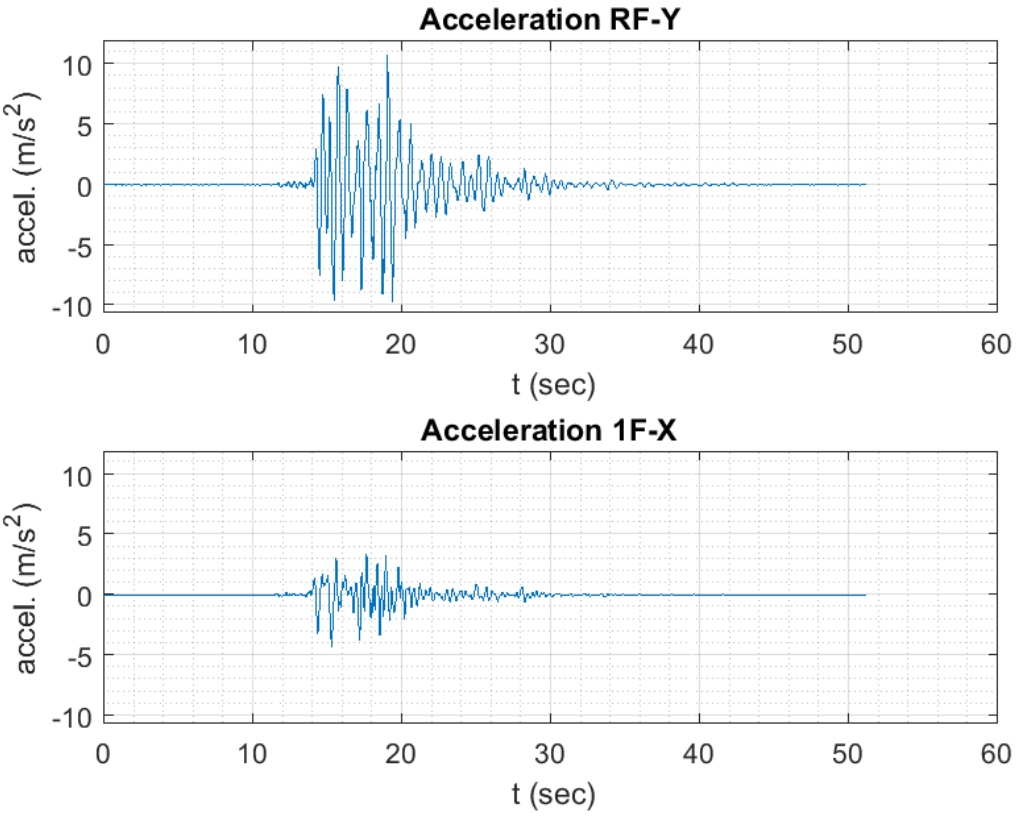

Fig. 8.10. Input acceleration in Y direction of four-story RC Building on the NIED E-Defense shake table. The record is JMA-Kobe motions (1995) scaled by 50 % [30].

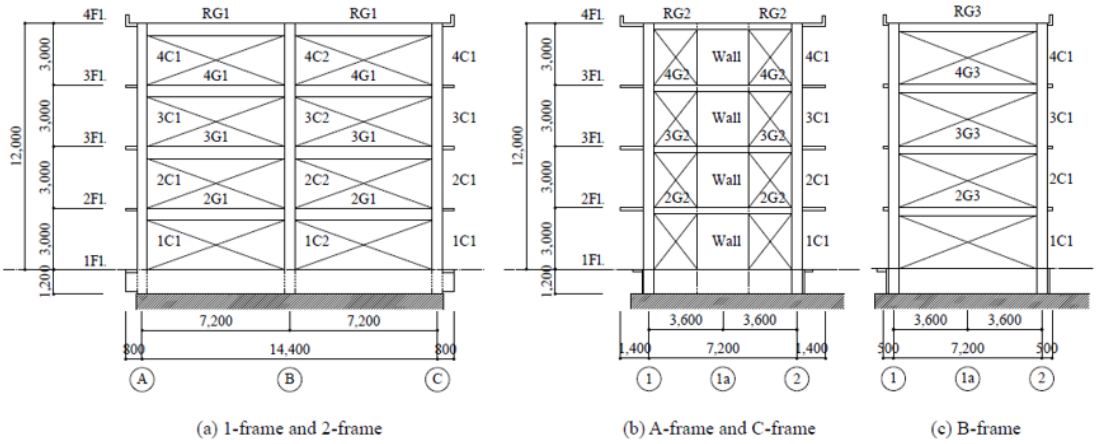

Fig. 8.11. Elevation of four-story RC building on the NIED E-Defense shake table [30].

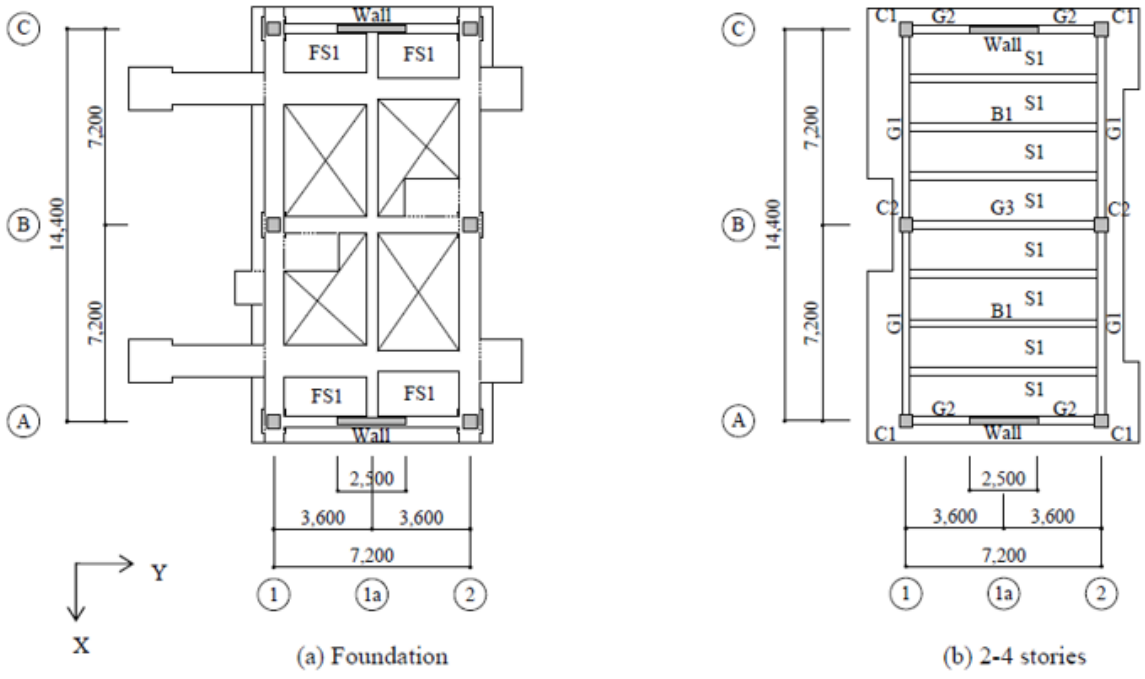

Fig. 8.12. Plan of four-story RC building on the NIED E-Defense shake table [30].

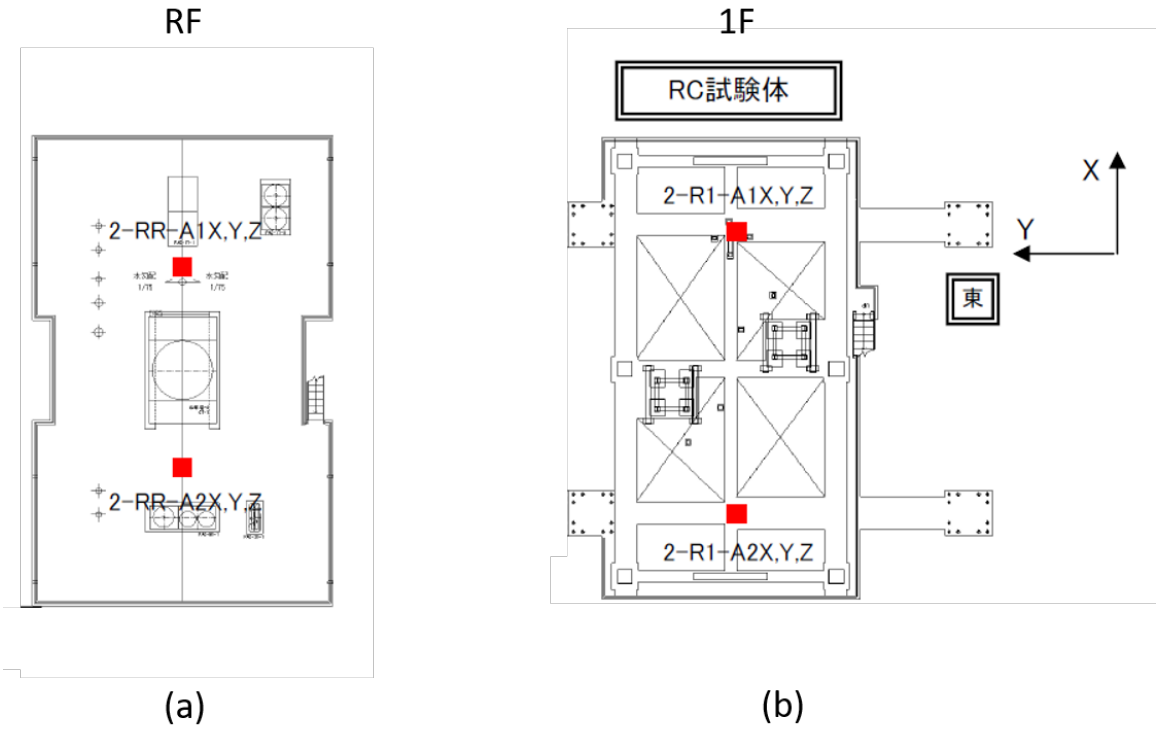

Fig. 8.13. Sensor locations of four-story RC building on the NIED E-Defense shake table [30].

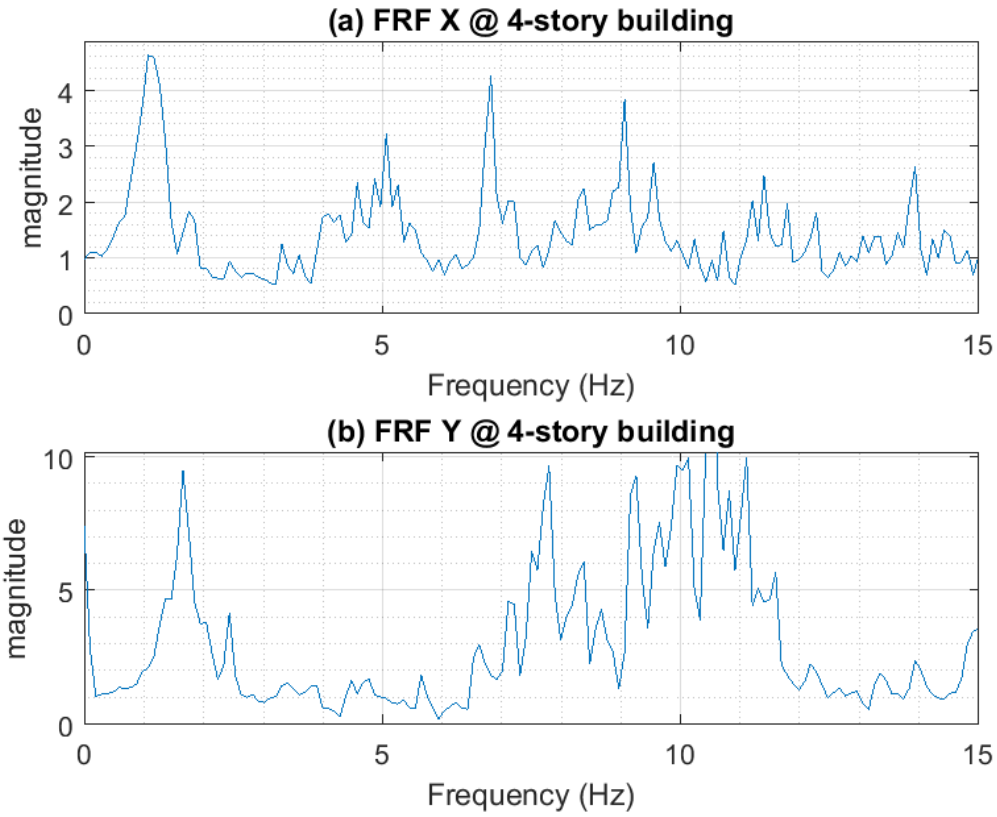

Fig. 8.14. The frequency response function of the four-story RC building. The plot was smoothed by Welch's method with Hamming window of 20% signal length.

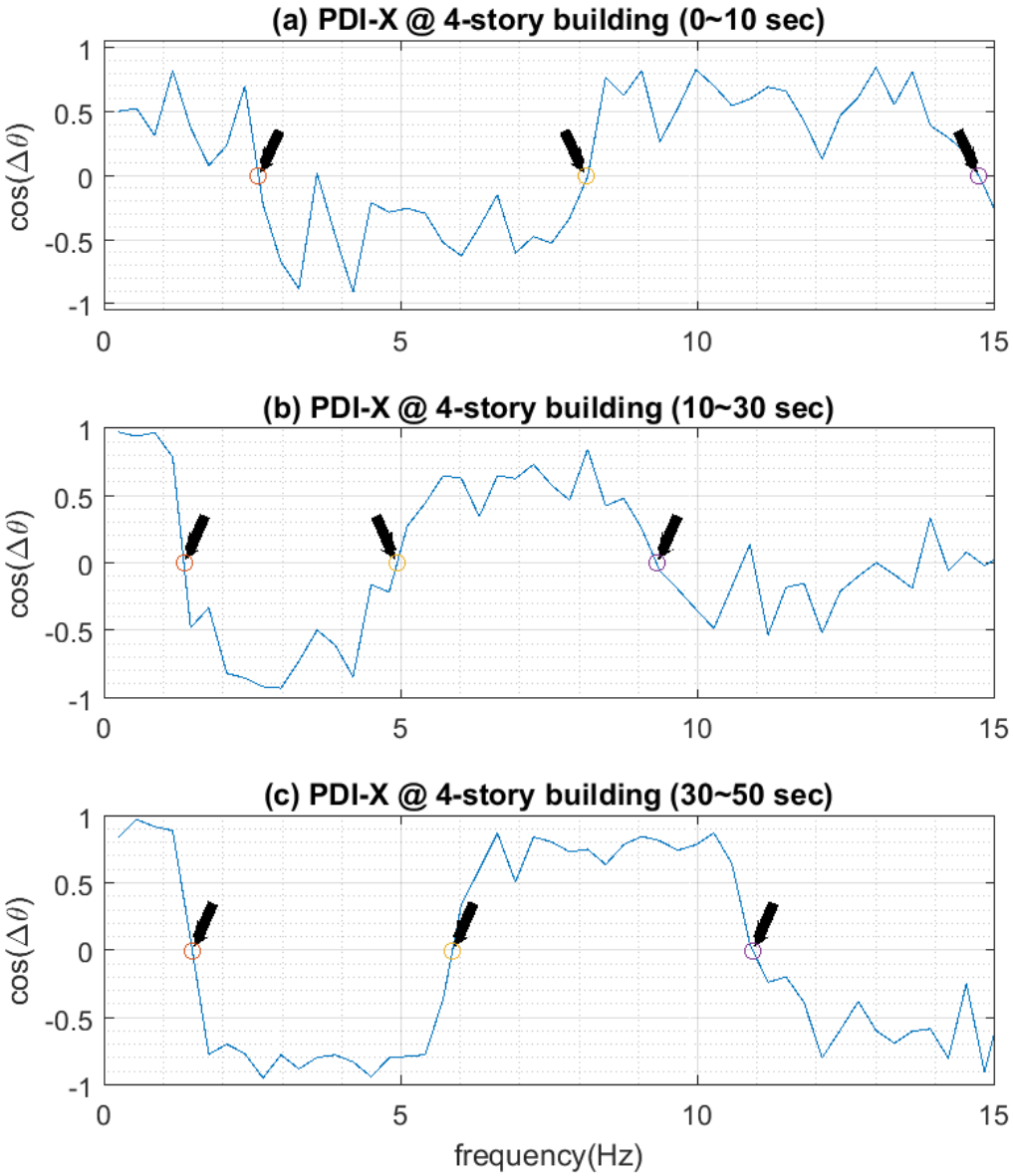

Fig. 8.15. The Time-PDI plots in X direction of the four-story RC building. f_{nx}= (a):[2.61, 8.12, 14.75]Hz, (b):[1.35, 4.94, 9.32]Hz, (c):[1.49, 5.88, 10.94]Hz.

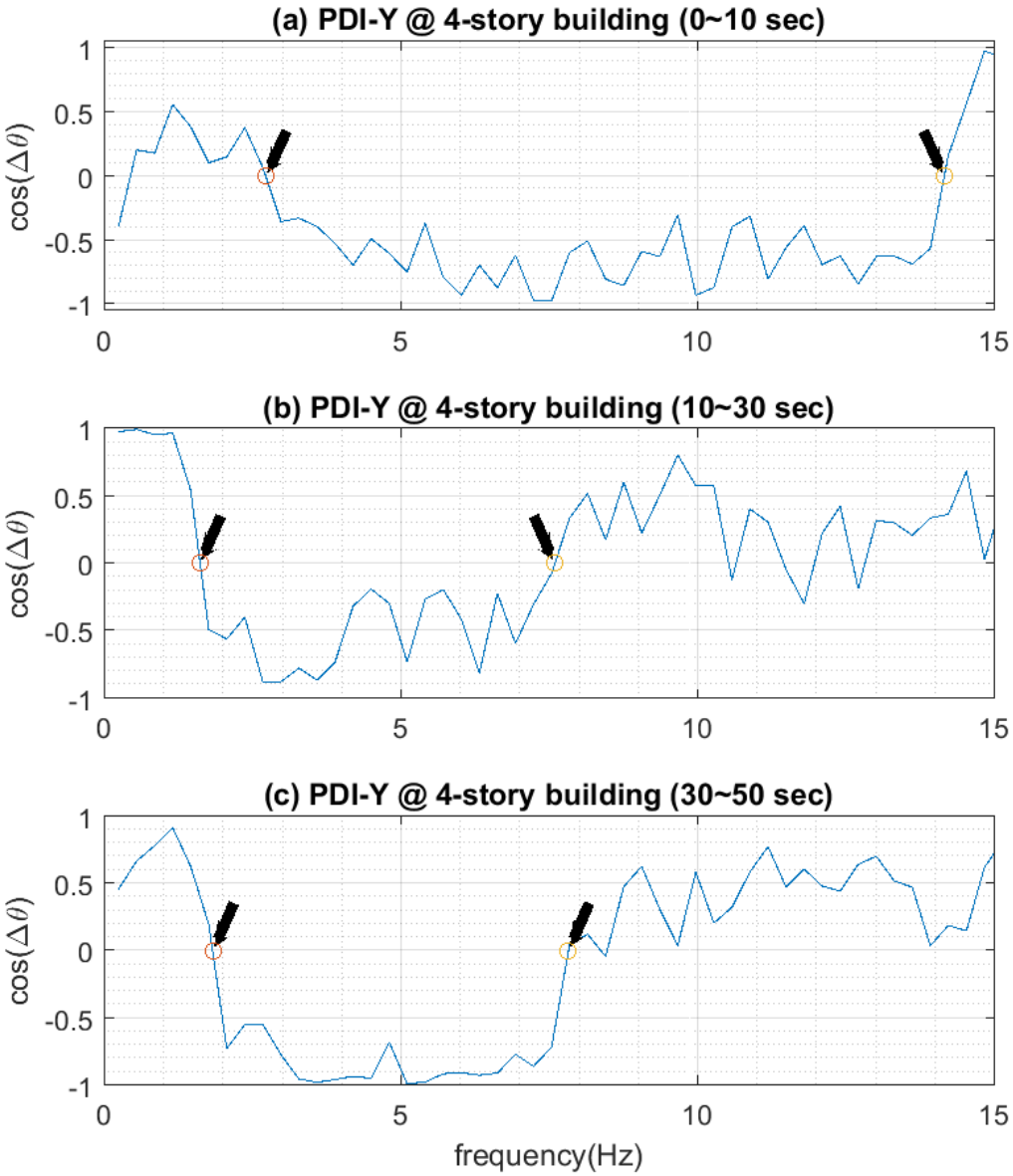

Fig. 8.16. The Time-PDI plots in Y direction of the four-story RC building. f_{ny}= (a):[2.73, 14.17]Hz, (b):[1.62, 7.60]Hz, (c):[1.84, 7.83]Hz.

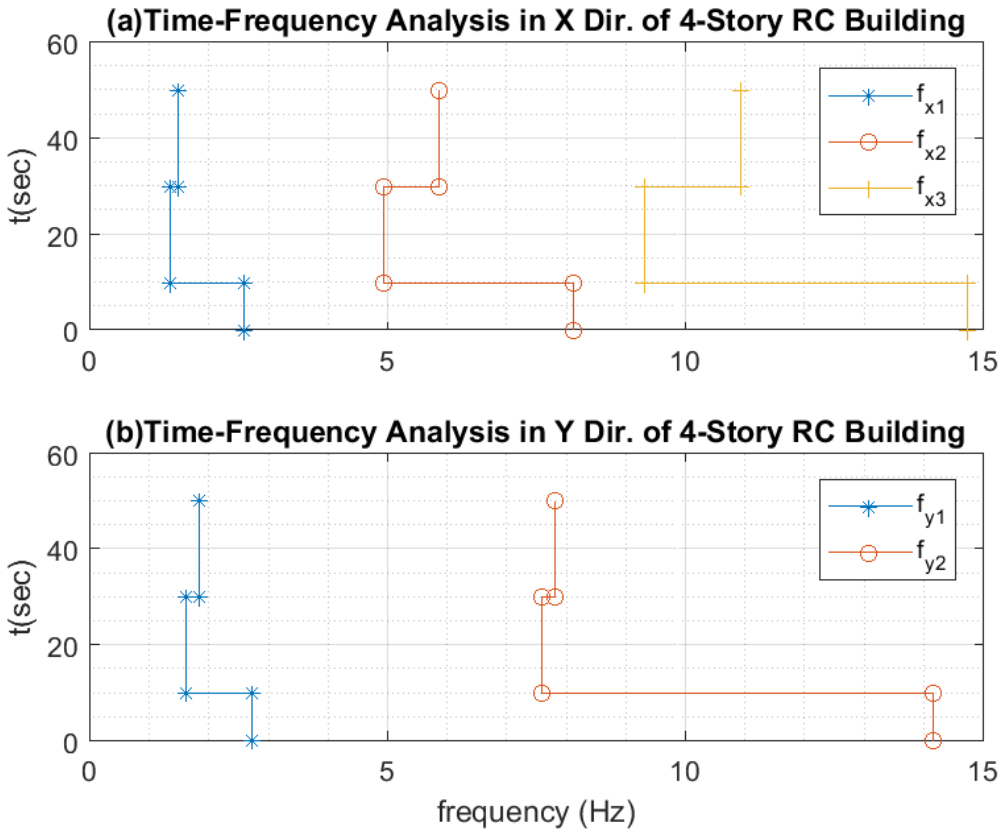

Fig. 8.17. The time-frequency analysis of the four-story RC building.

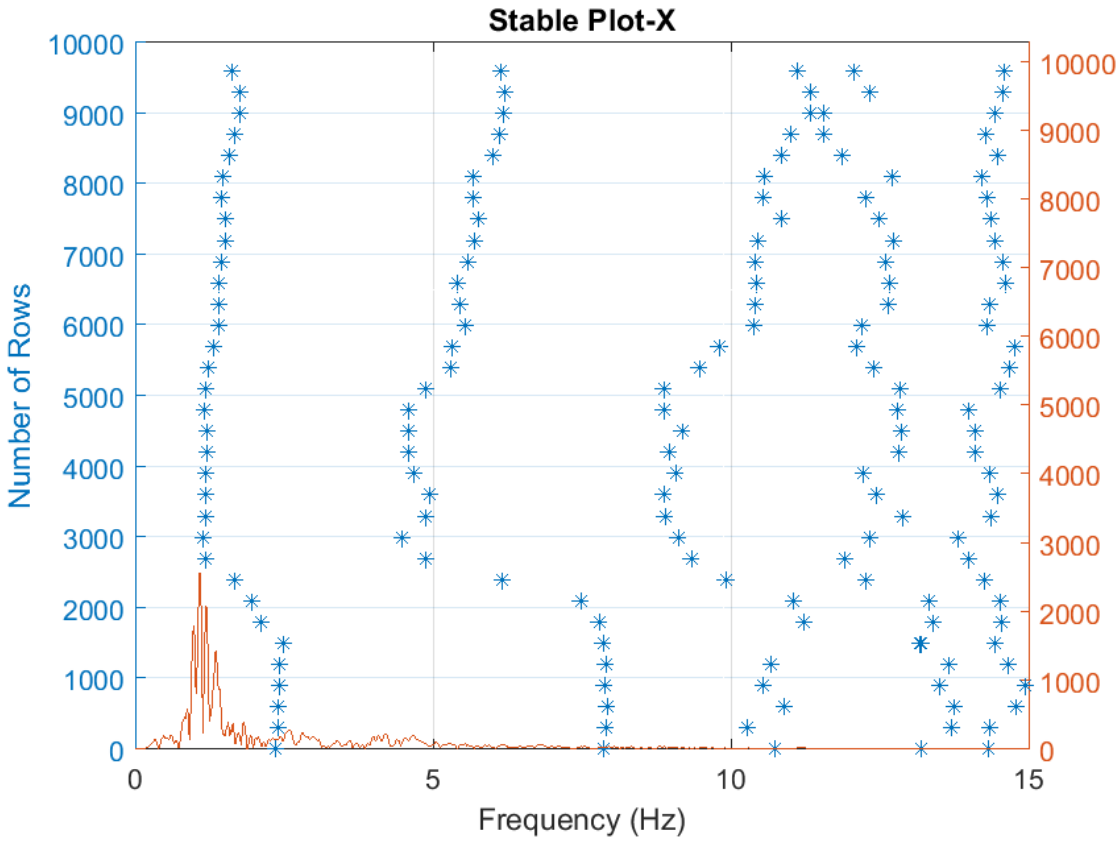

Fig. 8.18. The stable plot by the subspace method in X direction of the four-story RC building. In this case, the conversion of time and rows is 51.24 seconds=10,248 rows. For example, T= 0∼10 sec represents Row= 0 ∼2,050.

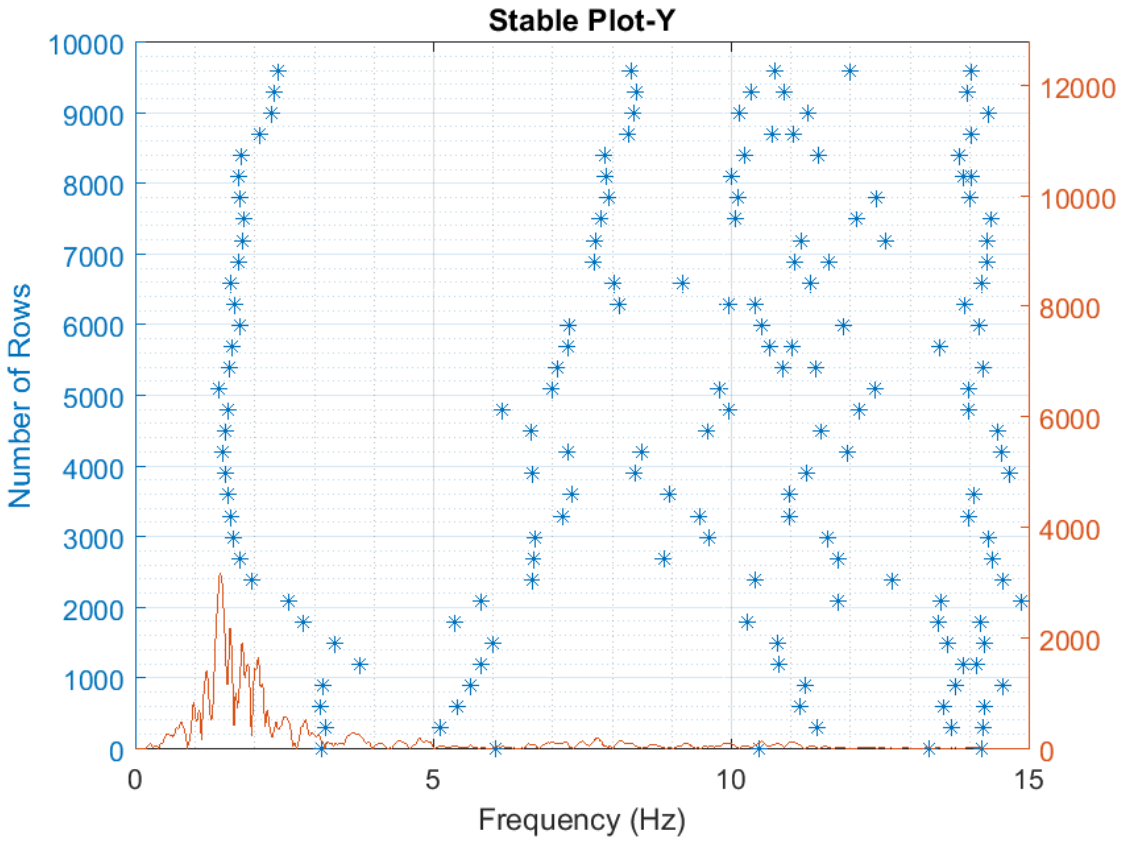

Fig. 8.19. The stable plot by the subspace method in Y direction of the four-story RC building. In this case, the conversion of time and rows is 51.24 seconds=10,248 rows. For example, T= 0∼10 sec represents Row= 0 ∼2,050.

9. SUMMARY

9.1 Objectives and Scope

The objective of this research is to develop a method for identifying the frequencies and order of natural modes of buildings using dynamic response records obtained in them. The core idea of the proposed method is based on the fact that there are patterns in the mode shapes of typical buildings. Therefore, the phase difference between modal displacements at different floors should also have patterns. For example, the pattern of relative motion between the roof and ground is "in-phase", "out-of-phase", "in-phase",and so on, i.e., between "in-phase" and "out-of-phase" switching regularly corresponding to mode order. Using common patterns of phase difference, the natural frequencies of buildings can be identified and so can the order modes.

Along with describing the proposed method, the scope of this research is to verify the proposed method with numerical models and to apply the proposed method to ten monitored buildings in U.S. and Taiwan selected from earthquake response databases, and one full-scale 4-story RC model tested on an earthquake simulator in Japan. The method is verified with the following simulations and earthquake strong motion data:

1. Numerical Models of 2DOF, 4DOF, 7DOF, and 10DOF building with equal mass, equal story height and stiffness k. Two kinds of input seismic force are used, including 1 Watt white noise for 60 seconds, and a record from 1999 the Ji-Ji earthquake record in WNT station from Taiwan database [31].

2. Numerical Models of 1-story, 5-story, 10-story and 26-story with equal mass per story, equal inter-story height and stiffness k. Ji-Ji earthquake(20 September 1999 at 17:47:12.6 UTC) record in WNT station is adopted to be the input acceleration.

3. Five buildings selected from the " Center for Engineering Strong Motion Data " website [2].

    - Case 1: Los Angeles, 8 story building of California State University, Northridge-17Jan1994.
    - Case 2: Newport Beach - 11-story Hospital, Northridge-17Jan1994.
    - Case 3: Los Angeles - 54 story Office Building, Northridge-17Jan1994.
    - Case 4: Los Angeles - 6-story Parking Structure, Northridge-17Jan1994.
    - Case 5: Los Angeles - 19 story Office Building, Northridge-17Jan1994.

4. Five buildings selected from the Taiwan's earthquake database [31].

    - Case 1: Building of Department of Civil Engineering, National Chung Hsin University (TCUBA3), Earthquake UT1999/ 7/ 7
    - Case 2: Building of Department of Civil and Construction Engineering, National Taiwan University of Science and Technology (TAPBA5), Earthquake UT2004/ 5/16
    - Case 3: Dormitory Building of Faculty & Staff, National Chiao Tung University (TCUBA6), Earthquake UT2002/ 2/12
    - Case 4: Headquarters building, Taiwan Power Company (TAPBA4), Earthquake UT1999/ 9/20
    - Case 5: National Chiao Tung University Library (TCUBAA), Earthquake UT1999/ 9/20

5. A full-scale, four-story RC building on the NIED E-Defense earthquake simulator [29], [30].

9.2 Method Description

The main procedure of PDI analysis are as follows:

1. Decompose frequency spectrum of roof and ground (or other assigned floor) by band pass FIR (finite impulse response) filter, frequency bandwidth of which is 0.05 or 0.1 Hz, into N sets to get acceleration records corresponding to each narrow frequency bandwidth. The cutoff frequencies in each corresponding band pass filter are (f_i, f_{i+1}), and $i = 1.....N$.

2. Find all the displacement curves of roof and ground (or other assigned floor) corresponding to each narrow frequency bandwidth in step one.

3. Calculate the phase difference [32] and the PDI corresponding to each narrow frequency bandwidth obtained from step 2 . Then, set of points $((f_i + f_{i+1})/2, PDI_i)$ can be obtained.

4. To Collect N pairs of points and drawing the Phase Difference Index(PDI) plot.

5. In PDI (Roof/Ground floor) plot, zero-crossing points are thought to be the natural frequencies. In PDI (Roof/2nd floor) plot, the frequency zones within each zero-crossing point indicates the corresponding frequency window for the associated natural frequency. In the PDI-torsion plot (calculated by a pair of accelerometers on the roof), the frequency corresponding to PDI=-1 (or close to -1) represents the natural torsional frequency.

6. The identification results from PDI curves are compared with peak-picking method in FRF plots.

7. In Time-PDI method, the displacement curves are truncated into two or more intervals, and the PDI of each truncated signal is calculated individually. The dynamic properties of the structure can be observed in the Time-PDI curve.

9.3 Conclusion

1. For the studied theoretical and actual buildings with modal properties listed in Tables 4.1∼4.8, Tables 5.1∼5.4, Tables 6.7∼6.11 and Tables 7.7∼7.11, the proposed method to estimate periods of linear building structures using phase differences (PDI) produced:

    - period estimates within 1.4% of theoretical estimates obtained with modal analysis (Chapter 4 & 5)
    - period estimates within 3.7% of values obtained by Naeim et al., 2005 and Loh et al., 2010 using the conventional peak-picking method for ten instrumented buildings, and
    - Higher-mode period estimates (for 2/3 to 1/5 of the total number of nominal modes) within 17% of values estimated from the rule of thumb indicating that the ratios of frequencies in a typical buildings follow the shear beam model, i.e., the sequence 1:3:5:7:9....

2. In cases with obvious nonlinear response, estimates produced by the proposed method (PDI) still could identify the variation of natural frequencies.

3. In cases in which the first mode and the torsional mode had similar periods, estimates produced by the proposed method (PDI) were less accurate because of aliasing.

4. No other method known to the writer can produce as many period estimates for a given structure as the proposed method does and with similar confidence. Another advantage of the proposed method is that it helps pairing period estimates and mode shapes.

10. RECOMMENDATIONS

Recommendations for future work include:

10.1 Method Application

1. Long term monitoring data analysis by PDI method:
   Using PDI plot to analyze a building over a long term of seismic response monitoring data and comparing results with other methods would be a good study to see how sensitive PDI is to small and slow changes, if any, in modal properties of a building .

2. Applying the PDI method to analyze monitored bridges:
   PDI plot may also apply to bridges because typical bridges have mode shape patterns.

10.2 Method Improvement

1. In this dissertation, PDI is taken as the arithmetic mean of each instantaneous phase difference in each time step. Although such definition has already achieved good identification results, it might be still worth, in mathematical terms, to try to use different weights based on such as amplitude of response or length of time interval, to calculate the PDI, and observe if there is any improvement.

2. In PDI calculation, the frequency spectrum is decomposed into 100$\sim$200 narrow frequency bands, and all bands are equal in width. The narrower bandwidth one uses, the higher order of FIR filter one needs, and the more time com-

puters need to do the calculation. Most of the time, a narrower frequency bandwidth is needed in the low frequency zone of high-rise buildings. Thus, changing frequency bandwidth (window size) might become a practical issue if the calculation time matters.

3. Currently all identification methods for buildings need manual post-processing to determine the mode order because the mode orders can not be interpreted only by spectrum in frequency-domain analysis or eigenvalues calculated in time-domain analysis. PDI plot may offer a different perspective to achieve the goal automatically using computer interpretation.

10.3 Other Suggestions

1. In numerical model tests, it is found that even a small amount of torsion blurs the FRF curves and PDI curves. The phenomenon deteriorates the quality of building monitoring, perhaps more than it is acknowledged in publications. Thus, it is better, if feasible, to install the accelerometer at the stiffness center to avoid the interference of torsion.

2. In order to obtain the PDI-T curve, it is recommended that a pair of accelerometers be installed at opposite sides on the roof (or in an upper floor).

3. For targeting the possible frequency bandwidth of each mode, it is strongly recommended that at least two accelerometers (in both principal directions) be installed on the second floor.

REFERENCES

REFERENCES

[1] C. W. B. Taiwan. Taiwan's structure strong earthquake monitoring system. [Online]. Available: http://gdms.cwb.gov.tw/gdms-build.php

[2] USGS. (2017, Jun.) Usgs earthquake monitoring of structures. [Online]. Available: https://earthquake.usgs.gov/monitoring/nsmp/buildings/

[3] G. A. Prieto, J. F. Lawrence, A. I. Chung, and M. D. Kohler, "Impulse response of civil structures from ambient noise analysis," *Bulletin of the Seismological Society of America*, vol. 100, no. 5A, pp. 2322–2328, 2010.

[4] C.-H. Loh, S.-H. Chao, J.-H. Weng, and T.-H. Wu, "Application of subspace identification technique to long-term seismic response monitoring of structures," *Earthquake Engineering & Structural Dynamics*, vol. 44, no. 3, pp. 385–402, 2015, eQE-14-0015.R2. [Online]. Available: http://dx.doi.org/10.1002/eqe.2475

[5] E. Reynders, "System identification methods for (operational) modal analysis: Review and comparison," *Archives of Computational Methods in Engineering*, vol. 19, no. 3, pp. 51–124, 2012. [Online]. Available: https://link.springer.com/article/10.1007/s11831-012-9069-x

[6] R. Astroza, H. Ebrahimian, J. P. Conte, J. I. Restrepo, and T. C. Hutchinson, "System identification of a full-scale five-story reinforced concrete building tested on the nees-ucsd shake table," *Structural Control and Health Monitoring*, vol. 23, no. 3, pp. 535–559, 2016, sTC-14-0172.R1. [Online]. Available: http://dx.doi.org/10.1002/stc.1778

[7] N. Nakata, W. Tanaka, and Y. Oda, "Damage detection of a building caused by the 2011 tohoku-oki earthquake with seismic interferometry," *Bulletin of the Seismological Society of America*, 2015.

[8] B. Petrovic, D. Bindi, M. Pilz, M. Serio, S. Orunbaev, J. Niyazov, F. Hakimov, P. Yasunov, U. T. Begaliev, and S. Parolai, "Building monitoring in bishkek and dushanbe by the use of ambient vibration analysis," *Geophysics*, vol. 58, p. 1, 2015.

[9] D. Huston, *Structural Sensing, Health Monitoring, and Performance Evaluation (Series in Sensors)*, 1st ed. CRC Press, 2010.

[10] A. K. Chopra, *Dynamics of structures: theory and applications to earthquake engineering.*, 4th ed. Pearson, 2012.

[11] Z.-F. Fu and J. He, *Modal Analysis*, 4th ed. Butterworth-Heinemann, 2001.

[12] P. V. O'Neil, *Advanced Engineering Mathematics*, 7th ed. Cengage learning, 2012.

[13] W. Wang, *Introduction to Digital Signal and System Analysis*. Ventus Publishing ApS, 2012. [Online]. Available: http://bookbcon.com

[14] L. Cohen, *Time-Frequency Analysis*, 1st ed. Prentice-Hall PTR, A Pearson Education Company, 2007.

[15] P. Diniz, E. da Silva, and S. Netto, *Digital Signal Processing: System Analysis and Design*. Cambridge University Press, 2002. [Online]. Available: https://books.google.com.tw/books?id=L9ENNEPbZ8IC

[16] H.-C. Chiu, "Stable baseline correction of digital strong-motion data," *Bulletin of the Seismological Society of America*, vol. 87, no. 4, pp. 932–944, 1997.

[17] Mathworks. Matlab detrend. [Online]. Available: https://www.mathworks.com/help/matlab/ref/detrend.html

[18] A. F. Shakal, M. J. Huang, and V. M. Graizer, *Strong-motion data processing, International Handbook of Earthquake & Engineering Seismology, Part B*. Academic Press, 2003, vol. 81B.

[19] J. O. S. III, *Mathematics of the Discrete Fourier Transform (DFT): with Audio Applications*, 2nd ed. W3K Publishing, 2007.

[20] P. Welch, "The use of fast fourier transform for the estimation of power spectra: A method based on time averaging over short, modified periodograms," *IEEE Transactions on Audio and Electroacoustics*, vol. 15, no. 2, pp. 70–73, Jun 1967.

[21] USGS. Center for engineering strong motion data. [Online]. Available: https://www.strongmotioncenter.org/

[22] ASCE, *Minimum Design Loads for Buildings and Other Structures*, asce 7-98 ed. American Society of Civil Engineers, 2000. [Online]. Available: http://ascelibrary.org/doi/abs/10.1061/9780784404454

[23] USGS. Northridge1994. [Online]. Available: https://pubs.usgs.gov/of/1996/ofr-96-0263/introduc.htm

[24] F. Naeim, S. Hagie, A. Alimoradi, and E. Miranda, "Automated post-earthquake damage assessment and safety evaluation of instrumented buildings," vol. 66, 01 2005.

[25] M. Rahmani and M. I. Todorovska, "1d system identification of a 54-story steel frame building by seismic interferometry," *Earthquake Engineering & Structural Dynamics*, vol. 43, no. 4, pp. 627–640, 2014.

[26] CWBT. Central weather bureau, taiwan. [Online]. Available: http://www.cwb.gov.tw/V7/earthquake/research.htm

[27] C.-H. Loh, *Application of CWB structural earthquake monitoring data to evaluate the horizontal/vertical building seismic design code of Taiwan, 2014*. Central Weather Bureau, Taiwan, 2014. [Online]. Available: http://scweb.cwb.gov.tw/research/64vol/MOTC-CWB-103-E-14.pdf

[28] ——, *Application of CWB structural earthquake monitoring data to evaluate the horizontal/vertical building seismic design code of Taiwan, 2015*. Central Weather Bureau, Taiwan, 2015. [Online]. Available: http://scweb.cwb.gov.tw/research/65vol/MOTC-CWB-104-E-16.pdf

[29] T. Nagae, T. Matsumori, H. Shiohara, T. Kabeyasawa, S. Kono, M. Nishiyama, J. Moehle, J. Wallace, R. Sause, and W. Ghannoum, "The 2010 e-defense shaking table test on four-story reinforced concrete and post-tensioned concrete buildings," 07 2014.

[30] J. Wallace, "U.s. instrumentation and data processing for the 4-story rc and post-tensioned e-defense building tests (nees-2011-1005)," May 2017. [Online]. Available: https://datacenterhub.org/resources/14266

[31] C. W. B. Taiwan. Taiwan's disastrous earthquake data base. [Online]. Available: http://www.cwb.gov.tw/V7/earthquake/research.htm

[32] G. M. Ballou, *Handbook for Sound Engineers*, 3rd ed. Focal Press, 2008.

[33] N. Satake, K.-i. Suda, T. Arakawa, A. Sasaki, and Y. Tamura, "Damping evaluation using full-scale data of buildings in japan," *Journal of structural engineering*, vol. 129, no. 4, pp. 470–477, 2003.

[34] Mathworks. Matlab detrend. [Online]. Available: https://www.mathworks.com/help/ident/ref/n4sid.html

APPENDICES

A. COMPARISON OF THREE METHODS FOR PHASE DIFFERENCE CALCULATION

In Chapter 3, three methods are introduced for phase difference calculation. In this chapter, the three methods are used in the same example to compare the differences. In the following content, we use Van Nuys 7 story hotel with Westwood Village earthquake in June 1st ,2014 as an example. The sensor locations in the hotel is shown as Fig. A.1. In this example, channel 9 and channel 16 are selected to be analyzed. There are three possible ways to calculate the phase difference between the Ch.16 (Ground) and Ch.9 (Roof):

1. Phase angle difference from Fourier Spectrum
2. Maximum cross correlation of two signals
3. Instantaneous frequency difference calculated by Hilbert Transform.

A.1 Basic Information

A.1.1 Station Information

- Station No.: CGS - CSMIP Station 24386
- Station name: Van Nuys - 7-story Hotel, LA
- Location: 34.220N, 118.471W
- Earthquake: Westwood Village Earthquake of 01 Jun 2014
- Epicenter: 34.100 N, 118.490W
- Distance between station and epicenter: 13.47 km
- Start Time: 6/02/14, 02:36:24.0 UTC
- Record Length(sec): 57.00

- Sample Rate(Hz): 200
- Sensor Locations plan : Fig. A.1
- Selected Sensor: Ch.09 (Roof), & Ch.16 (ground)
- Peak acceleration = -9.502 cm/sec^2 at 25.545 sec.
- Data Source : Center For Engineering Strong Motion Data
  http://www.strongmotioncenter.org/

A.1.2 PDI Plot by Three Methods

Fig.A.3 is the comparison of PDI plots in X direction by using three different methods (Fourier transform, Max cross correlation, and Hilbert transform).

Fourier transform

In the Fig.A.3-(a), the approximate 1st mode and 2nd mode (zero-crossing points with y-axis) can roughly be identified. However, the disadvantage is its obvious noise interference. Therefore, it seems not an ideal method to identify the natural mode.

Max. Cross-correlation

In the Fig.A.3-(b), the 1st mode and 2nd mode (zero-crossing points with y-axis) can be identified clearly. The curve is even smoother than Fig.A.3-(c) in the range of $f = [0 \sim 5]$ Hz. The only concern is that larger jumps occurring at f=9.5 Hz and f=13.2 Hz.

Hilbert Transform

In the Fig.A.3-(c), the 1st mode and 2nd mode (zero-crossing points with y-axis) can be identified clearly. Although there are some small fluctuations in the curve, in

general, the curve has no big jumps. Therefore, it would be easier to find zero-crossing points.

A.2 Conclusion

The Van Nuys 7-story hotel is used as an example to test the difference of (i) phase difference of Fourier Spectrum, (ii) maximum cross correlation of 2 signals, and (iii) instantaneous phase difference by Hilbert transform. All three methods can generate similar curves. However, the first one (true phase by Fourier spectrum) has more noise interference. The 2nd method and 3rd method have clearer resolution and thus can be studied further. From the adopted example, it is found that setting amplitude criteria or not does not affect the identification of the 1st mode.

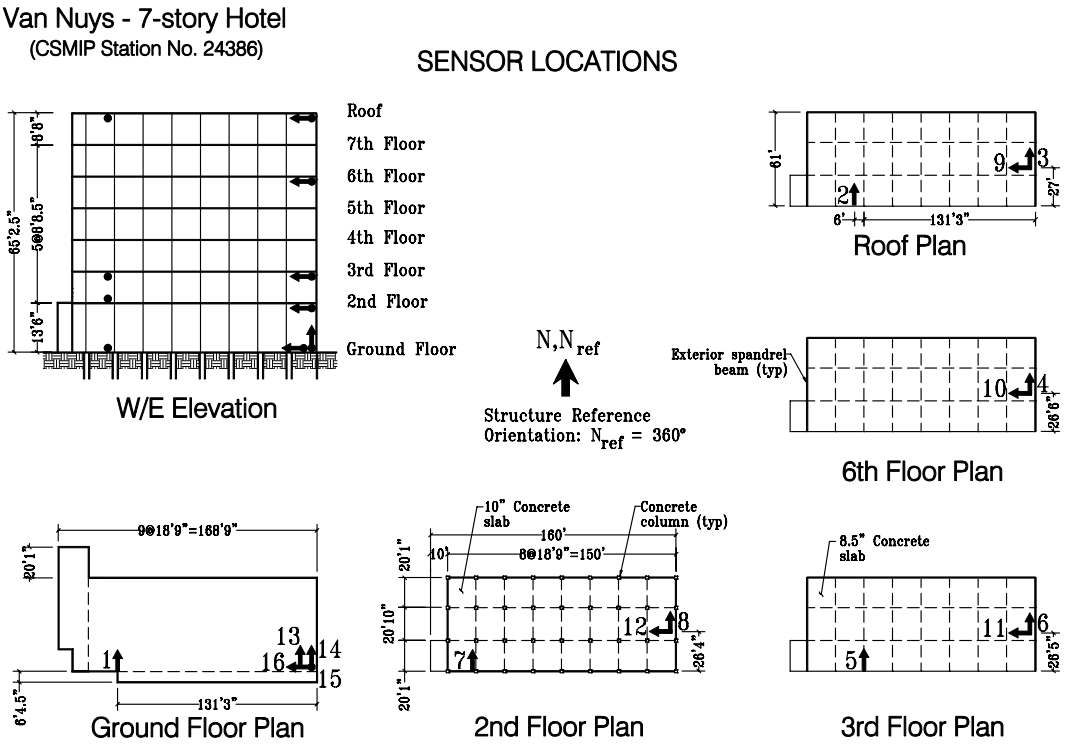

Fig. A.1. Sensor locations of Van Nuys 7-story building [21]

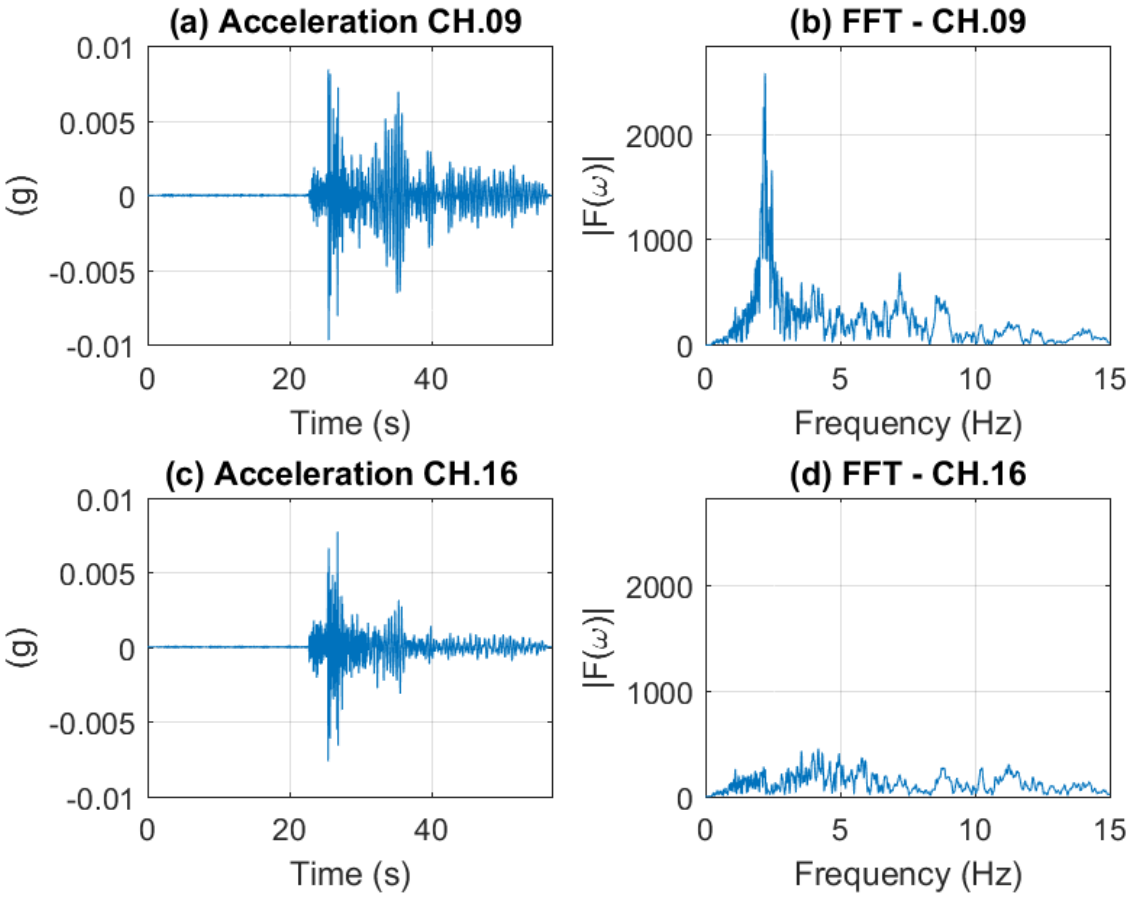

Fig. A.2. Acceleration records of Ch.09 & Ch.16 of Van Nuys 7-story building, Westwood Village Earthquake of 01 Jun 2014: (a) Acceleration time history curve of Ch.09, (b) Fourier Spectrum of Acceleration record of Ch.09, (c) Acceleration time history curve of Ch.16, (d) Fourier Spectrum of Acceleration record of Ch.16,

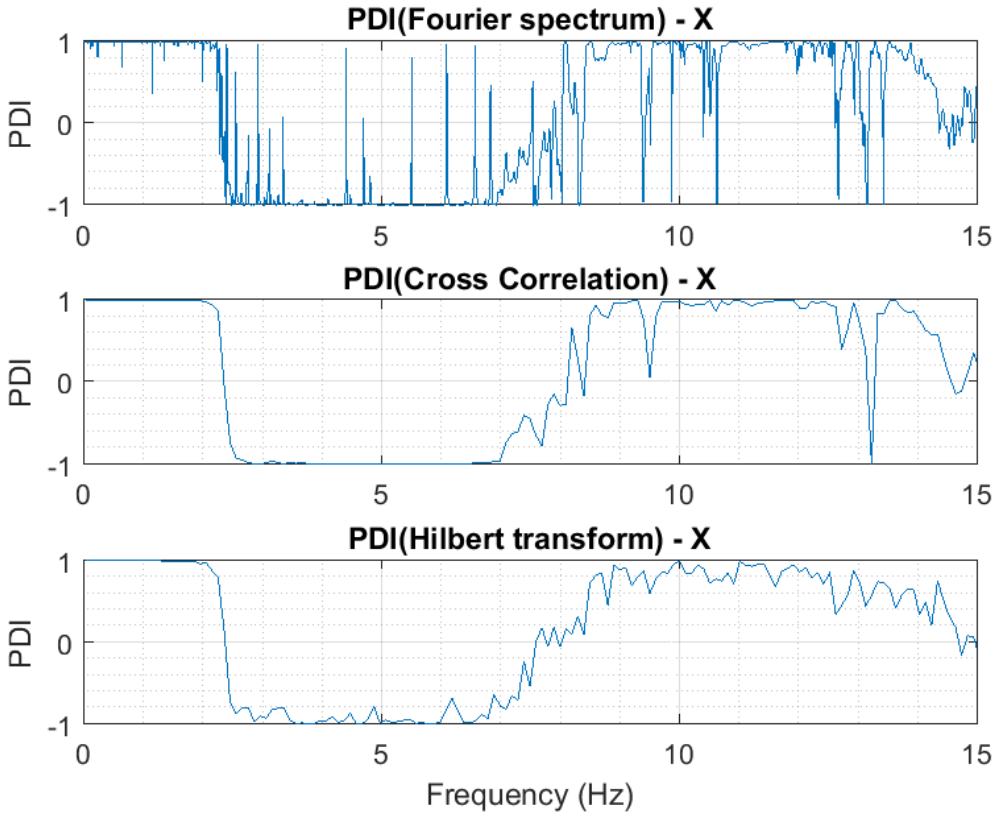

Fig. A.3. Comparison of three methods for PDI plot in X direction

B. AVOIDANCE OF SINGULARITY IN HILBERT TRANSFORM

B.1 Instantaneous Frequency of Analytic Signal

Hilbert transform sometimes is criticized for the singularity occurring at the low amplitude point. The following equation explains the how the singularities occur. For any given signal

$$f(t) = a \times (\cos\theta + i * \sin\theta) \tag{B.1}$$

let $x = \cos\theta, y = \sin\theta \rightarrow \theta = \arctan(\frac{y}{x})$

$$\omega = \frac{d\theta}{dt} = \frac{\frac{\mathrm{d}}{\mathrm{d}t}(\frac{y}{x})}{1 + (\frac{y}{x})^2} = \frac{1}{a^2}(x\frac{\mathrm{d}y}{\mathrm{d}t} - y\frac{\mathrm{d}x}{\mathrm{d}t}) \tag{B.2}$$

where:

a:amplitude of signal

ω:instantaneous frequency (rad/s)

If a (amplitude) is near zero, the frequency will become a singular point. To illustrate the limitation of Hilbert transform, we still use Van Nuys 7 story hotel with data from the Westwood Village earthquake in Jun. 1st ,2014 as an example to illustrate the phenomenon. Fig.B.1-(a) is the filtered signal of Ch.16 and Ch.9 of which the frequency bandwidth is [2∼2.1] Hz. For a narrow bandwidth frequency, the beat frequency may be observed obviously (shown as Fig.B.1-(a)). In the range of small amplitude, the corresponding phase difference becomes unstable (shown as Fig.B.1-(a)-b & c). Such singular points might cause imprecise results of phase difference index (PDI) since PDI is the average of phase difference of whole time steps.

B.2 Eliminating Singularity Points

To eliminate singular points of instantaneous frequency, we have to ignore the phase differences of small amplitude. However, the definition of small is rather subjective. In this dissertation, a standard procedure is proposed here, and the threshold of small amplitude is suggested to be the 0.1 maximum amplitude of filtered signal.

1. Calculating the instantaneous amplitude:

   The relationship of analytic signal and amplitude is:

   $$S_a(t) = s(t) + j\widehat{s}(t) \tag{B.3}$$

   The instantaneous amplitude :

   $$A(t) = |S_a(t))| \tag{B.4}$$

   Shown as Fig. B.2, (a) is Ch. 9 and (b) is Ch.16. The upper figure is the original filtered signal and the lower figure is the absolute amplitude envelope.

2. Defining a threshold of low amplitude:

   In this example, the threshold of low amplitude is defined as 0.1 maximum of filtered signal (shown as Fig. B.3). If the amplitude $< 0.1 \times max$ amplitude, the weight of PDI is 0. If the amplitude $> 0.1 \times max$ amplitude, the weight of PDI = 1.

3. Calculating the weighted PDI:

   After defining the threshold of low amplitude, we can calculate the weighted PDI and compare the weighted PDI with original PDI. The calculation equations can be expressed as below:

   $$PDI_{non-weighted} = \frac{1}{N_1} \times \sum_{i=1}^{N_1} PDI_i \tag{B.5}$$

   $$PDI_{weighted} = \frac{1}{N_2} \times \sum_{i=1}^{N_1} w(i) PDI_i \tag{B.6}$$

   where:

N_1: The length of $S_a(t)$

N_2: The length of $S_a(t)$ of which magnitude $\geq 0.1 \times max(|S_a(t)|)$

$w(i)$: weight of PDI

$=0$; if $PDI_i < 0.1 \times max(|S_a(t)|)$

$=1$; if $PDI_i \geq 0.1 \times max(|S_a(t)|)$

In the case of Van Nuys 7 story hotel with the condition of 0.1 max amplitude as threshold, the weighted PDI is 0.96 by using Eq.B.6, while the original PDI is 0.76 by using Eq.B.5.

B.3 Comparison of Different Amplitude Criteria

In last paragraph, we know that different criteria of low amplitude make different PDI value in each frequency bandwidth. Here, we use the same example with different criteria and observe the difference of PDI curve plot.

Figure B.5 includes four different criteria of amplitude limit condition: 0, 0.1 ,0.2 and 0.3. Four different amplitude criteria have approximate the same PDI curves, but are slightly different in details. At the first zero crossing point, four plots are almost the same. However, at the second zero crossing point, the four plots have different results. Although the differences seem tolerable, it is still worth to check if other cases have similar trend.

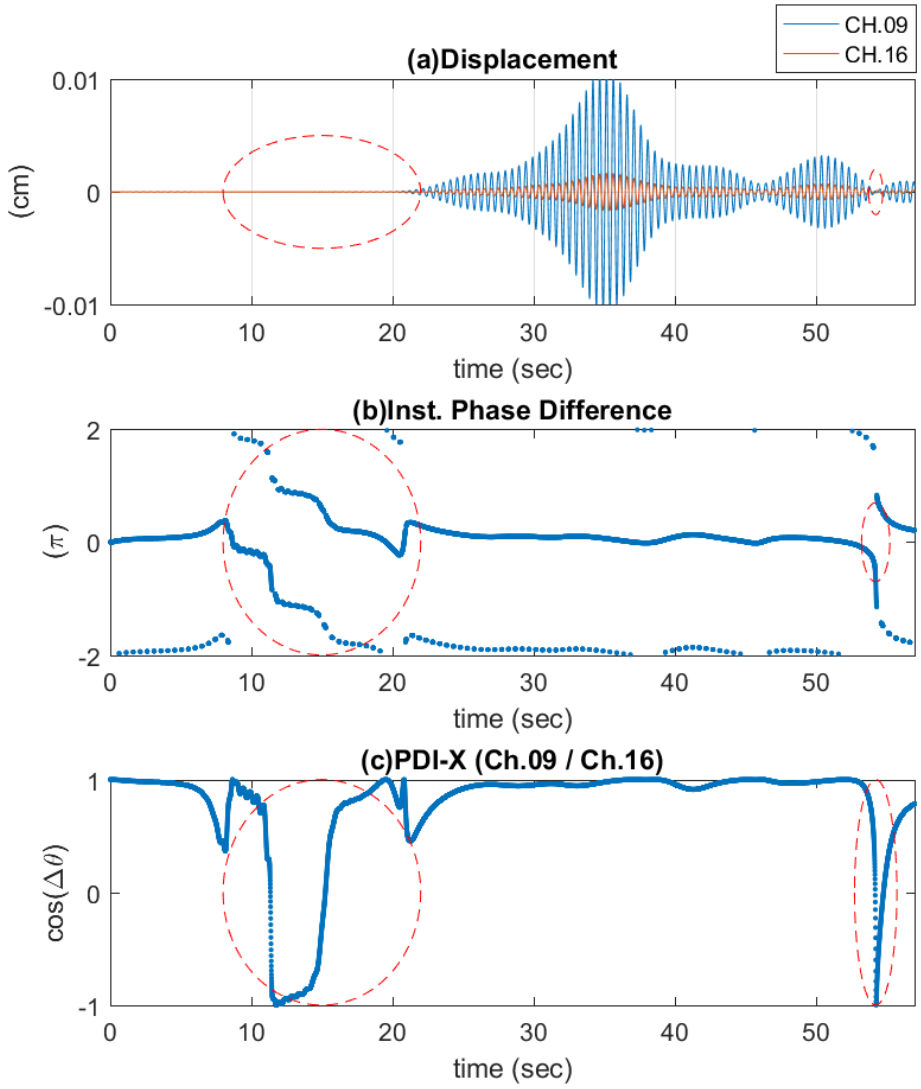

Fig. B.1. Singularity occurring in instantaneous frequency plot. (a) Ch.9 & Ch.16 filtered by band pass filter 2-2.1 Hz; (b). Instantaneous phase difference of Ch.9 & Ch.16; (c). PDI of Ch.9 & Ch.16.

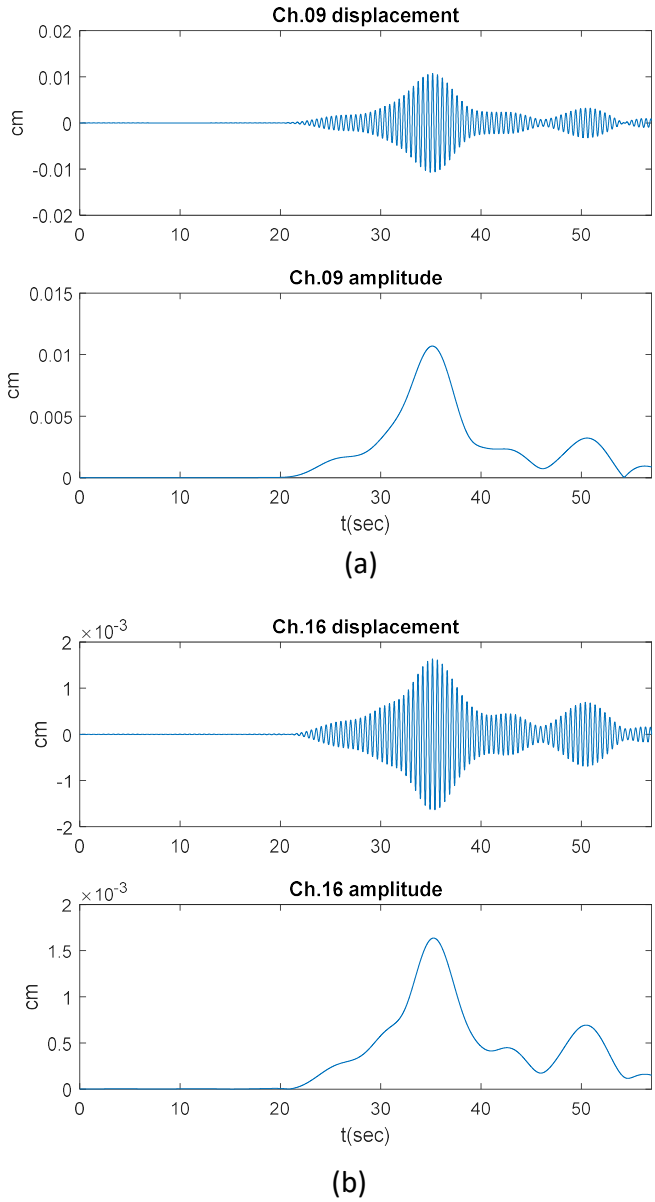

Fig. B.2. Envelope of Displacement curves (a)Displacement and amplitude of Ch.9; (b)Displacement and amplitude of Ch.16

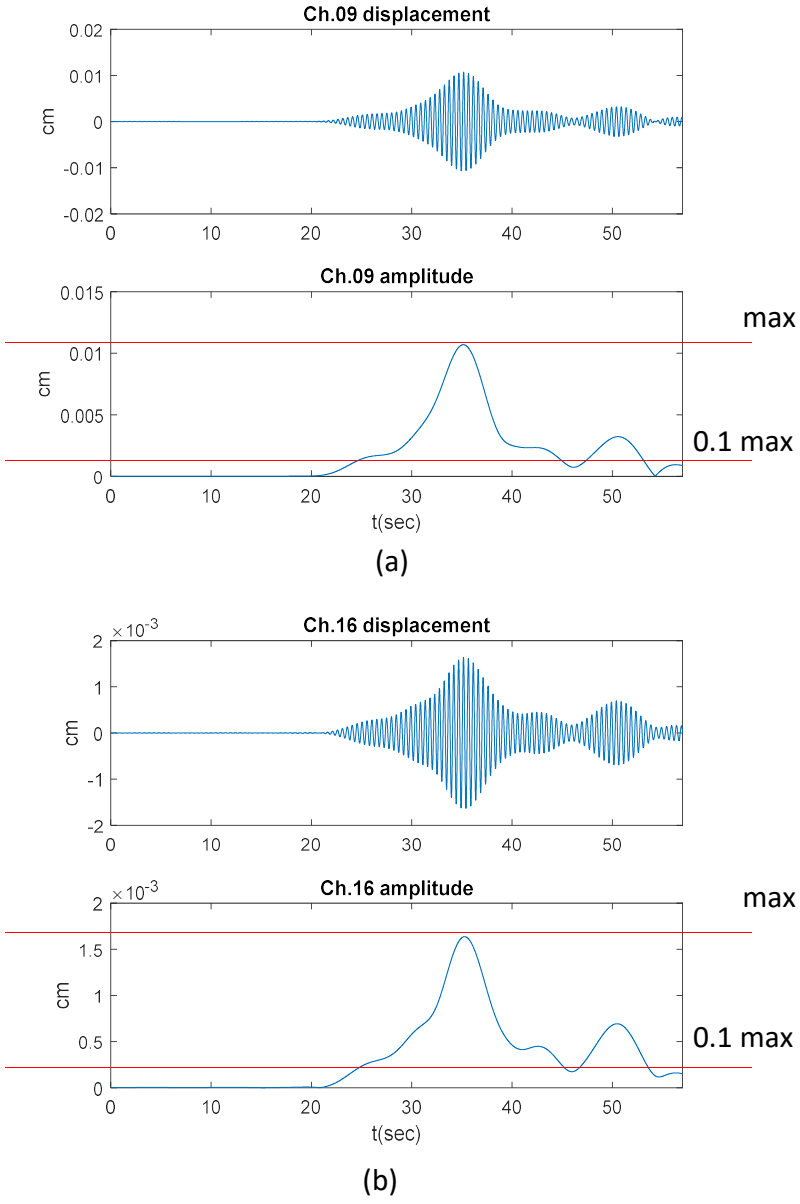

Fig. B.3. Threshold of Envelope (a)Red line represents max and 0.1 max amplitude of Ch.9; (b)Red line represents max and 0.1 max amplitude of Ch.16;

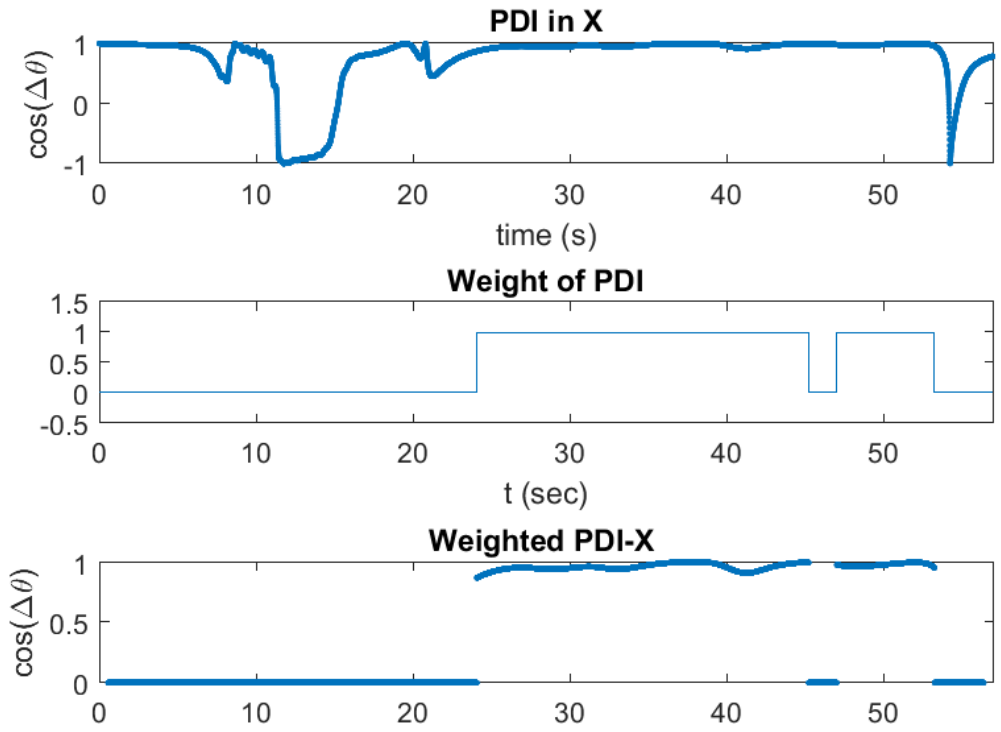

Fig. B.4. (a) Original PDI = 0.76; (b) Weighted PDI X.(weight= 0.1*max disp); (c) Weighted PDI-X=0.96

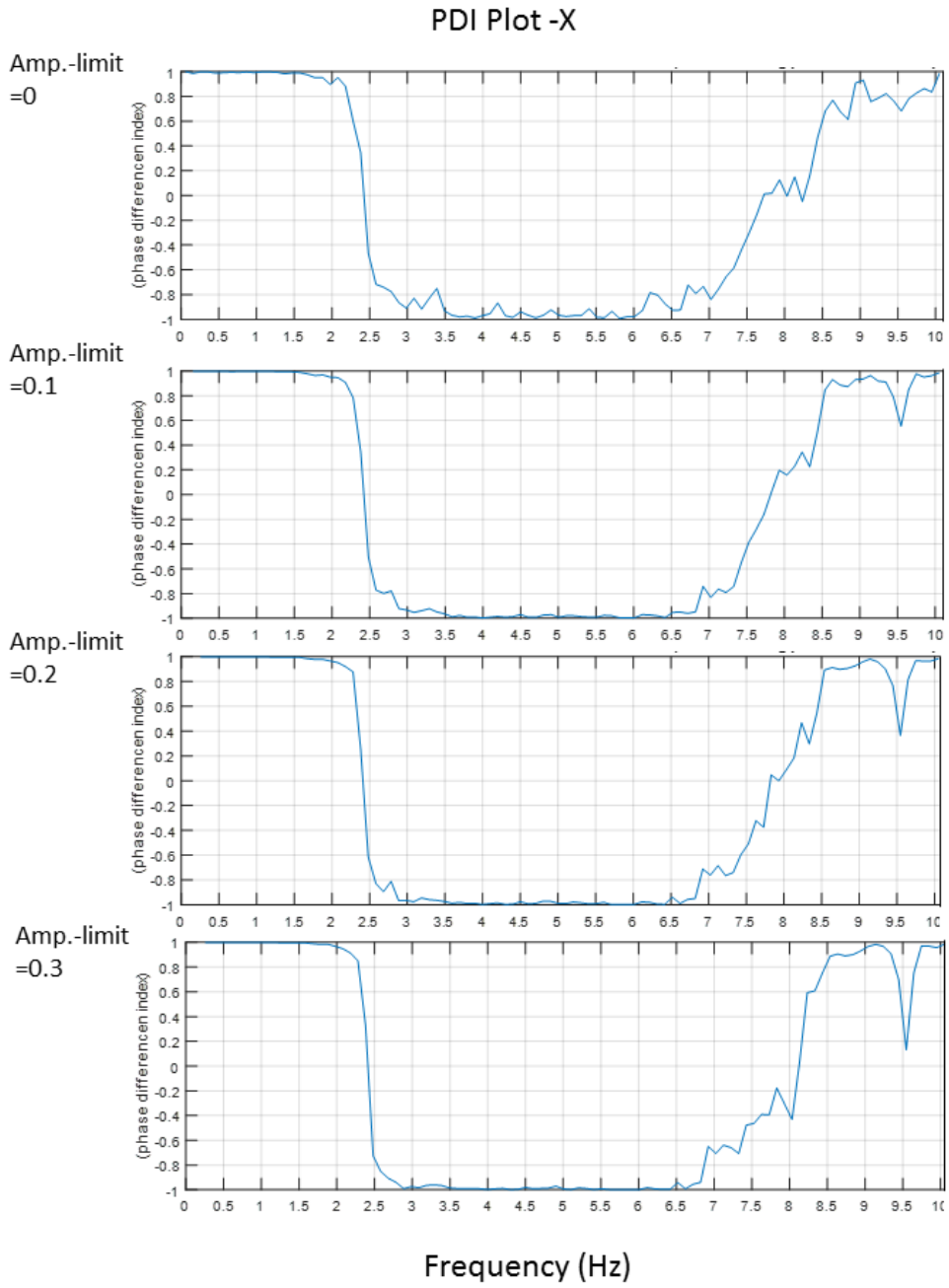

Fig. B.5. PDI Plots with different signal strength thresholds for consideration in PDI.

C. DETAILED ANALYSIS OF SMAPLE BUILDINGS IN U.S.

C.1 Case 1: Los Angeles- 8 story Building at California State University

C.1.1 Basic information

Case one is an 8 story building at California State University(CSMIP-STATION-24468). The structure is a reinforced concrete frame with shear walls at E-W sides from 2F to Roof. In this event, the maximum displacement is 10.22 cm (Ch.6). The corresponding drift is 10.24 cm (relative to Ch.16), and the drift ratio is 0.3%. The detailed information is shown in Table 6.2.

C.1.2 Sensors Information

There are 16 accelerometers in three levels of this building. The location of sensors are shown in Figure C.1. Eight sensors in this building are chosen to be studied. The channels and corresponding floors are listed in Table C.1.

C.1.3 Identification Result

Parameter for PDI plots

In case one, the adopted parameters are as listed:

- Observed frequency bandwidth: $0 \sim 5$ Hz
- Unit narrow frequency bandwidth: 0.05 Hz
- Order of FIR bandpass filter: 990
- Window length of Hamming window (for FRF plot): 25% data length.

X Direction

The PDI plot in X direction of this building is shown in Fig. C.2 which comprises three parts:

a. Phase difference index plot (Roof vs. ground)

   In Fig. C.2-(a), there are three zero-crossing points, which represent the natural frequencies of the building (the fourth and other points are not recognizable).

   – zero-crossing points of PDI-X: [0.64, 1.84, 4.04] Hz

   A suspected zero-crossing point occurs in $f \approx 3$ Hz, but it is not a natural mode frequency. The reason is explained in the next section.

b. Phase difference index plot (Roof vs. 2F)

   In Fig. C.2-(b) plot, the coordinate plot is separated by the PDI curve. PDI=1 means the roof and the second floor moving in the same direction i.e. moving in-phase. On the contrary, PDI=-1 means the roof and the second floor moving in the opposite directions, i.e. moving out-of-phase. The available acceleration had been bandpass filtered with cutoff frequency= $[(0.15 \sim 0.3)\ (23 \sim 25)]$ Hz in advance. Thus, the signals below $f = 0.2$ Hz can be ignored. Upon a visual review, we can divide the PDI coordinate into four parts:

   $\sim$ $0 < f < 0.2$: Ignored area.

   $\sim$ $0.2 < f < 0.8$: RF and 2F move in-phase

   $\sim$ $0.8 < f < 3.6$: RF and 2F move out-of-phase

   $\sim$ $f > 3.6$: RF and 2F move in-phase

   Since the PDI is from Roof/2F, the $LMOI(8)_{18} = 8$. Therefore, the plot may offer a useful information to assist evaluators to identify the modes of buildings. For example, in Fig. C.2-(a), $f = 3$ Hz seems to be a zero-crossing point, but the (b) plot can help people to exclude this spurious mode. A possible explanation for the spurious mode is that $f = 3 \sim 3.2$ is the 3rd torsional mode. By observing Fig. C.2-(a) and C.3-(a), responses around $f = 3.2$ Hz occur in

both plots. However, the guess can not be proven since the 3rd torsional mode can not be identified in Fig.C.9 and C.5.

c. Frequency response function plot (Roof vs.ground)

Figure C.2-(c) is a traditional FRF plot, and evaluators can judge the natural frequencies by peak-picking method. In this case, the first mode frequency is 0.64 Hz while higher modes are not clear.

Y Direction

The PDI plot in Y direction of this building is shown in Fig. C.3 which comprises three parts:

a. Phase difference index plot (Roof vs. ground)

In Fig. C.3-(a), there are three zero-crossing points, which represent the natural frequencies of the building (the fourth and higher zero-crossing points are not recognizable).

- zero-crossing points of PDI-Y: [0.64, 2.00, 4.2] Hz

b. Phase difference index plot (Roof vs. 2F)

In Fig. C.3-(b) plot, the coordinate plot is separated by the PDI curve. PDI=1 means the roof and the second floor moving in the same direction i.e. moving in-phase. On the contrary, PDI=-1 means the roof and the second floor moving in the opposite directions, i.e. moving out-of-phase. The available acceleration had been bandpass filtered with cutoff frequency= $[(0.15 \sim 0.3)\ (23 \sim 25)]$ Hz in advance. Thus, the signals below $f = 0.2$ Hz can be ignored. Upon a visual review, we can divide the PDI coordinate into four parts:

$\sim$ $f < 0.2$: Ignored area.

$\sim$ $0.2 < f < 0.85$: RF and 2F move in-phase

$\sim$ $0.8 < f < 3.9$: RF and 2F move out-of-phase

$\sim$ $f > 3.9$: RF and 2F move in-phase

Since the PDI is from Roof/2F, the $LMOI(8)_{18} = 8$. The PDI (Rf/2F) should provide enough information. The above three intervals:$0.2 < f < 0.85$,$0.8 < f < 3.9$, and $f > 3.9$ indeed indicate the corresponding natural frequency in Y direction.

c. Frequency response function plot (Roof vs.ground) Figure C.3-(c) is a traditional FRF plot, and evaluators can judge the natural frequencies by peak-picking method. In this case, the first mode is about 0.62 Hz while higher modes are not clear.

Rotation

In this building, two pairs of channels, namely, (Ch. 2 & 10) and (Ch. 3 & 11) are used to draw the torsional PDI plots:

1. The PDI-T plot of RF pair (Ch. 2 & 10) is shown in Fig. C.4-(a)
2. The PDI-T plot of 2F pair (Ch. 3 & 11) is shown in Fig. C.5-(a)
3. The Torsion spectrum is shown in Fig. C.4-(b) and Fig. C.5-(b)

Figure C.4 is not a good plot to identify the torsional mode because no apparent frequency corresponds to PDI=-1. We can only guess approximately the torsional modes are around $[0.7 \sim 0.9], [2.4 \sim 3], [4.7 \sim 4.8]$ Hz.

Figure C.5 is much better than Figure C.4 for torsional identification. At least, we can confirm that the 1st torsional mode is around 0.7 Hz. In addition, by observing the interval of $f = 2 \sim 3$ Hz, it can be confirmed that the second torsional mode is $f = 2.3$ Hz.

C.1.4 Comparison with Existing Research

From the above discussion and existing research, a comparison of results are given in the table 6.7. The comparison shows that the three methods acquire the same identification results for the first mode.

C.2 Case 2: 11 Story Hospital in Newport Beach

C.2.1 Basic Information

Case two is a 11 story building at Newport Beach, California. The structure is a reinforced concrete frame with perimeter concrete shear walls. But only shear wall in the south side is continuous through the height of the building. In this event(Northridge Earthquake), the maximum displacement is 3.57 cm (Ch.15). The corresponding drift is 2.69 cm (relative to Ch.16), and the drift ratio is 0.06%. The detailed information is shown in Table 6.3.

C.2.2 Sensors Information

There are 18 accelerometers in four levels of this building. The location of sensors are shown in Figure C.6. Ten sensors in this building are chosen to be studied. The channels and corresponding floors are listed in Table C.2.

C.2.3 Identification Result

Parameter for PDI plots

In case one, the adopted parameters are as listed:

- Observed frequency bandwidth: $0 \sim 8$ Hz
- Unit narrow frequency bandwidth: 0.1 Hz
- Order of FIR bandpass filter: 990
- Window length of Hamming window (for FRF plot): 25% data length.

X Direction

The PDI plot in X direction of this building is shown in Fig. C.7 which comprises three parts:

a. Phase difference index plot (Roof vs. ground)

   In Fig. C.7-(a), there are three zero-crossing points, which represent the natural frequencies of the building (the fourth and after points are not recognizable).

   – zero-crossing points of PDI-X: [1.24, 3.85, 5.91] Hz

b. Phase difference index plot (Roof vs. 3F)

   In Fig. C.7-(b) plot, the coordinate plot is separated by the PDI curve. PDI=1 means the roof and the second floor moving in the same direction i.e. moving in-phase. On the contrary, PDI=-1 means the roof and the second floor moving in the opposite directions, i.e. moving out-of-phase. From visual judgment, we can approximately divide the PDI coordinate into three parts:

   $\sim$ $0 < f < 1.4$: RF and 3F move in-phase

   $\sim$ $1.4 < f < 2.6$: Interfered by torsion $f_t = 2$Hz.

   $\sim$ $2.6 < f < 5$: RF and 2F move out-of-phase

   Since the PDI is from Roof/3F, the $LMOI(11)_{18} = 6$. The PDI (Rf/3F) should still provide enough information.The phase difference index is 1, -1, 1, -1....in the first 6 modes. Thus, it still helps us to locate the interval of 1st and 2nd mode.

c. Frequency response function plot (Roof vs. ground)

Figure C.7-(c) is a traditional FRF plot, and evaluators can judge the natural frequencies by peak-picking method. In this case, the first mode is 1.15 Hz, the second mode is 3.8 Hz while other higher modes are not clear.

Y Direction

The PDI plot in Y direction of this building is shown in Fig. C.8 which comprises three parts:

a. Phase difference index plot (Roof vs. ground)

   In Fig. C.8-(a), there are three zero-crossing points, which represent the natural frequencies of the building (the fourth and after points are not recognizable).

   – Zero-crossing points of PDI-Y: [1.41, 4.55, 7.95] Hz

b. Phase difference index plot (Roof vs. 2F)

   From visual judgment, we can approximately divide the PDI coordinate into three parts:

   $\sim$ $f < 1.5$: RF and 2F move in-phase.

   $\sim$ $1.5 < f < 5.8$: RF and 2F move out-of-phase

   $\sim$ $f > 5.8$: RF and 2F move in-phase

   Since the PDI is from Roof/3F, the $LMOI(11)_{18} = 6$. The PDI (Rf/3F) should still provide enough information. The plot offers a useful information to assist evaluators to identify the modes of buildings because in Fig. C.8-(a) the divided intervals match the corresponding modes properly.

c. Frequency response function plot (Roof vs. ground) Figure C.8-(c) is a traditional FRF plot, and evaluators can judge the natural frequencies by peak-picking method. In this case, the first mode is 1.34 Hz, the second mode is 4.7 Hz while other higher modes are not clear.

Rotation

In this building, two pairs of channels, namely, (Ch. 14 & 15) and (Ch. 10 & 12) are used to draw the torsional PDI plots:

1. The PDI plot of RF pair (Ch.14 & 15) is shown in Fig. C.9-(a)
2. The PDI plot of 6F pair (Ch.10 & 12) is shown in Fig. C.10-(a)
3. The Torsion spectra are shown in Fig. C.9-(b) and Fig. C.10-(b)

In Fig. C.9, we can observe a very clear torsional mode$f = 2$ Hz, while the second torsional mode is not so clear.

Figure C.10 is a little better than Figure C.9 for torsional identification. In addition to that the first torsional mode is identified as 2 Hz, we can also tell that the second torsional mode is approximate 5.8 Hz.

C.2.4 Comparison with Existing Research

From the above discussion and existing research, a comparison result is shown as the table 6.8. The comparison shows that the three methods acquire the same identification results for the first mode. In addition, the PDI plots can identify more modes than traditional peak picking method.

C.3 Case 3: Los Angeles - 54 story Office Building

C.3.1 Basic Information

Case three is a 54 story building at Los Angeles, California(CSMIP-STATION-24629). The structure is a moment resisting perimeter steel frame. In this event (Northridge Earthquake), the maximum displacement is 16.76 cm (Ch.18). The corresponding drift is 17.41 cm (relative to Ch.18), and the drift ratio is 0.09%. The detailed information is shown in Table 6.4.

C.3.2 Sensors Information

There are 20 accelerometers in six levels of this building. The location of sensors are shown in Figure C.11. Nine sensors in this building are chosen to be studied. The channels and corresponding floors are listed in Table C.3.

C.3.3 Identification Result

Parameter for PDI plots

In case one, the adopted parameters are as listed:

- Observed frequency bandwidth: $0 \sim 4$ Hz
- Unit narrow frequency bandwidth: 0.04 Hz
- Order of FIR bandpass filter: 3000
- Window length of Hamming window (for FRF plot): 25% data length.

X Direction

The PDI plot in X direction of this building is shown in Fig. C.12 which comprises three parts:

a. Phase difference index plot (Roof vs. ground)

   In Fig. C.12-(a), there are nine zero-crossing points, which represent the natural frequencies of the building (the tenth and after points are not recognizable).

   – zero-crossing points of PDI-X:

   $f_{nx} = [0.18, 0.53, 0.85, 1.21, 1.57, 2.00, 2.50, 2.80, 3.18]$ Hz

b. Phase difference index plot (Roof vs. 20F)

   In Fig. C.12-(b), the coordinate plot is separated by the PDI curve. PDI=1 means the roof and the second floor moving in the same direction i.e. moving in-phase. On the contrary, PDI=-1 means the roof and the second floor moving in the opposite directions, i.e. moving out-of-phase.

   However, the plot is not as useful as in the previous cases because the PDI is between Roof and 20F rather than 2F. Since the PDI is from Roof/20F, the $LMOI(54)_{1,34} = 2$. It means we can target only the first two modes from Fig. C.12-(b). When we check the Fig. C.12-(a) and (c), the third and fourth modes

just correspond to the third zone of Fig. C.12-(b), which means the aliasing occurs.

c. Frequency response function plot (Roof vs.ground) Figure C.12-(c) is a traditional FRF plot, and evaluators can judge the natural frequencies by peak-picking method. In this case, we can determine the first five modes by peak picking method, and the rest modes are not recognizable.
$f_n = [0.18, 0.52, 0.85, 1.22, 1.52]$Hz

Y Direction

The PDI plot in Y direction of this building is shown in Fig. C.13 which comprises three parts:

a. Phase difference index plot (Roof vs. ground)
In Fig. C.13-(a), there are nine zero-crossing points, which represent the natural frequencies of the building (the tenth and after points are not recognizable).
   - zero-crossing points of PDI-Y:
$f_{ny} = [0.16, 0.52, 0.86, 1.21, 1.55, 1.89, 2.35, 2.74, 3.02]$ Hz

b. Phase difference index plot (Roof vs. 20F)
In Fig. C.13-(b) plot, the coordinate plot is separated by the PDI curve. The situation in Y direction is similar to that in the X direction. Since the PDI is from Roof/20F, the $LMOI(54)_{1,34} = 2$. It means we only can target the first two modes from Fig. C.13-(b). When we check the Fig. C.13-(a) and (c), the third and fourth modes just correspond to the third zone of Fig. C.13-(b), which means the aliasing occurs.

c. Frequency response function plot (Roof vs.ground)
Figure C.13-(c) is a traditional FRF plot, and evaluators can judge the natural frequencies by peak-picking method. In this case, we can determine the first five modes by peak picking method, and the rest modes are not recognizable.
$f_{ny} = [0.15, 0.49, 0.82, 1.16, 1.46]$Hz

Rotation

In this building, two pairs of channels, namely, (Ch. 19 & 20) in the penthouse and (Ch. 12 & 14) in the 36F are used to draw the torsional PDI plots:

1. The PDI plot of penthouse pair(Ch. 19 & 20) is shown in Fig. C.14-(a)
2. The PDI plot of 36F pair(Ch. 12 & 14) is shown in Fig. C.15-(a)
3. The Torsion spectra are shown in Fig. C.14-(b) and Fig. C.15-(b)

In Fig. C.14, we can observe six very clear torsional mode. The plot (a) and (b) correspond to each other very well and:
$f_{nt} = [0.37, 0.98, 1.48, 2.10, 2.55, 3.25]Hz$

Figure C.15 is not so good as figure C.14 for torsional identification. In plot (a), the second mode is missing and in plot (b), the second and the forth mode are missing. Except for those missing modes, the identification result of Fig. C.15 are the same in Fig. C.14.

C.3.4 Comparison with Existing Research

From the above discussion and existing research, a comparison is shown as the table 6.9. In this case, we refer to another paper for additional comparison [25]. The results are listed below:

1. The comparison table shows that the four methods acquire equal identification results for the first mode.
2. In addition, the PDI plots can identify more modes than traditional peak picking method.
3. PDI plots are able to identify the torsional modes with precise graphical solutions.
4. PDI analysis results are very close to Rahmani's research [25] in the first six modes including torsional modes.

C.4 Case 4: Los Angeles - 6-story Parking Structure

C.4.1 Basic Information

Case four is a 6 story parking structure in Los Angeles, California. The structure is a concrete slabs supported on precast concrete beams and columns with concrete shear walls. In this event(Northridge Earthquake), the maximum displacement is 6.99 cm (Ch.10). The corresponding drift is 4.25 cm (relative to Ch.3), and the drift ratio is 0.34%. The detailed information is shown in Table 6.5.

C.4.2 Sensors Information

There are 14 accelerometers in three levels of this building. The location of sensors are shown in Figure C.6. Nine sensors in this building are chosen to be studied. The channels and corresponding floors are listed in Table C.2.

C.4.3 Identification Result

Parameter for PDI plots

In case one, the adopted parameters are as listed:

- Observed frequency bandwidth: $0 \sim 10$ Hz
- Unit narrow frequency bandwidth: 0.1 Hz
- Order of FIR bandpass filter: 2000
- Window length of Hamming window (for FRF plot): 25% data length.

X Direction

The PDI plot in X direction of this building is shown in Fig. C.17 which comprises three parts:

a. Phase difference index plot (Roof vs. ground)

   In Fig. C.17-(a), there are two zero-crossing points, which represent the natural frequencies of the building (the third and after points are not recognizable).

   – zero-crossing points of PDI-X: [1.95, 5.70] Hz

b. Phase difference index plot (Roof vs. 4F)

   In Fig. C.17-(b) plot, the coordinate plot is separated by the PDI curve. PDI=1 means the roof and the second floor moving in the same direction i.e. moving in-phase. On the contrary, PDI=-1 means the roof and the second floor moving in the opposite directions, i.e. moving out-of-phase. From visual judgment, we can approximately divide the PDI coordinate into four parts:

   $\sim$ $0 < f < 2.2$: RF and 4F move in-phase

   $\sim$ $2.2 < f < 6.1$: RF and 4F move out-of-phase

   $\sim$ $6.1 < f < 8$: RF and 4F move in-phase

   $\sim$ $8 < f < 10$: RF and 4F move out-of-phase

   Since the PDI is from Roof/4F, the $LMOI(6)_{1,4} = 1$. It means we only can target the first modes from Fig. C.12-(b). But when we check the Fig. C.12-(b), we find the plot is not bad. However, the Fig. C.12-(a) and (c) only can identify the first two modes, which makes the (b) plot less useful.

c. Frequency response function plot (Roof vs.ground)

   Figure C.17-(c) is a traditional FRF plot, and evaluators can judge the natural frequencies by peak-picking method. In this case, the first mode is about 1.9 $\sim$ 2 Hz, and the second mode is close to 6 Hz.

Y Direction

The PDI plot in Y direction of this building is shown in Fig. C.18 which comprises three parts:

a. Phase difference index plot (Roof vs. ground)

   In Fig. C.18-(a), there is one zero-crossing points, which represents the natural frequencies of the model (the fourth and after points are not recognizable).

   – zero-crossing points of PDI-Y: 2.6 Hz

b. Phase difference index plot (Roof vs. 4F)

   From visual judgment, we can approximately divide the PDI coordinate into two parts:

   ∼ $f < 3.7$: RF and 4F move in-phase.

   ∼ $3.7 < f$: The phase cannot be determined because the curve fluctuates about the y axis.

   Since the PDI is from Roof/4F, the $LMOI(6)_{1,4} = 1$. It means we can target only the first modes from Fig. C.13-(b).

c. Frequency response function plot (Roof vs.ground)

   Figure C.18-(c) is a traditional FRF plot, and evaluators can judge the natural frequencies by peak-picking method. In this case, the first mode is about 2.4 Hz, the second mode and higher modes are not clear. In the FRF plot, there are two obvious peaks. In this case, the torsional frequency just happened to be the same as the 1st mode in y direction. The second peak should be the frequency response of torsion, but we need to collect more earthquake records and identify the building with different inputs to make sure the answer.

Rotation

In this building, two pairs of channels, namely, (Ch. 9 & 11) and (Ch. 6 & 7) are used to draw the torsional PDI plots:

1. The PDI plot of RF pair(Ch. 9 & 11) is shown in Fig. C.19-(a)
2. The PDI plot of 4F pair(Ch. 6 & 7) is shown in Fig. C.20-(a)
3. The torsion spectra are shown in Fig. C.19-(b) and Fig. C.20-(b)

In Fig. C.19, we can observe a very clear torsional mode: $f_{nt} = [2.5, 6.55]$ Hz.

C.4.4 Comparison with Existing Research

From the above discussion and existing research, a comparison result is shown as the table 6.10. The comparison shows that the three methods acquire similar identification results but the errors are bigger than the previous cases. It is probably because the system is not linear elastic during the Northridge earthquake. The phase plot only consider the moving direction of the floor rather than the signal strength in the spectrum. To fix the problem is another issue and not discussed in the section, but if we use more earthquake records input to analyze the building, such as small earthquakes. we should gain more information about the building.

C.5 Case 5: Los Angeles - 19 story Office Building

C.5.1 Basic Information

Case five is a 19 story Office Building in Los Angeles, California(CSMIP-STATION-24643). The structure is moment resisting steel frames in the longitudinal and X-braced steel frames in the transverse direction. In this event(Northridge Earthquake), the maximum displacement is 30.92 cm (Ch.10). The corresponding drift is 32.51 cm (relative to Ch.4), and the drift ratio is 0.93%. The detailed information is shown in Table 6.6.

C.5.2 Sensors Information

There are 15 accelerometers in three levels of this building. The location of sensors are shown in Figure C.21. Nine sensors in this building are chosen to be studied. The channels and corresponding floors are listed in Table C.5.

C.5.3 Identification Result

Parameter for PDI plots

In case one, the adopted parameters are as listed:

- Observed frequency bandwidth: $0 \sim 5$ Hz
- Unit narrow frequency bandwidth: 0.1 Hz
- Order of FIR bandpass filter: 2000
- Window length of Hamming window (for FRF plot): 25% data length.

X Direction

The PDI plot in X direction of this building is shown in Fig. C.22 which comprises three parts:

a. Phase difference index plot (Roof vs. ground)
   In Fig. C.22-(a), there are five zero-crossing points, which represent the natural frequencies of the building (the sixth and after points are not recognizable).
   - zero-crossing points of PDI-X: [0.30, 1.23, 2.58, 3.83, 4.78] Hz

b. Phase difference index plot (Roof vs. 2F)
   In Fig. C.22-(b) plot, the coordinate plot is separated by the PDI curve. PDI=1 means the roof and the second floor moving in the same direction i.e. moving in-phase. On the contrary, PDI=-1 means the roof and the second floor moving in the opposite directions, i.e. moving out-of-phase. From visual judgment, we can approximately divide the PDI coordinate into four parts:
   $\sim$ $0 < f < 0.3$: RF and 2F move in-phase
   $\sim$ $0.3 < f < 1.35$: RF and 2F move out-of-phase
   $\sim$ $1.35 < f < 2.95$: RF and 2F move in-phase
   $\sim$ $2.95 < f < 4.75$: RF and 2F move out-of-phase

The plot is useful because the PDI is from Roof/2F. The phase difference indices of this plot theoretically are 1, -1, 1, -1....in sequence. As expected, the identified frequencies bandwidth indeed correspond to the first four natural frequencies in X direction (identified in C.22-(a)) accordingly.

c. Frequency response function plot (Roof vs. ground)

Figure C.22-(c) is a traditional FRF plot, and evaluators can judge the natural frequencies by peak-picking method. In this case, the identified modes in X direction are:

f_n =[0.29, 1.21, 1.61]

(The higher modes are not recognizable.)

Y Direction

The PDI plot in Y direction of this building is shown in Fig. C.18 which comprises three parts:

a. Phase difference index plot (Roof vs. ground)

In Fig. C.18-(a), there are three zero-crossing points, which represent the natural frequencies of the building (the fourth and after points are not recognizable).

- zero-crossing points of PDI-Y: [0.23, 0.72, 1.28, 1.77, 2.33, 2.87, 3.47, 4.19, 4.71] Hz

b. Phase difference index plot (Roof vs. 2F)

From visual judgment, we can approximately divide the PDI coordinate into two parts:

$\sim$ $f < 0.27$: RF and 2F move in-phase.

$\sim$ $0.27 < f < 0.8$: RF and 2F move out-of-phase.

$\sim$ $0.8 < f < 1.3$: RF and 2F move in-phase.

$\sim$ $1.3 < f < 2.0$: RF and 2F move out-of-phase.

$\sim$ $2.0 < f < 2.6$: RF and 2F move in-phase.

The plot is useful because the PDI comes from Roof/2F. The phase difference indices of this plot theoretically are 1, -1, 1, -1....in sequence. As expected, the identified frequencies bandwidth indeed correspond to the first six natural frequencies in Y direction (identified in C.23-(a)) accordingly. However, when $f > 3$, plot (a) and (b) do not match properly. Because only one earthquake record of this building is provided, we do not have other data to Fig. out the problem.

c. Frequency response function plot (Roof vs.ground)
Figure C.23-(c) is a traditional FRF plot, and evaluators can judge the natural frequencies by peak-picking method. In this case, the first three modes are: [0.24, 0.70, 1.19] Hz (The higher modes are not clear.)

Rotation

In this building, two pairs of channels, namely, (Ch. 13 & 14) and (Ch. 10 & 11) are used to draw the torsional PDI plots:

1. The PDI plot of RF pair (Ch.13 & 14)is shown in Fig. C.24-(a)
2. The PDI plot of 8F pair (Ch.10 & 11)is shown in Fig. C.25-(a)
3. The torsion spectra are shown in Fig. C.19-(b) and Fig. C.25-(b)

In Fig. C.24-(a), clear torsional modes can be observed:
$f_{nt} = [0.23, 0.93, 1.99, 3.10]$ Hz.

C.5.4 Comparison with Existing Research

From the above discussion and reference [24] , a comparison result is shown as the table 6.11. It shows that the three methods acquire similar identification results for the first mode, but the errors are still bigger than the previous cases. It is probably because the system is not linear elastic during the Northridge earthquake. According to the earthquake data, the maximum acceleration in the building is 0.65g, a quite

huge acceleration for a typical structure. To fix the problem is another issue and not discussed in the section, but if we use more earthquake records input to analyze the building, such as other small earthquakes, we should obtain more useful information about the building.

Table C.1.
Selected Sensors in CSMIP-STATION-24468

Direction	**Floor**	**Channel NO.**
X	RF	6
	2F	7
	GF	16
Y	RF	10
	2F	11
	GF	1
T	RF	2 &10
	2F	3 &11

Sensor maps : Fig.C.1

Table C.2.
Selected Sensors in CSMIP-STATION-13589

Direction	**Floor**	**Channel NO.**
X	RF	15
	2F	8
	GF	5
Y	RF	13
	2F	6
	GF	3
T	RF	14 &15
	6F	10 &12

Sensor maps : Fig.C.6

Table C.3.
Selected Sensors in CSMIP-STATION-24629

Direction	**Floor**	**Channel NO.**
X	Penthouse	18
	20F	8
	GF	3
Y	Penthouse	20
	20F	10
	GF	5
T	Penthouse	19 &20
	36F	12 &14

Sensor maps : Fig.C.11

Table C.4.
Selected Sensors in CSMIP-STATION-24655

Direction	**Floor**	**Channel NO.**
X	RF	10
	4F	6
	GF	3
Y	RF	12
	4F	8
	GF	5
T	RF	9 &11
	4F	6 &7

Sensor maps : Fig.C.16

Table C.5.
Selected Sensors in CSMIP-STATION-24643

Direction	**Floor**	**Channel NO.**
X	RF	13
	2F	8
	GF	2
Y	RF	15
	2F	9
	GF	4
T	RF	13 &14
	8F	10 &11

Sensor maps : Fig.C.21

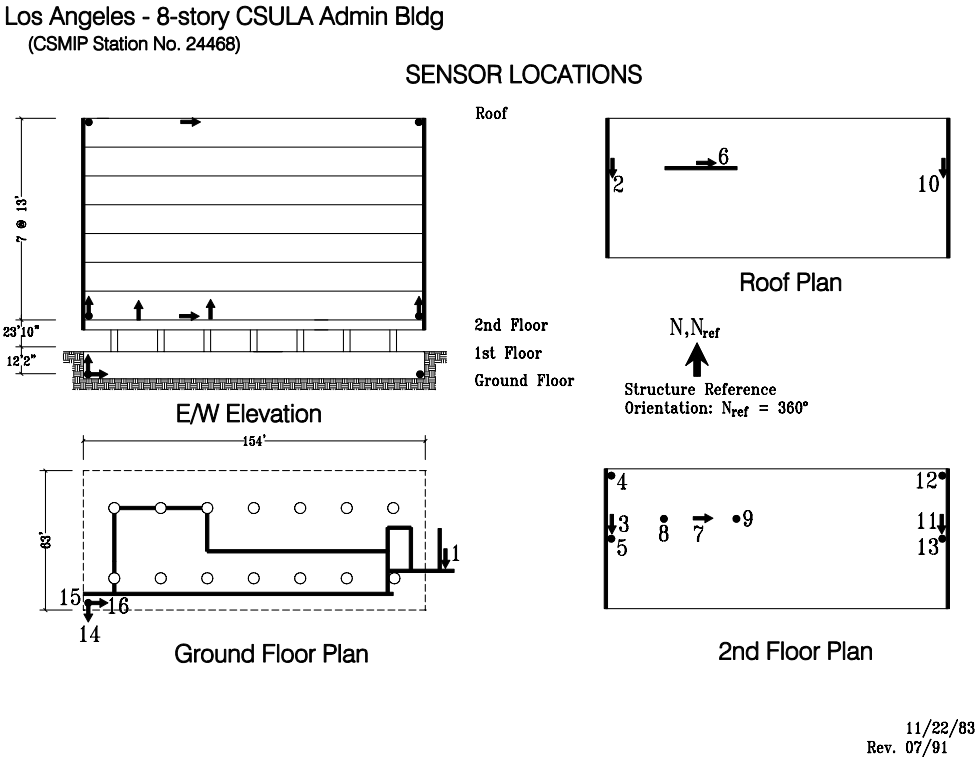

Fig. C.1. Sensor Locations for CSMIP-STATION-24468

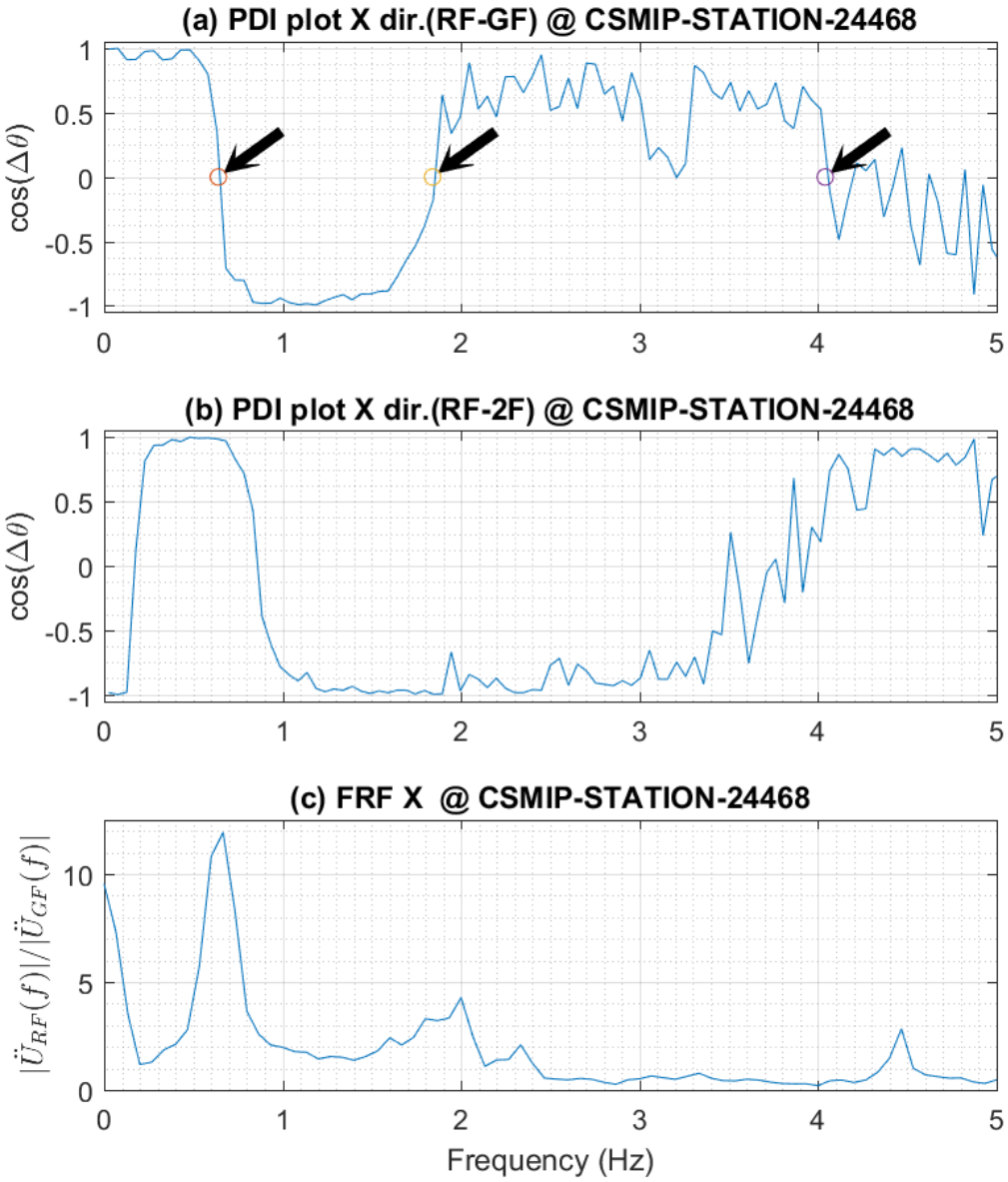

Fig. C.2. PDI plot of CSMIP-STATION-24468 in X direction. In Fig.(a), the black arrow marks point at the translational modes.

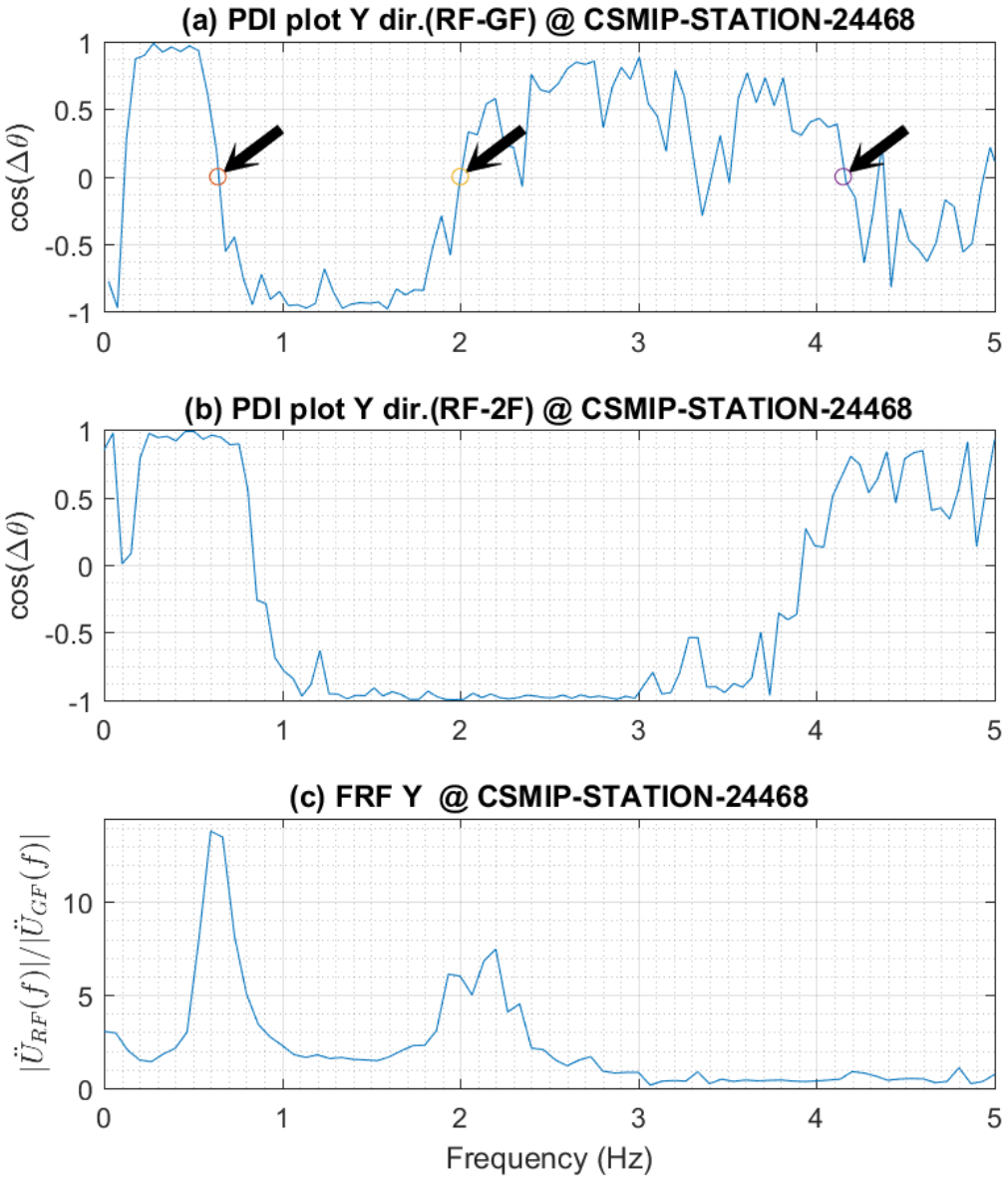

Fig. C.3. PDI plot of CSMIP-STATION-24468 in Y direction. In Fig.(a), the black arrow marks point at the translational modes.

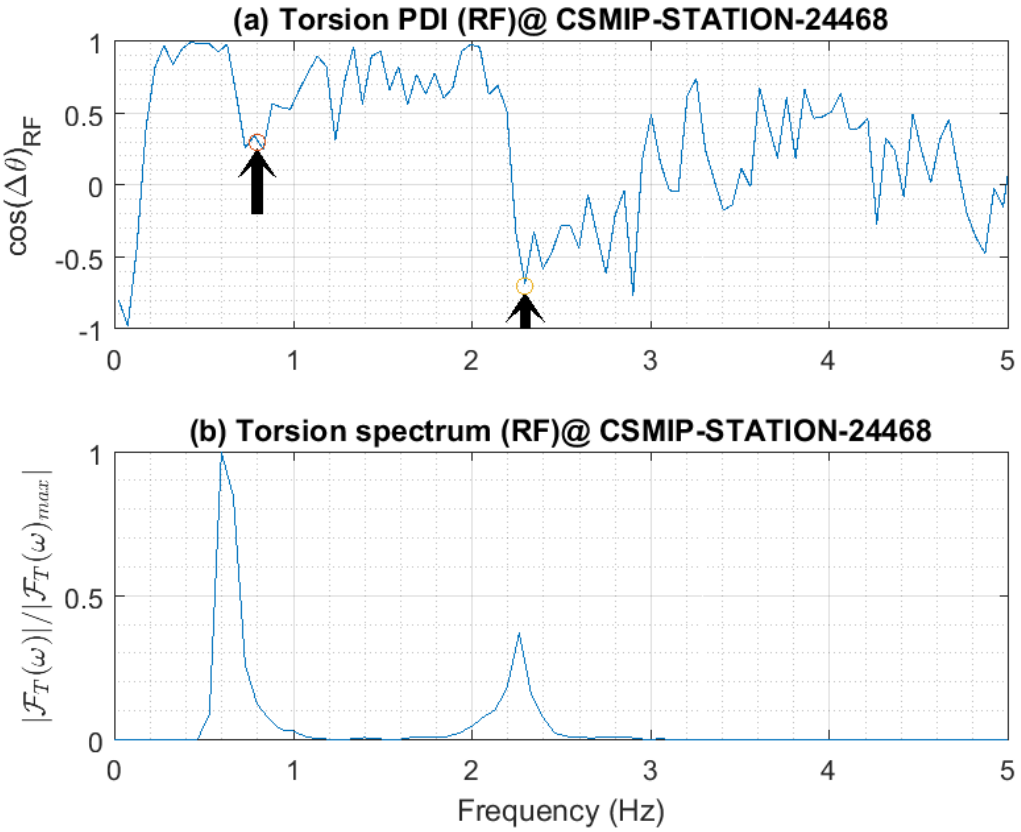

Fig. C.4. Torsional PDI plot of CSMIP-STATION-24468 (RF). (Ch.2 & 10). The black arrow marks point at the torsional modes.

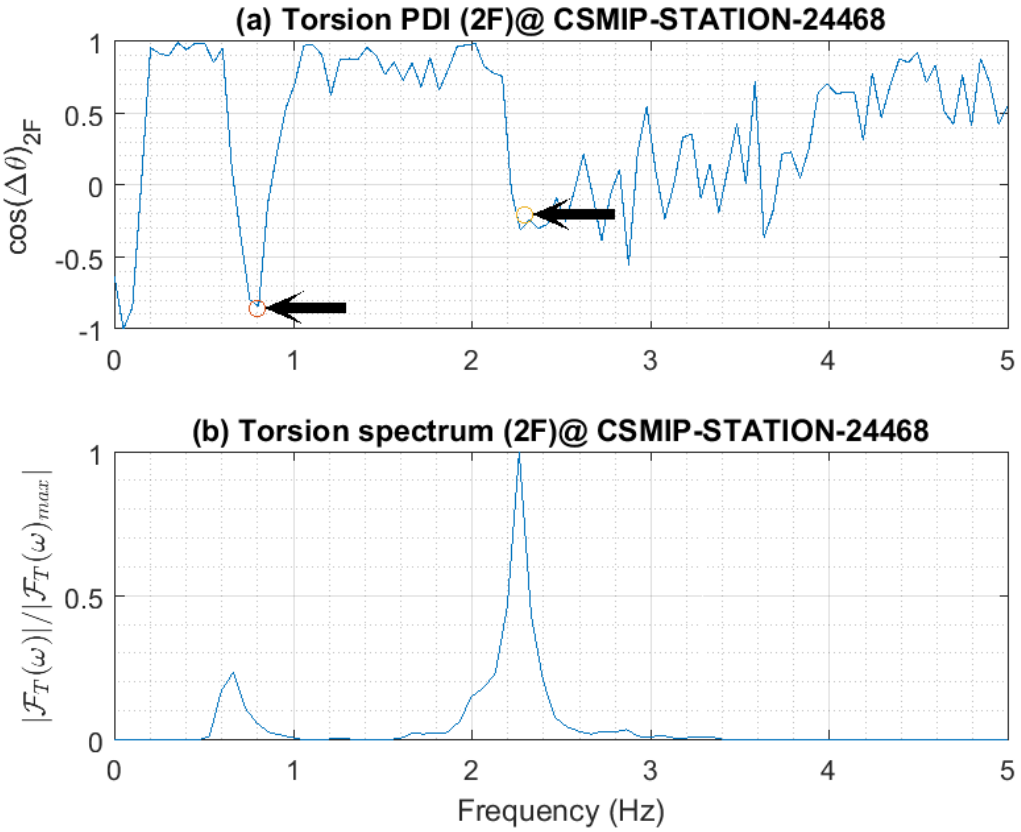

Fig. C.5. Torsional PDI plot of CSMIP-STATION-24468 (2F)(Ch.3 & 11). The black arrow marks point at the torsional modes.

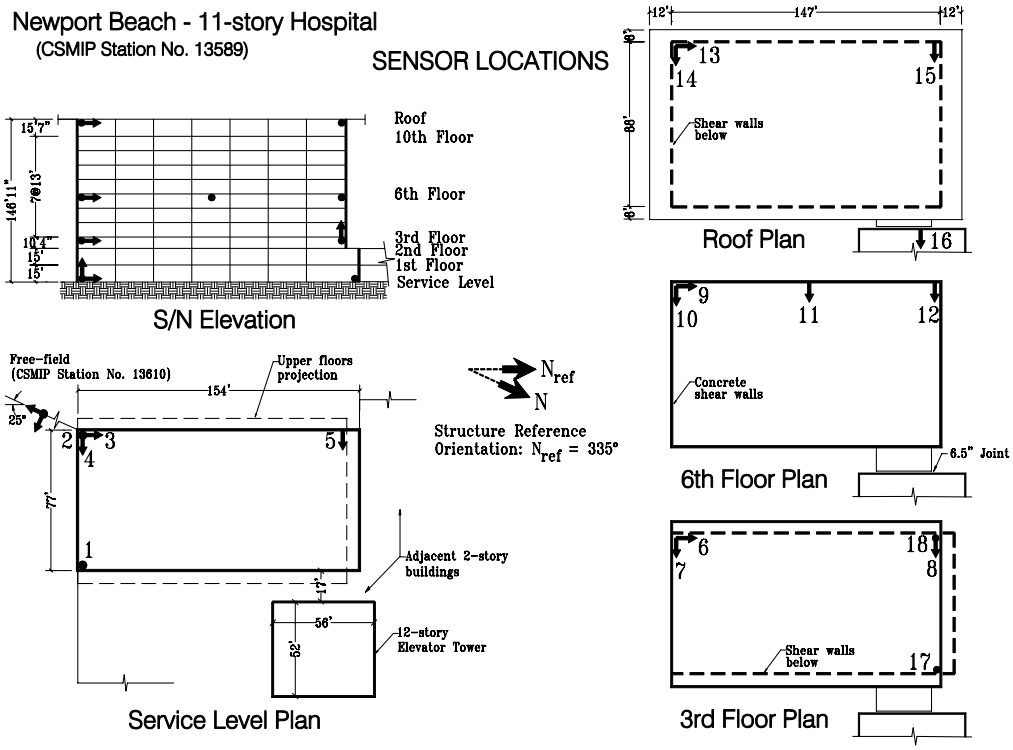

Fig. C.6. Sensor Locations for CSMIP-STATION-13589

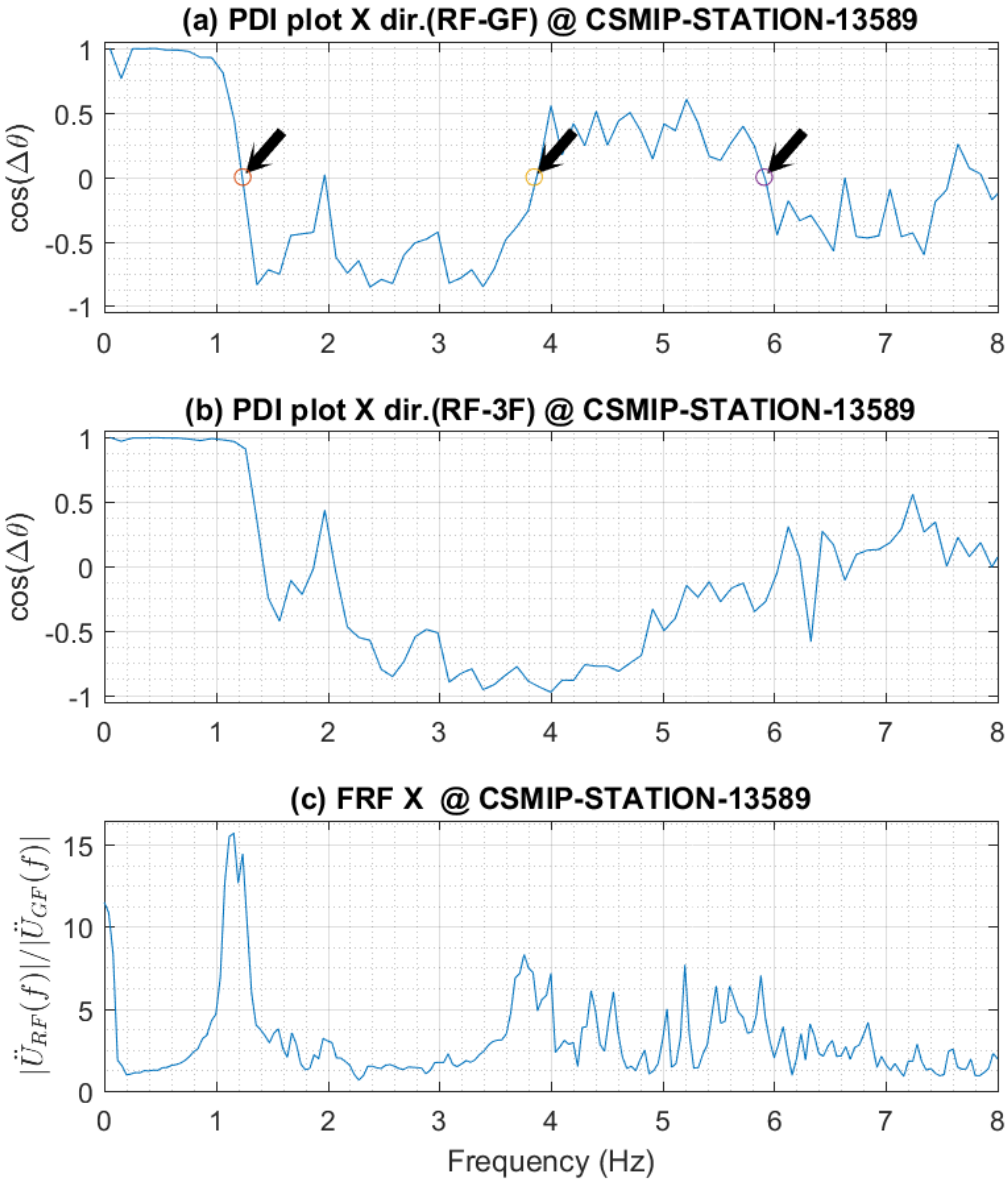

Fig. C.7. PDI plot of CSMIP-STATION-13589 in X direction. In Fig.(a), the black arrow marks point at the translational modes.

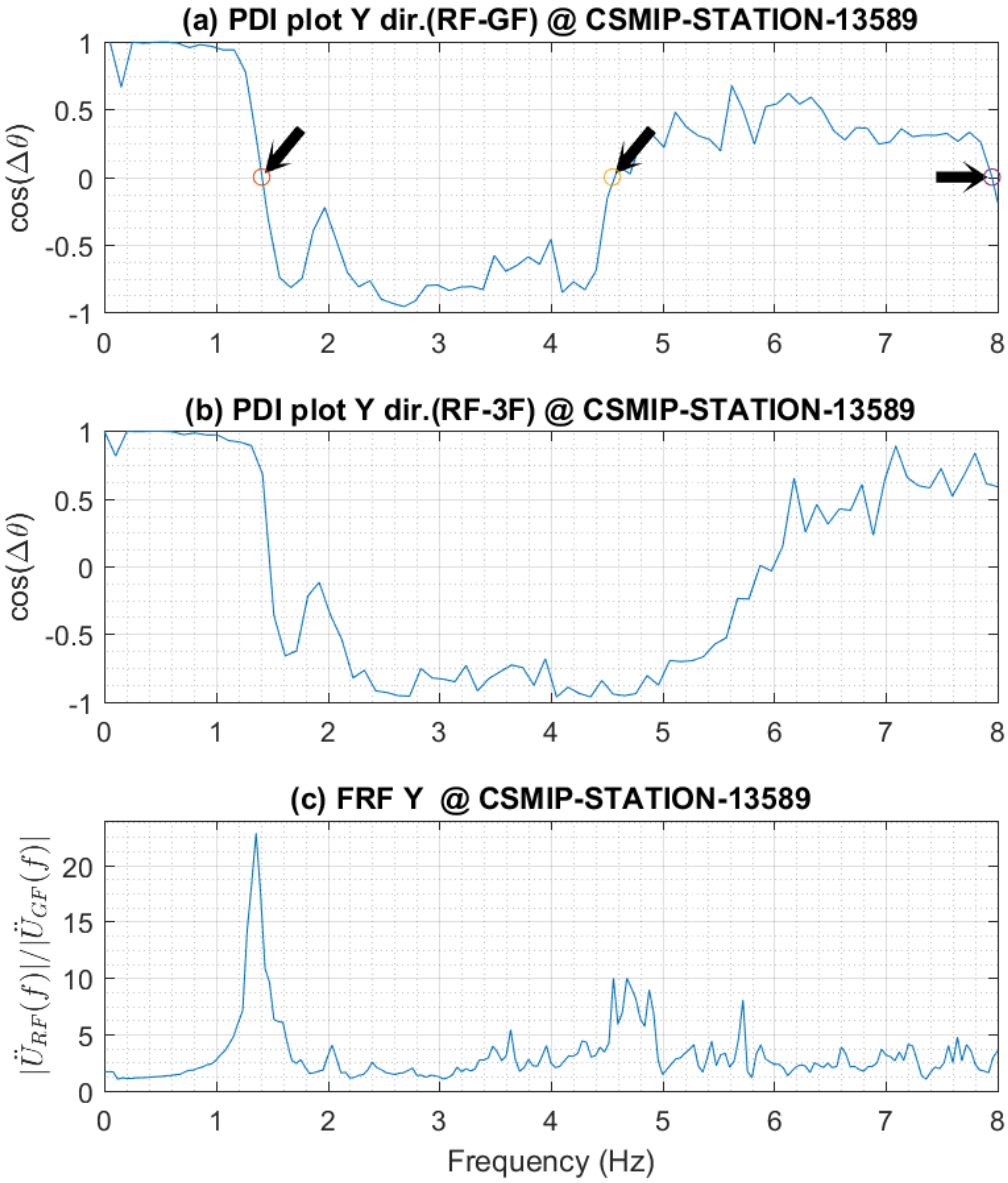

Fig. C.8. PDI plot of CSMIP-STATION-13589 in Y direction. In Fig.(a), the black arrow marks point at the translational modes.

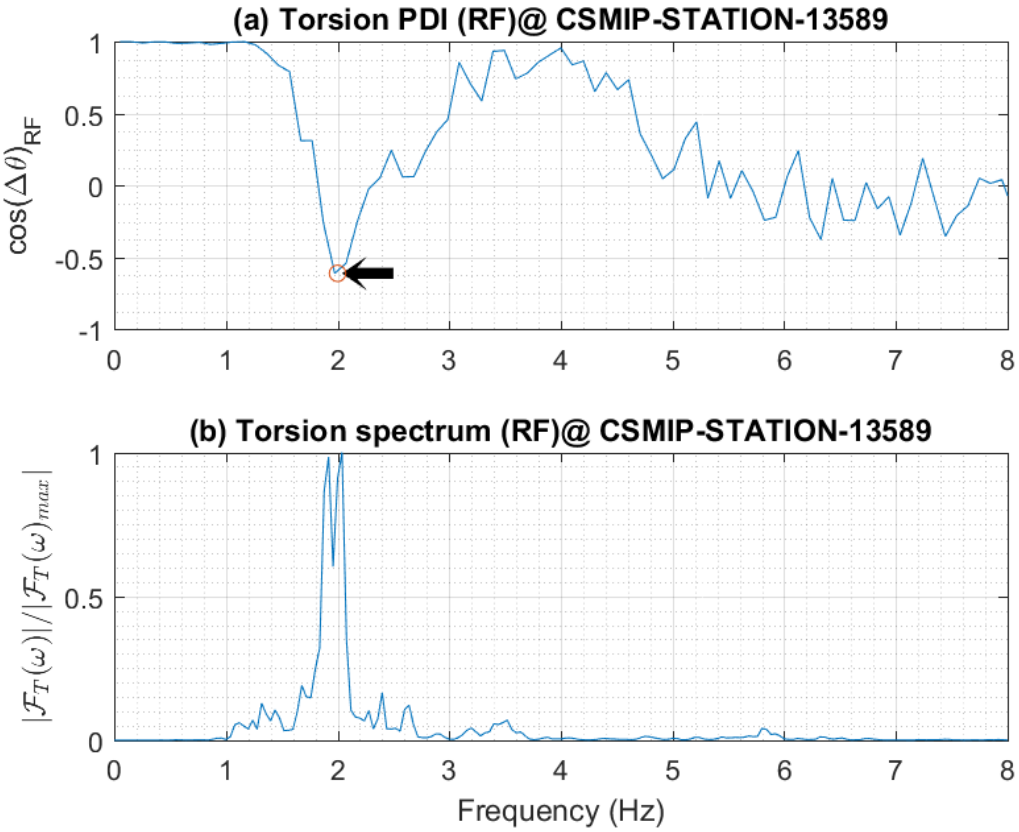

Fig. C.9. Torsional PDI plot of CSMIP-STATION-13589 (RF) (Ch. 14 & 15). The black arrow marks point at the torsional modes.

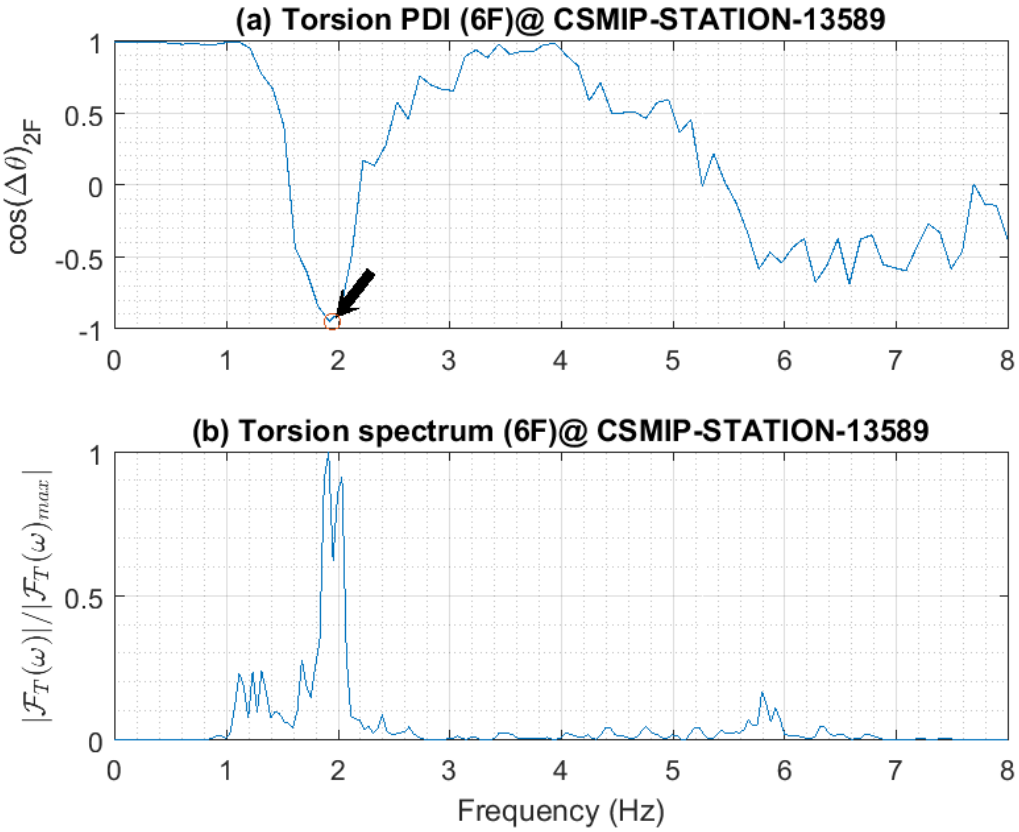

Fig. C.10. Torsional PDI plot of CSMIP-STATION-13589 (6F) (Ch. 10 & 12). The black arrow marks point at the torsional modes.

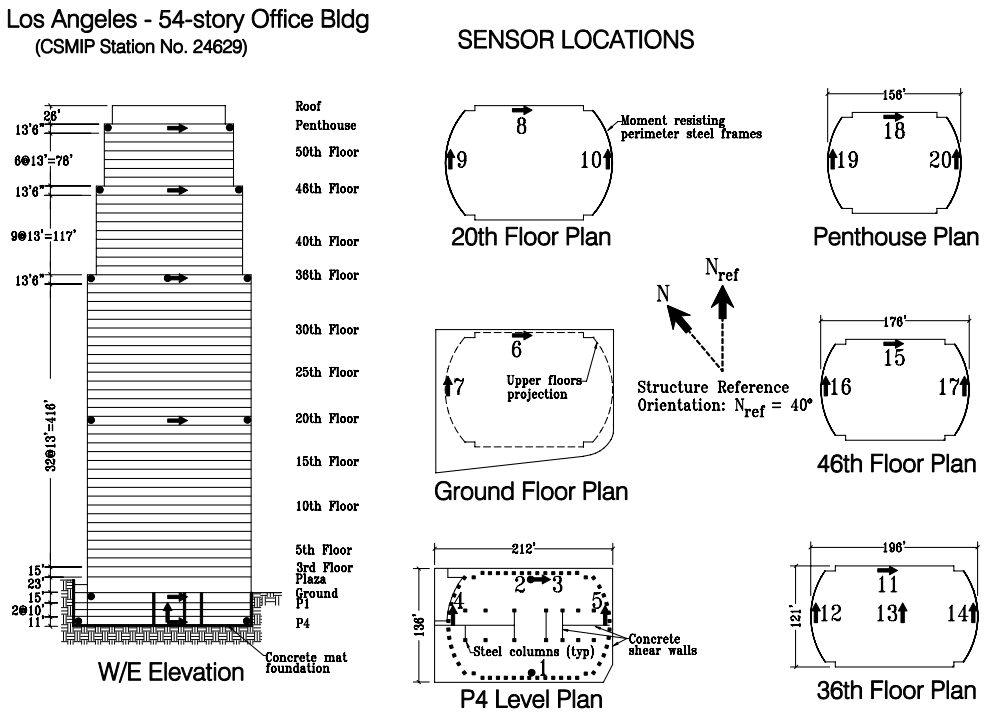

Fig. C.11. Sensor Locations for CSMIP-STATION-24629

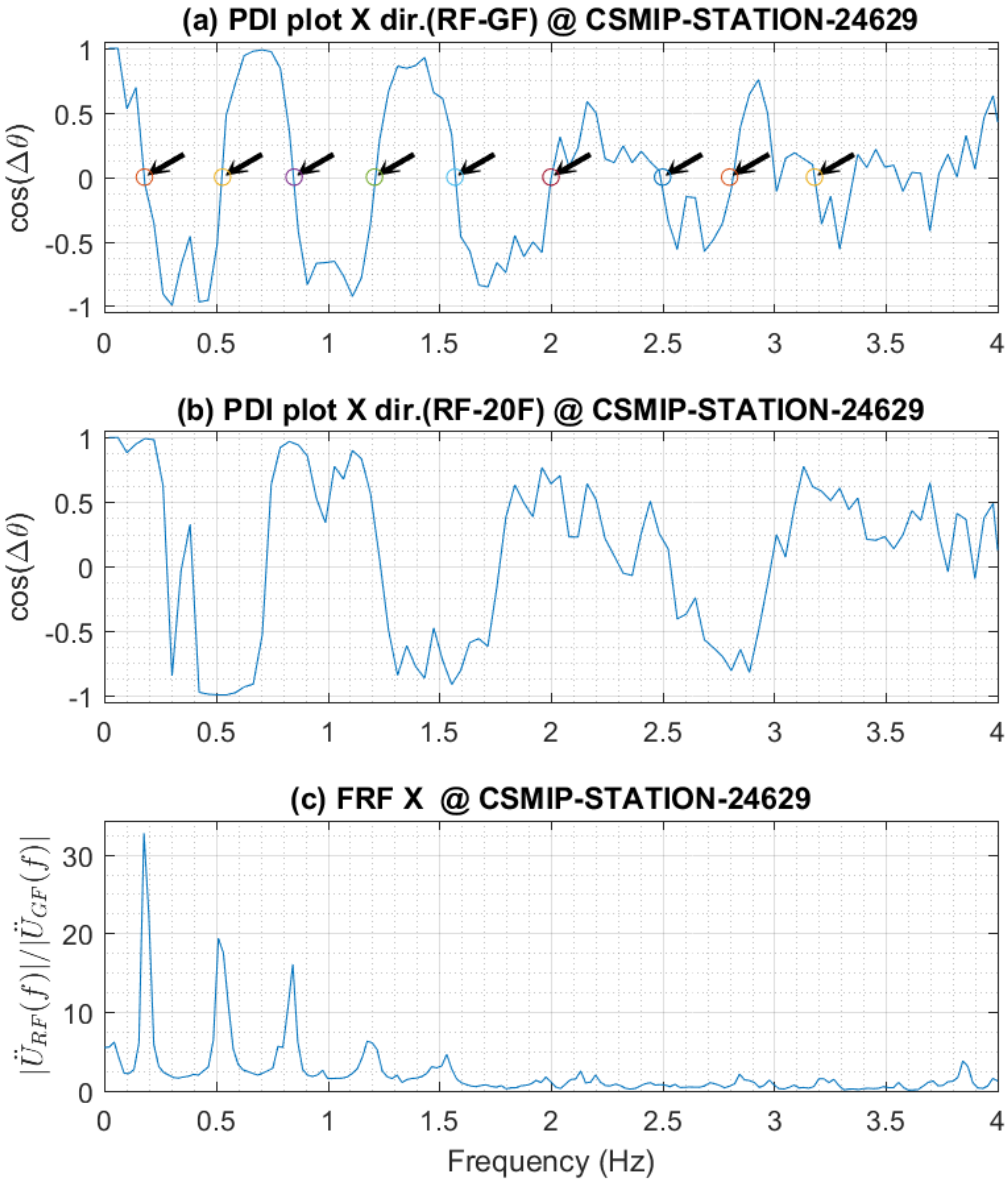

Fig. C.12. PDI plot of CSMIP-STATION-24629 in X direction. In Fig.(a), the black arrow marks point at the translational modes.

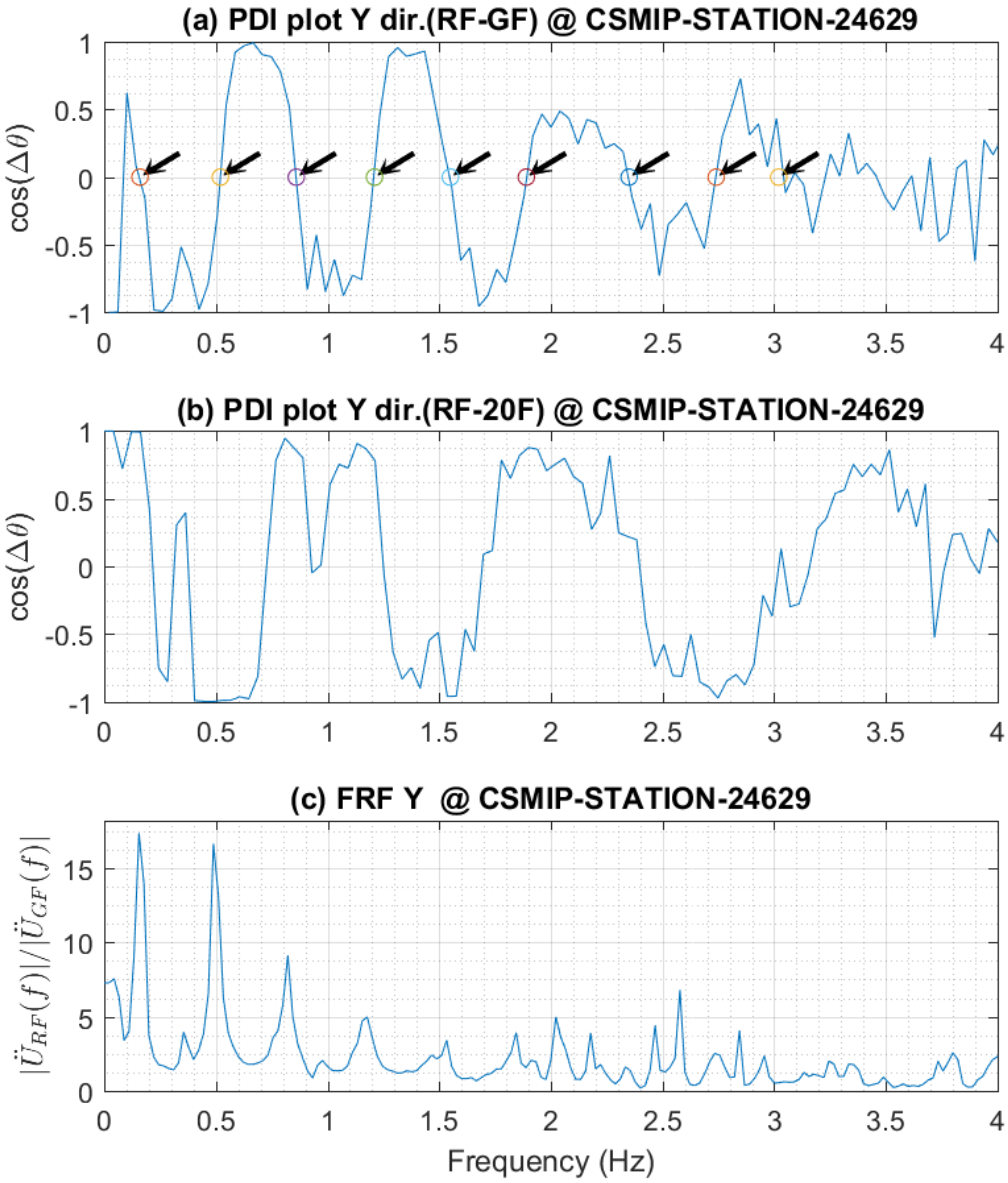

Fig. C.13. PDI plot of CSMIP-STATION-24629 in Y direction. In Fig.(a), the black arrow marks point at the translational modes.

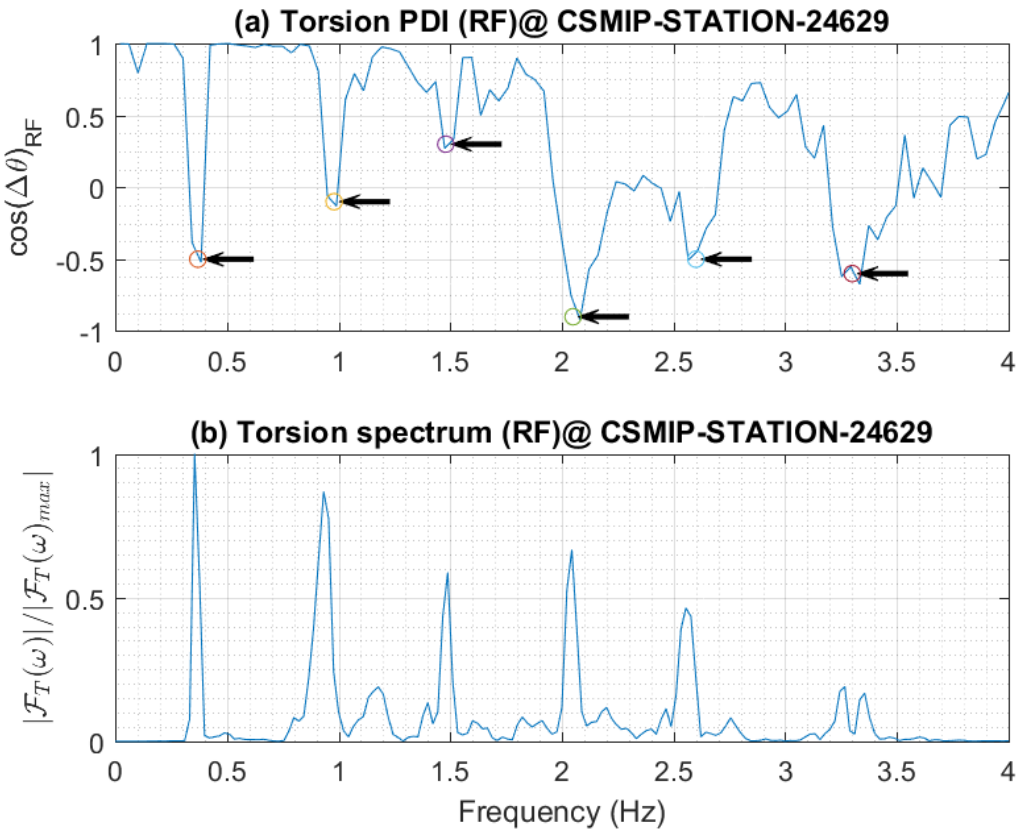

Fig. C.14. Torsional PDI plot of CSMIP-STATION-24629 (penthouse) (Ch. 19 & 20). The black arrow marks point at the torsional modes.

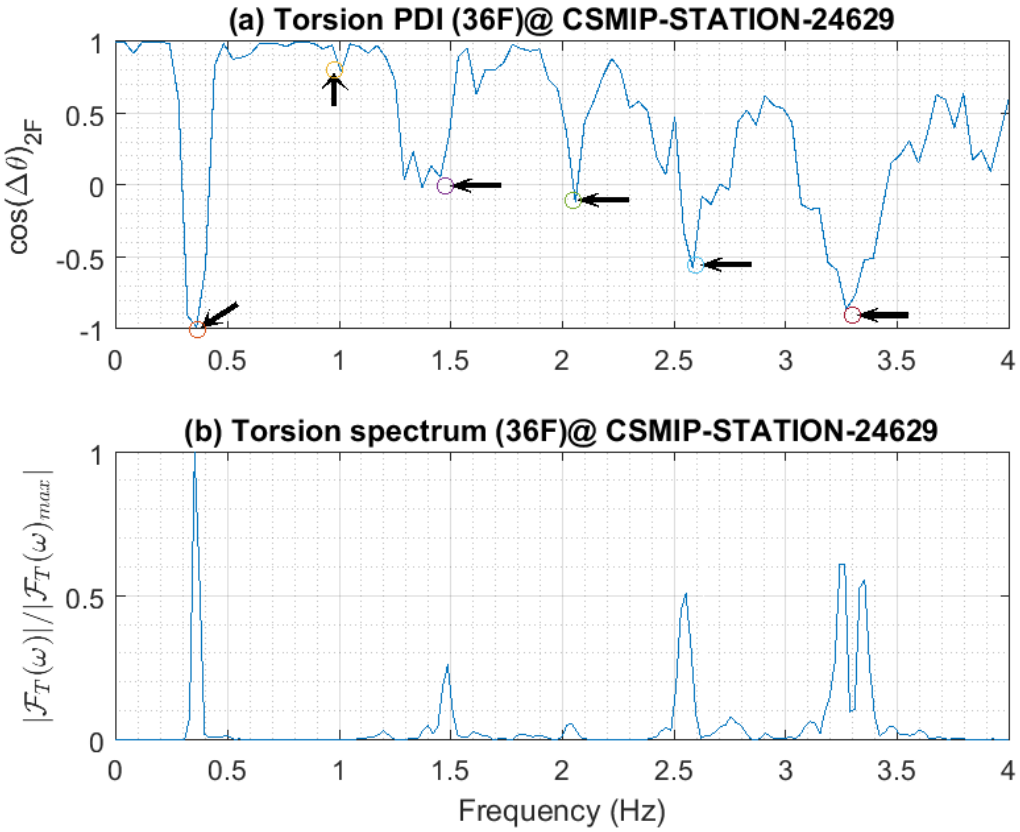

Fig. C.15. Torsional PDI plot of CSMIP-STATION-24629 (36F) (Ch. 12 & 14). The black arrow marks point at the torsional modes.

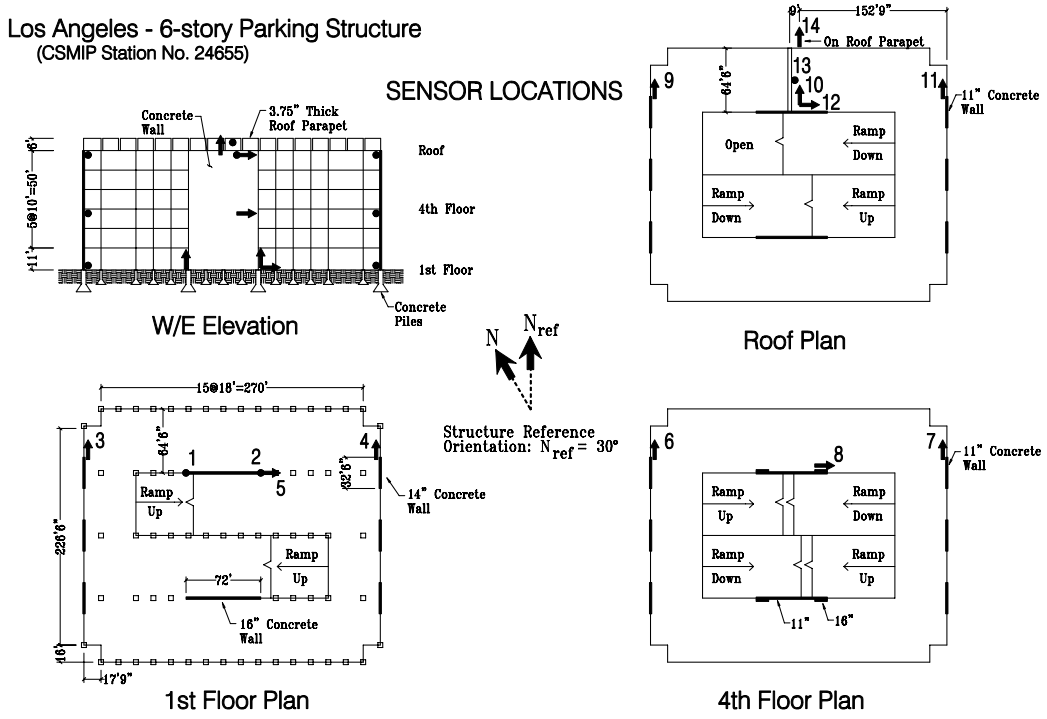

Fig. C.16. Sensor Locations for CSMIP-STATION-24655

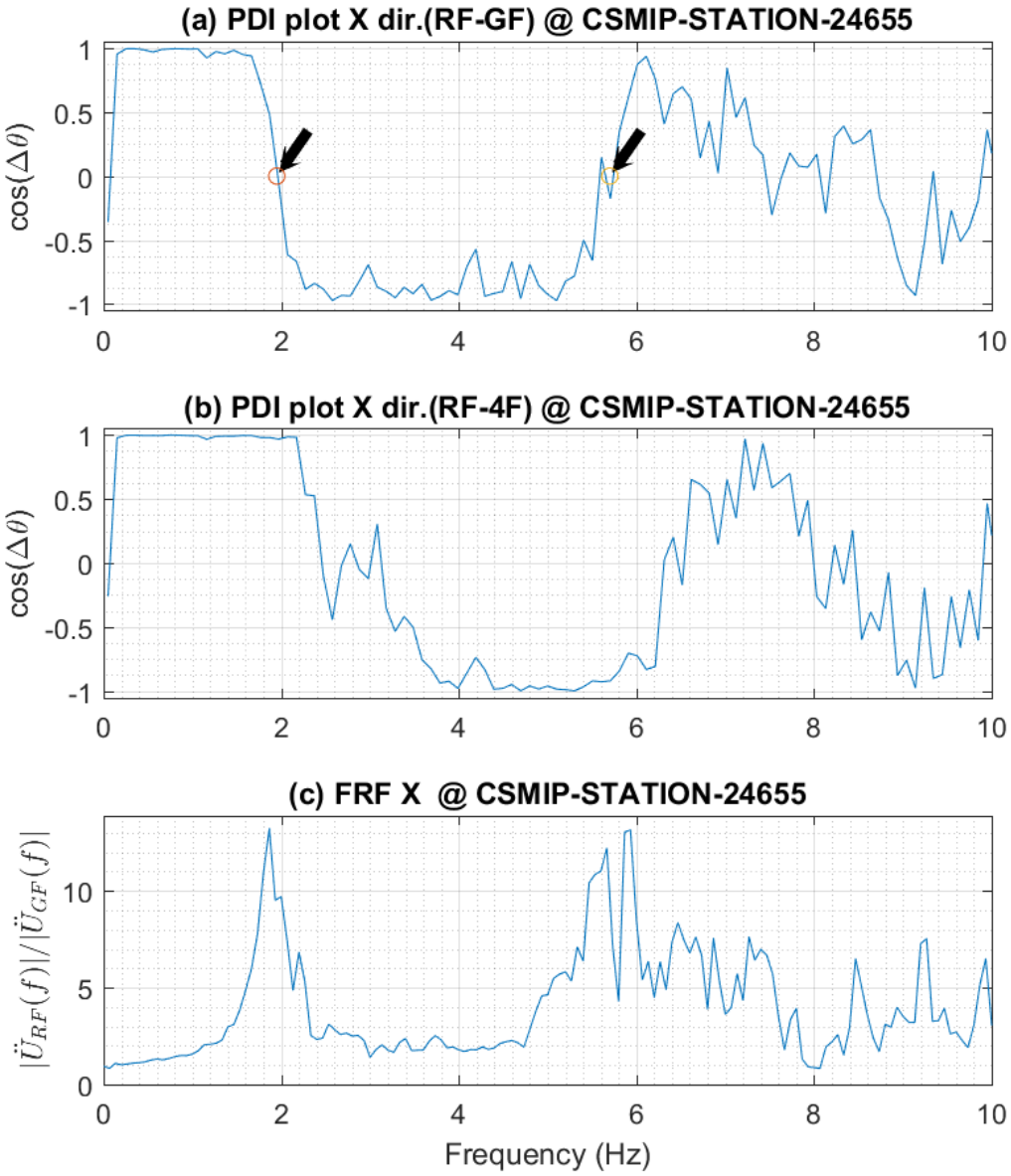

Fig. C.17. PDI plot of CSMIP-STATION-24655 in X direction. In Fig.(a), the black arrow marks point at the translational modes.

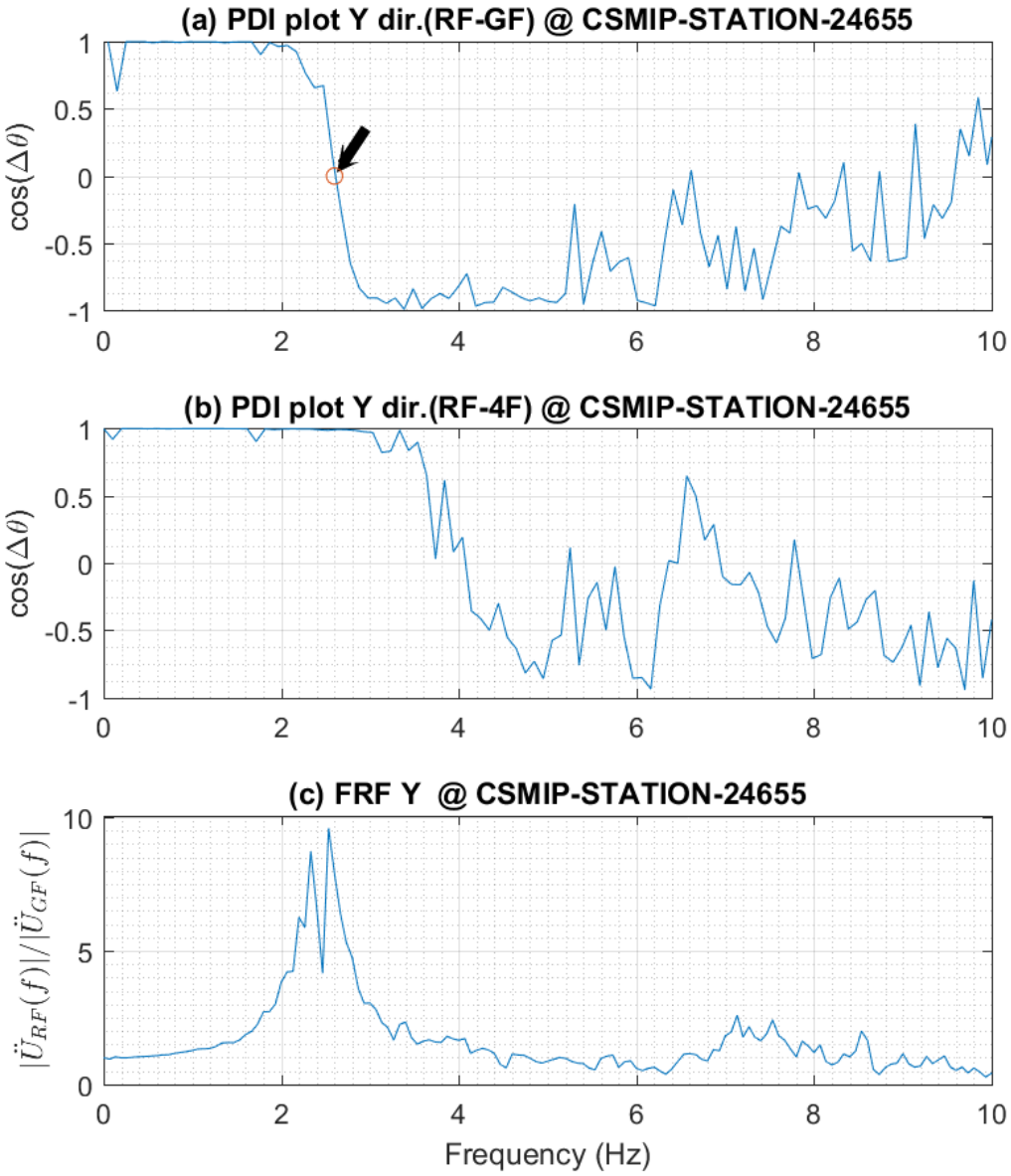

Fig. C.18. PDI plot of CSMIP-STATION-24655 in Y direction. In Fig.(a), the black arrow mark points at the translational mode.

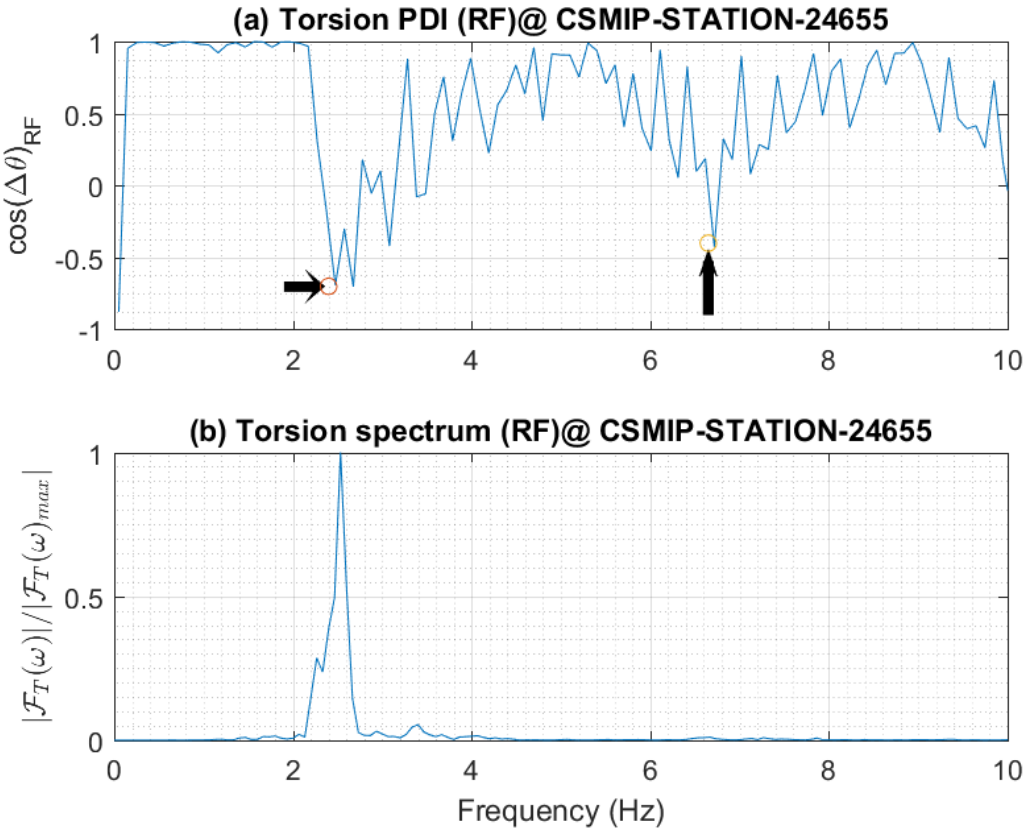

Fig. C.19. Torsional PDI plot of CSMIP-STATION-24655 (RF) (Ch. 9 & 11). The black arrow marks point at the torsional modes.

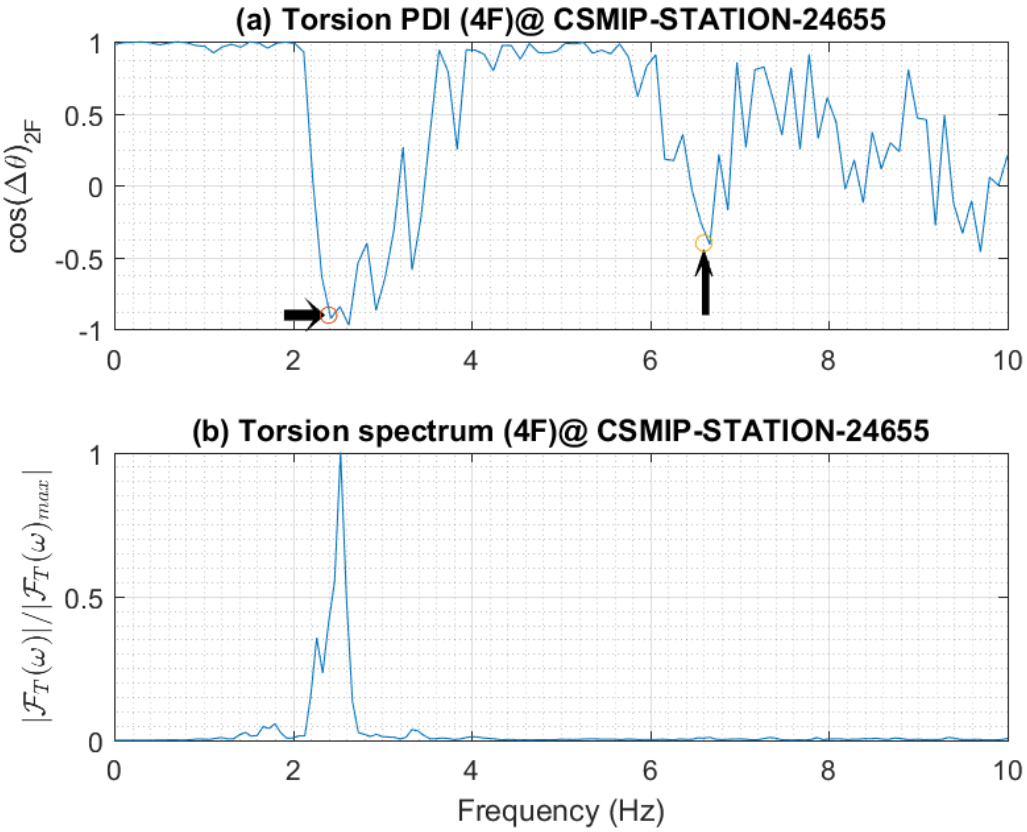

Fig. C.20. Torsional PDI plot of CSMIP-STATION-24655 (4F) (Ch. 6 & 7).The black arrow marks point at the torsional modes.

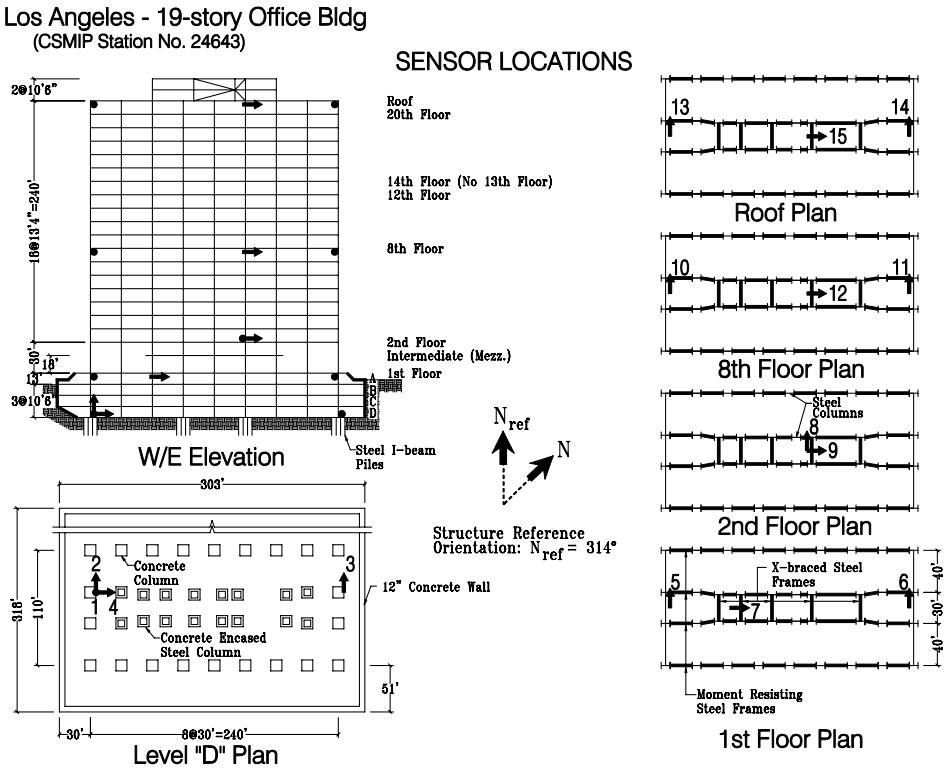

Fig. C.21. Sensor Locations for CSMIP-STATION-24643

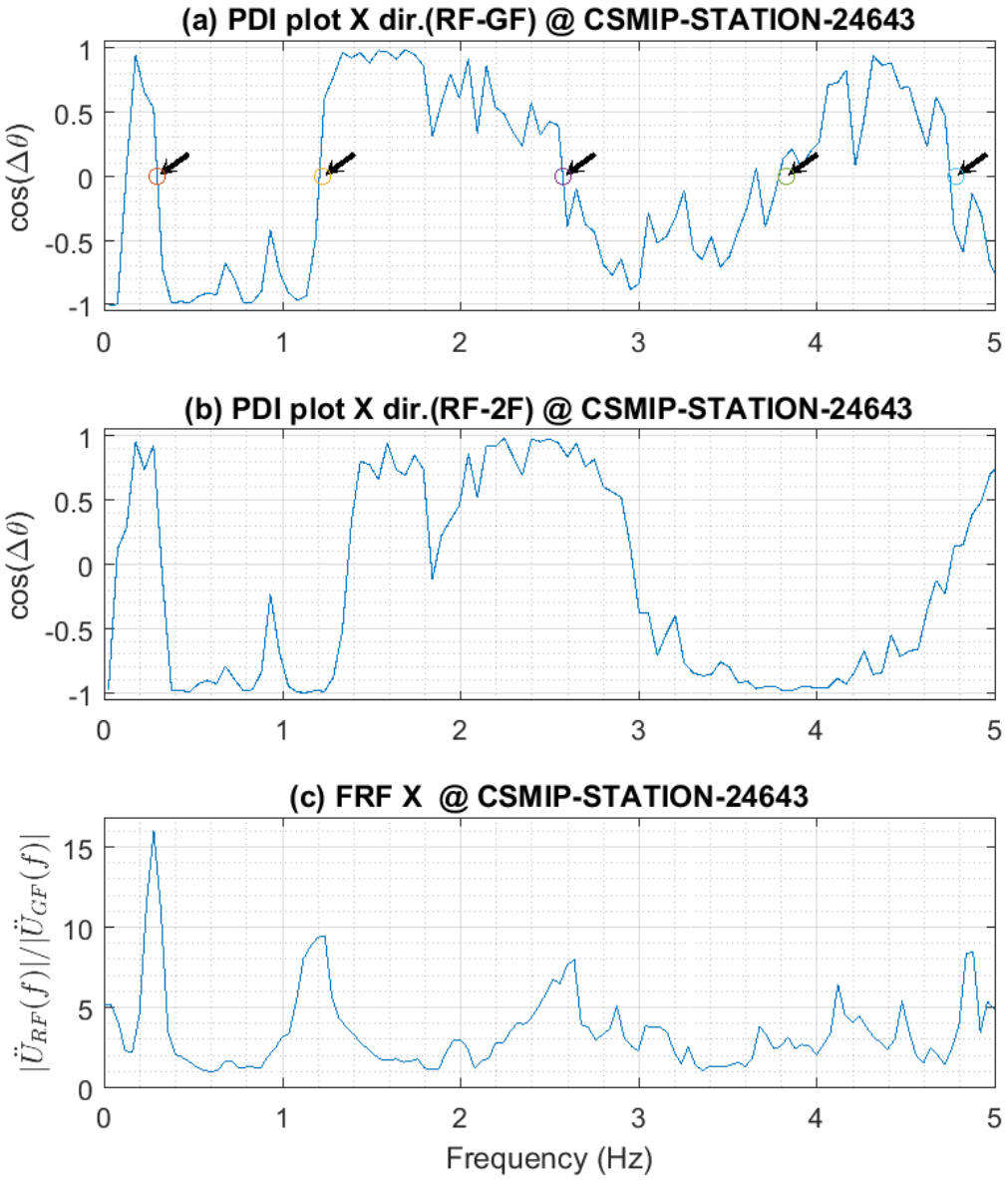

Fig. C.22. PDI plot of CSMIP-STATION-24643 in X direction. In Fig.(a), the black arrow marks point at the translational modes.

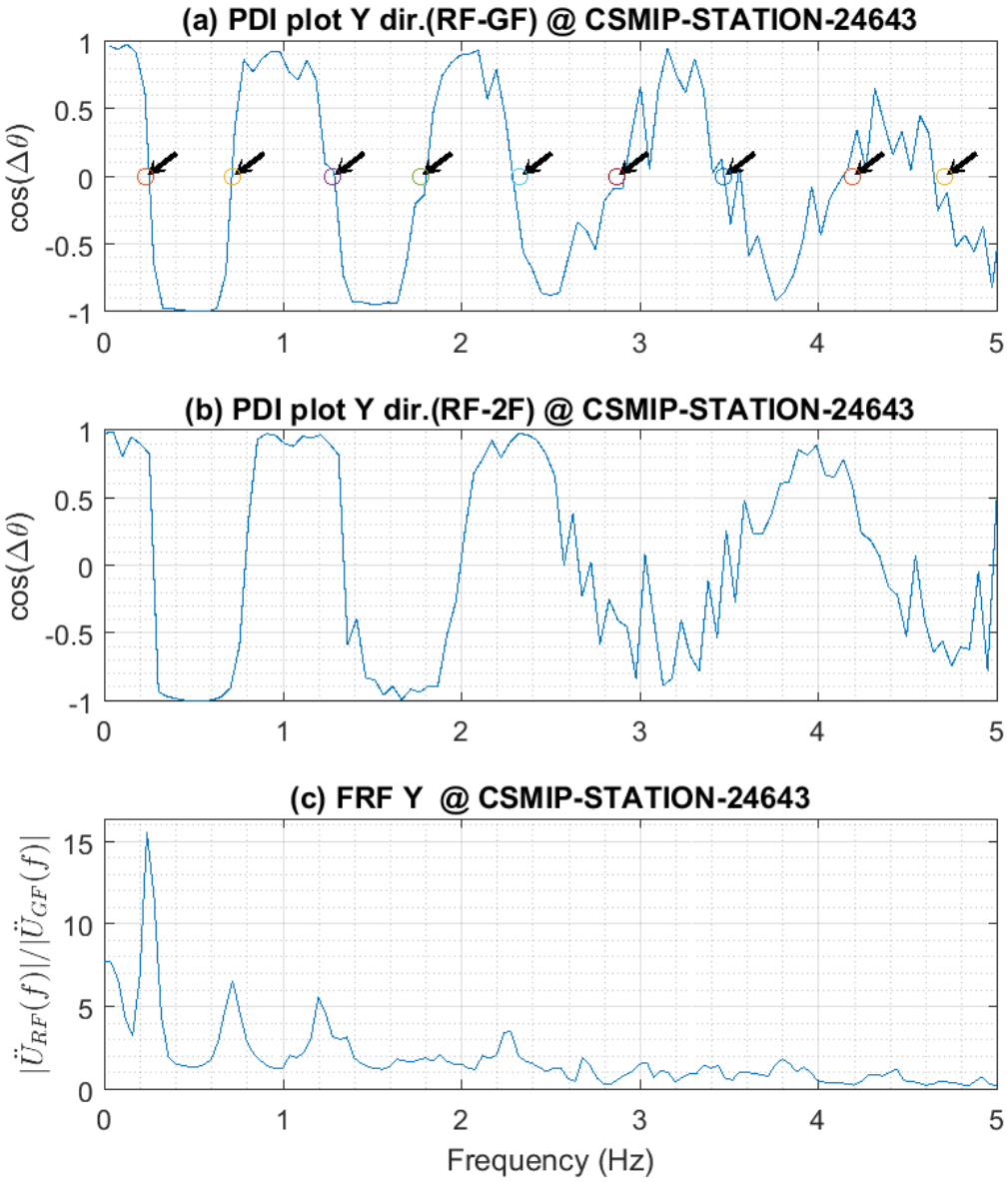

Fig. C.23. PDI plot of CSMIP-STATION-24643 in Y direction. In Fig.(a), the black arrow marks point at the translational modes.

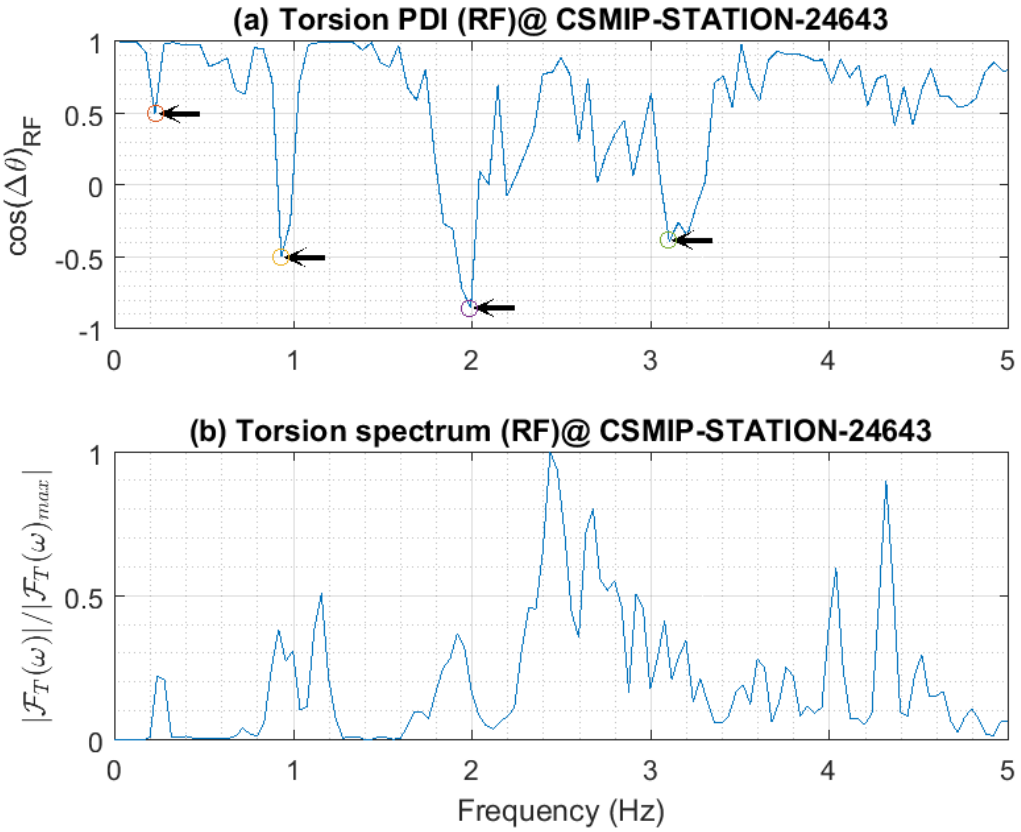

Fig. C.24. Torsional PDI plot of CSMIP-STATION-24643 (RF) (Ch.13& 14). The black arrow marks point at the torsional modes.

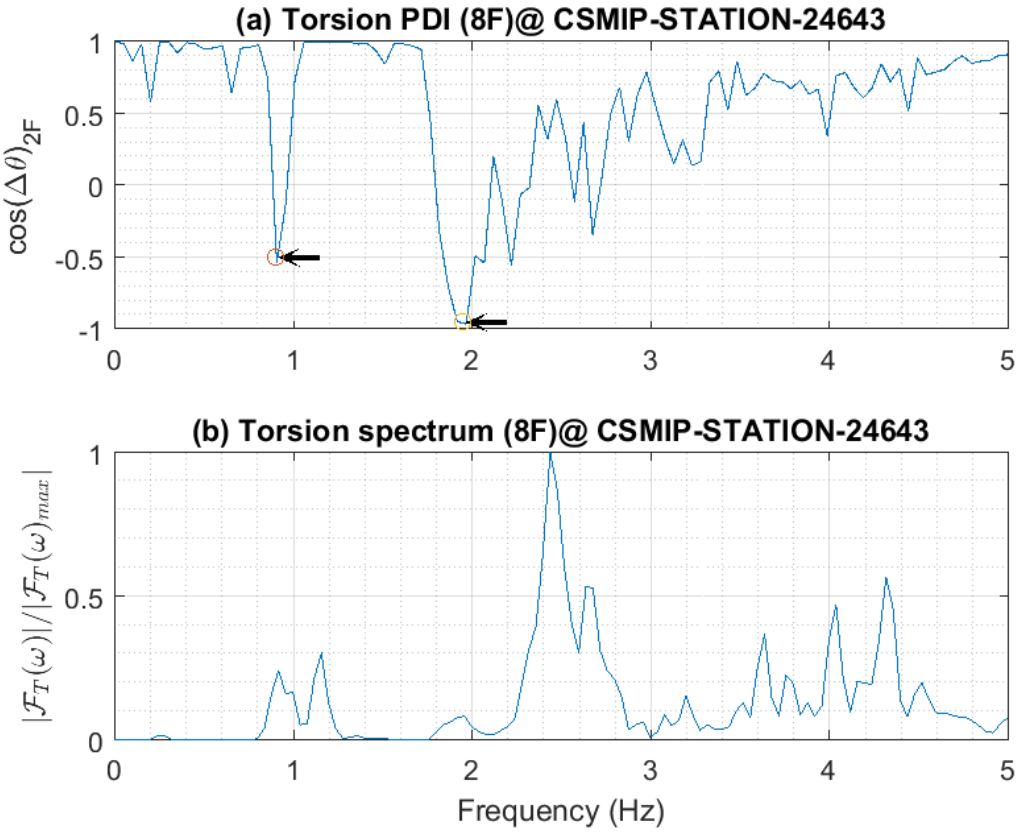

Fig. C.25. Torsional PDI plot of CSMIP-STATION-24643 (8F) (Ch.10& 11). The black arrow marks point at the torsional modes.

D. DETAILED ANALYSIS OF SAMPLE BUILDINGS IN TAIWAN

D.1 Case 1: Department of Civil Engineering Building, National Chung Hsin University (TCUBA3)

D.1.1 Basic information

Case one is a 7 story building at National Chung Hsin University, Taichung, Taiwan(TCUBA3). The structure is a reinforced concrete frame . In this event, the maximum displacement is 0.57 cm (Ch.22). The corresponding drift is 0.53 cm (relative to Ch.25), and the drift ratio is 0.02%. The detailed information is shown in Table 7.2.

D.1.2 Sensors Information

There are 29 accelerometers in this building. The location of sensors are shown in Figure D.1 and D.2. Eight sensors in this building are chosen to be studied. The channels and corresponding floors are listed in Table D.1.

D.1.3 Identification Result

Parameter for PDI plots

In case one, the adopted parameters are as listed:

- Observed frequency range: $0 \sim 10$ Hz
- Unit narrow frequency bandwidth: 0.05 Hz
- Order of FIR bandpass filter: 1500

- Window length of Hamming window (for FRF plot): 25% data length.

X Direction

The PDI plot in X direction of this building is shown in Fig.D.3 which comprises three parts:

a. Phase difference index plot (Roof vs. ground)

   In Fig.D.3-(a), there are two zero-crossing points, which represent the natural frequencies of the model (the third and after points are not recognizable).

   – zero-crossing points of PDI-X: [3.1, 9.3] Hz

b. Phase difference index plot (Roof vs. 4F)

   In Fig.D.3-(b) plot, the coordinate plot is separated by the PDI curve. From visual judgment, we can approximately divide the PDI coordinate into three parts:

   $\sim$ $0 < f < 3.31$: RF and 4F move in-phase

   $\sim$ $3.31 < f$: The PDI fluctuates along the y-axis

   Since the PDI is from Roof/4F, the $LMOI(6)_{1,4} = 1$. It means we only can target the first mode from plot (b). And Fig.D.3-(b) confirmed our assumption.

c. Frequency response function plot (Roof vs. ground)

   Figure D.3-(c) is a traditional FRF plot, and we can judge the natural frequencies by peak-picking method. In this case, the natural frequencies in X direction is: f= [3.05, 9.3] Hz. In addition, an obvious peak can be observed at f=3.9 Hz. In Chapter 5, the phenomenon was discussed, it might be caused by torsional force. By checking the PDI-T plot (Fig.D.5), it can be confirmed that f= 3.9 Hz is torsional mode.

Y Direction

The PDI plot in Y direction of this building is shown in Fig.D.4 which comprises three parts:

a. Phase difference index plot (Roof vs. ground)

   In Fig.D.4-(a), there are two obvious zero-crossing points, which represent the natural frequencies of the model. Maybe the earthquake is a small one so that higher modes are barely excited.

   - zero-crossing points of PDI-Y: [3.22, 8.78] Hz

b. Phase difference index plot (Roof vs. 4F)

   From visual judgment, we can approximately divide the PDI coordinate into three parts:

   $\sim$ $0 < f < 4.5$: RF and 9F move in-phase

   $\sim$ $4.5 < f$: The PDI fluctuates along the axis of y=-1.

   Since the PDI is from Roof/4F, the $LMOI(6)_{1,4} = 1$. It means we only can target the first modes from plot (b) . Figure D.4-(b) confirmed our assumption.

c. Frequency response function plot (Roof vs.ground)

   Figure D.4-(c) is a traditional FRF plot, and evaluators can judge the natural frequencies by peak-picking method. In this case, the natural frequencies are: f=3.12 Hz. In addition, an obvious peak can be observed at f=3.5 Hz. In Chapter 5, the phenomenon was discussed, it might be caused by torsional force. By checking the PDI-T plot (Fig.D.6), it can be confirmed that f= 3.9 Hz is a torsional mode. However, it is weired that the detected torsional mode in X direction is slightly difference from the identification result in Y direction. Similar results is also observed in torsion spectrum (Fig.D.5-(b) and D.6-(b)). Two obvious peaks can be seen in f=3.5 Hz and f=3.9 Hz, but the two peaks do not match the translational mode in X and Y direction. A possible explanation is that the building is not symmetric in plan and elevation. There is a sub-building

(3 story structure) attached at the right side of the main building, lengthening the dimension in Y direction. When the building shakes, the minor building somehow interferes the torsional period in different direction.

Rotation

In this building, two pairs of channels: (Ch. 15& 13) and (Ch. 21& 28) are used to draw the torsional PDI plots, i.e PDI-T plots:

1. The PDI-T plot of RF(Ch. 21& 28) is shown in Fig.D.5-(a)
2. The PDI-T plot of 4F(Ch. 15& 13) is shown in Fig.D.6-(a)
3. The torsion spectra are shown in Fig.D.5-(b) and Fig.D.6-(b)

From the above figures, we can observe three clear torsional modes: $f_{nt} = [3.8, 7.8]$ Hz.

D.1.4 Comparison with Existing Research

From the above discussion and existing research, a comparison of results is shown from PDI-analysis and from publications published by others as the Table 7.7. The comparison shows that the three methods, namely PDI, peak-picking and subspace method acquire similar identification results with tolerable errors.

The original plot of subspace method in [4] is not available. Therefore, this research analyzed the same earthquake data by subspace method again and produce the comparison plots as shown in Fig.D.7 and D.8. The adopted parameters of subspace method are listed as below:

- Order: 12
- Size of Hankel matrix: 150
- Sampling rate of signal: 50 Hz

Fig.D.7 and D.8 demonstrate the comparison of PDI-plot method, peak-picking method,and subspace method. It can be observed that three plots identify similar results of natural frequencies.

In addition, by aligning the PDI-X, PDI-Y, PDI-T together, we can identify the modal order of each identified frequency more easily. The triple PDI plot is shown in Fig.D.9. By initial check, the first three modes identified by Loh match well with the triple PDI(RF-GF)-XYT plots. Thus, it is proven that PDI-plot method can be an independent method for system identification.

D.2 Case 2: Building of Department of Civil and Construction Engineering, National Taiwan University of Science and Technology (TAPBA5)

D.2.1 Basic information

Case two is a eight story building at National Taiwan University of Science and Technology, Taipei, Taiwan(TAPBA5). The structure is a reinforced concrete frame . In this event, the maximum displacement is 0.084 cm (Ch.26). The corresponding drift is 0.078 cm (relative to Ch.1), and the drift ratio is 0.016%. The detailed information is shown in Table 7.3.

D.2.2 Sensors Information

There are 29 accelerometers in this building. The location of sensors are shown in Figure D.10 and D.11. Eight sensors in this building are chosen to be studied. The channels and corresponding floors are listed in Table D.2.

D.2.3 Identification Result

Parameter for PDI plots

In case two, the adopted parameters are as listed:

- Observed frequency range: $0 \sim 10$ Hz
- Unit narrow frequency bandwidth: 0.05 Hz
- Order of FIR bandpass filter: 2000
- Window length of Hamming window (for FRF plot): 25% data length.

X Direction

The PDI plot in X direction of this building is shown in Fig.D.12 which comprises three parts:

a. Phase difference index plot (Roof vs. ground)

   In Fig.D.12-(a), there are three zero-crossing points, which represent the natural frequencies of the model (the fourth and after points are not recognizable).

   – zero-crossing points of PDI-X: [1.48, 5.24, 9.27] Hz

b. Phase difference index plot (Roof vs. 2F)

   In Fig.D.12-(b) plot, the coordinate plot is separated by the PDI curve. PDI=1 means the roof and the second floor moving toward the same direction i.e. moving in-phase. On the contrary, PDI=-1 means the roof and the second floor moving toward the opposite direction, i.e. moving out-of-phase. From visual judgment, we can approximately divide the PDI coordinate into three parts:

   $\sim$ $0 < f < 1.94$: RF and 2F move in-phase

   $\sim$ $1.94 < f < 5.72$: RF and 2F move out-of-phase

   $\sim$ $5.72 < f$: RF and 2F move in-phase

   The plot is quite useful since the PDI is between Roof and 2F. The phase difference indices are not 1, -1, 1, -1....in sequence. The identified modes in X direction correspond to the interval accordingly. Therefore, it means that we can use the PDI(RF-2F) to locate the natural frequencies with more confidence.

c. Frequency response function plot (Roof vs. ground)

   Figure D.12-(c) is a traditional FRF plot, and evaluators can judge the natural

frequencies by peak-picking method. In this case, the natural frequencies in X direction is: f= [1.44, 5.45] Hz.

Y Direction

The PDI plot in Y direction of this building is shown in Fig.D.13 which comprises three parts:

a. Phase difference index plot (Roof vs. ground)

   In Fig.D.13-(a), there are two obvious zero-crossing points, which represent the natural frequencies of the model.

   - zero-crossing points of PDI-Y: [2.45, 7.7] Hz

b. Phase difference index plot (Roof vs. 2F)

   From visual judgment, we can approximately divide the PDI coordinate into three parts:

   $\sim$ $0 < f < 2.55$: RF and 9F move in-phase

   $\sim$ $2.55 < f < 8.4$: RF and 9F move out-of-phase

   $\sim$ $8.4 < f$: The PDI fluctuates along the y-axis

   Although the PDI plot is not RF/2F, the plot is still useful. The reason is the same as the condition in Y direction.

c. Frequency response function plot (Roof vs.ground)

   Figure D.13-(c) is a traditional FRF plot, and evaluators can judge the natural frequencies by peak-picking method. In this case, the natural frequencies are: f=2.29 Hz.

Rotation

In this building, two pairs of channels, namely (Ch.28 & 30) and (Ch. 21& 23) are used to draw the torsional PDI plots:

1. The PDI-T plot of RF(Ch.28 & 30) is shown in Fig.D.14-(a)
2. The PDI-T plot of 6F(Ch. 21& 23) pair is shown in Fig.D.15-(a)
3. The torsion spectra are shown in Fig.D.14-(b) and Fig.D.15-(b)

From Fig.D.14 and Fig.D.15, we can observe three torsional modes clearly: $f_{nt} = [1.75, 5.2, 9.2 \sim 9.4]$ Hz.

D.2.4 Comparison with Existing Research

From the above discussion and existing research, a comparison of results is shown from PDI-analysis and from publications published by others as the Table 7.8. The comparison shows that the three methods, namely PDI, peak-picking and subspace method acquire similar identification results with tolerable errors.

The original plot of subspace method in [4] is not available. Therefore, this research analyzed the same earthquake data by subspace method again and produce the comparison plots as shown in Fig.D.16 and D.17. The adopted parameters of subspace method are listed as below:

- Order: 10
- Size of Hankel matrix: 150
- Sampling rate of signal: 50 Hz

Fig.D.16 and D.17 demonstrate the comparison of PDI-plot method, peak-picking method,and subspace method. It can be observed that three plots identify similar results of natural frequencies.

Similar to the previous case, by aligning the PDI-X, PDI-Y, PDI-T together, we can identify the modal order of each identified frequency more easily. The triple PDI plot is shown in Fig.D.9. By initial check, the first three modes identified by Loh match well with the triple PDI(RF-GF)-XYT plots.

D.3 Case 3: Dormitory Building of Faculty & Staff, National Chiao Tung University (TCUBA6)

D.3.1 Basic information

Case two is a eight story building at National Taiwan University of Science and Technology, Taipei, Taiwan(TAPBA5). The structure is a reinforced concrete frame . In this event, the maximum displacement is 0.56 cm (Ch.20). The corresponding drift is 0.53 cm (relative to Ch.8), and the drift ratio is 0.014%. The detailed information is shown in Table 7.4.

D.3.2 Sensors Information

There are 29 accelerometers in this building. The location of sensors are shown in Figure D.19 and D.20. Eight sensors in this building are chosen to be studied. The channels and corresponding floors are listed in Table D.3.

D.3.3 Identification Result

Parameter for PDI plots

In case three, the adopted parameters are as listed:

- Observed frequency range: $0 \sim 10$ Hz
- Unit narrow frequency bandwidth: 0.1 Hz
- Order of FIR bandpass filter: 2000
- Window length of Hamming window (for FRF plot): 25% data length.

X Direction

The PDI plot in X direction of this building is shown in Fig.D.21 which comprises three parts:

a. Phase difference index plot (Roof vs. ground)

   In Fig.D.21-(a), there are two zero-crossing points, which represent the natural frequencies of the model (the third and after points are not recognizable).

   – zero-crossing points of PDI-X: [1.71, 5.85] Hz

b. Phase difference index plot (Roof vs. 2F)

   In Fig.D.21-(b) plot, the coordinate plot is separated by the PDI curve. PDI=1 means the roof and the second floor moving toward the same direction i.e. moving in-phase. On the contrary, PDI=-1 means the roof and the second floor moving toward the opposite direction, i.e. moving out-of-phase. From visual judgment, we can approximately divide the PDI coordinate into three parts:

   $\sim$ $0 < f < 1.8$: RF and 2F move in-phase

   $\sim$ $1.8 < f < 8.5$: RF and 2F move out-of-phase

   $\sim$ $8.5 < f$: The PDI fluctuates along the y-axis

   Although the PDI is between Roof and 2F, very limited information can be obtained. Because the building is " C "-shaped in plan, the structural behavior is dominated by the first mode accompanied with some torsional effects. In the frequency range of $f = 1 \sim 10$ Hz, only the first mode can be identified without ambiguity.

c. Frequency response function plot (Roof vs. ground)

   Figure D.21-(c) is a traditional FRF plot, and evaluators can judge the natural frequencies by peak-picking method. In this case, the natural frequencies in X direction is: f= 1.68 Hz.

Y Direction

The PDI plot in Y direction of this building is shown in Fig.D.22 which comprises three parts:

a. Phase difference index plot (Roof vs. ground)

   In Fig.D.22-(a), there are two obvious zero-crossing points, which represent the natural frequencies of the model (the third and after points are not recognizable).

   – zero-crossing points of PDI-Y: [2.18, 8.43] Hz

b. Phase difference index plot (Roof vs. 2F)

   From visual judgment, we can approximately divide the PDI coordinate into three parts:

   $\sim$ $0 < f < 2.48$: RF and 2F move in-phase

   $\sim$ $2.48 < f < 8.8$: RF and 2F move out-of-phase

   $\sim$ $8.8 < f$: The PDI fluctuates along the y-axis

c. Frequency response function plot (Roof vs.ground)

   Figure D.22-(c) is a traditional FRF plot, and evaluators can judge the natural frequencies by peak-picking method. In this case, the natural frequencies are: f=2.17 Hz.

Rotation

In this building, two pairs of channels: (Ch. 19& 23) and (Ch. 16& 18) are used to draw the torsional PDI plots:

1. The PDI-T plot of RF(Ch. 19& 23) is shown in Fig.D.23-(a)
2. The PDI-T plot of 7F(Ch. 16& 18) is shown in Fig.D.24-(a)
3. The torsion spectra are shown in Fig.D.23-(b) and Fig.D.24-(b)

In Fig.D.23, we can observe torsional modes at $f_{nt} = [2.4, 5.6, 8.4 - 9.4]$ Hz. This building is close to " C " shape i.e. an asymmetric plan. From Fig.D.20, an eccentric torsion might occur in X direction under seismic force. Therefore, one has to be very careful in mode frequency identification. Observing Fig.D.23-(b) and Fig.D.24-(b), we find that these are standard torsional spectra. Three observed frequency peaks

[1.6, 2.0, 2.4] Hz represent the approximate f_{1x}, f_{1y}, f_{1t}. Comparing with the identified f_{1x}, f_{1y} in previous sections, it can be inferred that $f_{1t} \approx 2.4$ Hz.

D.3.4 Comparison with Existing Research

From the above discussion and existing research, a comparison of results is shown from PDI-analysis and from publications published by others as the Table 7.9. The comparison shows that the three methods, namely PDI, peak-picking and subspace method acquire similar identification results with tolerable errors.

The original plot of subspace method in [4] is not available. Therefore, this research analyzed the same earthquake data by subspace method again and produce the comparison plots as shown in Fig.D.25 and D.26. The adopted parameters of subspace method are listed as below:

- Order: 12
- Size of Hankel matrix: 200
- Sampling rate of signal: 50 Hz

Fig.D.25 and D.26 demonstrate the comparison of PDI-plot method, peak-picking method,and subspace method. It can be observed that three plots identify similar results of natural frequencies.

Similar to the previous case, by aligning the PDI-X, PDI-Y, PDI-T together, we can identify the modal order of each identified frequency more easily. The triple PDI plot is shown in Fig.D.27. By initial check, the first three modes identified by Loh match well with the triple PDI(RF-GF)-XYT plots.

D.4 Case 4: Headquarters building, Taiwan Power Company (TAPBA4)

D.4.1 Basic information

Case four is a twenty six story headquarters building of Taiwan Power Company, Taipei, Taiwan(TAPBA4). The structure, finished in 1982, is the first steel rigid frame skyscraper in Taiwan . In this event, the maximum displacement is 10.44 cm (Ch.16). The corresponding drift is 11.80 cm (relative to Ch.7), and the drift ratio is 0.11%. The detailed information is shown in Table 7.5.

D.4.2 Sensors Information

There are 18 accelerometers in this building. The location of sensors are shown in Figures D.28 and D.29. Seven sensors in this building are chosen to be studied. The channels and corresponding floors are listed in Table D.4.

D.4.3 Identification Result

Parameter for PDI plots

In case four, the adopted parameters are as listed:

- Observed frequency range: $0 \sim 4$ Hz
- Unit narrow frequency bandwidth: 0.02 Hz
- Order of FIR bandpass filter: 5000
- Window length of Hamming window (for FRF plot): 25% data length.

X direction

The PDI plot in X direction of this building is shown in Fig.D.30 which comprises three parts:

a. Phase difference index plot (Roof vs. ground)

In Fig.D.30-(a), there are three zero-crossing points, which represent the natural frequencies of the model (the fourth and after points are not recognizable).

- zero-crossing points of PDI-X: [0.37,1.03,1.83] Hz

b. Phase difference index plot (Roof vs. 9F)

In Fig.D.30-(b) plot, the coordinate plot is separated by the PDI curve. PDI=1 means the roof and the ninth floor moving toward the same direction i.e. moving in-phase. On the contrary, PDI=-1 means the roof and the ninth floor moving toward the opposite direction, i.e. moving out-of-phase. From visual judgment, we can approximately divide the PDI coordinate into five parts:

$\sim$ $0 < f < 0.5$: RF and 9F move in-phase

$\sim$ $0.5 < f < 1.3$: RF and 9F move out-of-phase

$\sim$ $1.3 < f < 2.2$: RF and 9F move in-phase

$\sim$ $2.2 < f < 2.9$: RF and 9F move out-of-phase

$\sim$ $2.9 < f$: The PDI fluctuates along the y-axis

Although the PDI plot is not RF/2F, the plot is still useful. It is because for a tall building like this case, the mode contribution factors at roof and 9th floor have alternating signs in the first four modes. Thus, the phase difference indices are still 1, -1, 1, -1 in sequence. The identified modes in X direction correspond to the interval accordingly.

c. Frequency response function plot (Roof vs. ground)

Figure D.30-(c) is a traditional FRF plot, and evaluators can judge the natural frequencies by peak-picking method. In this case, the natural frequencies are: f=[0.35, 1.0, 1.82, 2.4] Hz.

Y Direction

The PDI plot in Y direction of this building is shown in Fig.D.31 which comprises three parts:

a. Phase difference index plot (Roof vs. ground)

   In Fig.D.31-(a), there are four obvious zero-crossing points, which represent the natural frequencies of the model (the fifth and after points are not recognizable).

   - zero-crossing points of PDI-Y: [0.4, 1.09, 2.0, 2.82] Hz

b. Phase difference index plot (Roof vs. 9F)

   From visual judgment, we can approximately divide the PDI coordinate into three parts:

   $\sim$ $0 < f < 0.4$: RF and 9F move in-phase

   $\sim$ $0.4 < f < 1.35$: RF and 9F move out-of-phase

   $\sim$ $1.35 < f < 2.5$: RF and 9F move in-phase

   $\sim$ $2.5 < f < 3.2$: RF and 9F move out-of-phase

   $\sim$ $3.2 < f$: The PDI fluctuates along the y-axis

   Although the PDI plot is not RF/2F, the plot is still useful. The reason is the same as the condition in X direction.

c. Frequency response function plot (Roof vs.ground)

   Figure D.31-(c) is a traditional FRF plot, and evaluators can judge the natural frequencies by peak-picking method. In this case, the natural frequencies are: f=[0.35, 1.2, 2.0] Hz.

Rotation

In this building, only one pair of channels, namely (Ch. 14& 17) can be used to draw the torsional PDI plots. Another pair [13, 16] is too close to the symmetry axis of this building, so the effect of torsion would not be obvious in measurements:

1. The PDI-T plot of RF is shown in Fig.D.32-(a)
2. The torsion spectra are shown in Fig.D.32-(b)

There is a great difficulty to identify the first torsional mode for a tall building. According to Satake et al. (2003), the relationship between the first translational mode and torsional mode for RC building [33] is:

$$T_{1t} = 0.77T_1 \tag{D.1}$$

where:

T_{1t}: period of first torsional mode

T_1 : period of first translational mode

A rough empirical equation for estimating the first translational period is [22]:

$$T_1 = 0.1N \tag{D.2}$$

where: N = number of stories above the base.

From Eq.D.1 and D.2, when the building is very tall, the first torsional mode would be very close to translational mode in frequency. For example, for a 30 story building, T_1 ≈3 (sec), i.e f_1 ≈0.33 (Hz), and T_{1t} ≈2.31 (sec), i.e f_{1t} ≈0.41 (Hz). The difference of f_1 and f_{1t} is only 0.08 Hz. It is so small that it is very hard to separate f_{1t} from f_1 in signal processing.

Nevertheless, from Fig.D.32, D.30 and D.31, we still can make a reasonable guess.

- From Fig.D.32-(b), the apparent responses occur at $f = 0.45$ Hz and $f = 1.2$ Hz. It is obvious that $f = 1.2$ is a torsional mode, but it cannot be determined if $f = 0.45$ is a torsional mode.
- From Fig.D.30-(b), the obvious PDI(RF/9F) index of " out-of-phase " occur at the range between $f = 1.21$ Hz and $f = 2.2$ Hz. In $f = 0.45$, PDI(RF/9F) index only equal to 0.6. This does not provide evidence to suggest that there is a torsional mode at f=0.4 Hz.

- Fig.D.31-(b) tells us that when $f = 1.2$, PDI(RF/9F) index is close to -1, implying that the roof and 9F move out-of-phase. Therefore, from the viewpoint of torsional mode shape, $f = 1.2$ cannot be the first torsional mode.

Base on the above ideas, we can bravely consider that $f \approx 0.45$ is the first torsional mode. The rest torsional modes are :f_t=[1.21, 2.2] Hz

D.4.4 Comparison with Existing Research

From the above discussion and existing research, a comparison of results is shown from PDI-analysis and from publications published by others as the Table 7.10. The comparison shows that the three methods, namely PDI, peak-picking and subspace method acquire similar identification results with tolerable errors.

The original plot of subspace method in [27] is not available. Therefore, this research analyzed the same earthquake data by subspace method again and produce the comparison plots as shown in Fig.D.33 and D.34. The adopted parameters of subspace method are listed as below:

- Order: 10
- Size of Hankel matrix: 50
- Sampling rate of signal: 10 Hz

Fig.D.33 and D.34 demonstrate the comparison of PDI-plot method, peak-picking method,and subspace method. It can be observed that three plots identify similar results of natural frequencies.

Similar to the previous case, by aligning the PDI-X, PDI-Y, PDI-T together, we can identify the modal order of each identified frequency more easily. The triple PDI plot is shown in Fig.D.35. By initial check, the first three modes identified by Loh match well with the triple PDI(RF-GF)-XYT plots.

D.5 Case 5: National Chiao Tung University Library (TCUBAA)

D.5.1 Basic information

Case five is a eight story library building of National Chiao Tung University, Hsin Chiu, Taiwan(TCUBAA). The structure is a RC rigid frame with mat foundation. In this event, the maximum displacement is 7.77 cm (Ch.24). The corresponding drift is 5.24 cm (relative to Ch.5), and the drift ratio is 0.15%. The detailed information is shown in Table 7.6.

D.5.2 Sensors Information

There are 25 accelerometers in this building. The location of sensors are shown in Figures D.36 and D.37. Eight sensors in this building are chosen to be studied. The channels and corresponding floors are listed in Table D.5.

D.5.3 Identification Result

Parameter for PDI plots

In case four, the adopted parameters are as listed:

- Observed frequency range: $0 \sim 10$ Hz
- Unit narrow frequency bandwidth: 0.1Hz
- Order of FIR bandpass filter: 2000
- Window length of Hamming window (for FRF plot): 25% data length.

X Direction

The PDI plot in X direction of this building is shown in Fig.D.38 which comprises three parts:

a. Phase difference index plot (Roof vs. ground)

   In Fig.D.38-(a), there are two zero-crossing points, which represent the natural frequencies of the model (the third and after points are not recognizable).

   – zero-crossing points of PDI-X: [1.48, 5.15] Hz

b. Phase difference index plot (Roof vs. 2F)

   In Fig.D.38-(b) plot, the coordinate plot is separated by the PDI curve. PDI=1 means the roof and the fourth floor moving toward the same direction i.e. moving in-phase. On the contrary, PDI=-1 means the roof and the fourth floor moving toward the opposite direction, i.e. moving out-of-phase. From visual judgment, we can approximately divide the PDI coordinate into three parts:

   $\sim$ $0 < f < 1.55$: RF and 2F move in-phase

   $\sim$ $1.55 < f < 5.4$: RF and 2F move out-of-phase

   $\sim$ $5.4 < f$: The PDI fluctuates along the y-axis

   The plot is quite useful since the PDI is between Roof and 2F. The phase difference indices are not 1, -1, 1, -1....in sequence. The identified modes in X direction correspond to the interval accordingly.

c. Frequency response function plot (Roof vs. ground)

   Fig.D.38-(c) is a traditional FRF plot, and evaluators can judge the natural frequencies by peak-picking method. In this case, the first mode is about 1.5 Hz, and the second mode is close to 4.9 Hz. It can be observed that there are more than two peaks ($f \approx 1.5$ & 1.8 Hz) around the first mode in the FRF plot. By Fig.D.38-(a), it is clear that $f \approx 1.5$ is the first mode. By Fig.D.40, $f \approx 1.8$ is not torsional mode. The remained possibility is that the building did not keep linear during the earthquake. To figure this out, the concept of time-frequency domain analysis will be introduced in the next chapter.

Y Direction

The PDI plot in Y direction of this building is shown in Fig.D.39 which comprises three parts:

a. Phase difference index plot (Roof vs. ground)

   In Fig.D.39-(a), there are two obvious zero-crossing points, which represent the natural frequencies of the model (the fourth and after points are not recognizable).

   - zero-crossing points of PDI-Y: [1.15, 4.05] Hz

b. Phase difference index plot (Roof vs. 2F)

   From visual judgment, we can approximately divide the PDI coordinate into three parts:

   $\sim$ $0 < f < 1.2$: RF and 2F move in-phase

   $\sim$ $1.2 < f < 4.4$: RF and 2F move out-of-phase

   $\sim$ $4.4 < f$: The PDI fluctuates along the y-axis

   The phase difference indices are not 1, -1, 1, -1....in sequence. The identified modes in Y direction correspond to the interval accordingly.

c. Frequency response function plot (Roof vs.ground)

   Figure D.39-(c) is a traditional FRF plot of this building in Y direction. By peak-picking method, the first mode is about 1.15 Hz, and the second mode is close to 4.4 Hz(although it is somewhat subjective). Similar to X direction, it can be observed that there are minor peaks at the right side of the first mode in the FRF plot. By Fig.D.39-(a), it is clear that $f \approx 1.5$ is the first mode. By Fig.D.40, the minor peak is not torsional mode, either. The remained possibility is that the building did not keep linear during the earthquake. To figure this out, the concept of time-frequency domain analysis will be introduced in the next chapter.

Rotation

In this building, two pairs of channels: (Ch. 24& 26) and (Ch. 27& 23) are used to draw the torsional PDI plots:

1. The PDI-T plot of RF(Ch. 24& 26 - Y dir.) is shown in Fig.D.40-(a)
2. The PDI-T plot of RF(Ch. 27& 23 - X dir.) is shown in Fig.D.41-(a)
3. The torsion spectra are shown in Fig.D.40-(b) and Fig.D.41-(b)

In Fig.D.40, we can observe torsional mode at $f_{nt} = 0.96$ Hz. However, Fig.D.41 indicates that $f \approx 1.5$ is the torsional mode.

This building is the structure type with large mass eccentricity in elevation and plan. From Fig.D.37, the area among column line 1 to line 5 is partially empty in lower stories. Lacking mass in lower left part brings large amount of torsion in X direction under lateral seismic forces. Such structural type explains the torsional spectrum in Fig.D.41-(a). The plot indicates $f \approx 1.4$ is torsional mode while Fig.D.40-(a) points out $f_{nt} = 0.96$. This is because the channel pair -[27, 23] is in X direction which has large response in X direction. Without the comprehensive judgment of all conditions for this building, it is difficult to determine the torsional mode of this building.

D.5.4 Comparison with Existing Research

From the above discussion and existing research, a comparison of results is shown from PDI-analysis and from publications published by others as the Table 7.11. The comparison shows that the three methods, namely PDI, peak-picking and subspace method acquire similar identification results with tolerable errors.

The original plot of subspace method in [28] is not available. Therefore, this research analyzed the same earthquake data by subspace method again and produce the comparison plots as shown in Fig.D.42 and D.43. The adopted parameters of subspace method are listed as below:

- Order: 10
- Size of Hankel matrix: 200
- Sampling rate of signal: 50 Hz

Fig.D.42 and D.43 demonstrate the comparison of PDI-plot method, peak-picking method,and subspace method. It can be observed that three plots identify similar results of natural frequencies.

Similar to the previous case, by aligning the PDI-X, PDI-Y, PDI-T together, we can identify the modal order of each identified frequency more easily. The triple PDI plot is shown in Fig.D.44. By initial check, the first three modes identified by Loh match well with the triple PDI(RF-GF)-XYT plots.

Table D.1.
Selected Sensors in TCUBA3

Direction	**Floor**	**Channel NO.**
X	RF	22
	4F	13
	GF	25
Y	RF	21
	4F	14
	GF	26
T	RF(Y dir.)	21 &18
	4F(X dir.)	15 &13

Sensor maps : Fig.D.1∼ Fig.D.2

Table D.2.
Selected Sensors in TAPBA5

Direction	**Floor**	**Channel NO.**
X	RF	26
	2F	12
	B1F	1
Y	RF	27
	2F	13
	B1F	2
T	4F(X dir.)	28 &30
	RF(X dir.)	21 &23

Sensor maps : Fig.D.10∼ Fig.D.11

Table D.3.
Selected Sensors in TCUBA6

Direction	**Floor**	**Channel NO.**
X	RF	20
	2F	11
	GF	8
Y	RF	19
	2F	10
	B1F	7
T	RF	19 &23
	7F	16 &18

Sensor maps : Fig.D.19∼ Fig.D.20

Table D.4.
Selected Sensors in TAPBA4

Direction	**Floor**	**Channel NO.**
X	RF	16
	19F	9
	GF	7
Y	RF	17
	19F	10
	B1F	8
T	RF	14 &17

Sensor maps : Fig.D.28∼ Fig.D.29

Table D.5.
Selected Sensors in TCUBAA

Direction	**Floor**	**Channel NO.**
X	RF	23
	2F	13
	B1	4
Y	RF	24
	2F	14
	B1	5
T	RF(Y dir.)	24 &26
	RF(X dir.)	27 &23

Sensor maps : Fig.D.36∼ Fig.D.37

Unit: cm

TCUBA3-Elevation

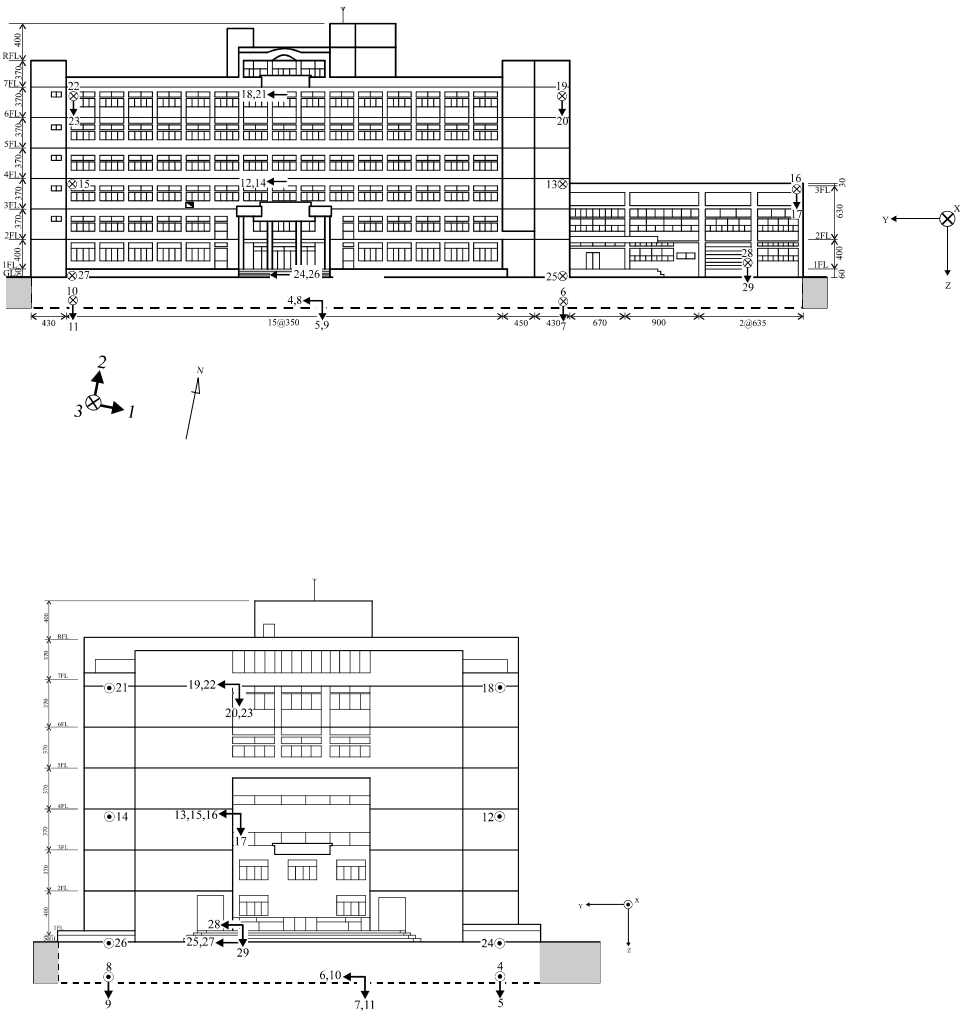

Fig. D.1. Elevation of TCUBA3

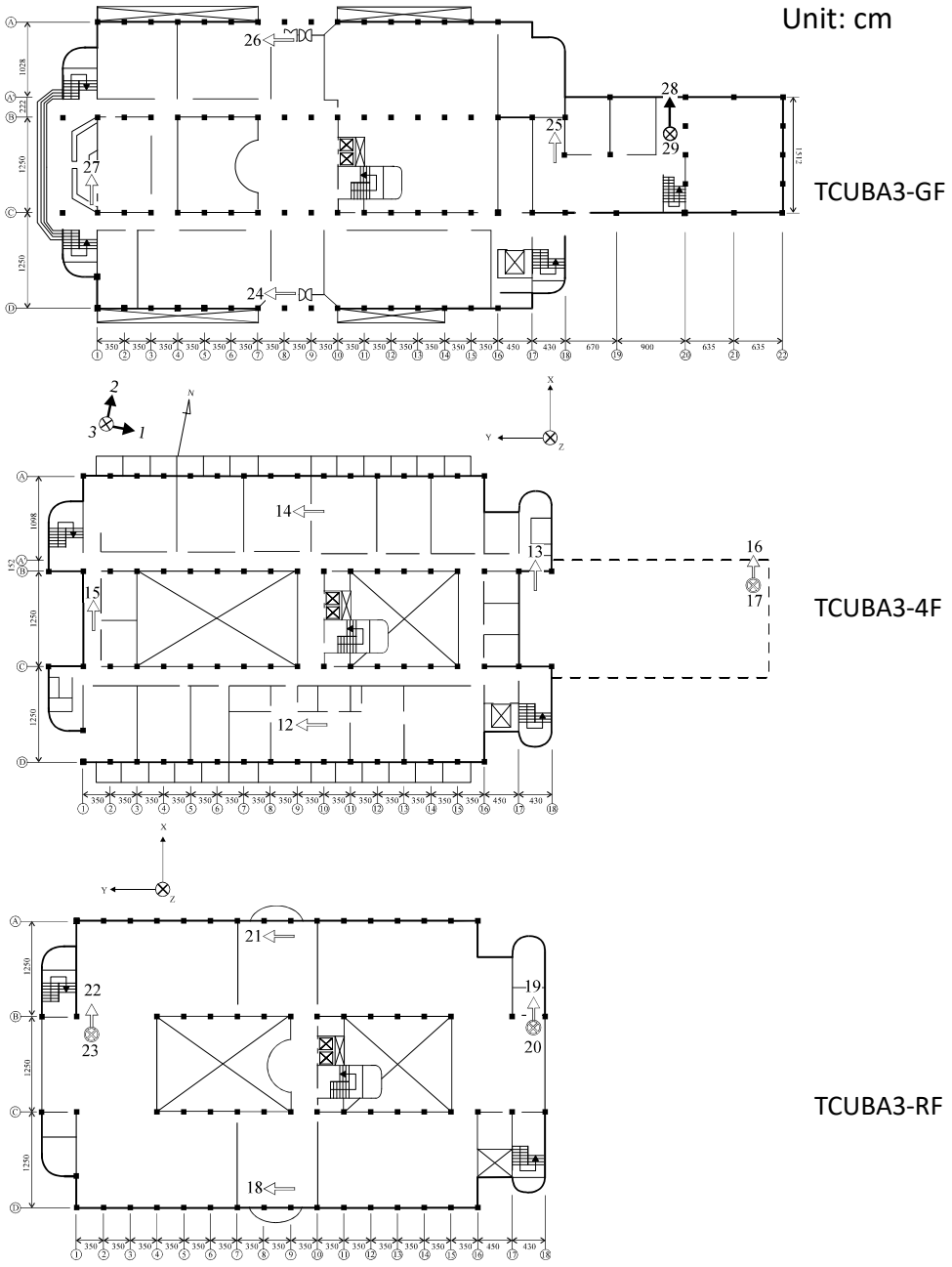

Fig. D.2. Building Plan of TCUBA3

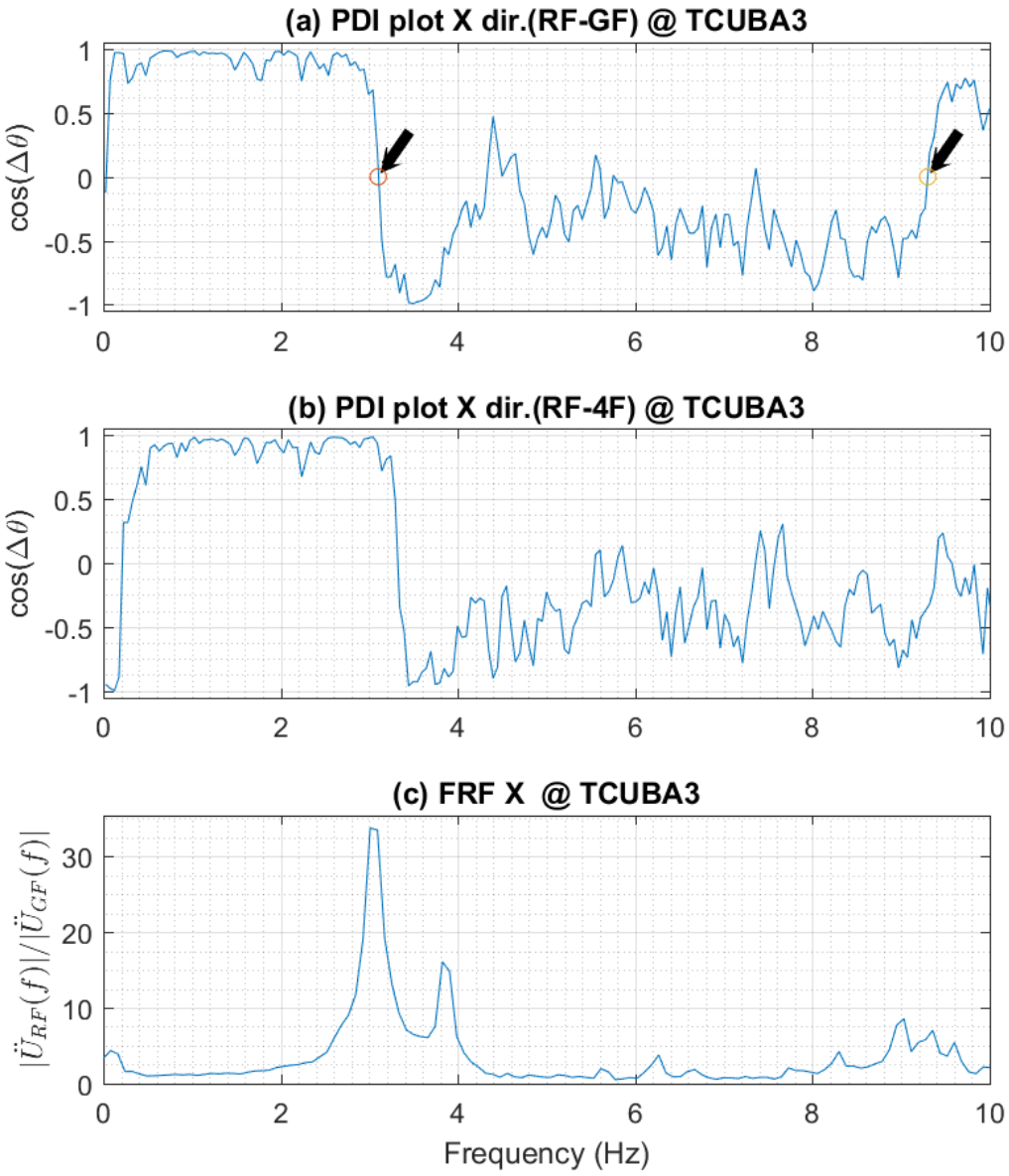

Fig. D.3. PDI plot of TCUBA3 in X direction. The black arrow marks point at the identified modes.

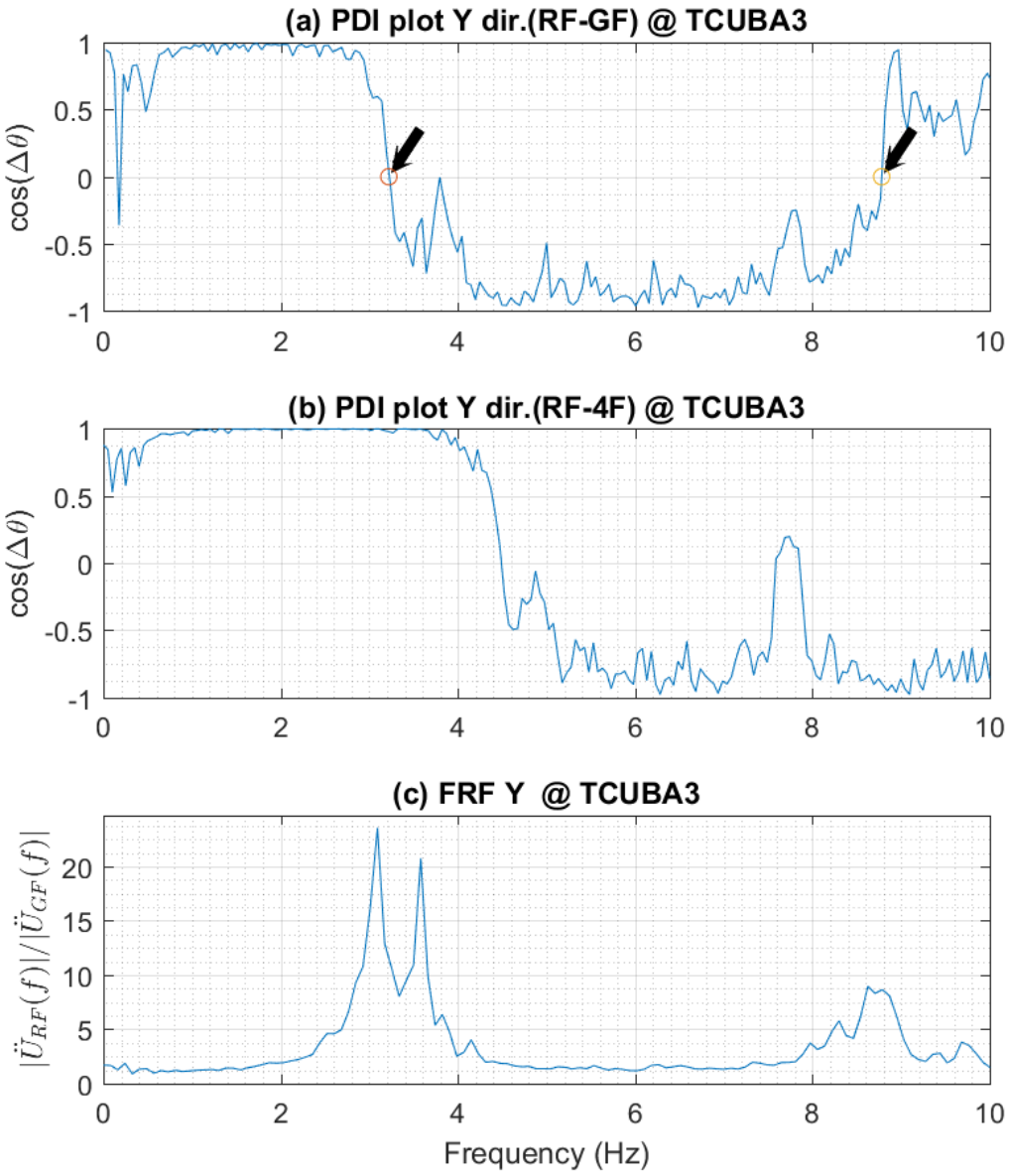

Fig. D.4. PDI plot of TCUBA3 in Y direction. The black arrow marks point at the identified modes.

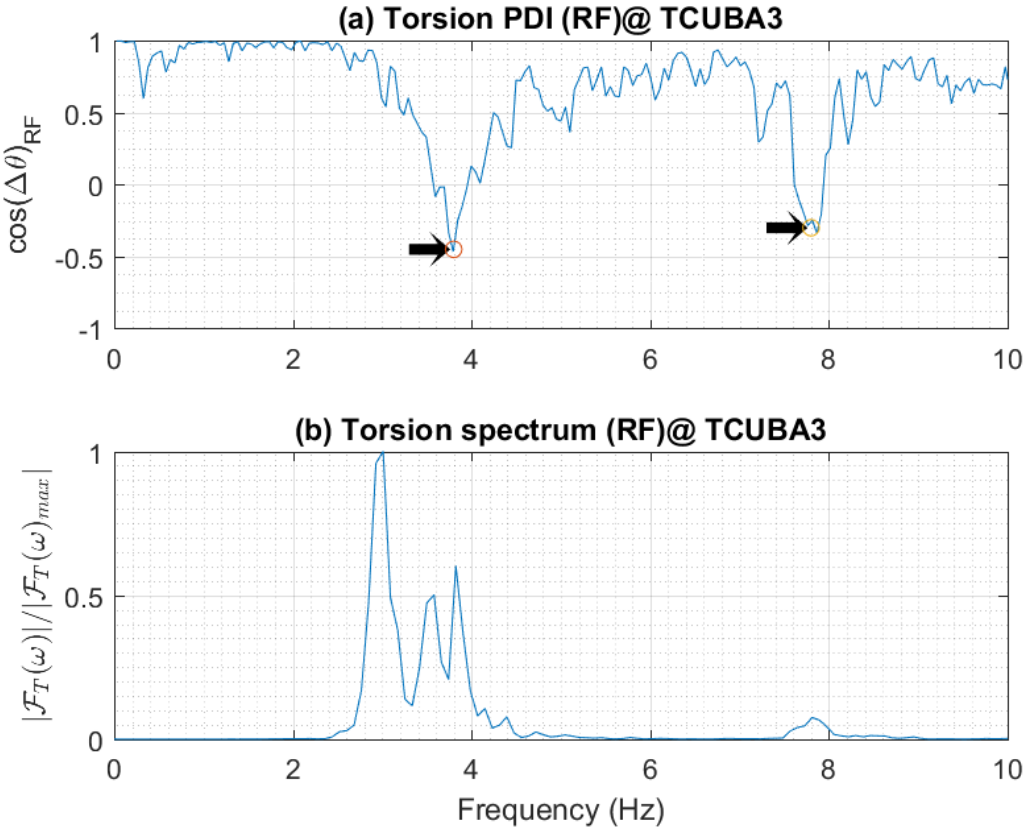

Fig. D.5. Torsional PDI plot of TCUBA3 (RF)(Ch. 21 & 28). The black arrow marks point at the identified modes.

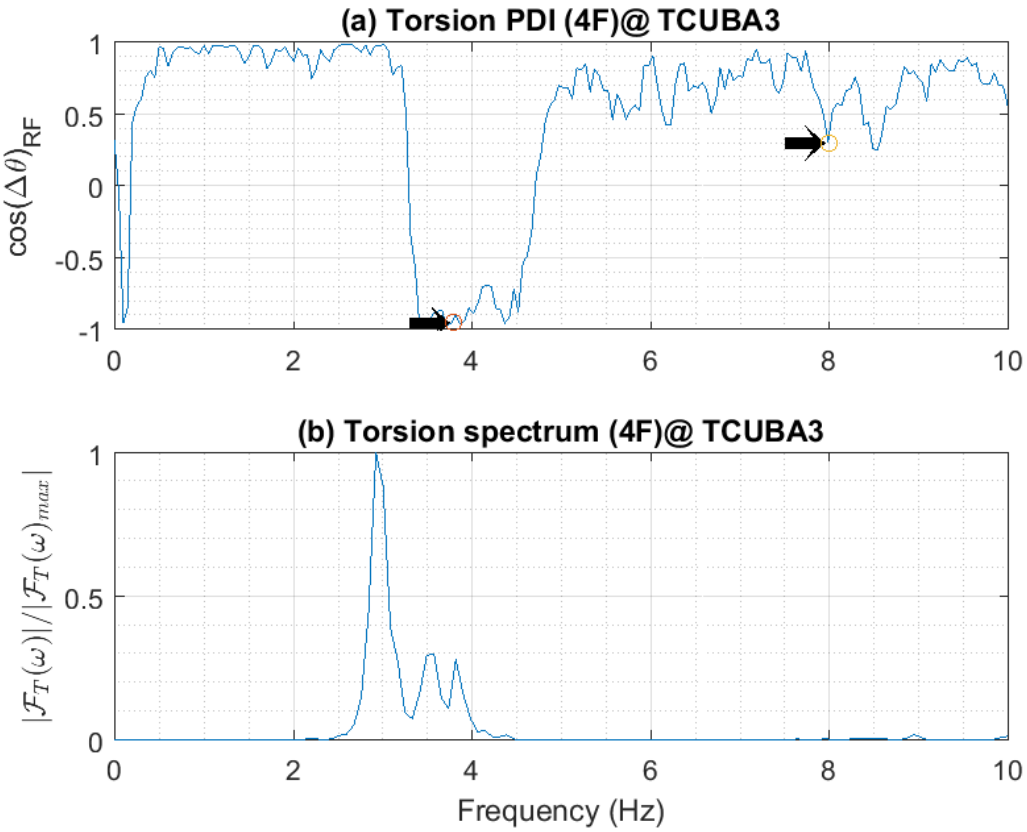

Fig. D.6. Torsional PDI plot of TCUBA3 (4F)(Ch. 15 & 13). The black arrow marks point at the identified modes. The results is from referring to the Fig.D.5.

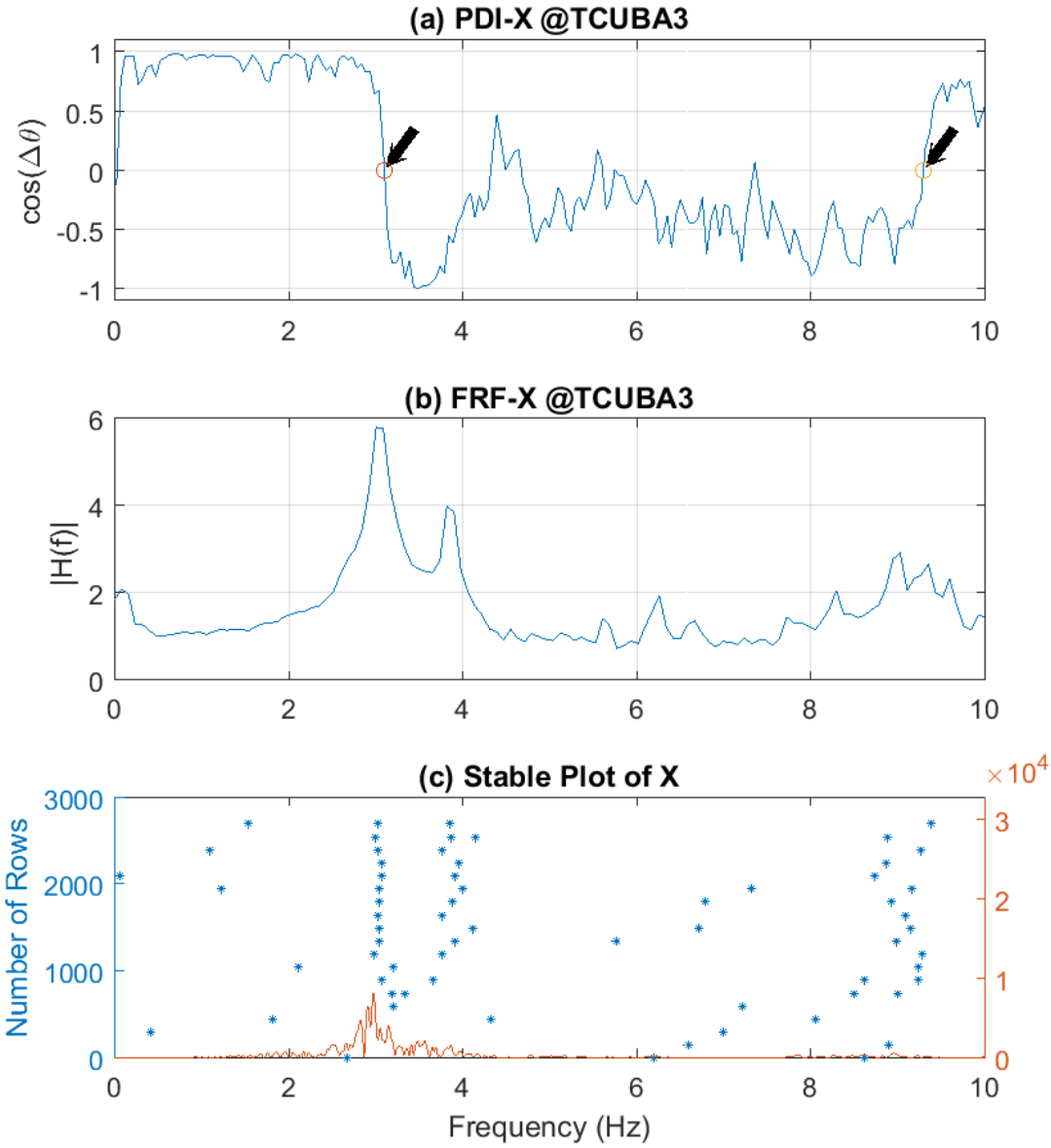

Fig. D.7. Comparison of three methods @ TCUBA3 in X direction.(a) PDI plot method, (b) peak-picking method, (c) subspace method. The black arrow marks point at the identified modes.

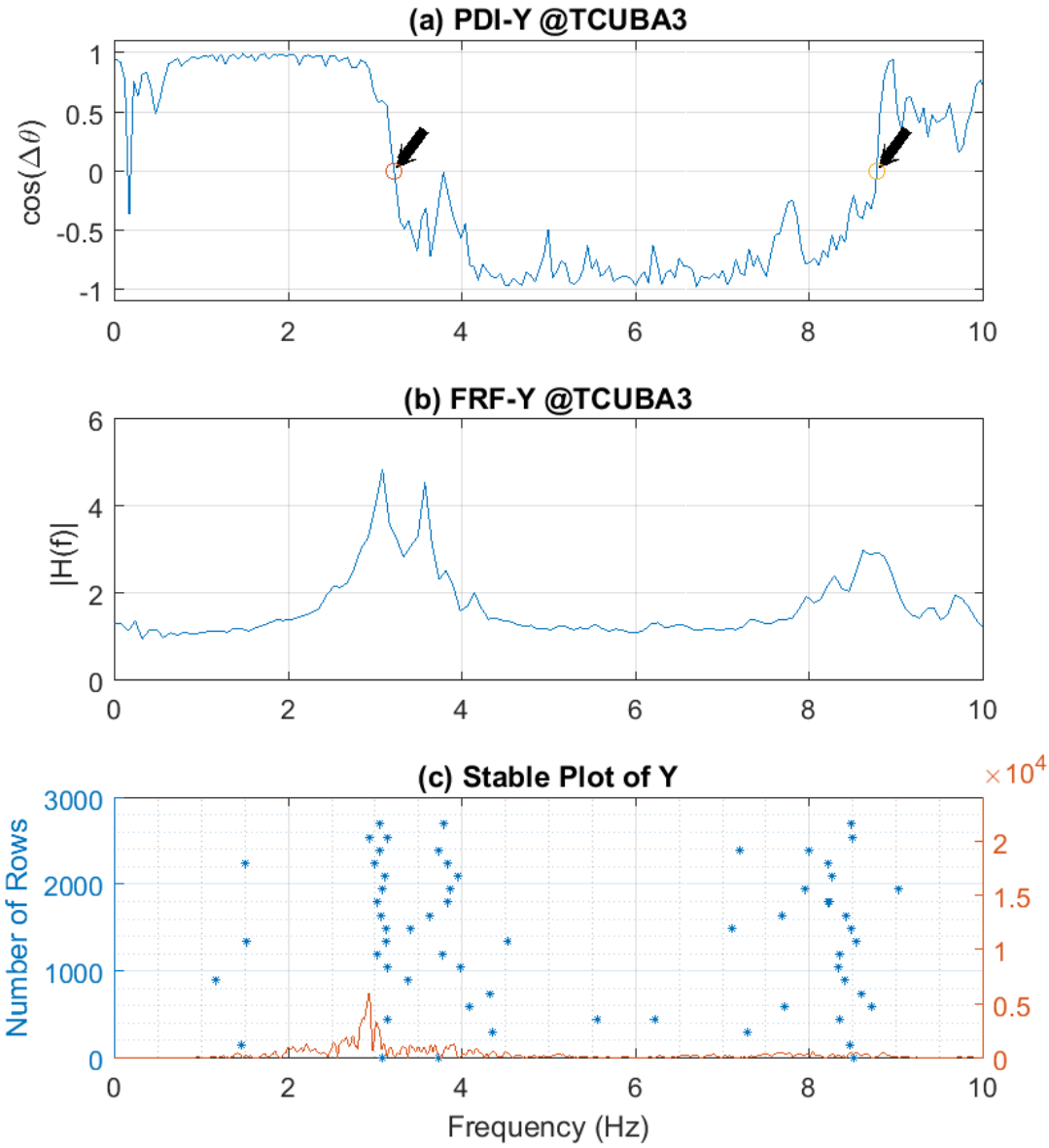

Fig. D.8. Comparison of three methods @ TCUBA3 in Y direction.(a) PDI plot method, (b) peak-picking method, (c) subspace method

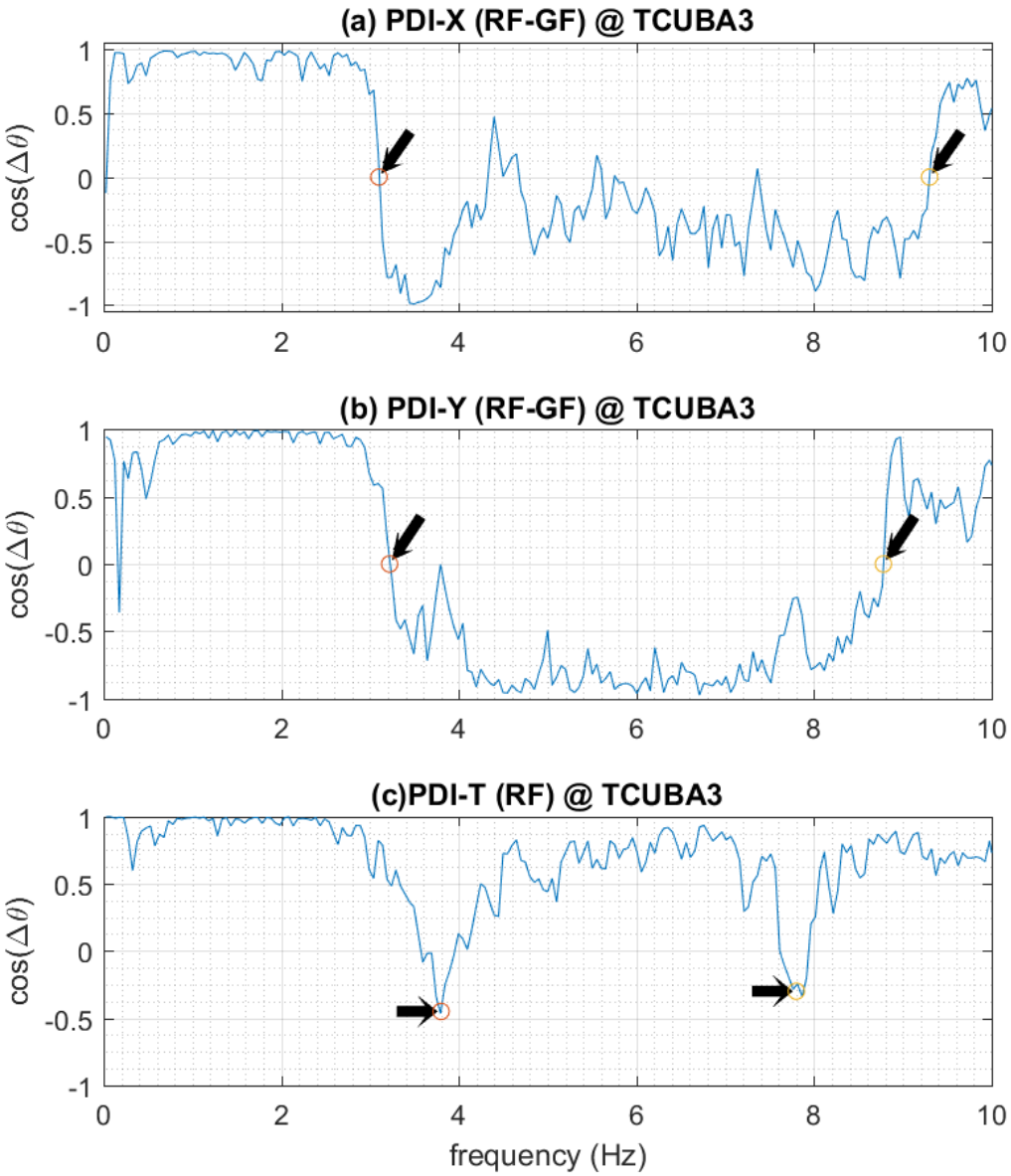

Fig. D.9. Triple PDI plots of TCUBA3 (X,Y and Torsion).The black arrow marks point at the identified modes.

TAPBA5-Elevation (X direction)

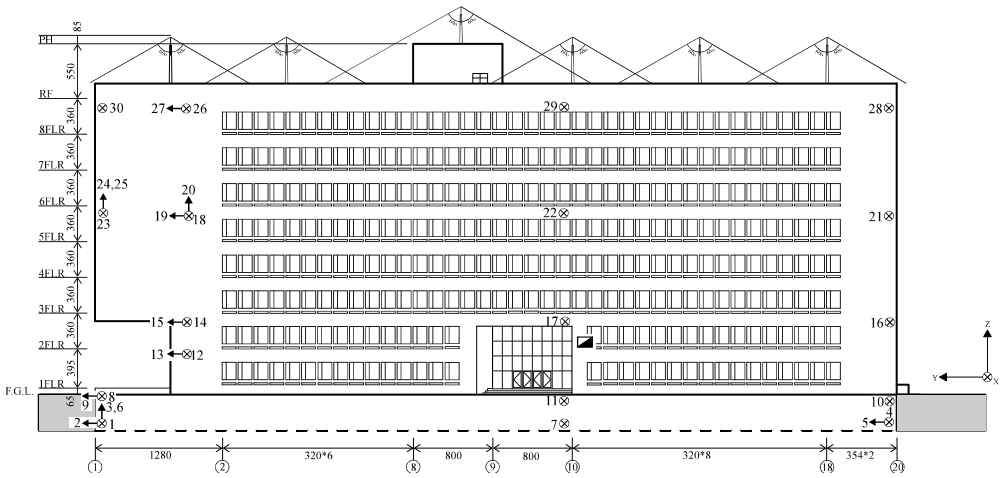

TAPBA5-Elevation (Y direction)

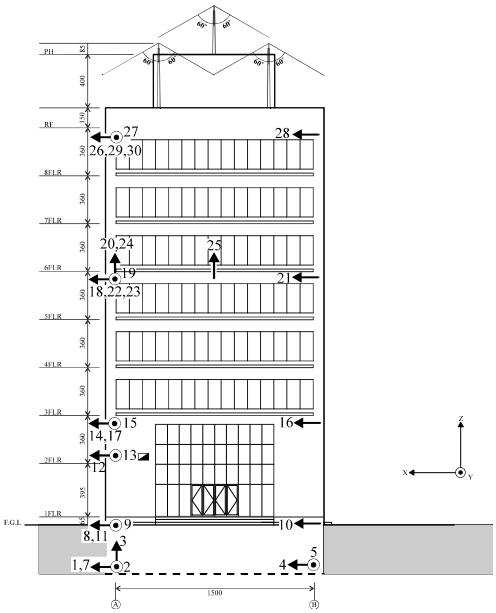

Fig. D.10. Elevation of TAPBA5

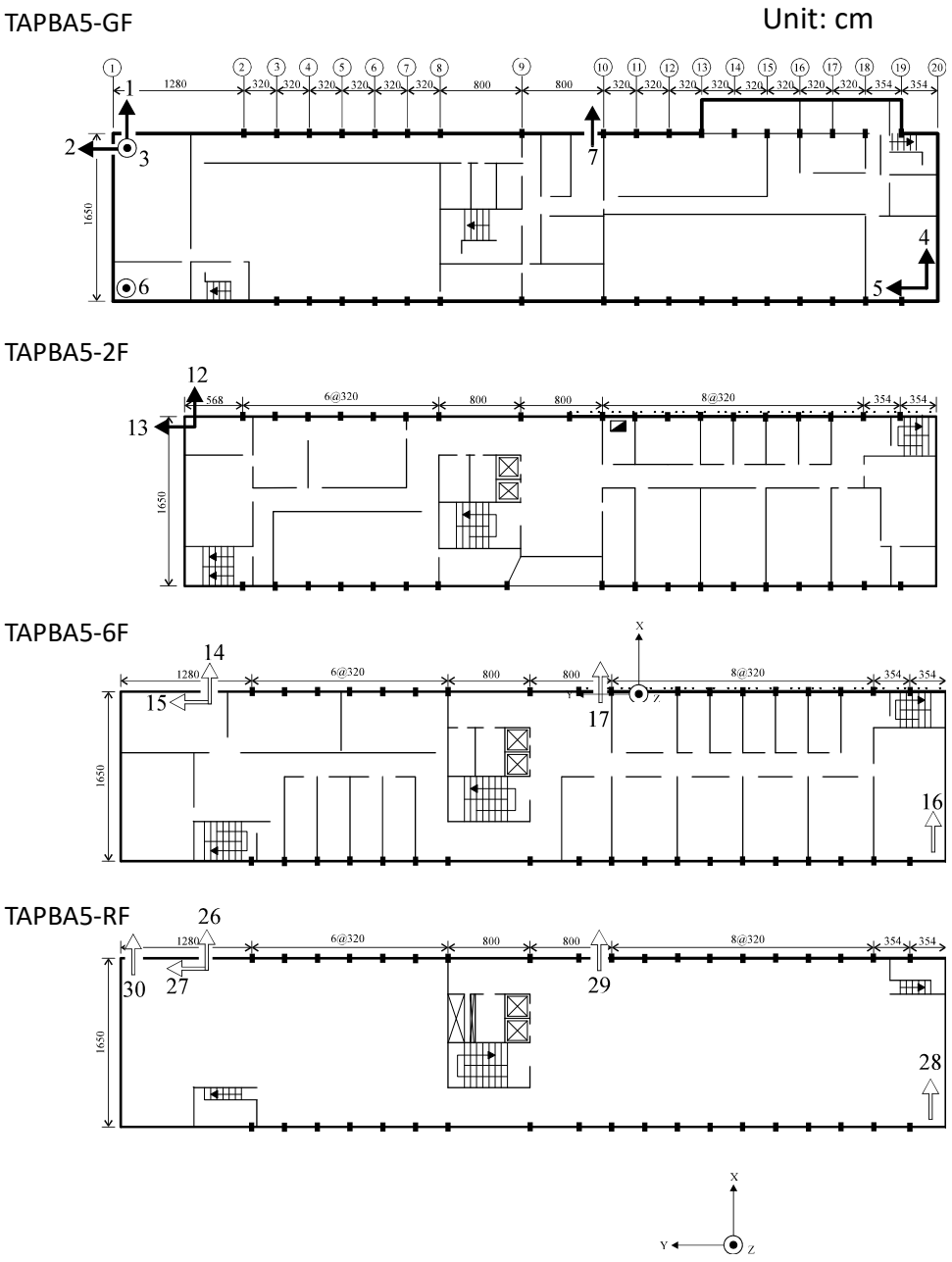

Fig. D.11. Building Plan of TAPBA5

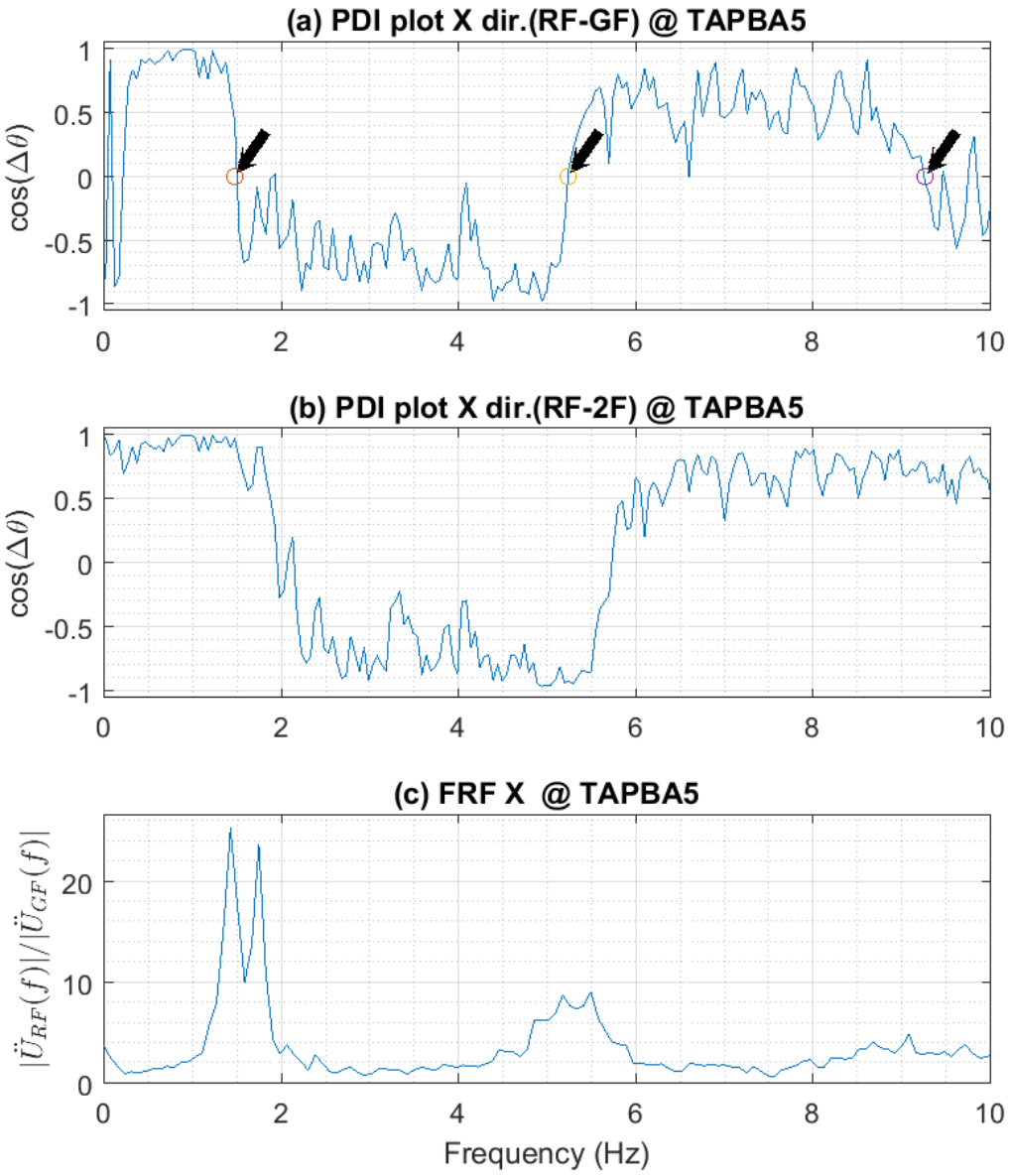

Fig. D.12. PDI plot of TAPBA5 in X direction. The black arrow marks point at the identified modes.

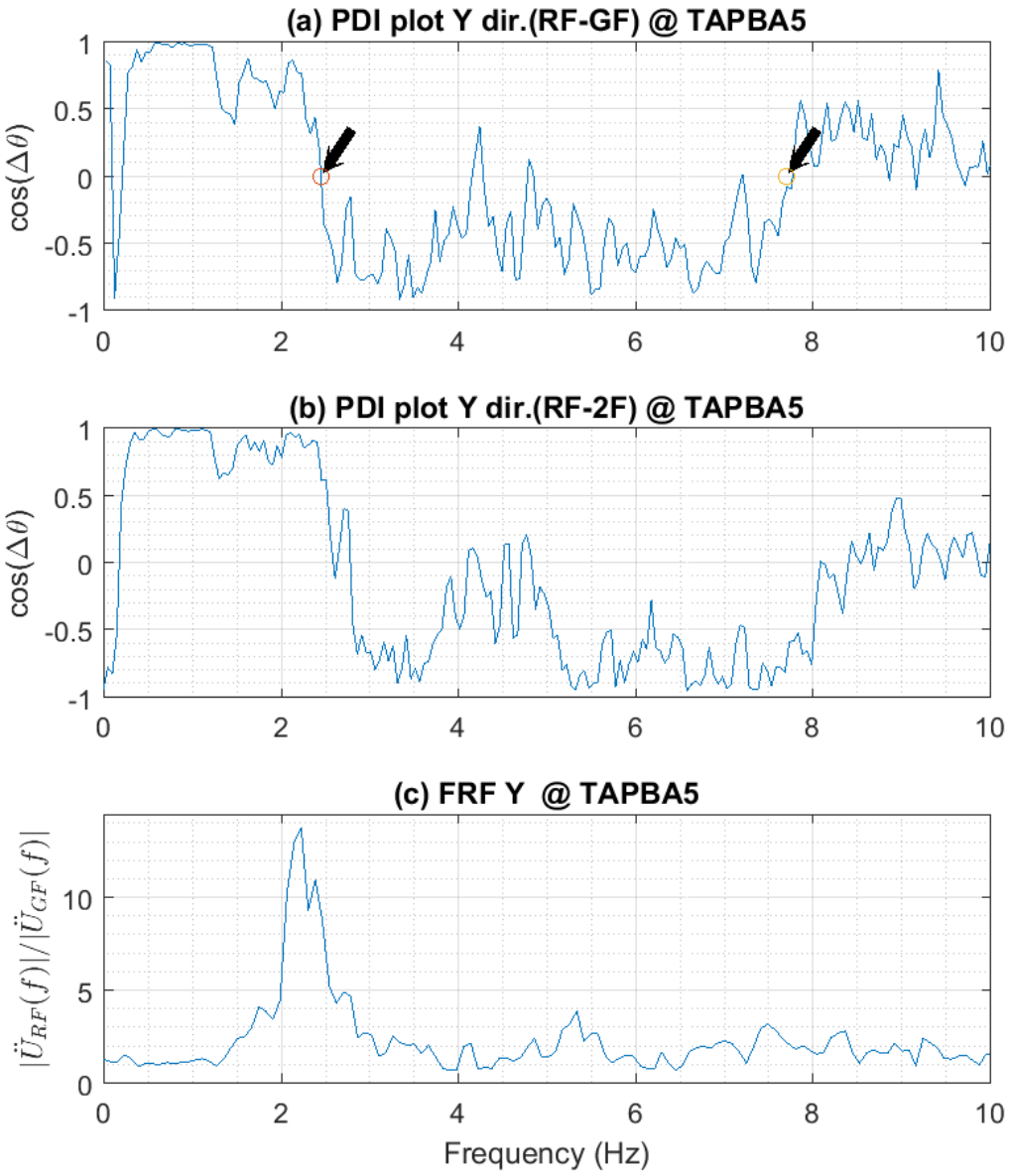

Fig. D.13. PDI plot of TAPBA5 in Y direction. The black arrow marks point at the identified modes.

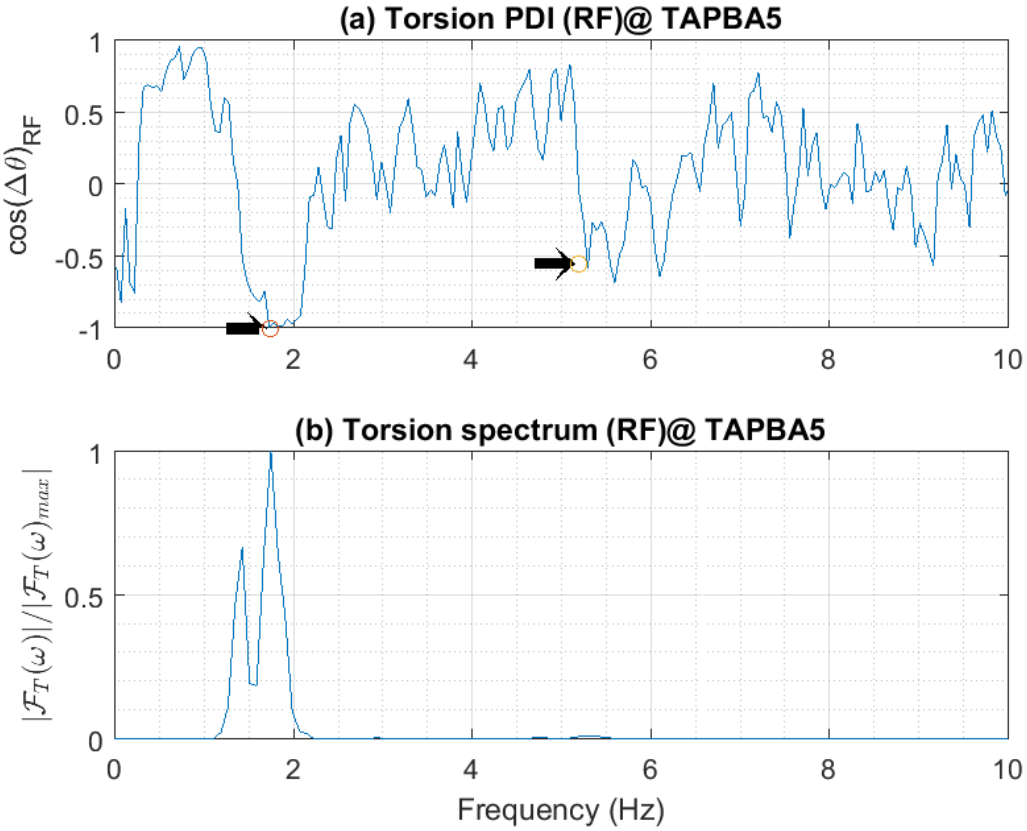

Fig. D.14. Torsional PDI plot of TAPBA5 (RF)(Ch. 28 & 30). The black arrow marks point at the identified modes.

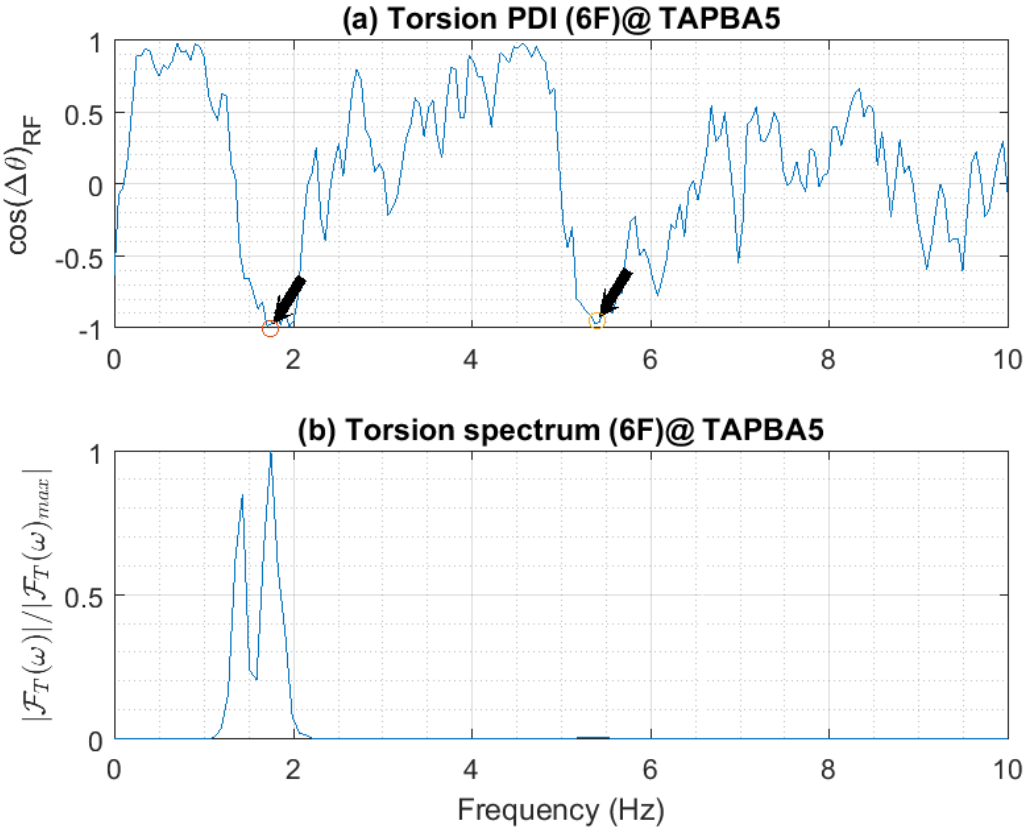

Fig. D.15. Torsional PDI plot of TAPBA5 (6F)(Ch. 21 & 23). The black arrow marks point at the identified modes.

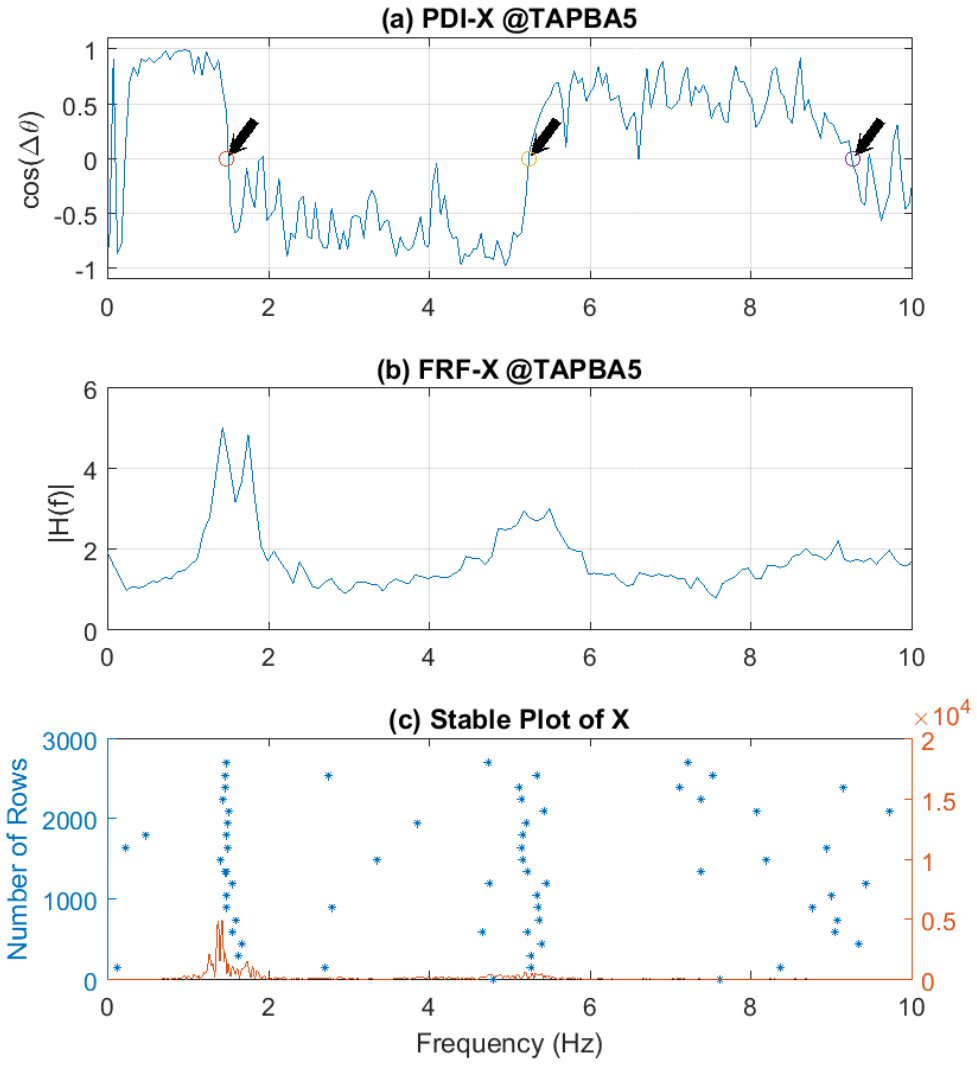

Fig. D.16. Comparison of three methods @ TAPBA5 in X direction.(a) PDI plot method, (b) peak-picking method, (c) subspace method. The black arrow marks point at the identified modes.

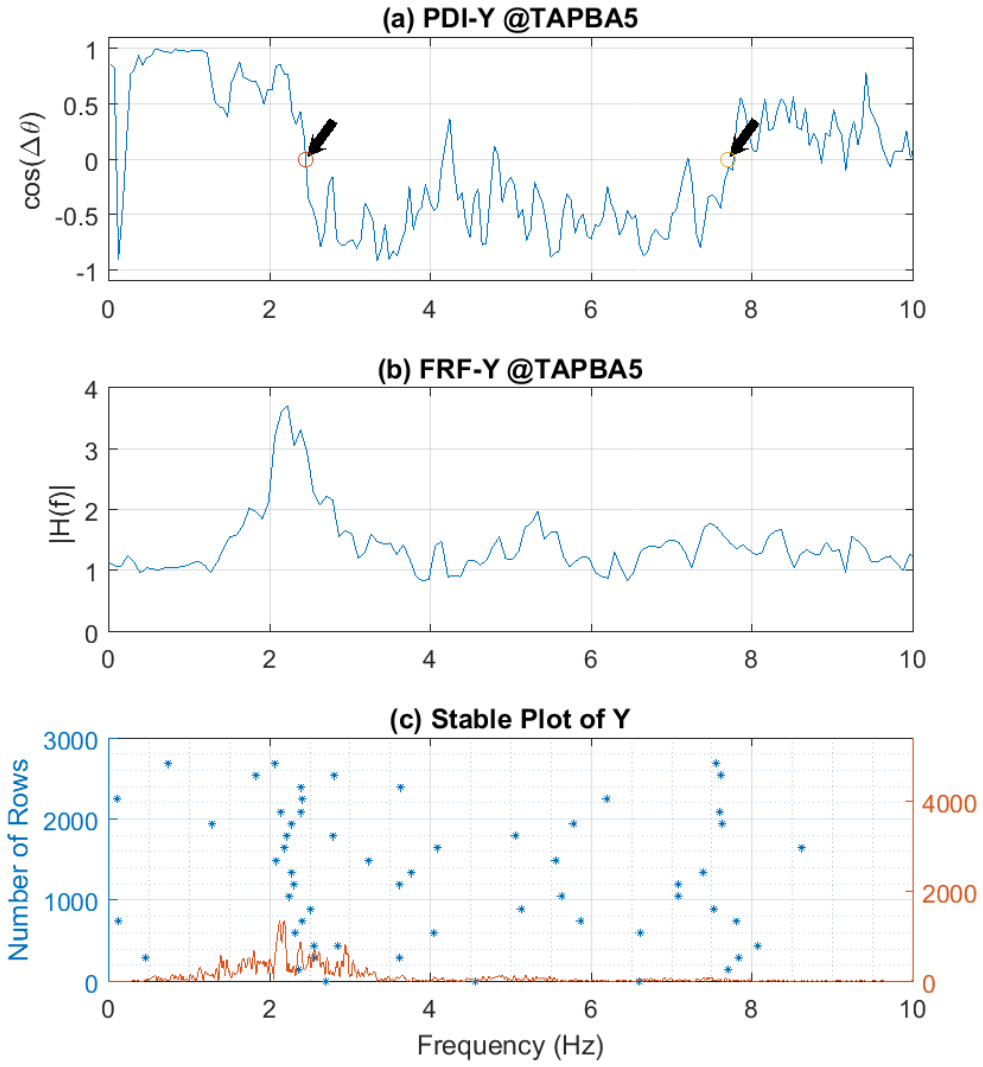

Fig. D.17. Comparison of three methods @ TAPBA5 in Y direction.(a) PDI plot method, (b) peak-picking method, (c) subspace method. The black arrow marks point at the identified modes.

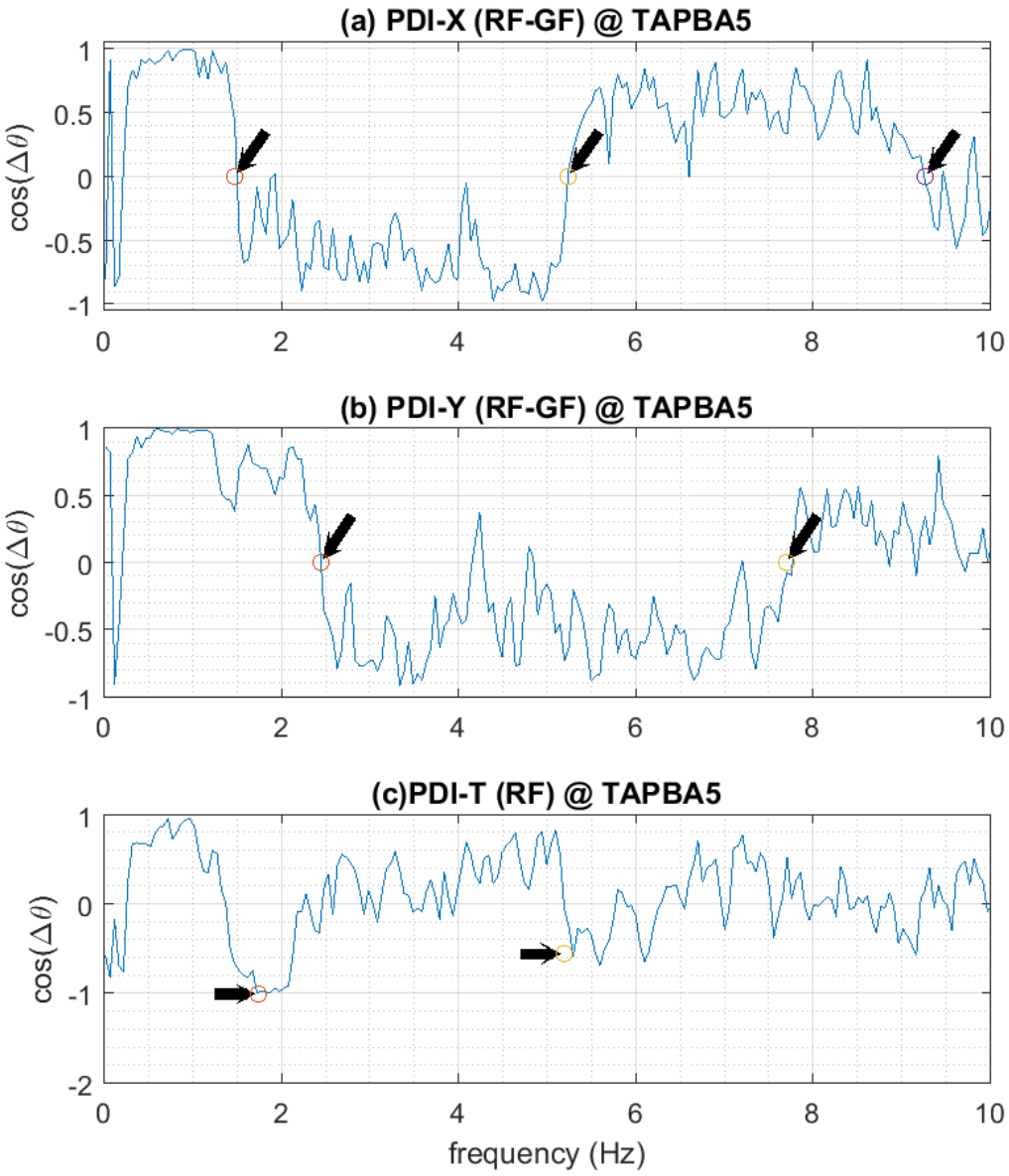

Fig. D.18. Triple PDI plots of TAPBA5 (X,Y and Torsion). The black arrow marks point at the identified modes.

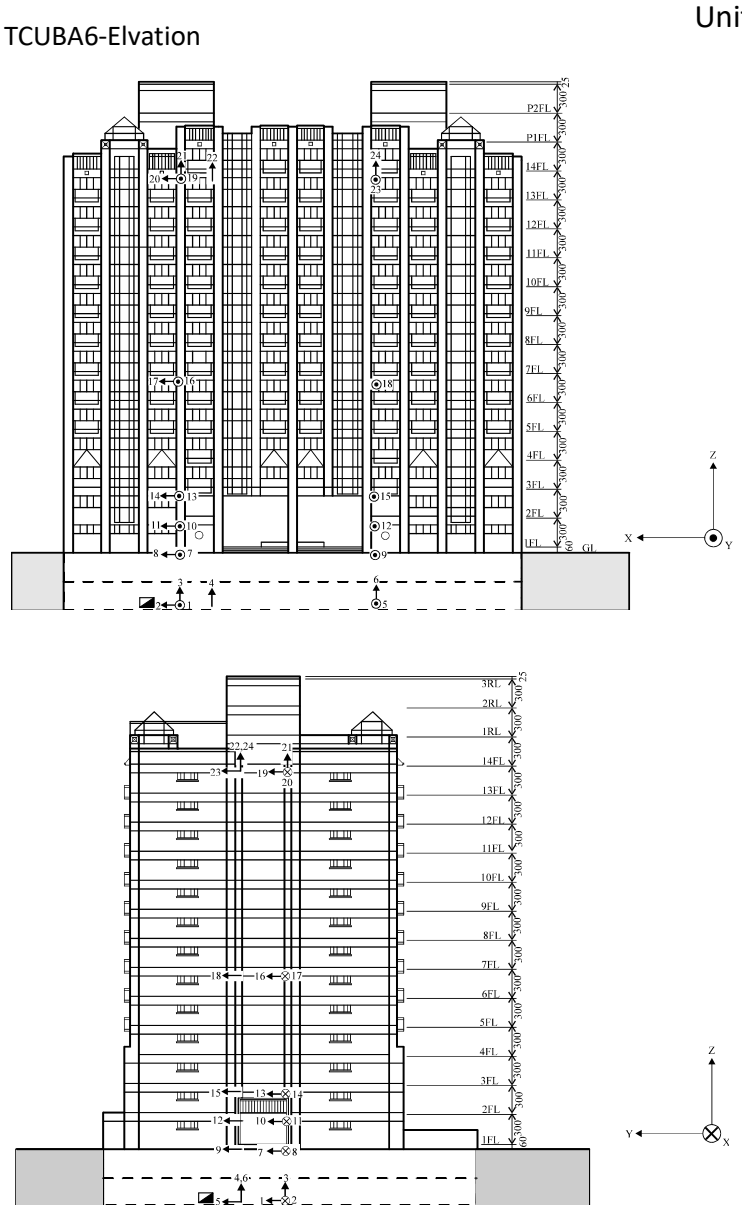

Fig. D.19. Elevation of TCUBA6

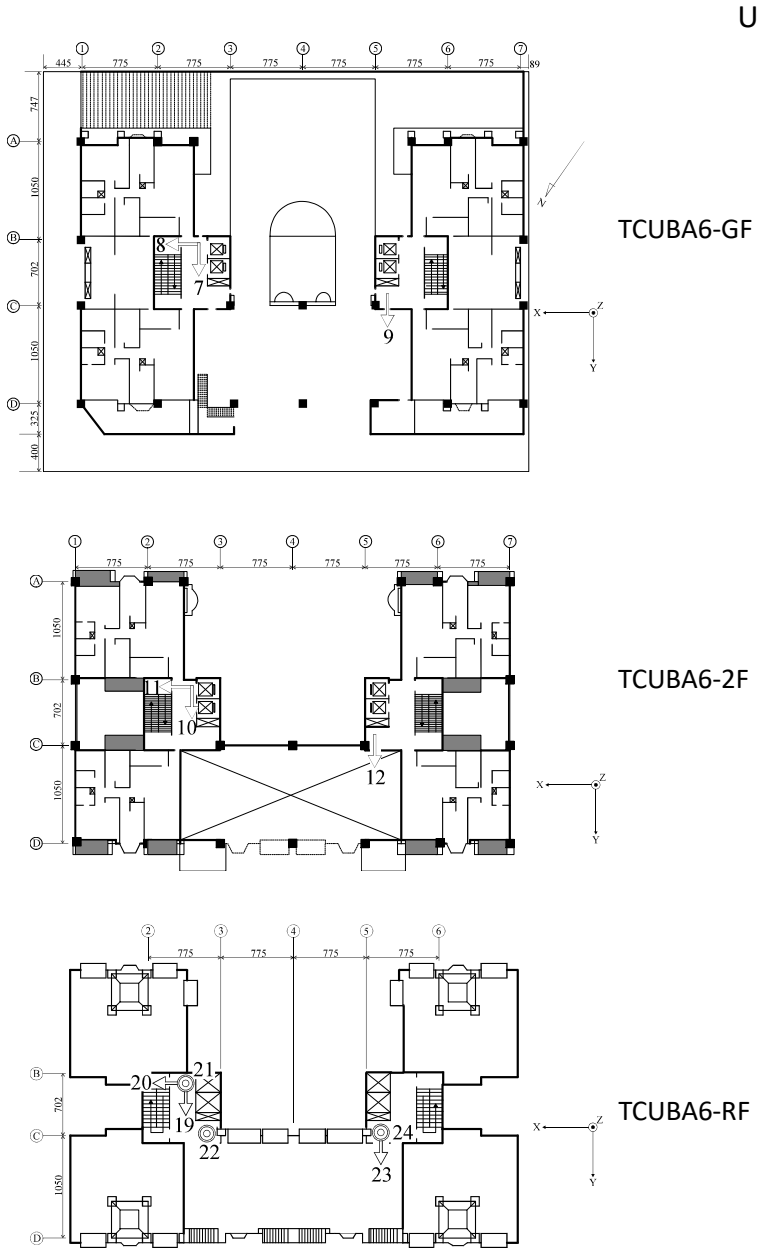

Fig. D.20. Building Plan of TCUBA6

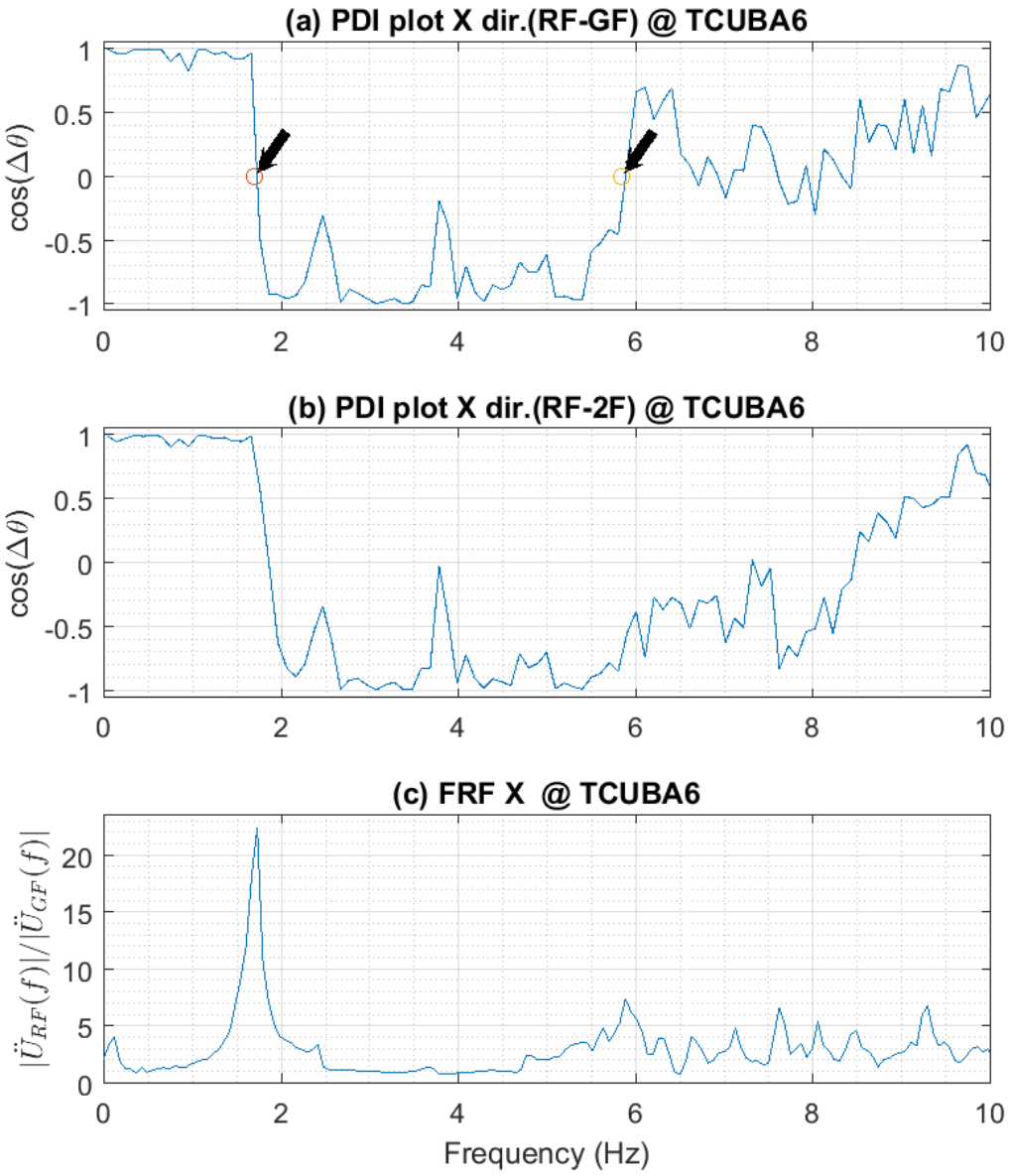

Fig. D.21. PDI plot of TCUBA6 in X direction. The black arrow marks point at the identified modes.

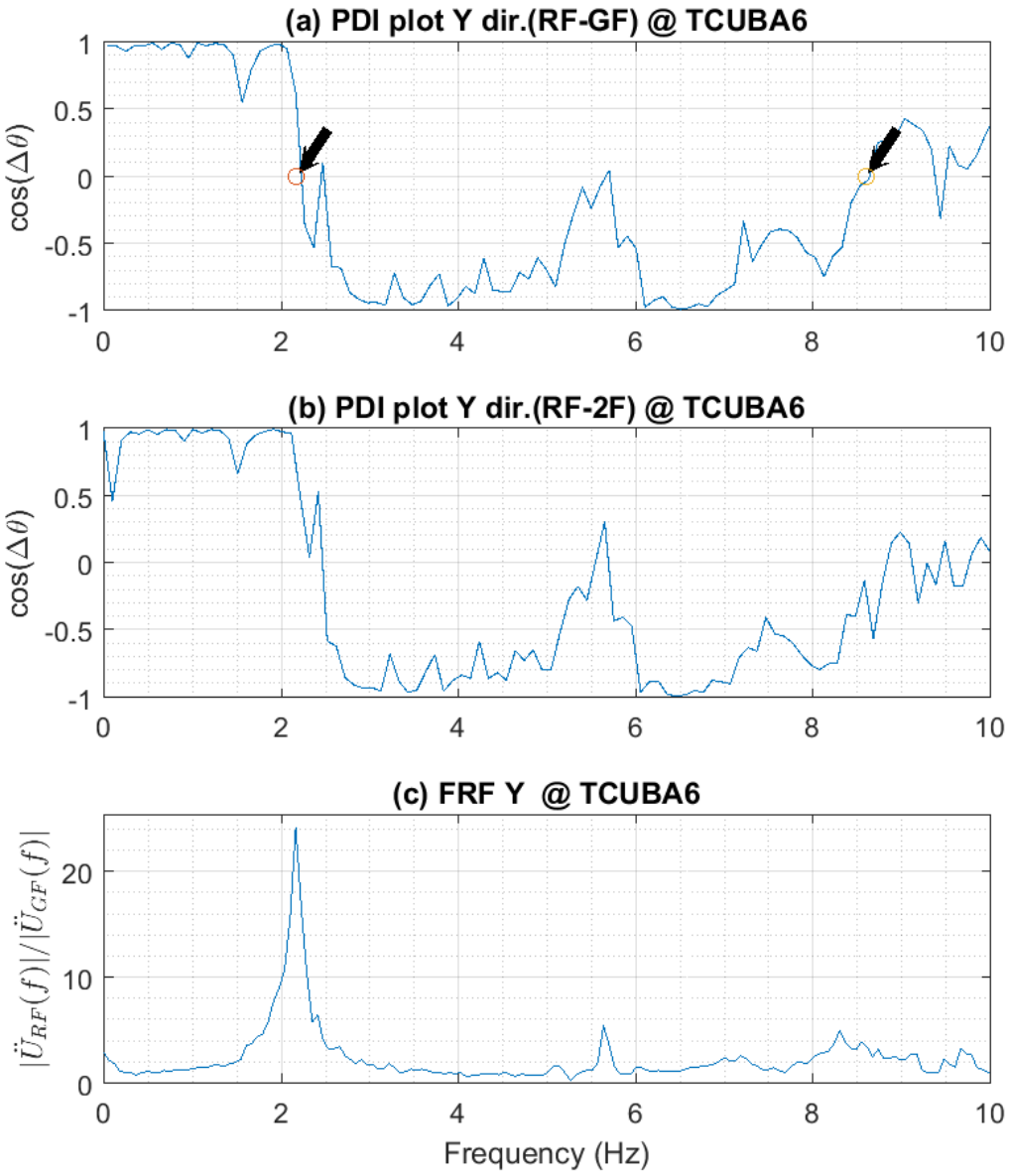

Fig. D.22. PDI plot of TCUBA6 in Y direction. The black arrow marks point at the identified modes.

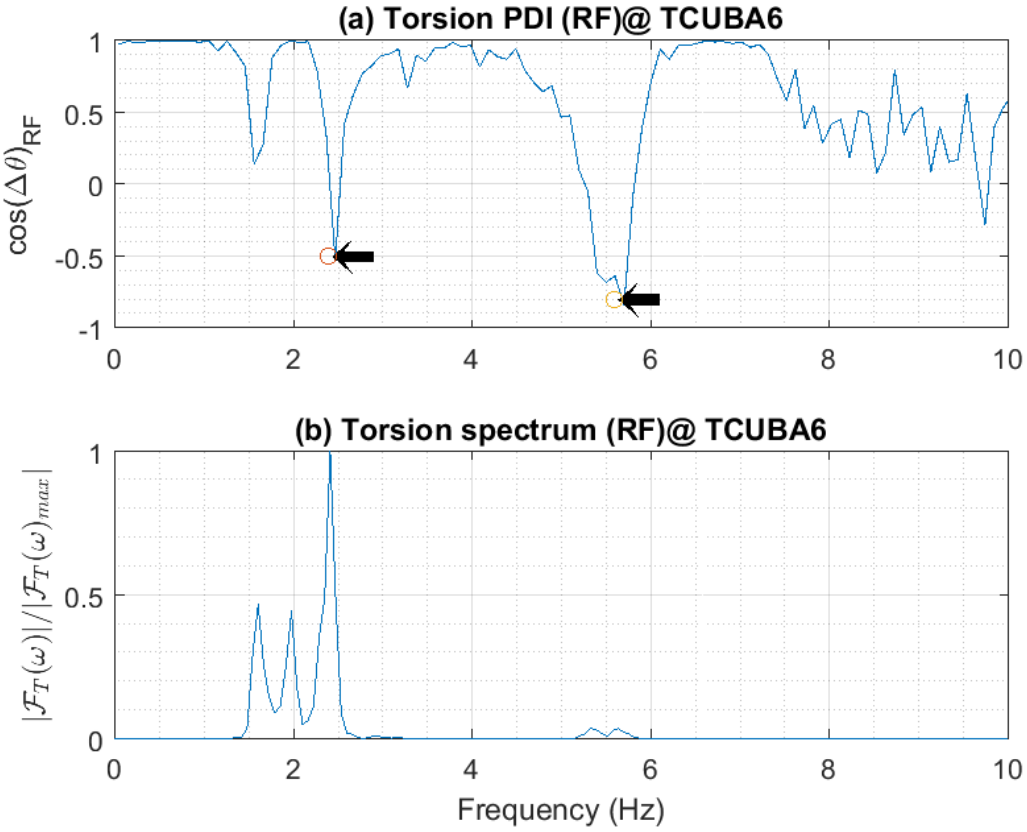

Fig. D.23. Torsional PDI plot of TCUBA6 (RF)(Ch. 19 & 23). The black arrow marks point at the identified modes.

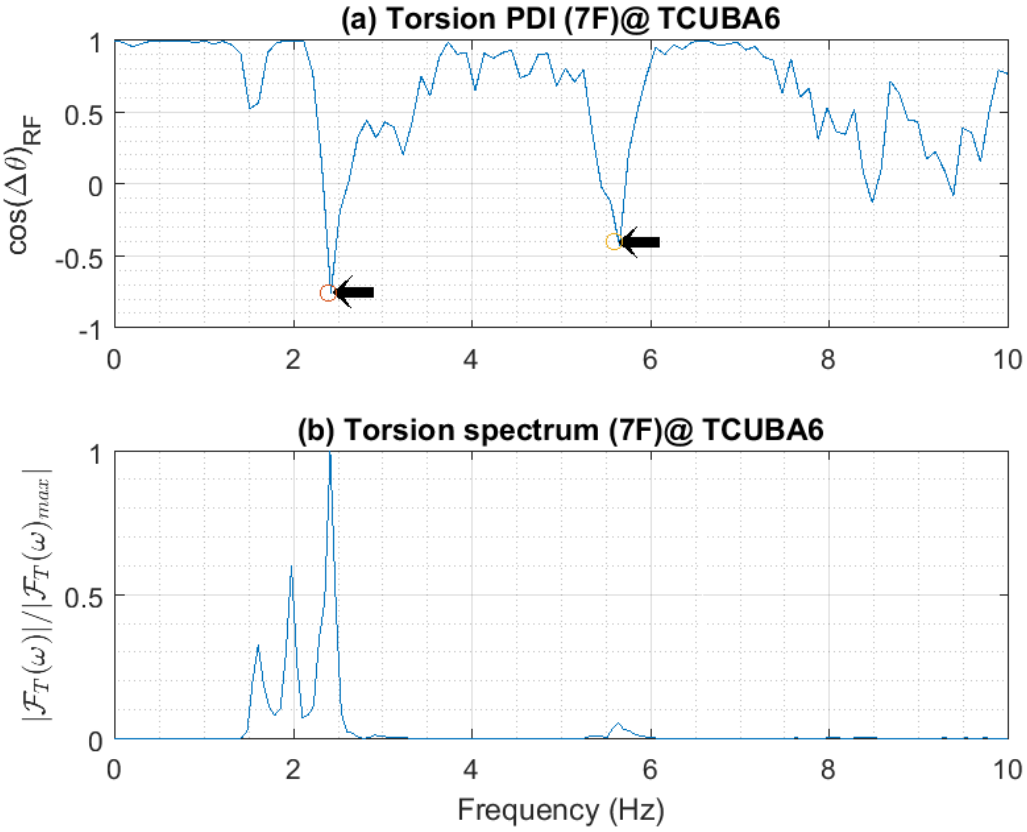

Fig. D.24. Torsional PDI plot of TCUBA6 (7F)(Ch. 16 & 18). The black arrow marks point at the identified modes.

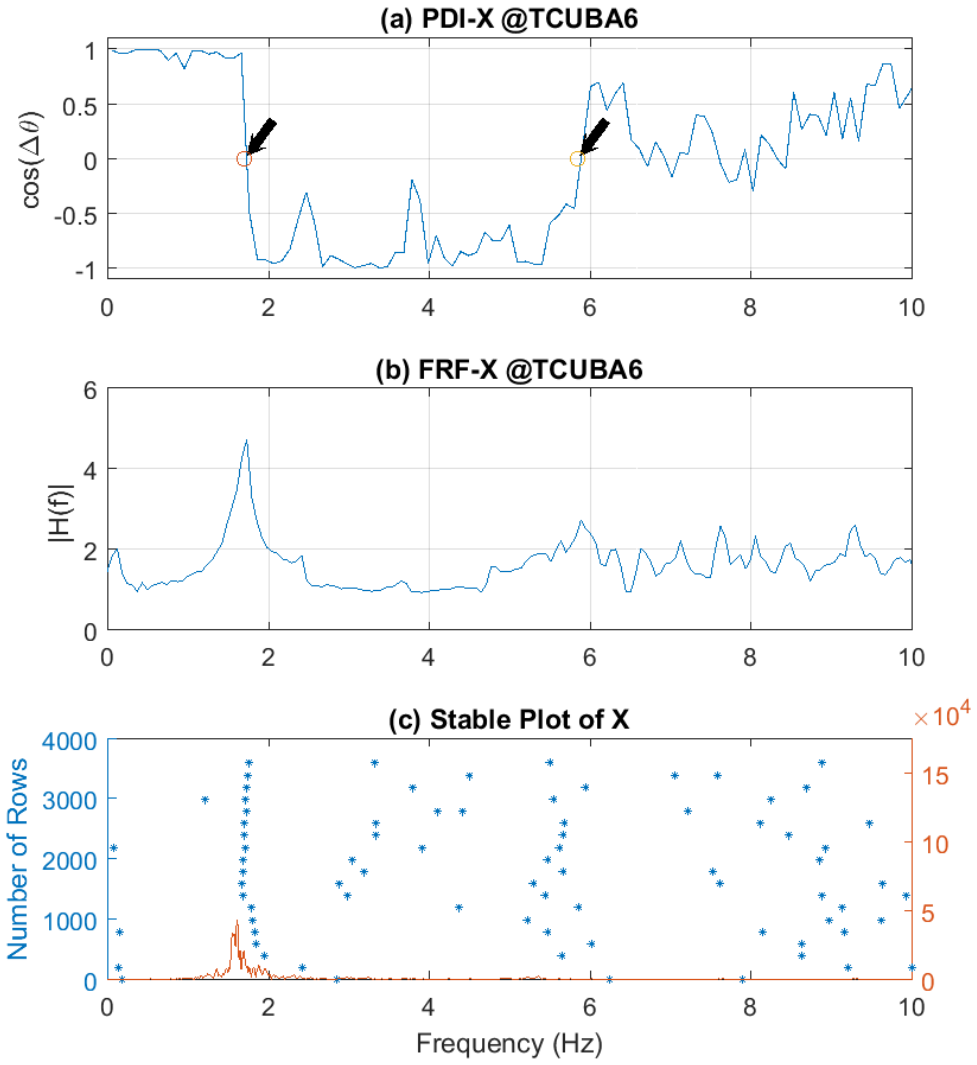

Fig. D.25. Comparison of three methods @ TCUBA6 in X direction.(a) PDI plot method, (b) peak-picking method, (c) subspace method. The black arrow marks point at the identified modes.

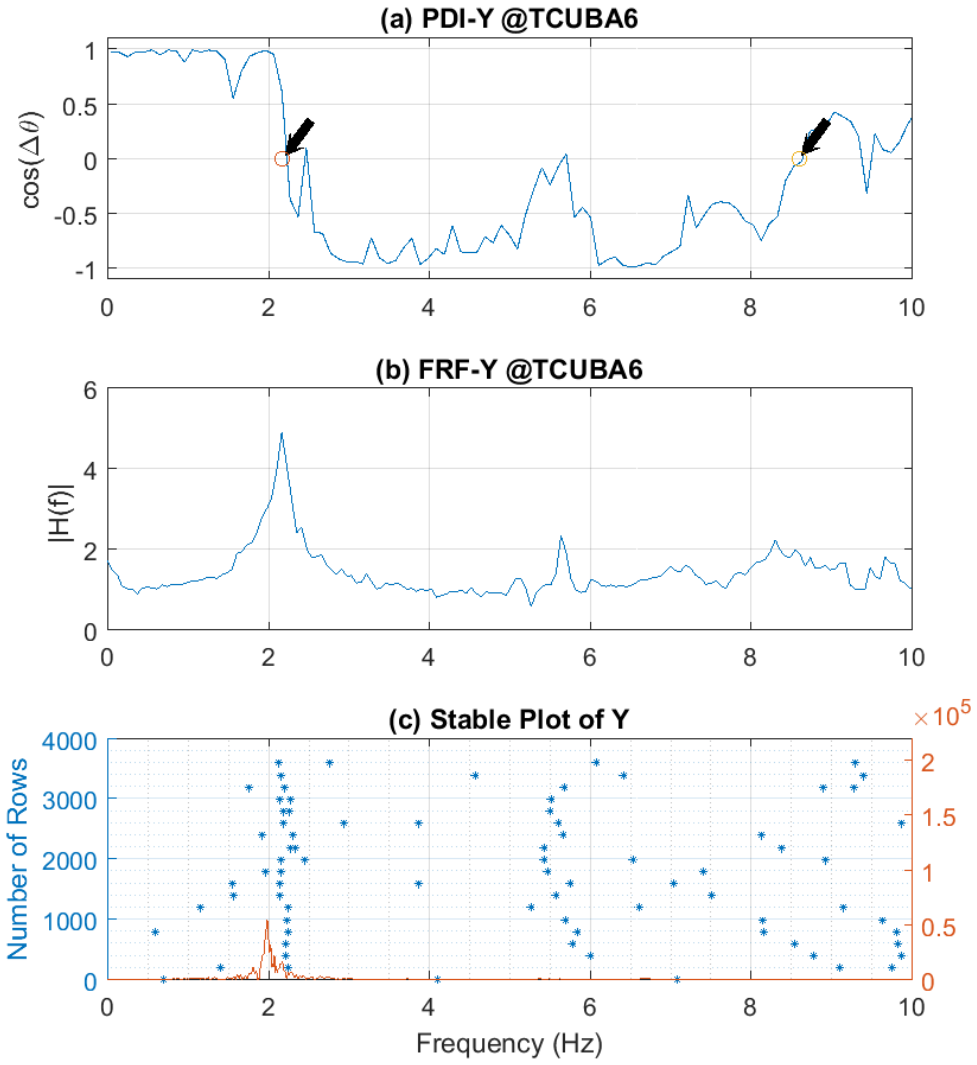

Fig. D.26. Comparison of three methods @ TCUBA6 in Y direction.(a) PDI plot method, (b) peak-picking method, (c) subspace method. The black arrow marks point at the identified modes.

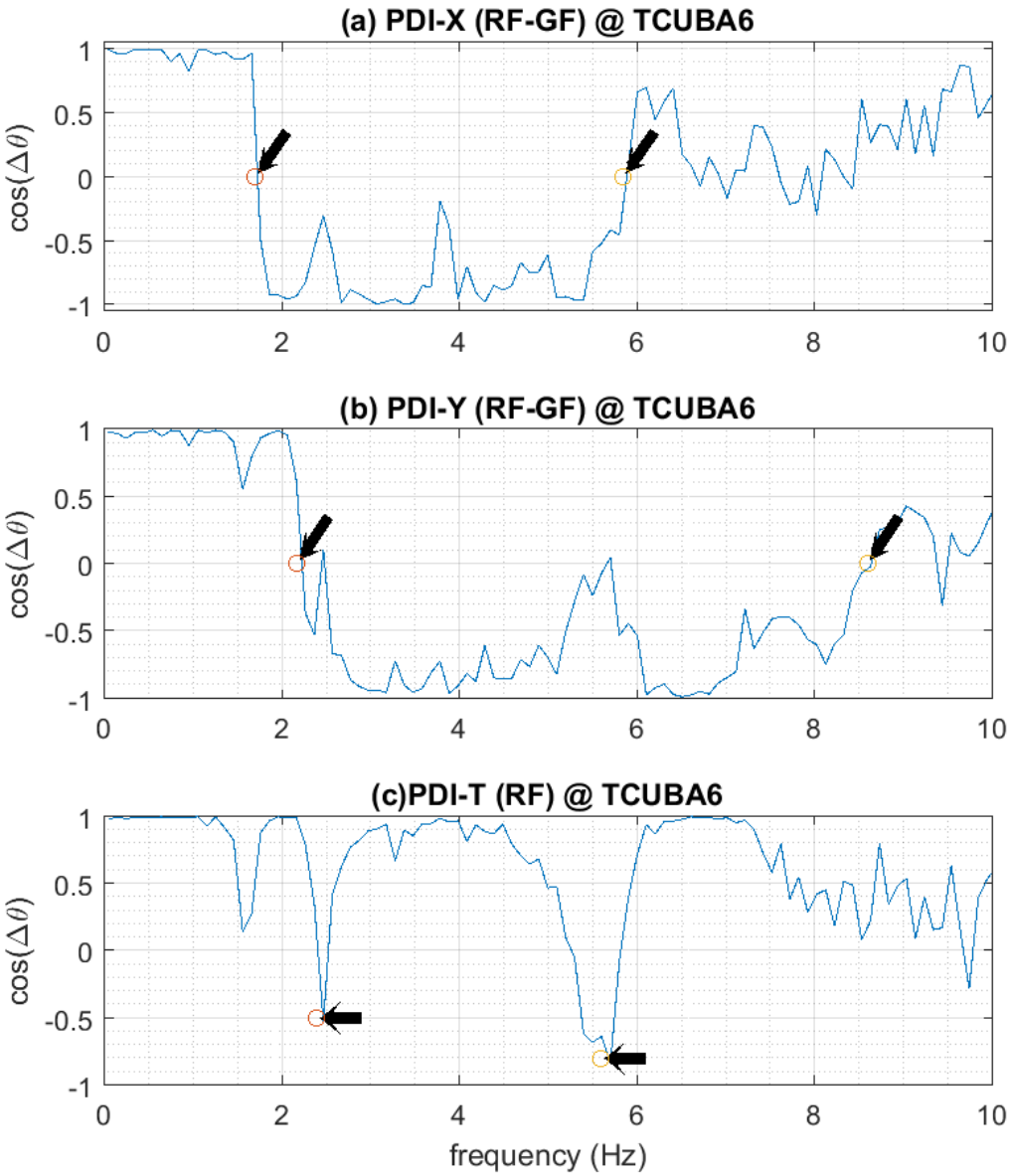

Fig. D.27. Triple PDI plots of TCUBA6 (X,Y and Torsion). The black arrow marks point at the identified modes.

TAPBA4-Elvation

Unit: cm

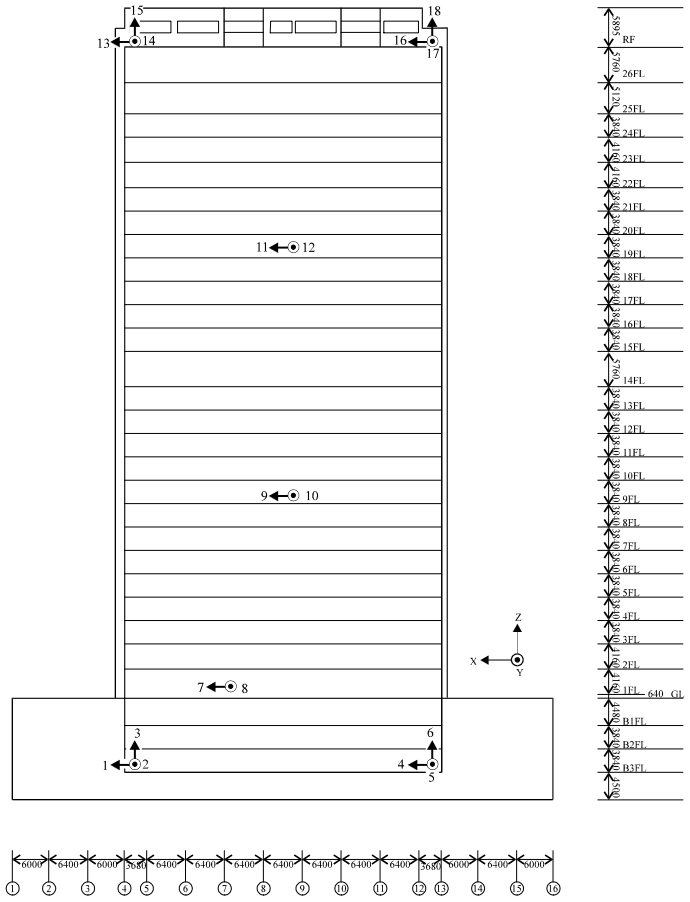

Fig. D.28. Elevation of TAPBA4

Unit: cm

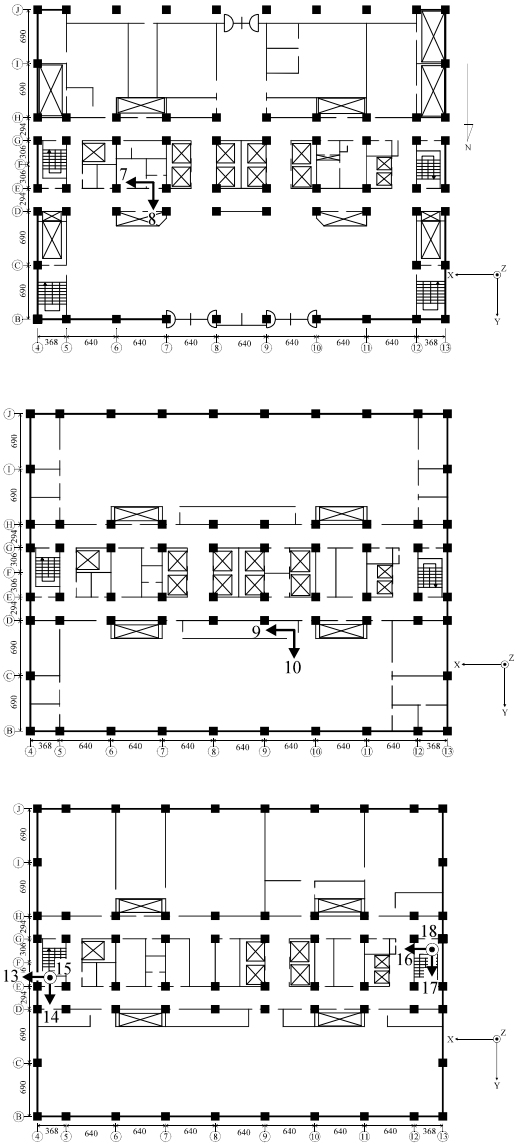

Fig. D.29. Building Plan of TAPBA4

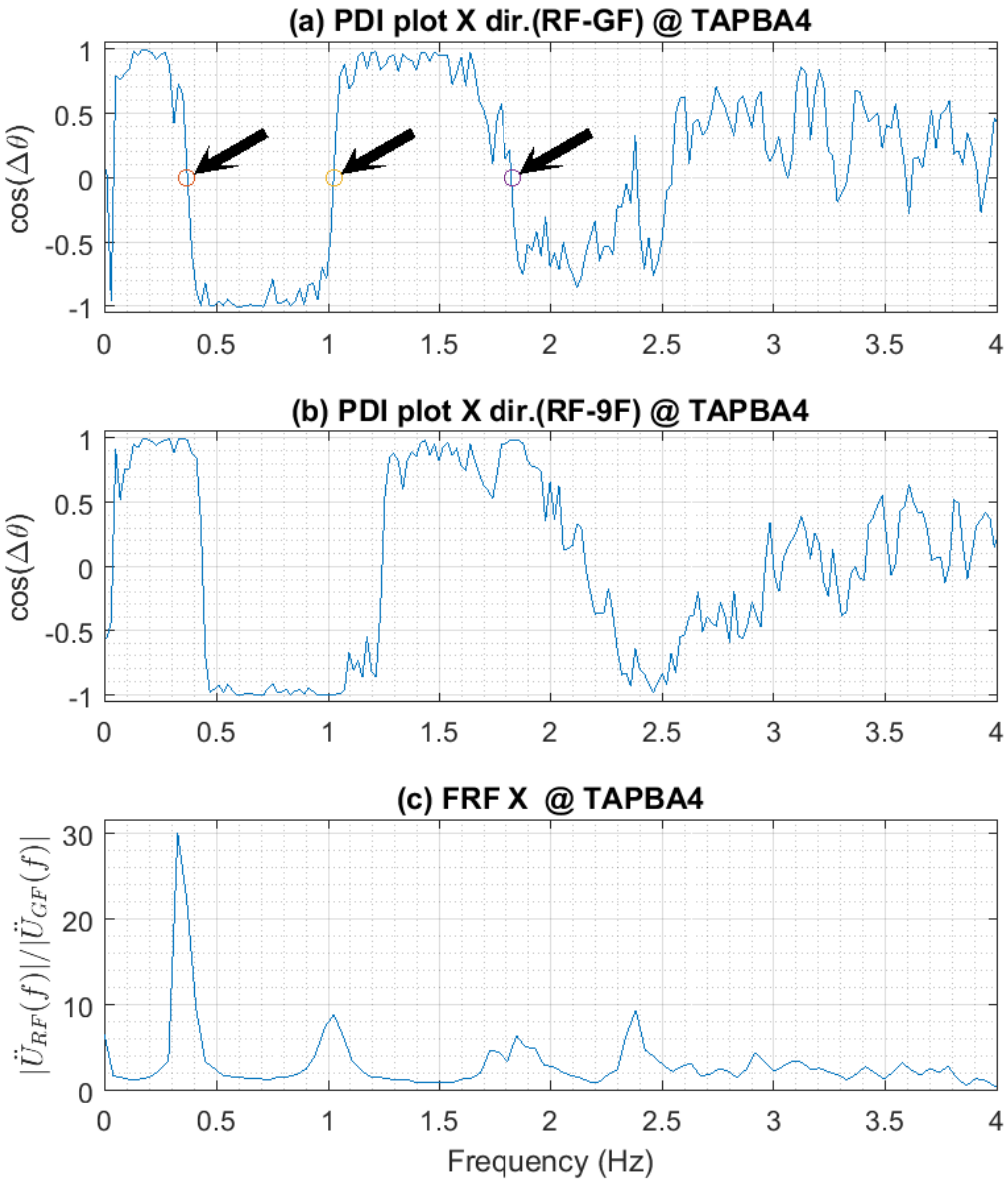

Fig. D.30. PDI plot of TAPBA4 in X direction. The black arrow marks point at the identified modes.

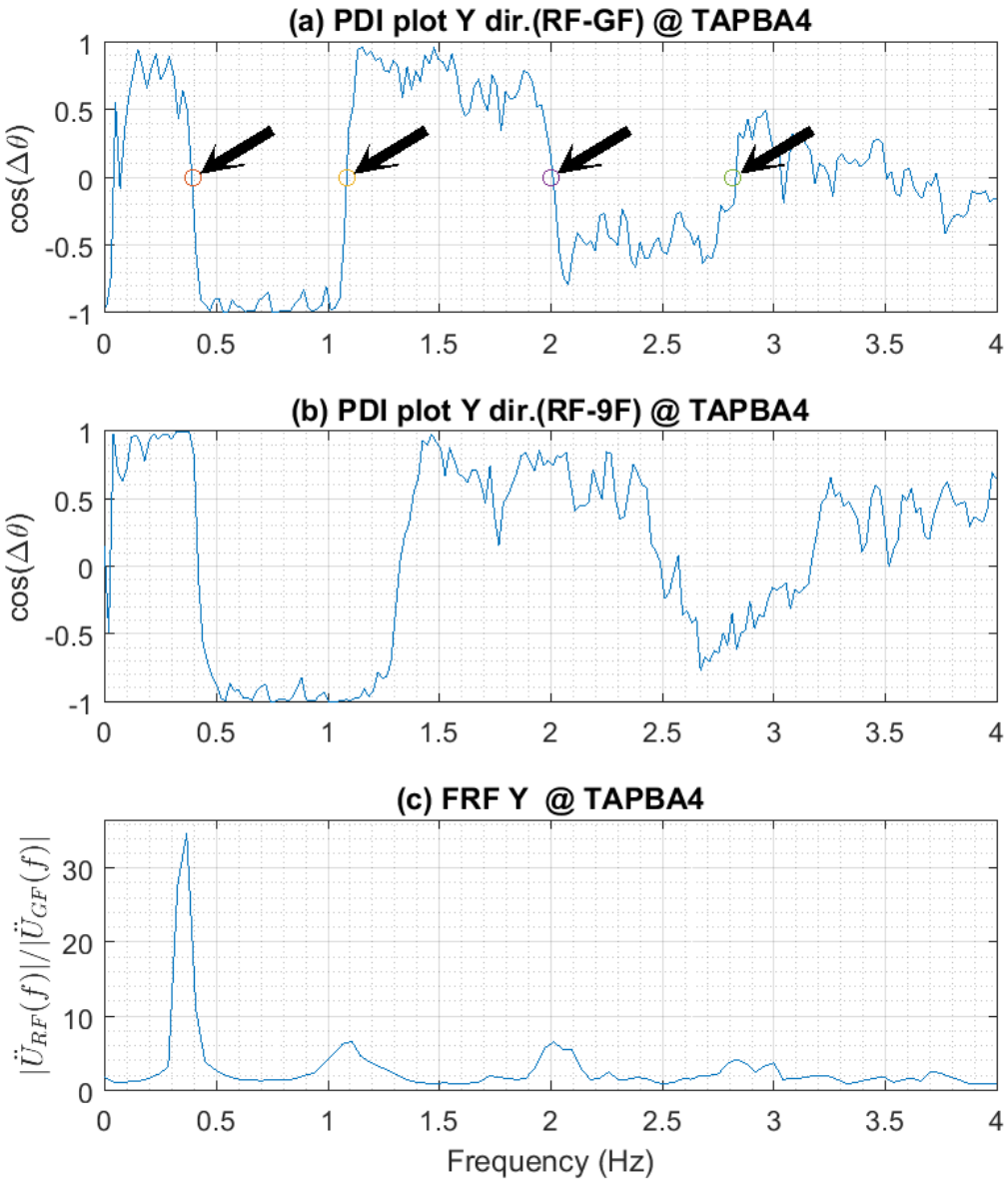

Fig. D.31. PDI plot of TAPBA4 in Y direction. The black arrow marks point at the identified modes.

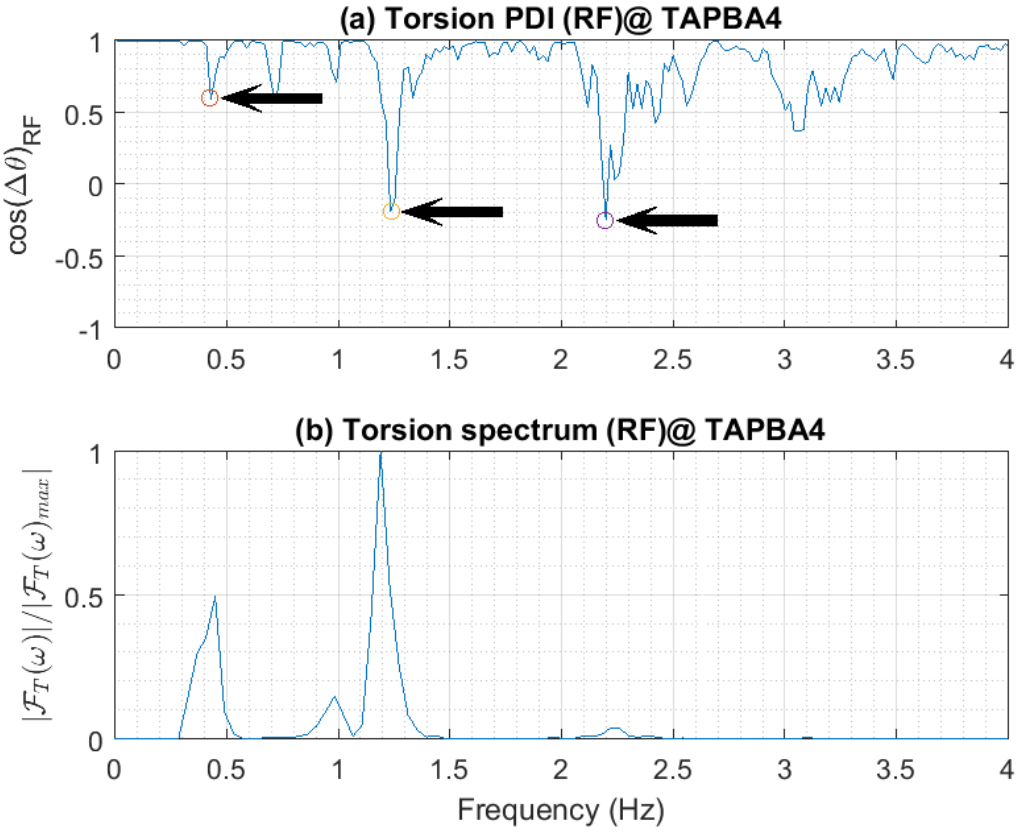

Fig. D.32. Torsional PDI plot of TAPBA4 (RF)(Ch. 14 & 17). The black arrow marks point at the identified modes.

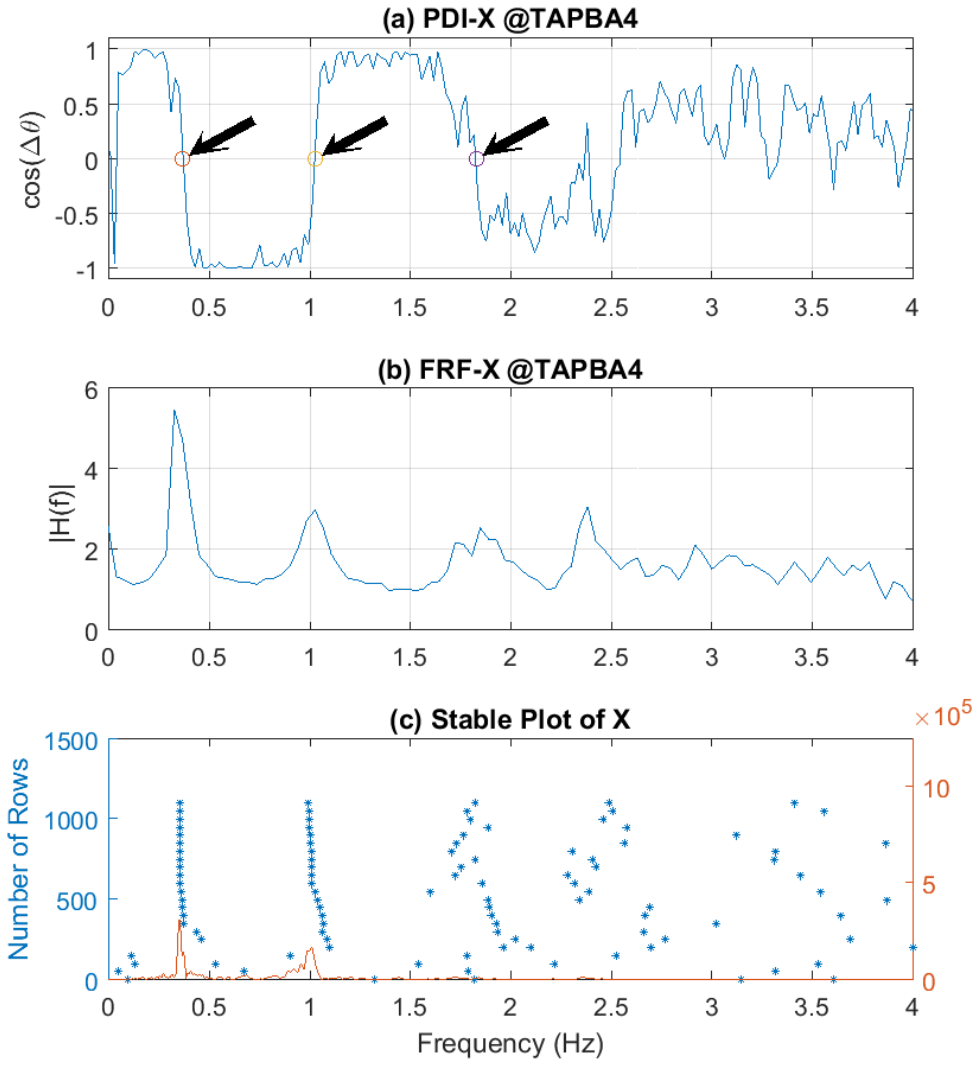

Fig. D.33. Comparison of three methods @ TAPBA4 in X direction.(a) PDI plot method, (b) peak-picking method, (c) subspace method. The black arrow marks point at the identified modes.

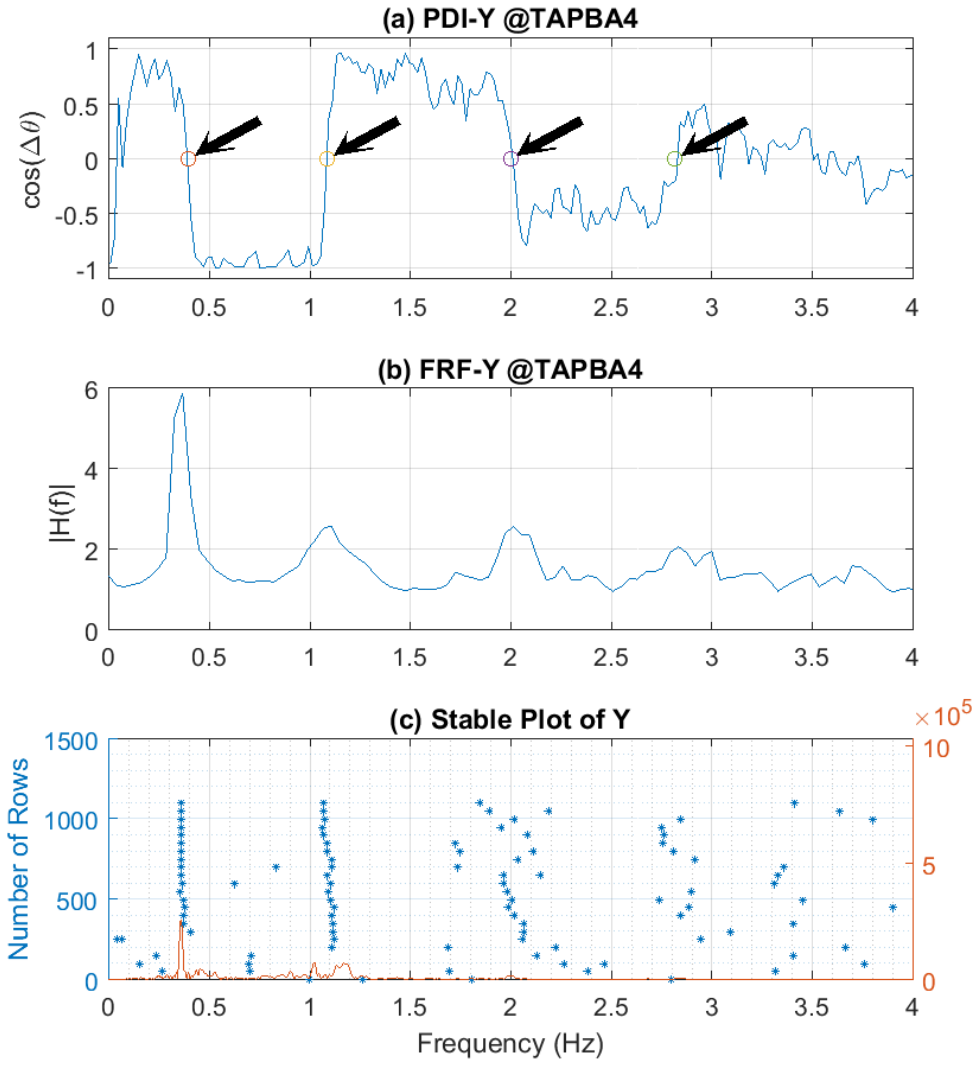

Fig. D.34. Comparison of three methods @ TAPBA4 in Y direction.(a) PDI plot method, (b) peak-picking method, (c) subspace method. The black arrow marks point at the identified modes.

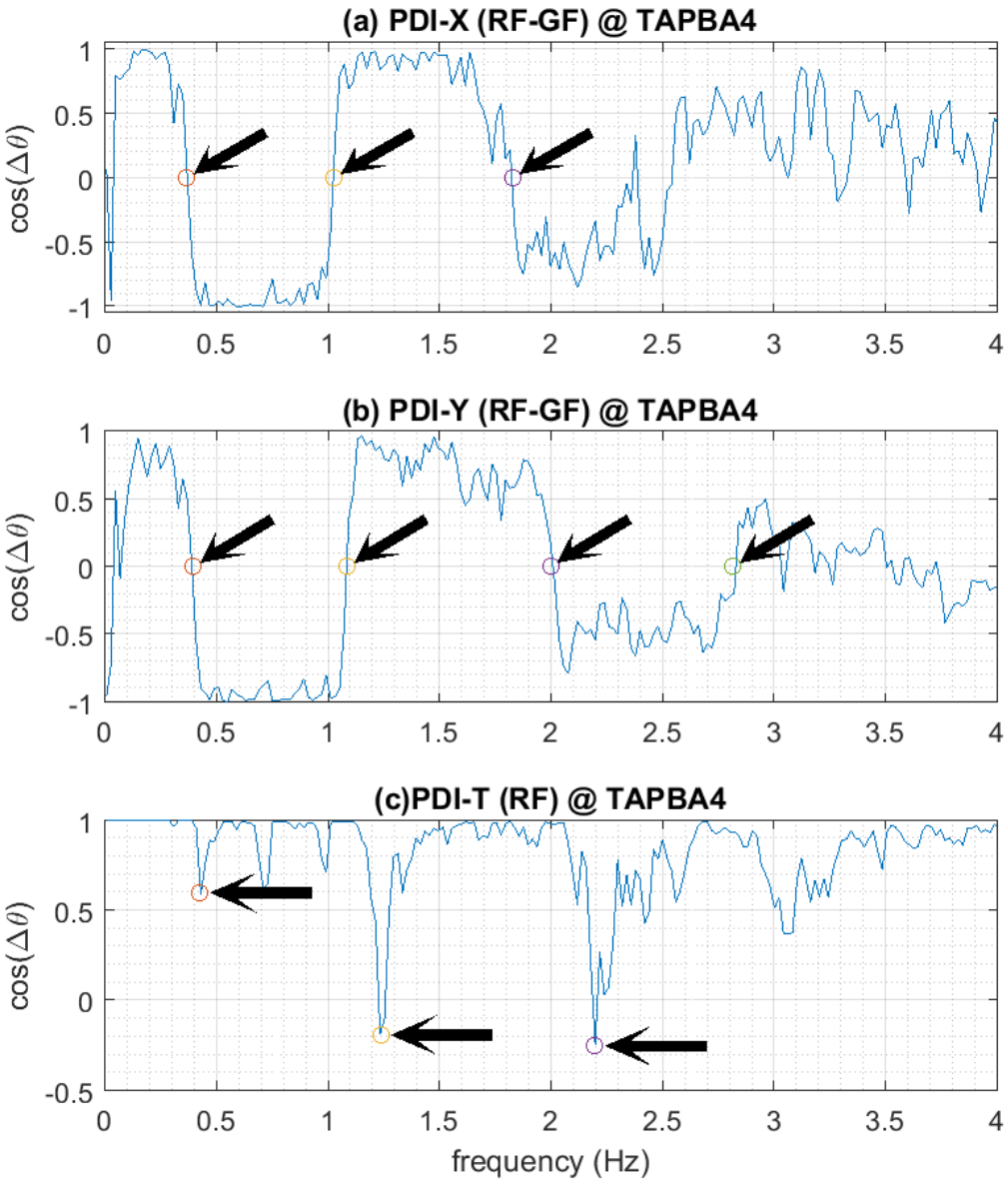

Fig. D.35. Triple PDI plots of TAPBA4 (X,Y and Torsion). The black arrow marks point at the identified modes.

Unit: cm

(a) TCUBAA-Elevation

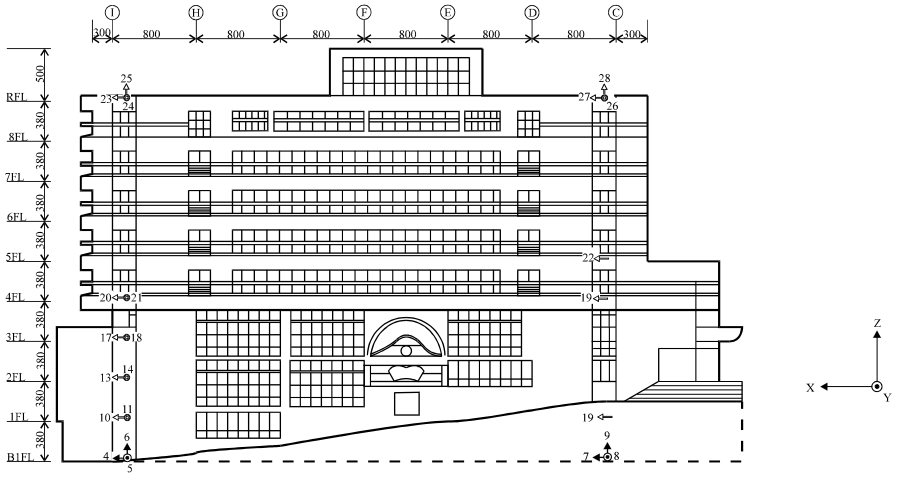

(b) TCUBAA-Plan

TCUBAA-RF

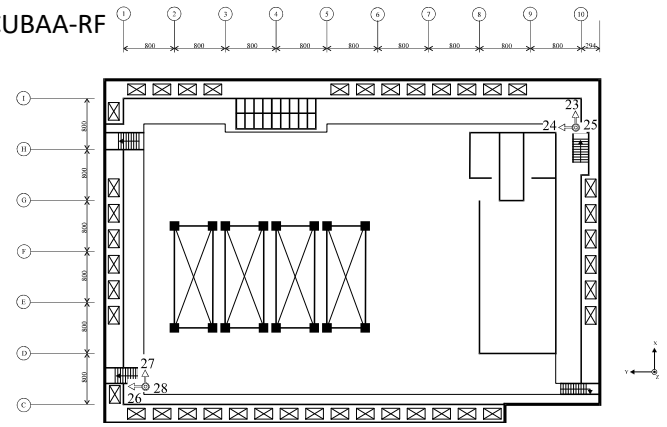

Fig. D.36. (a)Elevation of TCUBAA, (b) Roof Plan of TCUBAA

TCUBAA-Plan

Unit: cm

TCUBAA-B1

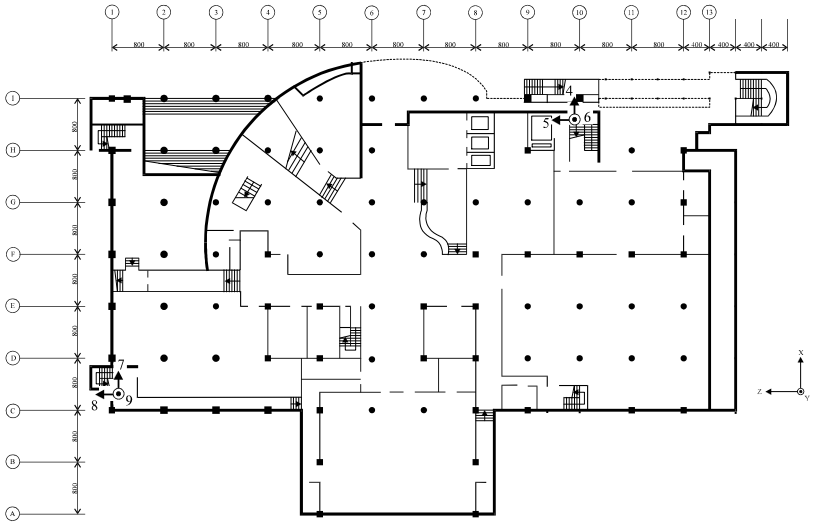

TCUBAA-2F

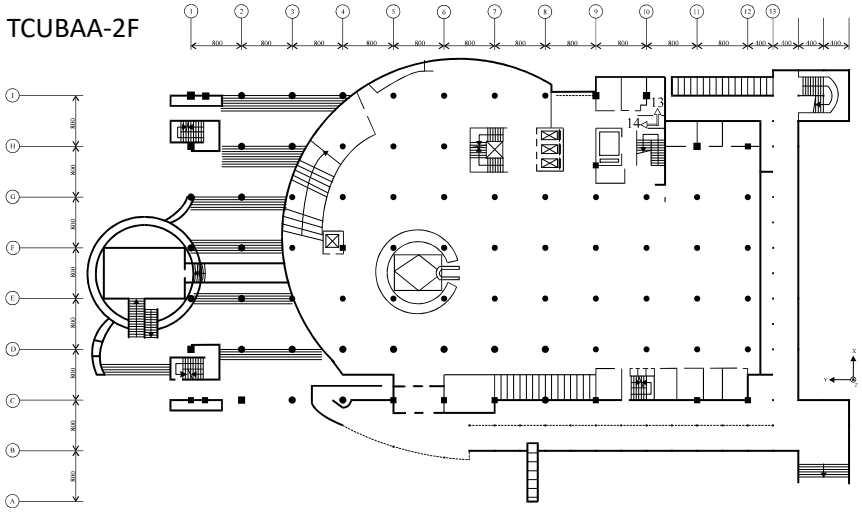

Fig. D.37. Building Plan of TCUBAA (2F and GF)

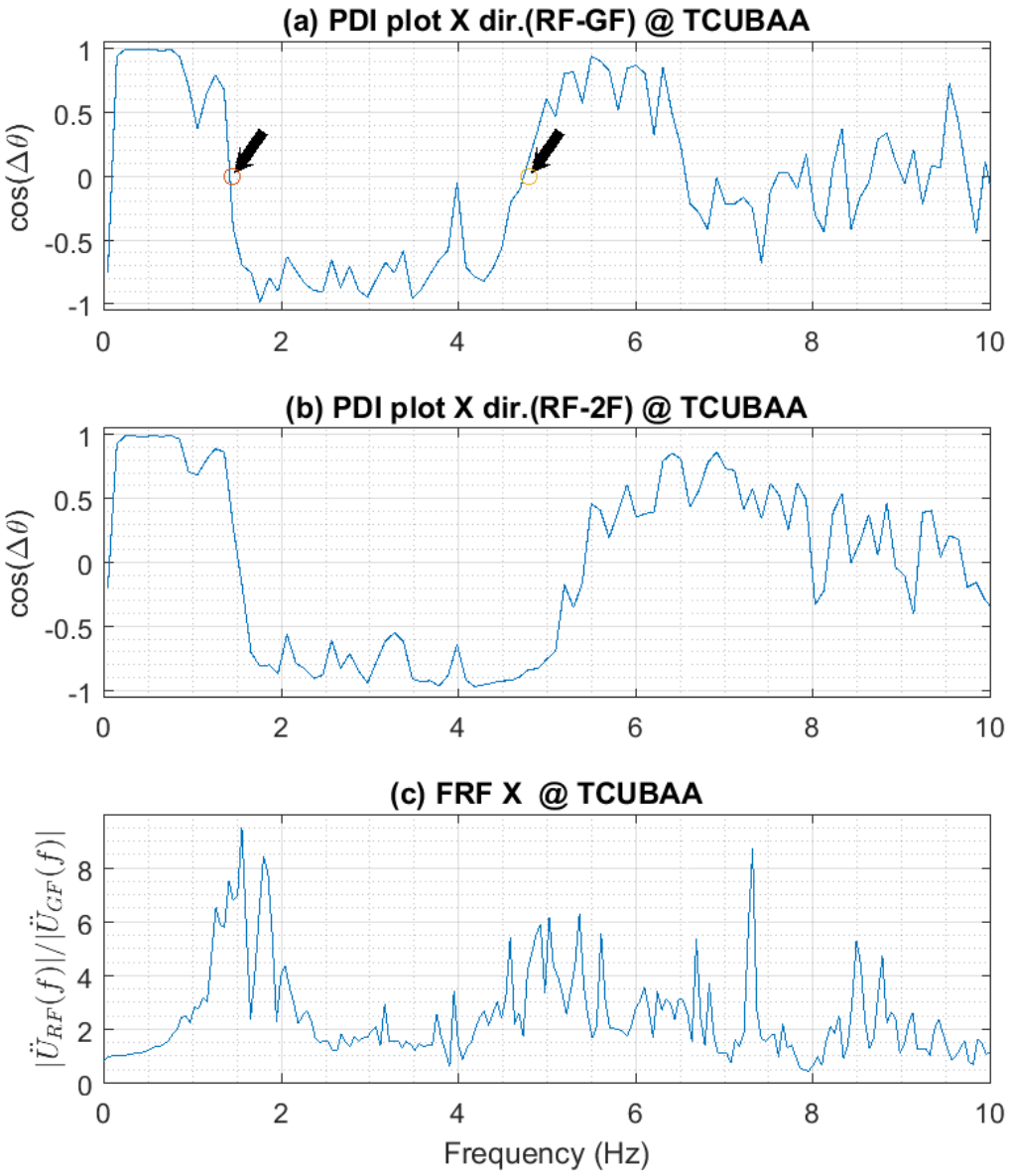

Fig. D.38. PDI plot of TCUBAA in X direction. The black arrow marks point at the identified modes.

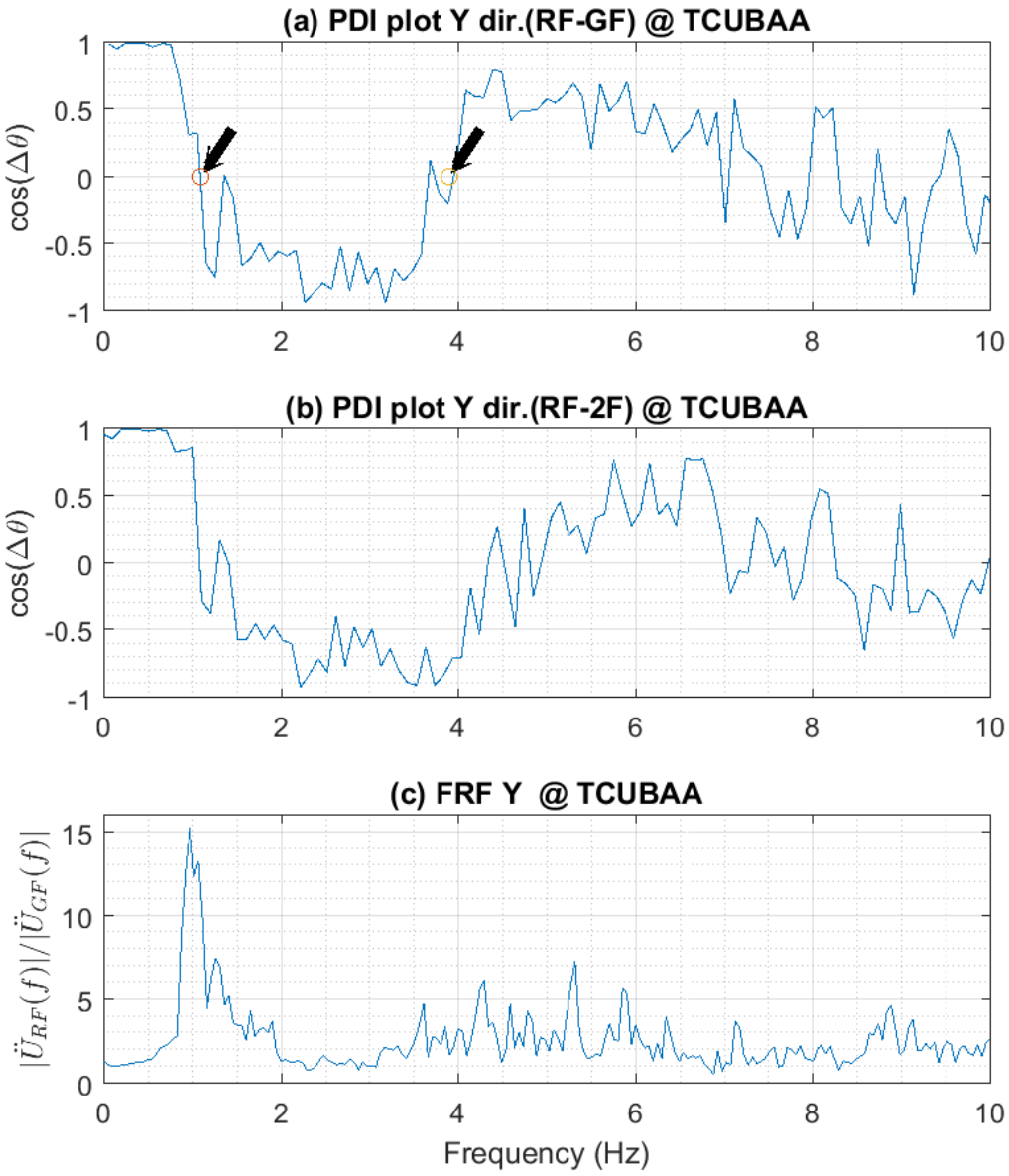

Fig. D.39. PDI plot of TCUBAA in Y direction. The black arrow marks point at the identified modes.

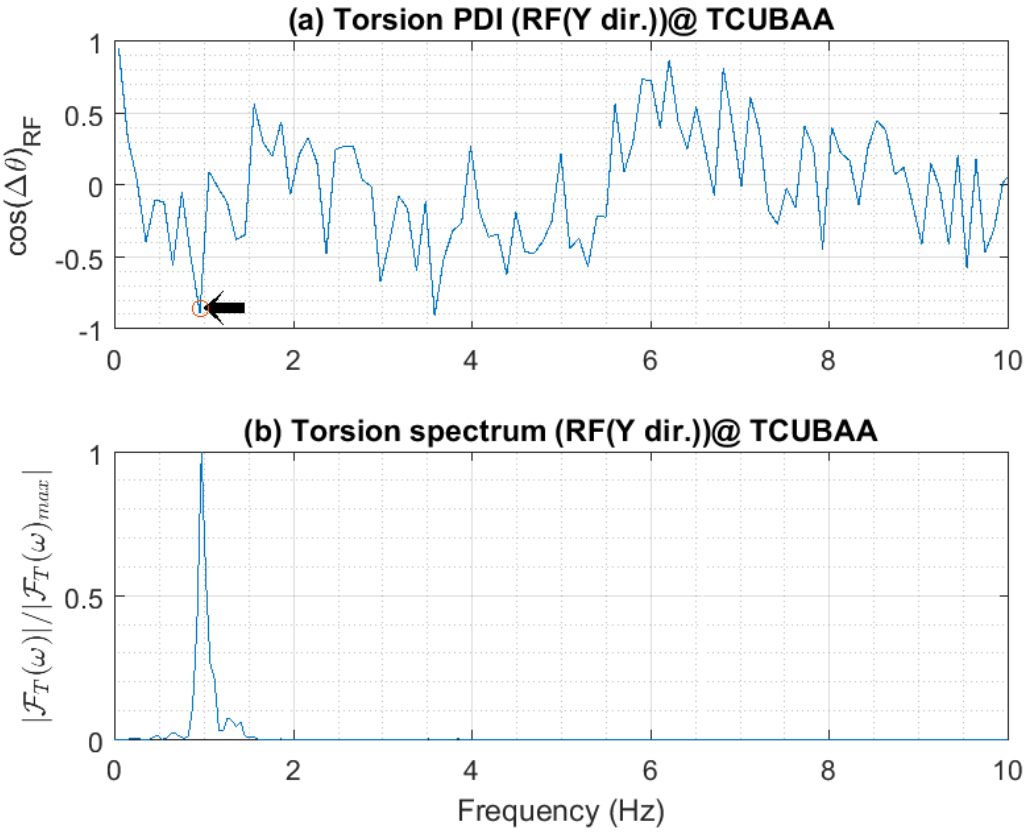

Fig. D.40. Torsional PDI plot of TCUBAA (RF-Y dir.)(Ch. 24 & 26). The black arrow marks point at the identified modes.

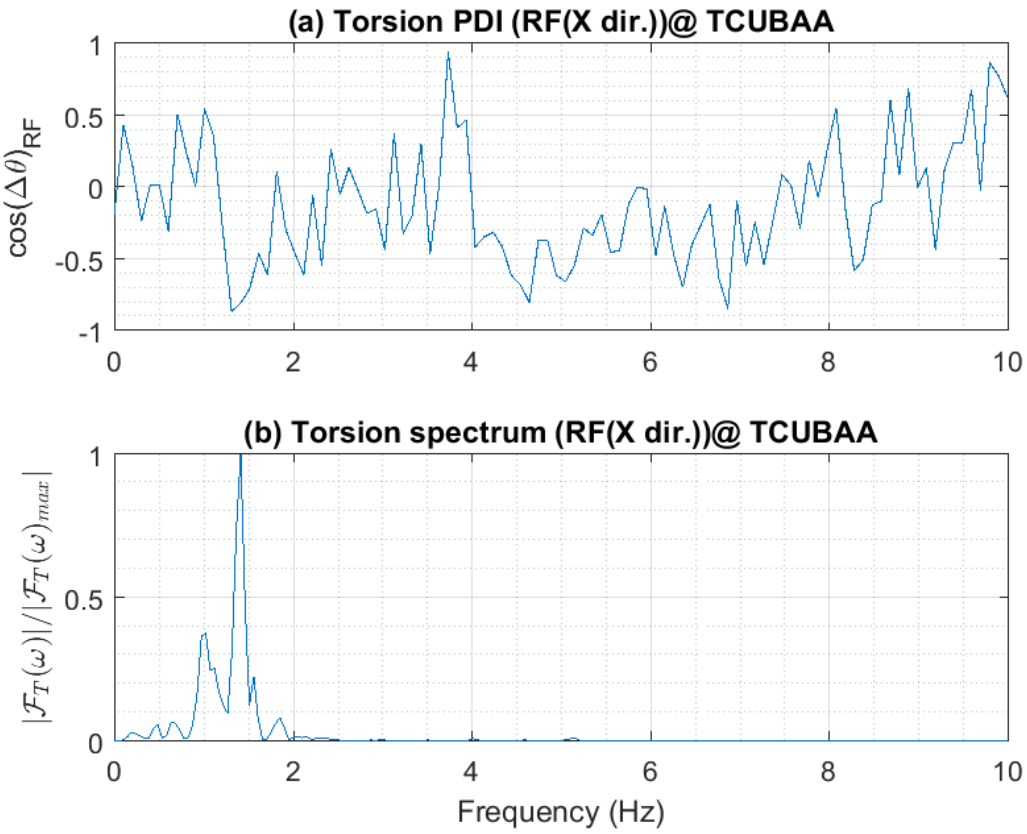

Fig. D.41. Torsional PDI plot of TCUBAA (RF-X dir.)(Ch. 27 & 23). The result is different from Fig.D.40 because of mass eccentricity in X direction.

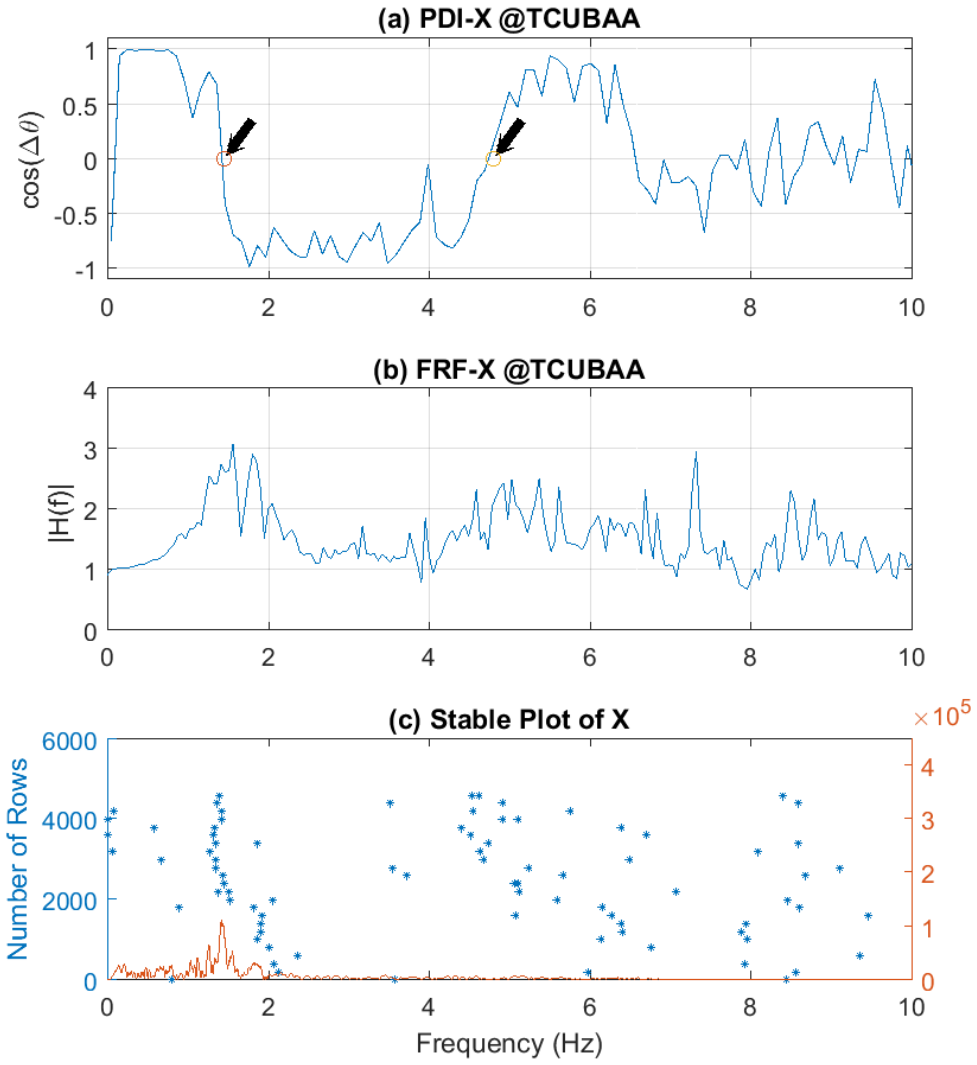

Fig. D.42. Comparison of three methods @ TCUBAA in X dir.(a) PDI plot method, (b) peak-picking method, (c) subspace method. The black arrows mark point at the identified modes.

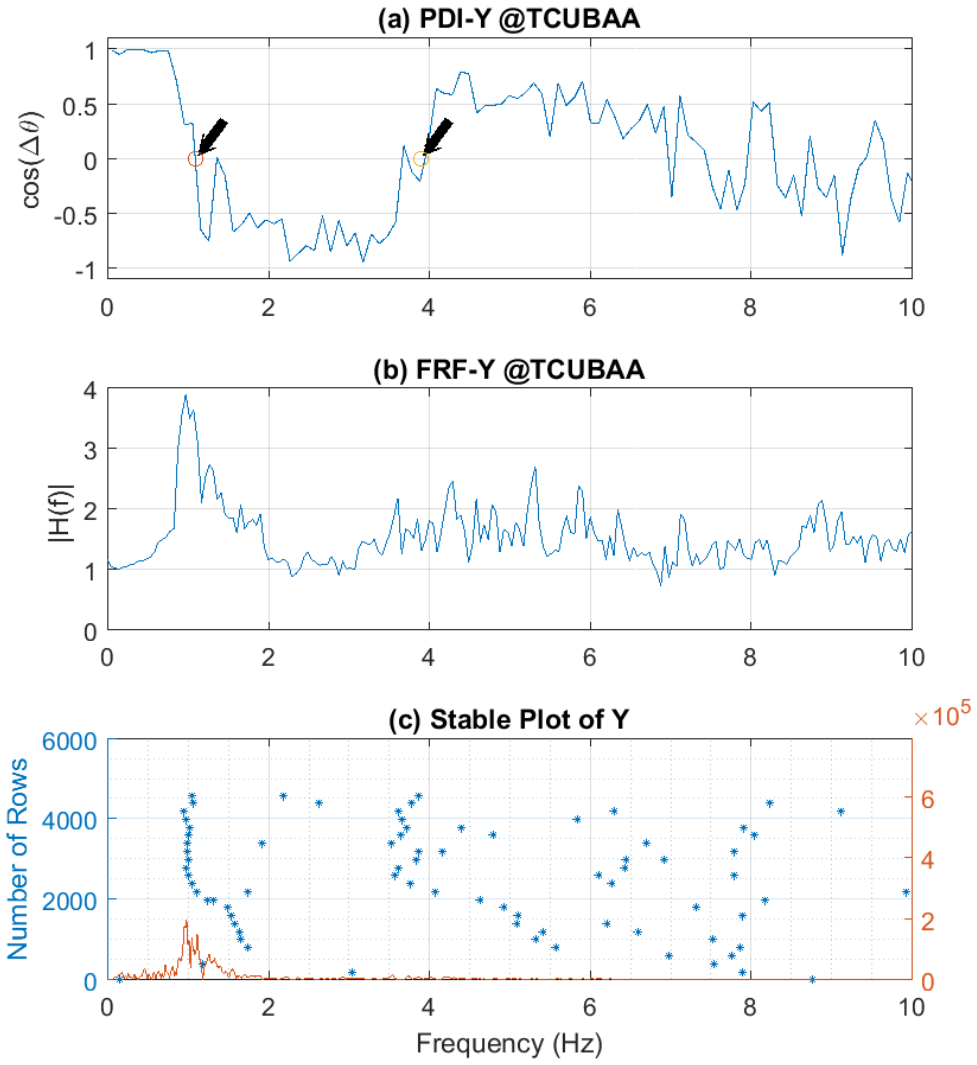

Fig. D.43. Comparison of three methods @ TCUBAA in Y dir.(a) PDI plot method, (b) peak-picking method, (c) subspace method. The black arrows mark point at the identified modes.

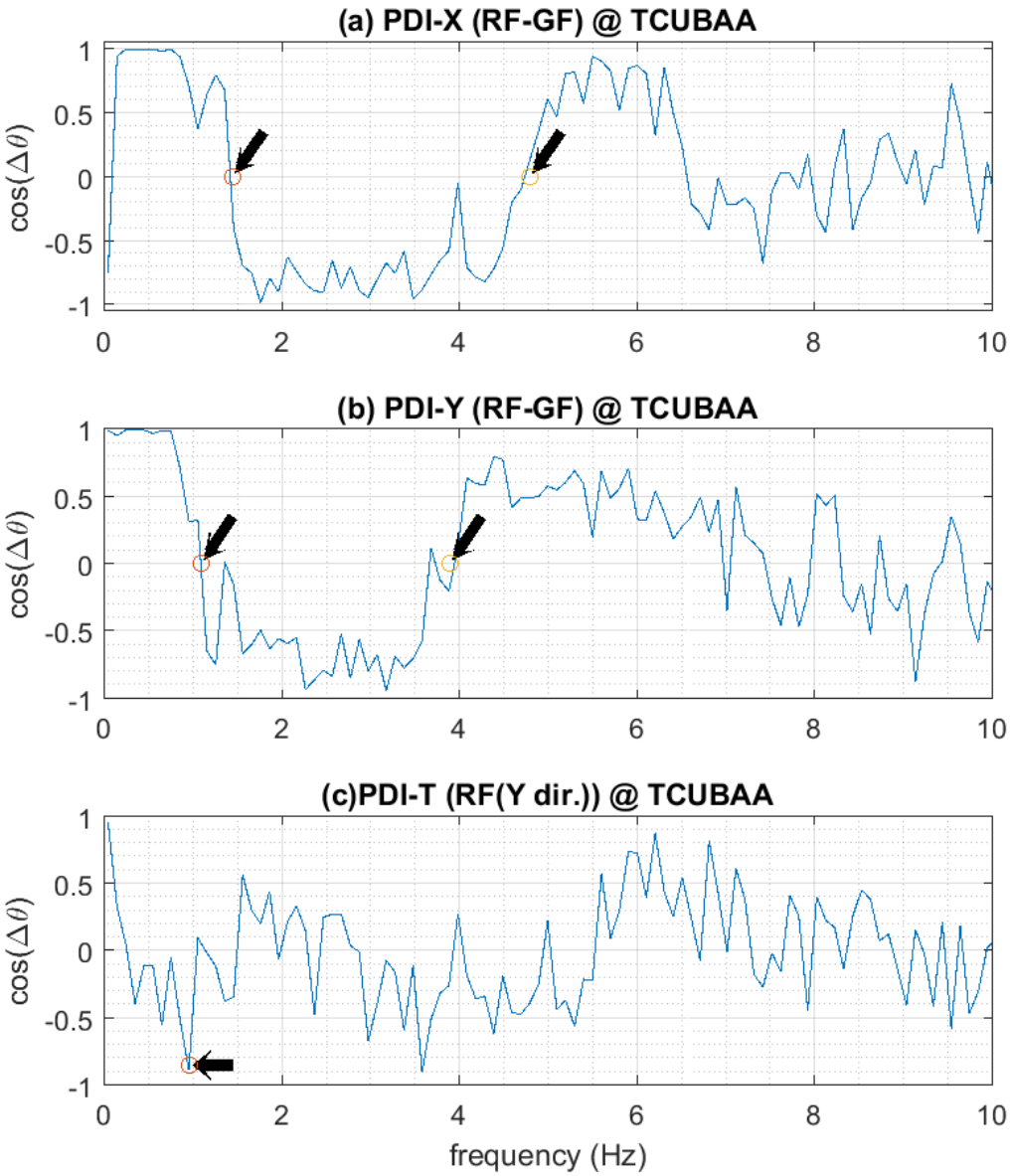

Fig. D.44. Triple PDI plots of TCUBAA (X,Y and Torsion). The black arrow marks point at the identified modes.

E. INTRODUCTION OF THE SUBSPACE METHOD

E.1 Introduction

The subspace identification method(SIM) had been widely applied to structural system identification. The theory in SIM was originated from the impulse response (Markov parameter) of the state space model. The skills of these methods are based on knowledge from linear algebra, system theory, and statistics [4]. First, one has to understand the concept of state space .

E.1.1 State Space Concept

To consider N degrees of freedom system:

$$[M]\{\ddot{x}\} + [C]\{\dot{x}\} + [K]\{x\} = \Pi[u(t)] \tag{E.1}$$

Now, a new variable vector is defined to transform eq. E.1 to a eigenvalue problem:

$$\{X\} = \begin{Bmatrix} x \\ \dot{x} \end{Bmatrix} \tag{E.2}$$

Eq. E.1 becomes:

$$\left\{\dot{X}\right\} = [A]\{X\} + [B]\{u(t)\} \tag{E.3}$$

where:

$$[A] = \begin{bmatrix} [0] & [I] \\ -[M]^{-1}[K] & -[M]^{-1}[C] \end{bmatrix} \tag{E.4}$$

$$[B] = \begin{bmatrix} [0] \\ [M]^{-1}\Pi \end{bmatrix} \tag{E.5}$$

The same notion can also be applied to the measured signal from the system.

$$y(t) = C_a\ddot{x} + C_v\dot{x} + C_d x \tag{E.6}$$

where:C_a, C_v and C_d is the output location matrices of acceleration, velocity and displacement.

$y(t)$ can also be expressed in state space form:

$$y(t) = CX + Du \tag{E.7}$$

E.1.2 Subspace Method

From above, the traditional MDOF equations can be transformed to a state space form. Consider a system that combined the stochastic system with additive sensor noises:

$$\dot{x}(t) = Ax(t) + Bu(t) + Ke(t) \tag{E.8}$$

$$y(t) = Cx(t) + Du(t) + e(t) \tag{E.9}$$

where: A, B, C,and D are state-space matrices. K is the disturbance matrix. $u(t)$ is the input, $y(t)$ is the output, $x(t)$ is the vector of nx states and $e(t)$ is the disturbance [34]. In this research, $Ke(t)$ and $e(t)$ can be regarded as the white noise recorded in the system.

As long as a system can be expressed as a state space form with discrete data of input and output. It is feasible to work out the problem by the subspace method. In Matlab, some convenient tools such as the "n4sid" command can be easily used to calculated the A,B,C,D matrices in Eq. E.8 and Eq. E.9. Among those matrices, A is the most important. By analyzing the eigenvalues of A matrix, the natural frequencies and mode shape can be found by the following equation. Assume λ_i is the eigenvalues of A matrix:

$$\Lambda_i^c = \frac{ln\lambda_i}{\Delta t} \tag{E.10}$$

$$\lambda_i^c, \bar{\lambda_i^c} = a_i \pm b_i j \tag{E.11}$$

where:

- $a_i = -\xi_i \omega_i$
- $b_i = \omega_i \sqrt{1 - \xi_i^2}$
- Δt : time step

Therefore the natural frequency of the system:

$$\omega_i = \sqrt{a_i^2 + b_i^2}(rad/s) \tag{E.12}$$

$$f_i = \frac{\omega_i}{2\pi}(Hz) \tag{E.13}$$

From Eq. E.12 and Eq. E.13, the natural frequencies can be obtained.

VITA

VITA

Li-Hui Cheng was born on 15 June 1974 and grew up in Taipei, Taiwan. He received a bachelor's degree in Agricultural Engineering from National Taiwan University in June 1996 and a master's degree in Civil Engineering from National Central University, Taiwan in June 1998.

From 1998 to 2000, Cheng served his military service in National Security Bureau, Taiwan. After his military service, he passed the government employee exam and began his first job in Public Works Bureau of Taipei County Government. Meanwhile, he also passed the National Exams of Structure Engineer and Civil Engineer in Taiwan.

From 2000 to 2014, he held different positions, namely, as associate technical specialist(Apr. 2000 $\sim$ Oct. 2005), technical specialist (Oct. 2005 $\sim$ Mar. 2008), chief of planning and design section(Mar.2008 $\sim$ Aug.2013), and then promoted to deputy chief engineer of New Construction Office, New Taipei City Government(Aug. 2013 $\sim$ Jul. 2014).

In 2012, the author received a scholarship from the Taiwan government, and arrived at Purdue University in August 2014 to begin work on his Ph.D. dissertation. Cheng completed his degree in December 2017.